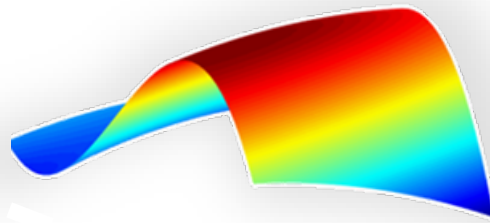


Synergistic hydrothermal liquefaction of waste materials

Ph.D. Thesis



Juliano Souza dos Passos
Department of Biological and Chemical Engineering

Aarhus University
January 2022



The present Doctor of Philosophy thesis was submitted to the Aarhus University's (AU) Graduate School of Technical Sciences (GSTS) – Denmark. This project received funding from:

- European Union's Horizon 2020 research and innovation grant agreement No. 764734 (HyFlexFuel – Hydrothermal Liquefaction: enhanced performance and feedstock flexibility for efficient biofuel production);
- Aarhus University's Centre for Circular Bioeconomy (CBIO);
- Aarhus University's Graduate School of Technical Sciences (GSTS).

The project took place at AU's facilities in Aarhus and Foulum, Denmark from February 1st, 2019 to January 31st, 2022. The research described here was carried out in the Hydrothermal Processing Research Group, department of Biological and Chemical Engineering, under supervision of Associate Professor Patrick Biller and co-supervision of Associate Professor Marianne Glasius. Also in connection with this project, activities were performed in the Department of Petroleum Technology and Alternative Fuels, University of Chemistry and Technology Prague, Czech Republic from July, 16th to September, 10th, 2021, under supervision of Assistant Professor Petr Straka. This thesis is composed of 10 chapters. Out of those, 3 are published papers – namely chapters 2, 5 and 6. Another 3 chapters are manuscripts mostly in final versions – namely chapters 3, 8 and 9. Published material is appended in the thesis using original publishers' formatting. All chapters in this thesis have as main author the PhD student Juliano Souza dos Passos with co-authorship noted when necessary at the beginning of each chapter.

Main Supervisor:

Patrick Biller

Associate Professor

Department of Biological and Chemical Engineering - Process and Materials Engineering

pbiller@bce.au.dk

Co-Supervisor:

Marianne Glasius

Associate Professor

Department of Chemistry

glasius@chem.au.dk

ISBN: 978-87-7507-527-0

DOI: 10.7146/aui.450

Acknowledgements

I would like to thank first and foremost my wife, Natália for supporting me in this journey. You are my family and best friend. Without you I could not have finished this work with the same joy and happiness. Thank you for being part of my life.

I thank my family and friends for all moral support, even in long distance. I thank my parents, Maria Aparecida and Genivaldo, my sister and brother for everything they mean to me. [Obrigado família por tudo que vocês já fizeram e fazem por mim.] I would like to mention the names of Jean Gonçalves, Marcos Laurentino, Mette and Simon Kristensen that represent to me what friendship means, and thank all other friends I encountered during this time in Denmark for all support you provided. If you've participated in my life during the past years, please feel embraced right now and know that I owe you my deepest gratitude.

I would like to express my profound gratitude to Patrick Biller, my main supervisor, for all his inputs and fruitful discussions. Thanks for keeping your doors open and for everything you taught me during the past three years. I also thank Ib Johansen for introducing me to Patrick and keeping an eye on me and this project. I believe this work gave me two good friends.

I thank my co-supervisor Marianne Glasius for her support and fruitful discussions. I'd like to thank Ib Johansen, Konstantinos Anastasakis, Marianne Glasius and Natália H. M. dos Passos for proofreading this thesis. Also, I thank all my colleagues in Aarhus University's Biological and Chemical Engineering Department for the good work environment and for both technical and comical discussions. Aisha, Aidan, Aikaterini, Andrej, Carmen, Cecilie, Cristiane, Emil, Gossaye, Konstantinos, Laura, Lars, Louise, Mads, Morten, Thalles, Theis, Thomas and all others at Hangøvej and L38, thanks a lot.

I thank all staff at UCT Prague that received me with enthusiasm and the will to collaborate and discuss ideas. In specific, thank you Petr Straka and Milos Auersvald for the excellent discussions and all collaboration. I hope this is the first of many!

I gratefully acknowledge all funding that made this PhD project real, from European Commission's Horizon 2020, from Aarhus University CBIO and GSTS.

Preface

Subcritical hydrothermal liquefaction (HTL) of mixed waste streams is the key concept tying this thesis together. By subcritical HTL, this work refers to hot, compressed, liquid-state water at temperatures ranging from 300 to 373 °C. The thesis is separated into two major areas: the interaction of synthetic polymers with biomass waste in the HTL process and; the interaction of different biomass waste streams with each other. This thesis is organized in three parts to highlight the research approach and the discoveries throughout the PhD project.

Part I describes HTL of synthetic polymers alone, in an effort to evaluate subcritical HTL processing of synthetic materials in one publication and assess how modern HTL methods can handle these materials. Here, it is discussed the types of reactions found for each of the 12 most used synthetic polymers under hot and compressed water. This evaluation will prove to be of utmost importance to understand the behavior of synthetic materials in presence of other types of organic molecules under HTL.

Part II describes the interaction of synthetic polymers and biomass, specifically lignocellulosic types in the appended papers from the author. The first paper evaluates the interaction of each of the 12 selected polymers with lignocellulosic biomass in a fixed ratio under typical subcritical HTL conditions. Benefits and drawbacks of the approach are identified and discussed. The most promising advantage identified was the combined processing of polyurethane foam with lignocellulosic, which was explored further in another paper appended, where batch and continuous processing of these materials are reported, accompanied with advanced mass spectrometry evaluation of the produced oil.

Part III explores the interactions of cow manure and wheat straw as representatives of wet and dry agricultural waste materials, respectively rich and poor in protein content. The advantages gained by synergistic effects identified during co-HTL of both are modelled and tested in pilot processing in the first manuscript of this part. The resulting biocrudes are evaluated in bench scale upgrading via catalytic hydrotreatment in a separate manuscript, where the possible benefits and drawbacks of this approach are discussed.

The last chapter of this thesis brings up conclusions and other considerations about the approach suggested. Here, the great benefits of increasing HTL efficiencies via combined waste processing are highlighted. Together with it, further comments about opportunities identified are elaborated. The reader can find all supporting information in the appendix section of this thesis, at the end of the document. To ease your reading, please use the bookmarks tool of this PDF document.

List of abbreviations

ABS	- Poly (acrylonitrile butadiene styrene)
CHN	- Carbon, Hydrogen and Nitrogen elemental analysis
CHNS	- Carbon, Hydrogen, Nitrogen and sulfur elemental analysis
CM	- Cow Manure
co-HTL	- Combined Hydrothermal Liquefaction
DTG	- Derivative Thermogravimetry
FT-ICR	- Fourier Transform Ion Cyclotron Resonance
FTIR	- Fourier Transform Infra-Red
GC	- Gas Chromatography
HDPE	- High Density Polyethylene
HTL	- Hydrothermal Liquefaction
IEA	- International Energy Agency
LCA	- Life-Cycle Assessment
LDPE	- Low Density Polyethylene
MS	- Mass Spectrometry
PA	- Polyamide
PA6	- Polyamide 6
PA66	- Polyamide 6-6
PC	- Polycarbonate
PE	- Polyethylene
PET	- Polyethylene Terephthalate
PP	- Polypropylene
PUR	- Polyurethane
PVC	- Polyvinyl Chloride
TAN	- Total Acid Number
TGA	- Thermogravimetric Analysis
TIC	- Total ion chromatogram
WS	- Wheat Straw

List of Publications

This thesis contains the following peer-reviewed publications:

dos Passos, J. S.; Glasius, M.; Biller, P. Screening of Common Synthetic Polymers for Depolymerization by Subcritical Hydrothermal Liquefaction. *Process Saf. Environ. Prot.* 2020, *139*, 371–379. doi.org/10.1016/j.psep.2020.04.040.

dos Passos, J. S.; Glasius, M.; Biller, P. Hydrothermal Co-Liquefaction of Synthetic Polymers and Miscanthus Giganteus : Synergistic and Antagonistic Effects. *ACS Sustain. Chem. Eng.* 2020. doi.org/10.1021/acssuschemeng.0c07317

dos Passos, J. S.; Chiaberge, S.; Biller, P. Combined Hydrothermal Liquefaction of Polyurethane and Lignocellulosic Biomass for Improved Carbon Recovery. *Energy and Fuels* 2021, *35* (13), 10630–10640. doi.org/10.1021/acs.energyfuels.1c01520.

This thesis contains the following unpublished manuscripts:

dos Passos, J. S.; Nowak, M.; Biller, P. Hydrothermal liquefaction of polyolefins and polystyrene for chemical recycling: steam explosion as a pretreatment step and the effects of combined supercritical processing. *Unpublished manuscript.* 2019.

dos Passos, J. S.; Matayeva, A.; Biller, P. Enhanced biocrude and carbon recovery from cow manure and wheat straw combined hydrothermal liquefaction via mixed feedstock optimization: from batch to continuous processing. *Unpublished manuscript.* 2021

dos Passos, J. S.; Straka, P.; Auersvald, M.; Biller, P. Upgrading of hydrothermal liquefaction biocrudes from mono- and co-liquefaction of cow manure and wheat straw via hydrotreating followed by distillation. *Unpublished manuscript.* 2022

Other relevant publications by the author in this thesis' field of research

Biller, P.; Johannsen, I.; dos Passos, J. S.; Ottosen, L. D. M. Primary Sewage Sludge Filtration Using Biomass Filter Aids and Subsequent Hydrothermal Co-Liquefaction. *Water Res.* 2018, *130*, 58–68. doi.org/10.1016/j.watres.2017.11.048.

Thomsen, L.; Carvalho, P. N.; dos Passos, J. S.; Anastasakis, K.; Bester, K.; Biller, P. Hydrothermal Liquefaction of Sewage Sludge; Energy Considerations and Fate of Micropollutants during Pilot Scale Processing. *Water Res.* **2020**, *183*, 116101. doi.org/10.1016/j.watres.2020.116101.

Abstract

Synthetic polymers constitute one of the largest fractions of solid waste worldwide. From 1950 to 2015, roughly 12 Gton of these materials were deposited either in landfills or in the environment. The absolute majority of these materials are energetically dense, fossil-derived and non-biodegradable, which causes accumulation in the environment, threatening both marine and terrestrial ecosystems. Chemical recycling of these materials can be a management strategy to alleviate pollution and to reuse otherwise wasted energy in the form of solid materials.

Agricultural crop residues are composed of both wet and dry streams, summing up to 3600 Mton year⁻¹ (2013 estimate) of wasted resources globally. Besides that, around 3120 Mton year⁻¹ (2017 estimate) of animal manure is generated worldwide. Nowadays, these agribusiness byproducts are underutilized and their conversion to liquid biofuels may present an untapped opportunity to provide the sustainability needed in sectors dependent on liquid hydrocarbons as an energy source.

This thesis focuses on understanding how synthetic polymers and agricultural waste interact under hydrothermal liquefaction (HTL) conditions, identifying opportunities and evaluating the engineering challenges to apply the technology in combined processing of waste streams. This work evaluates the possibility of recovering monomer-like structures from synergistic combined HTL (co-HTL) of synthetic materials and lignocellulosic biomasses. It also evaluates how biocrudes derived from highly synergistic co-HTL behave in downstream processing for biofuel production when compared to single-feedstock biocrudes.

HTL uses the reactivity of hot-compressed water in near-critical conditions to convert carbon-based materials into useful short chain organic compounds. The interaction of different feedstock materials under this condition allows a beneficial process efficiency and enlarges the opportunities to apply this process in waste handling scenarios.

Literature about HTL processing of synthetic polymers present significant achievements within the field, however the non-standardized approach for several studies lead to contradictory results, generating a knowledge gap between laboratory results and practical applications. Here, results of subcritical HTL processing are presented for the 12 most used synthetic polymers worldwide, both individually and combined with lignocellulosic materials. When evaluating synthetic polymers alone, it is found that materials containing heteroatoms in the backbone of the polymer structure are prone to hydrolysis under subcritical water, while carbon-carbon bonds are preserved. In practice, polymers derived from addition polymerization such as polyolefins and polystyrene do not depolymerize under subcritical water, while condensation polymers and others containing heteroatoms in the backbone are decomposed into molecules similar to their original monomers.

When these materials are combined with lignocellulosic ones, the synthetic parts containing nitrogen heteroatoms tend to synergistically interact with the organic-derived molecules and act synergistically increasing biocrude production. The reactivity of nitrogen species in synthetic polymers was directly proportional to the intensity of the synergies verified. The largest synergy identified was for polyurethane combined processing due to the presence of

highly reactive amines bonded to aromatic groups. This finding led to an improved combined processing of polyurethane foam and lignocellulosic materials, reaching pilot processing carbon and energy efficiencies of 71 and 75%, respectively.

The combination of wet and dry agribusiness waste fractions in HTL processing was evaluated using cow manure and wheat straw, respectively, as representatives. Their combination also leads to enhanced biocrude and carbon recovery during subcritical HTL processing through nitrogen species reactions with lignocellulosic-derived compounds. The formation of heteroatom-containing aromatics acts as a carbon carrier to the biocrude products. With this approach, pilot HTL processing carbon yields were enhanced from 40 to 60 wt%, while also providing superior total energy efficiencies (up to 50% based on organic input and output including heating utilities). This increase in carbon efficiency generates further benefits in the production of hydrotreated products, with biomass-to-hydrotreated products carbon balances increasing from 34 wt% for wheat straw in single HTL to 43 wt% in co-HTL of wheat straw and cow manure. The distillation of hydrotreated products depicts that the nitrogen-containing molecules tend to have higher concentration in heavier fractions, which may be an opportunity for more targeted processing of these fractions. Overall, production of biofuels enlarged via co-HTL mainly due to HTL superior carbon and energy yields.

Both synthetic-organic and organic-organic waste combined HTL, the reactions involving nitrogen compounds generate high synergistic effects towards biocrude formation. When increasing product stability through nitrogenated species, a consequent increased difficulty for their removal in following hydrotreatment oil upgrading is also verified. Nevertheless, the enhanced carbon and energy recovery and enlarged scope of HTL technologies attained via combination of waste materials is an opportunity to take advantage of these sub-utilized streams.

Resumé

Syntetiske polymerer udgør en af de største fraktioner af fast affald på verdensplan. Fra 1950 til 2015 blev omkring 12 GT af disse materialer enten afbrændt, deponeret eller havnede i miljøet. Størstedelen af disse materialer er fossil-afledte og ikke-bionedbrydelige, hvilket forårsager ophobning i miljøet, og udgør dermed en trussel for både marine og terrestriske økosystemer. Kemisk genanvendelse af disse materialer kan være en løsning for at afhjælpe forurening og genbruge ellers spildte ressourcer fra disse kilder.

Landbrugsafgrøderester sammensat af både våde og tørre strømme udgør op til 3600 Mton år⁻¹ (2013 skøn) af dårligt udnyttede ressourcer globalt. Derudover genereres der omkring 3120 Mton år⁻¹ (2017 skøn) husdyrgødning på verdensplan. I dag er disse biprodukter fra landbruget underudnyttet, og deres omdannelse til flydende biobrændstoffer kan udgøre en uudnyttet mulighed for at levere den nødvendige bæredygtighed i sektorer, der er afhængige af flydende kulbrinter som energikilde.

Denne afhandling fokuserer på at forstå, hvordan syntetiske polymerer og landbrugsaffald interagerer under hydrotermisk forflydning eller liquefaction (HTL). Afhandlingen vilt identificere muligheder og evaluere de tekniske udfordringer ved at anvende teknologien i kombineret behandling af affaldsstrømme. HTL bruger reaktiviteten af varmt komprimeret vand under næsten kritiske forhold til at omdanne kulstofbaserede materialer til nyttige kortkædede organiske forbindelser. Samspelet mellem forskellige råmaterialer under disse forhold muliggør en fordelagtig proceseffektivitet og udvider mulighederne for at anvende denne proces i affaldshåndteringsscenerier.

Litteraturen om HTL omdannelse af syntetiske polymerer beskriver betydelige resultater inden for området, men den ikke-standardiserede tilgang i flere undersøgelser fører til modstridende resultater, hvilket genererer en videnskloft mellem laboratorieresultater og praktiske anvendelser. I denne afhandling er resultater fra subkritisk HTL-bearbejdning beskrevet for de 12 mest anvendte syntetiske polymerer på verdensplan individuelt og sammen med lignocellulosematerialer. Ved evaluering af syntetiske polymerer alene fandt vi ud af, at materialer indeholdende heteroatomer i polymerstrukturens rygrad er tilbøjelige til omdannelse under HTL betingelser, mens carbon-carbon-bindinger bevares. I praksis depolymeriserer polymerer afledt af additions polymerisation, såsom polyolefiner og polystyren, ikke, mens kondensations- og additionspolymerer, der indeholder heteroatomer i rygraden, nedbrydes til molekyler svarende til deres oprindelige monomerer.

Når disse materialer kombineres med lignocelluloseholdige, har de syntetiske dele, der indeholder nitrogenheteroatomer, en tendens til synergistisk at interagere med de organisk afledte molekyler, hvilket øger produktionen af biocrude. Reaktiviteten af kvælstofforbindelser i syntetiske polymerer var direkte proportional med omfanget af de verificerede synergier. Den største identificerede synergi var for polyurethan med biomasse omdannelse på grund af tilstedeværelsen af meget reaktive aromatiske aminer. Denne opdagelse førte til en forbedret kombineret omdannelse af polyurethanskum og lignocellulosematerialer. Pilotforarbejdning nåede en kulstof- og energieffektivitet på henholdsvis 71 og 75%.

Kombinationen af våde og tørre affaldsfraktioner fra landbruget i HTL-omdannelse blev evalueret med henholdsvis kogødning og hvedehalm som repræsentanter. Denne kombination fører til forbedret bioråolie udbytte og kulstofgenvinding under subkritisk HTL-omdannelse. Dette skyldes kvælstofforbindelsernes reaktioner med lignocellulose-afledte forbindelser. Dannelsen af heteroatomholdige aromater fungerer som en kulstofbærer til bioråprodukterne. Med denne tilgang blev pilot-HTLkulstofudbyttet øget fra 40 til 60 vægt%, samtidig med at det gav bedre total energieffektivitet (op til 50% baseret på organisk input inklusive tilført procesenergi).

Både i syntetisk-organisk og organisk-organisk affald genererer kombinerede HTL-reaktioner, der involverer nitrogenforbindelser, høje synergistiske effekter ved biocrude-dannelse. Når produktstabiliteten øges gennem kvælstofforbindelser, medfører det samtidig en øget resistens mod fjernelse af disse ved hydrogenering i forbindelse med raffinering. Ikke desto mindre er den forbedrede kulstof- og energigenvinding og det udvidede marked for HTL-teknologier opnået via kombination af affaldsmaterialer en mulighed for at drage fordel af disse underudnyttede strømme.

Resumo

Polímeros sintéticos constituem uma das maiores frações de resíduos sólidos em todo o mundo. De 1950 a 2015, cerca de 12 Gton desses materiais foram depositados em aterros ou no meio ambiente. A maioria absoluta desses materiais são energeticamente densos, derivados de combustíveis fósseis e não biodegradáveis, ameaçando os ecossistemas marinhos e terrestres por seu acúmulo nestes. A reciclagem química destes materiais pode ser uma estratégia para reduzir a poluição e reutilizar a energia desperdiçada na forma de materiais sólidos.

Resíduos de culturas agrícolas podem ser divididos dentre úmidos e secos, juntos totalizando 3600 Mton ano⁻¹ (estimativa de 2013) de recursos desperdiçados globalmente. Além disso, cerca de 3120 Mton ano⁻¹ (estimativa de 2017) de esterco animal são gerados em todo o mundo. Atualmente, esses subprodutos do agronegócio são sub-utilizados e sua conversão em biocombustíveis líquidos pode representar uma oportunidade inexplorada para fornecer a sustentabilidade necessária em setores dependentes de hidrocarbonetos líquidos como fonte de energia.

Esta tese se concentra em entender como polímeros sintéticos e resíduos agrícolas interagem sob processamento via liquefação hidrotérmica (HTL), identificando oportunidades e avaliando os desafios de engenharia para aplicar a tecnologia no processamento combinado de resíduos. Este trabalho avalia a possibilidade de recuperação de moléculas semelhantes a monômeros via HTL combinada (co-HTL) de materiais sintéticos e biomassas lignocelulósicas. Além disso, também é discutido como bio-petróleos derivados da co-HTL se comportam no seu pós-processamento para produção de biocombustíveis quando comparados a bio-petróleos de matéria-prima única.

A HTL usa a reatividade da água comprimida a quente em condições quase críticas para converter materiais à base de carbono em compostos orgânicos úteis de cadeia curta. A interação de diferentes matérias-primas nesta condição beneficia as eficiências do processo e amplia as oportunidades de aplicação deste em estratégias de manuseio de resíduos.

A literatura sobre processamento HTL de polímeros sintéticos apresenta resultados significativas dentro da área, porém a abordagem não padronizada de diversos estudos leva a conclusões contraditórias, gerando um distanciamento entre resultados laboratoriais e aplicações práticas. Nesta tese, são apresentados resultados do processamento via HTL subcrítica dos 12 polímeros sintéticos mais utilizados em todo o mundo, tanto individualmente quanto combinados com materiais lignocelulósicos. Ao avaliar apenas polímeros sintéticos, verifica-se que materiais contendo heteroátomos na estrutura base do polímero são propensos a hidrólise sob água subcrítica, enquanto as ligações carbono-carbono são preservadas. Na prática, polímeros derivados de polimerização por adição, como poliolefinas e poliestireno, não despolimerizam sob água subcrítica, enquanto polímeros de condensação e outros contendo heteroátomos na cadeia principal são decompostos em moléculas semelhantes aos seus monômeros originais.

Quando esses materiais são combinados com os lignocelulósicos, as partes sintéticas contendo heteroátomos de nitrogênio tendem a interagir sinergicamente com as moléculas derivadas

de materiais biológicos e aumentam a produção de bio-petróleo. A reatividade das espécies nitrogenadas presentes em polímeros sintéticos foi diretamente proporcional à intensidade das sinergias verificadas. A maior sinergia identificada foi para o processamento combinado de poliuretano e lignocelulósicos, devido à presença de aminas altamente reativas ligadas a grupos aromáticos. Essa descoberta levou à um melhoramento na HTL de espuma de poliuretano e materiais lignocelulósicos, atingindo altas eficiências com base no carbono e energia processados em escala piloto, respectivamente de 71 e 75%.

A combinação das frações úmidas e secas de resíduos agroindustriais no processamento via HTL foi avaliada usando esterco de vaca e palha de trigo, respectivamente, como representantes das duas categorias de rejeito. Sua combinação também leva a uma melhora na produção de biopetróleo e eficiência em base de carbono durante o processamento subcrítico via HTL. O efeito se dá também por meio de reações de espécies de nitrogênio com compostos derivados de lignocelulósicos. A formação de aromáticos contendo nitrogênio como heteroátomo arrasta carbono para os produtos do bio-petróleo. Com essa abordagem, os rendimentos do processamento via HTL em planta piloto foram aumentados de 40 para 60% em peso de carbono, além de também melhorar a eficiência energética total para valores superiores aos comuns em HTL (até 50% com base na entrada e saída orgânica, incluindo equipamentos auxiliares de aquecimento). Esse aumento na eficiência de carbono gera benefícios adicionais no balanço produtivo de hidrocarbonetos, com balanços de carbono para produtos hidrogenados aumentando de 34% (palha de trigo) para 43% em co-HTL de palha de trigo e esterco de vaca. A destilação de produtos hidrogenados mostra que as moléculas contendo nitrogênio tendem a ter maior concentração em frações mais pesadas, o que pode ser uma oportunidade para o refino direcionado dessas frações. Em geral, a produção de biocombustíveis aumentou via co-HTL principalmente devido aos rendimentos superiores de carbono e energia do processo.

Tanto para as misturas orgânico-sintéticas quanto as orgânico-orgânicas tratadas via HTL, as reações envolvendo compostos de nitrogênio geram altos efeitos sinérgicos para a formação de bio-petróleo. Ao aumentar a estabilidade do produto por meio de espécies nitrogenadas, verifica-se também um consequente aumento na dificuldade para a sua remoção no refino via hidrogenação catalítica do óleo. No entanto, a melhora na conversão de carbono e energia e o escopo ampliado das tecnologias de HTL obtidas por meio da combinação de materiais residuais é uma oportunidade de aproveitar esses resíduos subutilizados.

Contents

Part I - Hydrothermal liquefaction of synthetic	3
Chapter 1 - Introduction to synthetic polymers' current scenario	4
1.1. Synthetic polymers contribution and harm to society and the environment	4
1.2. Current fate of synthetic polymers.....	5
1.3. Thermal processes for chemical recycling of synthetic polymers	6
Chapter 2 - Paper 1 - Screening of common synthetic polymers for depolymerization by subcritical hydrothermal liquefaction	8
2.1. Reflections	8
Chapter 3 - Manuscript 1 - Hydrothermal liquefaction of polyolefins and polystyrene for chemical recycling: steam explosion as a pre-treatment step and the effects of combined supercritical processing	18
REFERENCES PART I	26
Part II - Synthetic polymers and biomass co-HTL	28
Chapter 4 - Introduction	29
4.1. Carbon, circular economy and materials.....	29
4.2. HTL of synthetic polymers and biological materials	30
4.2.1. Synthetic polymers and biomolecules under subcritical water.....	30
4.2.2. Algae and synthetic polymers.....	30
4.2.3. Lignocellulosic biomass and synthetic polymers	31
Chapter 5 - Paper 2 – Hydrothermal Co-Liquefaction of Synthetic Polymers and <i>Miscanthus Giganteus</i>: Synergistic and Antagonistic Effects	32
5.1. Reflections	32
Chapter 6 - Paper 3 – Combined Hydrothermal Liquefaction of Polyurethane and Lignocellulosic Biomass for Improved Carbon Recovery	45
6.1. Reflections	45
References Part II	57
Part III - HTL of mixed organic wastes	59
Chapter 7 - Introduction	60
7.1. Assessment of potential energy in agricultural waste streams for fossil fuel replacement	60
7.2. Energy considerations of thermochemical processes for biomass waste conversion to biofuels.....	63
7.3. Combined HTL models based on biomolecules and their applicability	65
7.4. Real waste HTL predictive models	66

Contents

Chapter 8 - Manuscript 2 – Enhanced biocrude and carbon recovery from cow manure and wheat straw combined hydrothermal liquefaction via mixed feedstock optimization: from batch to continuous processing.....	68
8.1. Reflections	68
Chapter 9 - Manuscript 3 – Upgrading of hydrothermal liquefaction biocrudes from mono- and co-liquefaction of cow manure and wheat straw via hydrotreating followed by distillation	82
9.1. Reflections	82
Chapter 10 - Thesis conclusions and perspectives	100
References Part III	102
SUPPLEMENTARY INFORMATION – Chapter 2 - Paper 1 - Screening of common synthetic polymers for depolymerization by subcritical hydrothermal liquefaction	105
SUPPLEMENTARY INFORMATION – Chapter 5 - Paper 2 – Hydrothermal co-liquefaction of synthetic polymers and Miscanthus Giganteus; synergistic and antagonistic effects	112
SUPPLEMENTARY INFORMATION – Chapter 6 - Paper 3 – Combined hydrothermal liquefaction of polyurethane and lignocellulosic biomass for improved carbon recovery.....	123
SUPPLEMENTARY INFORMATION – Chapter 8 – Manuscript 2 – Enhanced biocrude and carbon recovery from cow manure and wheat straw combined hydrothermal liquefaction via mixed feedstock optimization: from batch to continuous processing	132
SUPPLEMENTARY INFORMATION – Chapter 9 – Manuscript 3 – Upgrading of hydrothermal liquefaction biocrudes from mono- and co-liquefaction of cow manure and wheat straw via hydrotreating and distillation	140

Part I

Hydrothermal liquefaction of synthetic polymers

Chapter 1

Introduction to synthetic polymers' current scenario

1.1. Synthetic polymers contribution and harm to society and the environment

The post war world of the 1950's brought with it a revolution on material handling by introducing synthetic resins mass production. Different synthetic materials based on fossil reserves (oil, coal and gas) chemical refining widened market possibilities on transportation, food, feed, clothing, and all other imaginable market fractions. From the simple act of buying salad in the supermarket to building super-computers and spacecrafts, synthetic polymers largely contribute to modern society and undeniably bring value to it.^{1,2}

Generally, after synthetic polymers' final consumer use, the material is disposed and managed according to current waste handling systems. The lifetime of a product heavily depends on application sector¹ (Figure 1). The largest contributor to synthetic polymers waste is the packaging-related applications, which are dominated by single-use polyolefins, e.g. polyethylene (PE), polypropylene (PP), polystyrene (PS), etc. For these reasons, plastics quickly became one of the most produced and wasted materials in human history.¹ When such an amount of waste material goes through poorly designed systems, leakage to the environment is unavoidable.

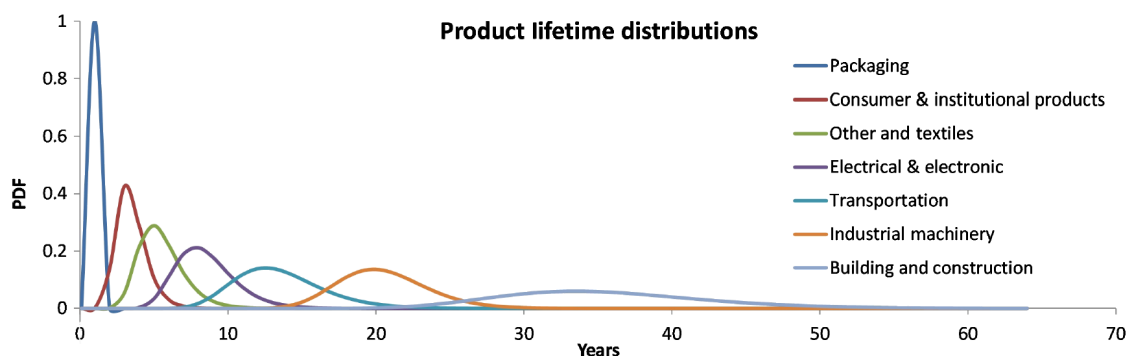


Figure 1 - Product lifetime distributions of synthetic polymers by application sector plotted as log-normal probability distribution functions (PDF) (adapted from¹)

It is known since the 1970's that synthetic polymers leakage to the environment was happening and accumulation into land and water bodies was a focus of concern due to several possible consequences. These consequences are all related to one of the most important characteristics of these materials: virtually no possible biological degradation.³ However, it was not until 2010's alarming numbers on plastic ocean pollution that this matter caught the eyes of public opinion and became a matter of concern in public forums and reports.⁴

The now acknowledged threat to both terrestrial^{5,6} and marine^{3,4,7} ecosystems posed by plastic debris pollution urges for action towards a better waste generation and handling system that keeps the recognized contributions of synthetic resins to society and handles its harm to environment. Business as usual operations cannot continue if global environment equilibrium and preservation are

the pursued objectives of current industrial setups.² More specifically, mismanaged synthetic resin waste has to be tackled urgently to avoid the likely worsening scenario we face, as pointed by several recent forecasts^{1-3,8,9} (Figure 2).

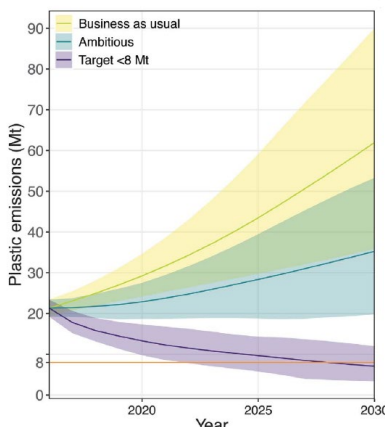


Figure 2 – Global plastic waste emissions forecast 2020-2030 (adapted from⁹)

Even though remarkable efforts are being made by several parties globally, it is still unlikely that pollution levels will decrease in the near future.⁹ These efforts can be illustrated by e.g. European Union’s plastic strategy¹⁰ and Circular Plastics Alliance¹¹; United Nations’ global plastic platform¹²; World Economic Forum’s Global Plastic Action Partnership¹³; plastic bottle partially successful history of recycling¹⁴; pyrolysis pilot and demonstration plants¹⁵ and more recently; supercritical water-based processing alternatives demonstration plants.^{16,17} Given the near future forecast, flexible technologies capable of handling the large variety of synthetic polymers used nowadays with the aim of chemically recycling those are still desired and should be pursued.

1.2. Current fate of synthetic polymers

When fossil reserves are converted into synthetic polymers, there are only a few options for their fate. They can be in use by a consumer; being recycled for once, (not often) twice or (rarely) a third time; discarded in landfills or; incinerated releasing CO₂. For the first two options, consumption and recycling, the status is temporary and the current unavoidable final disposal fate – landfilling or incineration – will happen eventually (see Figure 1).¹ The recycling processes can be divided into primary, secondary, tertiary and quaternary recycling. Primary recycling focuses in single-type pure streams mainly found within manufacturing plants, which are directly processed mechanically, e.g. trims, production errors. Secondary recycling deals with already used products that need pre-treatment steps before mechanical processing, e.g. PET bottles, fishing nets. Tertiary recycling focuses in the monomer recovery of synthetic materials, using e.g. pyrolysis, cracking, gasification and chemolysis. Quaternary recycling, despite called “recycling”, is simply the chemical energy utilization via combustion.^{15,18} All these recycling categories point out the linearity of this material balance, which conducts carbon from fossil to waste with only a few detours.

The most common plastic recycling strategy is mechanical recycling, which is limited to primary and secondary schemes. In short, single-type plastic streams are re-melted and mixed with virgin feedstock to produce new products. Because re-melting processes heavily impact mechanical properties of such polymers via polymer degradation and impurities introduction, typically only a

limited amount of recycled plastic can be added to brand new products (often up to 20-30%).¹⁹ I.e. if pure mechanically recycled polymers are used when producing products, the subsequent product will have lower quality than its first form. This effect can also be named downgrading recycling, which decreases value through the production and recycling chain.²⁰

The tertiary recycling technique is the most promising approach to recover virgin product quality, as it aims for monomer recovery. This tactic is often called chemical recycling and can be split into two segments: chemolysis and thermolysis.¹⁵ Principally, chemolysis uses chemical properties of a solvent or environment to interact with the polymer chain and depolymerize it, while thermolysis relies on temperature to increase kinetic energy of polymeric chain atoms and break bonds among them forming smaller molecules. Using such strategies synthetic resins can be broken down to their initial chemical building blocks, which in turn yield high grade synthetic resins.¹⁵ Such processes (e.g. pyrolysis, solvolysis, hydrocracking, gasification, hydrothermal liquefaction) have the potential of bringing circularity to the material balance of synthetic resins, as subsequent products yielded from those will have the same quality as original fossil refining.

1.3. Thermal processes for chemical recycling of synthetic polymers

Conventional pyrolysis is the direct use of thermal energy for breaking bonds of synthetic polymers in an inert medium. It requires moderate to high temperatures (450-700 °C) and is very effective for polyolefins, i.e. it breaks carbon-carbon bonds effectively.¹⁵ Several different reactor types are described in literature, with examples of commercial industrial facilities.²¹ Catalytic pyrolysis is an option to reduce the breaking temperature (down to 350 °C) needed for certain polymers, and several catalyst options are listed in literature. Though studies on stability and long-term operation are scarce, commercial catalytic pyrolysis plants are known, with several examples in literature dating back the 1980s.^{15,22,23} Both conventional and catalytic pyrolysis thrive using feedstock materials with little impurities. However, these processes are particularly sensitive towards feedstock polymers containing nitrogen or oxygen heteroatoms, and chlorine.

While pyrolysis processes try to avoid breaking molecules further than monomer-like structures, gasification uses even higher temperature (500-1800 °C) than pyrolysis to do so. The final product of such process is typically a combustible gas rich in H₂, CO and other small hydrocarbons, which can in turn be used as source of energy or chemical feedstock for platform chemicals.¹⁵ The limitations of gasification are similar to the ones of pyrolysis, mainly being the difficulty on handling diverse material with contaminants or heteroatom-containing synthetic materials, besides the even larger energy expenditure to maintain the process. Even so, a few examples of industrial facilities can be found, with none presenting major success stories.¹⁵

More recently, hydrothermal liquefaction (HTL) has taken attention for its potential for synthetic polymer processing.²⁴⁻²⁶ HTL can be performed using sub-critical water, with temperatures ranging from 300 to 374 °C and, supercritical water, with temperatures > 374 °C.²⁷ Typically, HTL is focused on processing biomass for biocrude production, though some of its characteristics can also be exploited for synthetic polymers. When HTL is conducted under subcritical conditions, liquid water under pressure and its properties are prone to break bonds of feedstock molecules forming smaller molecules and reacting with them for stable products. On the other hand, when supercritical

conditions are in place, water becomes even more reactive and increases its carbon-carbon bond cleaving potential.

In the context of tertiary recycling of synthetic polymers, HTL can be qualified as a mix of chemolysis and thermolysis. In one hand, it relies on hot compressed water as media for chemical reactions to take place with the chosen feedstock. On the hand, at supercritical conditions, thermal cracking is favored, while the presence of water as solvent interferes with the chemical bond cleaving mechanisms.²⁷ As HTL is typically used with different types of biomasses, which usually contain high amounts of oxygen per kg of feed, synthetic polymers offer the opportunity of inputting a higher concentration of carbon in the process. However, they also bring increased difficulty for conversion and very specific conditions for each type of polymer.

Chapter 2

Paper 1 - Screening of common synthetic polymers for depolymerization by subcritical hydrothermal liquefaction

dos Passos, J. S.; Glasius, M.; Biller, P. Screening of Common Synthetic Polymers for Depolymerization by Subcritical Hydrothermal Liquefaction. *Process Saf. Environ. Prot.* **2020**, *139*, 371–379. <https://doi.org/10.1016/j.psep.2020.04.040>.

Article history:

Received: March 23rd, 2020

Revised: April 24th, 2020

Published: May 1st, 2020

Keywords:

Hydrothermal liquefaction

Chemical recycling

Depolymerization

Circular economy

Polymers

Plastic

2.1. Reflections

This chapter tries to answer a major question remaining after critically reviewing literature about HTL applied to synthetic polymers: how should these results be compared? In many ways, literature findings were contradictory, however, as the HTL methods applied in each study were different, it was difficult to elucidate the applicability of the results and the efficiency of these processes. For instance, polyamide 6 had been reported by several groups²⁸⁻³⁰ with the agreement that it does depolymerize in presence of hot compressed water, but with very different outcomes in each study. Another example would be polyethylene terephthalate (PET), which was reported by several groups³¹⁻³⁴, some reporting 100% recovery of monomers, while others claiming a mix of molecules derived from monomers was found at the same temperature with an oil-like fraction. ABS and PS were described in literature as materials that result in high oil yields in subcritical conditions or, that no decomposition was observed at all.^{30,35-37}

The disagreement in methods reported made it difficult to anticipate the behavior of each type of polymer, hindering the development of a combined HTL approach for synthetic polymers and biomasses. In this sense, the paper appended in this chapter allowed us to better understand what yields result using the currently established method for batch HTL. This method is based on fast heating rate bomb-type reactors. After understanding the synthetic polymers individual behavior under HTL, combined approaches suggested in Part II can be explored with higher reliability.



Screening of common synthetic polymers for depolymerization by subcritical hydrothermal liquefaction



Juliano Souza dos Passos^{a,c}, Marianne Glasius^{b,c}, Patrick Biller^{a,c,*}

^a Biological and Chemical Engineering, Aarhus University, Høngøvej 2, DK-8200 Aarhus N, Denmark

^b Department of Chemistry, Aarhus University, Langelandsgade 140, DK-8000 C, Denmark

^c Aarhus University Centre for Circular Bioeconomy, Blichers Allé 20, DK-8830, Tjele, Denmark

ARTICLE INFO

Article history:

Received 23 March 2020

Received in revised form 24 April 2020

Accepted 27 April 2020

Available online 1 May 2020

Keywords:

Hydrothermal liquefaction

Chemical recycling

Depolymerization

Circular economy

Polymers

Plastic

ABSTRACT

Hydrothermal liquefaction could potentially utilize mixed plastic wastes for sustainable biocrude production, however the fate of plastics under HTL is largely unexplored for the same reaction conditions. In this study, we evaluate how synthetic waste polymers can be depolymerized to bio-crude or platform chemicals using HTL at typical conditions expected in future commercial applications with and without alkali catalyst (potassium hydroxide). We evaluate different characteristics for HTL processing of polyacrylonitrile-butadiene-styrene (ABS), Bisphenol-A Epoxy-resin, high-density polyethylene (HDPE), low density PE (LDPE), polyamide 6 (PA6), polyamide 66 (PA66), polyethylene terephthalate (PET), polycarbonate (PC), polypropylene (PP), polystyrene (PS) and polyurethane (PUR) at 350 °C and 20 min residence time. Polyolefins and PS showed little depolymerization due to lack of reactive sites for hydrolysis. HTL of PC and Epoxy yielded predominantly bisphenol-A in oil fraction and phenols in aqueous phase. PA6 and PA66 yielded one of its monomers caprolactam and a range of platform chemicals in the aqueous phase. PET produces both original monomers. PUR yields a complex oil containing similar molecules to its monomers and longer hydrocarbons. Our results show how HTL can depolymerize several different synthetic polymers and highlights which of those are the most attractive or are unsuitable for subcritical processing.

© 2020 Institution of Chemical Engineers. Published by Elsevier B.V. All rights reserved.

1. Introduction

Our modern society relies on an unsustainable linear production of goods, entailing the extraction of natural resources, refining and production of consumer goods and commodities followed by final disposal. The unavoidable end-of-life products of such processes are either mechanically recycled, disposed of in landfills or undergo combustion if suitable (Korhonen et al., 2018). The latter option, despite reducing solid residues in landfills, releases CO₂ in the atmosphere while recovering heat as the lowest value commodity.

Circular economy is an alternative mode of production (Ghosh and Agamuthu, 2018; Korhonen et al., 2018) in which industry considers waste streams generated by society as its own source of raw materials. Innumerable implementation challenges are present here, e.g. mixed materials where each substance should be diverted to a different sector; combined goods, which include synthetic

polymers, inorganic salts and metals fused together. Scientists around the world are trying to solve this problem by creating more efficient and less costly innovative solutions. The hydrothermal liquefaction (HTL) technology is a promising alternative to fulfil these requirements, as it is highly flexible in dealing with both pure waste streams and mixed ones (Biller et al., 2018).

The HTL concept has been investigated since as early as in 1982 (Coorporation, 1982), with different approaches being introduced over the years (Foudriaan and Peferoen, 1990), however early efforts aimed at substituting crude oil with bio-based feedstock for political reasons instead of climate concerns. Nowadays, the latter reason has encouraged many research groups to investigate the HTL processing efficiency and its technical feasibility in depth (Anastasakis et al., 2018; Skaggs et al., 2018). HTL has proven so far to be a technology able to with a wide range of organic waste feedstocks (Anastasakis et al., 2018; Castello and Pedersen, 2018; Skaggs et al., 2018) and synthetic polymers (Pedersen and Conti, 2017) for the production of a bio-crude which can readily be upgraded to transportation fuels (Castello et al., 2019). To this date HTL research has primarily focused on biofuel production from

* Corresponding author.

E-mail address: pbiller@eng.au.dk (P. Biller).

biomass and wastes while the utilization of waste polymers has received little attention.

Single synthetic polymers subcritical HTL has been reported for specific materials in several publications, including reports on HTL of: high-impact polystyrene, poly-acrylonitrile-butadiene-styrene (ABS), polycarbonate and polyamide 6 (Iwaya et al., 2006; Zhao et al., 2018a); epoxy printed circuit boards (Yildirim et al., 2015); polyethylene naphthalate and terephthalate (Arai et al., 2010; Zenda and Funazukuri, 2008); polystyrene-butadiene (Park et al., 2001); polyurethane (Dai et al., 2002). These studies show that monomers, other valuable chemical compounds or an oil product may be recovered using HTL. However, comparable data on the depolymerization mechanisms of these polymers is unavailable, as different reactor setups, residence times, heating rates, temperatures and pressures reported in literature make it difficult to assess if the current HTL technologies used for biomasses and organic waste (Anastasakis et al., 2018; Biller et al., 2018, 2016) are suited for synthetic polymers as well. In general, current subcritical HTL technology relies on fast heating rate reactors with moderate residence time (15–20 min), working close to water saturation pressure in the range of 300–360 °C and, depending on feedstock, applying alkali catalysis (e.g. K_2CO_3 , KOH).

The present study investigates how HTL can be applied as a generic valorization process for synthetic polymers using the same conditions as in modern biomass liquefaction. We hypothesize that HTL of polymer waste has positive and negative aspects that must be unraveled for each synthetic material in order to assess if they can be included in a combined HTL waste treatment processes for e.g. mixed municipal waste or as a standalone technology for chemical plastic recycling. Batch experiments were conducted to evaluate how the most used synthetic polymers behave when processed using fast heating rate reactors and short residence times. We give a comprehensive overview of the fate of the most common waste polymers at a given condition to allow a fully comparative assessment for future implementation in the circular economy.

2. Materials

A total of 12 different commercial polymers – poly-acrylonitrile-butadiene-styrene (ABS), Bisphenol-A based Epoxy resin, high density polyethylene (HDPE), low density polyethylene (LDPE), non-colored plastic cable ties of polyamide 6 (PA6), Sigma-Aldrich polyamide 6/6 (PA66), polyethylene terephthalate plastic bottles (PET), polycarbonate (PC), polypropylene cups (PP), polystyrene cups (PS) and polyurethane foam (PUR) – were milled using a Polymix® PX-MFC 90D knife mill equipped with a 2 mm sieve before the HTL procedure. Sigma-Aldrich Poly(vinyl chloride) (PVC) was used as acquired (powder).

3. Methods

3.1. HTL procedure

Reactions were performed using custom made Swagelok® bomb-type 20 mL reactors following already described procedures (Biller et al., 2016). Two sets of experiments were conducted in duplicates, one with pure water and one with alkali catalyst (KOH). In each experiment, 0.50 g of polymer was added to the reactor with 8.5 g of water or alkali aqueous solution (17.2 g/L). The feed dry matter concentration of the experiments (5.6 %) is lower than commonly applied in continuous systems (typically 15–20 %) (Castello and Pedersen, 2018). Such dry matter content was chosen to standardize loadings for all polymers tested, as some polymers were difficult to fill into the limited reactor space due to their low density. Reactors were sealed and submerged

into a pre-heated fluidized sand bath for 20 min at 350 °C, which results in a heating time of 4 min (average heating rate of 82 °C min⁻¹). This heating rate approximates the heating profile of a modern continuous HTL plant with integrated heat recovery, where a similar heating rate of 75–100 °C min⁻¹ was applied and a total reaction time of approximately 14 min. (Anastasakis et al., 2018) The reactors were then quenched in a water bath, cleaned and weighted. The gas produced during the HTL reaction was carefully vented and the reactor re-weighted to determine the mass of gas generated. The aqueous phase (AP) was transferred to a 15 mL centrifuge tube and centrifuged for 5 min at 4000 rpm. To recover the oil phase, 30 mL of methanol was used to wash remaining solids both in the reactor and in the AP centrifuge tube. After filtering the methanol, an aliquot of 1 mL was withdrawn for gas chromatography/mass spectrometry (GC/MS) analysis, while the remaining liquid was evaporated overnight at 35 °C in a convection oven to determine the oil weight. Solid residues were dried at 105 °C overnight in a convection oven and AP mass was determined by difference. All yields were based on the mass of polymer initially used.

3.2. Elemental analysis

An Elementar vario Macro Cube elemental analyser (Langensfeld, Germany) was used to determine the CHNS content of all raw materials, solid residues and oil products in duplicate, average values are reported. The combustion chamber was operated at 1150 °C and the reduction tube at 850 °C, with a helium flow of 600 mL min⁻¹.

3.3. ATR-FTIR

A Bruker Alpha Platinum Attenuated Total Reflectance Fourier-transform infrared spectroscopy (ATR FTIR) spectrometer was used to collect 24 spectra from 4000 to 400 cm⁻¹ with resolution of 2 cm⁻¹. The ATR crystal was cleaned using 96 % ethanol and baseline signal was checked between measurements. Solid samples were compressed against the diamond crystal and liquid/grease samples were rubbed on top for measurements.

3.4. GC/MS

Analysis were performed using an Agilent 7890B GC coupled to a quadrupole mass filter MS (Agilent, 5977A). For oil analysis, 1.0 µL of the aliquot retrieved from sample work-up was directly injected (inlet temperature of 280 °C, split ratio 20:1, helium flow 1 mL.min⁻¹) after internal standard addition (4-bromotoluene) on a VF-5 ms column (64.9 m x 0.25 mm x 0.25 µm). The following GC oven temperature program was performed: 60 °C hold for 2 min; ramp to 200 °C (5 °C.min⁻¹); ramp to 320 °C (20 °C.min⁻¹); hold for 5 min. Compounds were identified with authentic standards, NIST17 mass spectra library or based on literature references. Quantification was conducted using an 8-point calibration curve for selected compounds.

For AP analysis, the methyl chloroformate derivatization method was used (see reference (Madsen et al., 2016) for full details). Catalysts and methyl chloroformate were added to the AP to methylate water soluble compounds. Later, chloroform containing internal standard (4-bromotoluene) was used to extract these compounds to an organic phase, which was then analyzed using GC/MS.

4. Results and discussion

Fig. 1a and 1b show the mass balance for all polymers tested. The polymers are divided into (a) polymers which are prone to

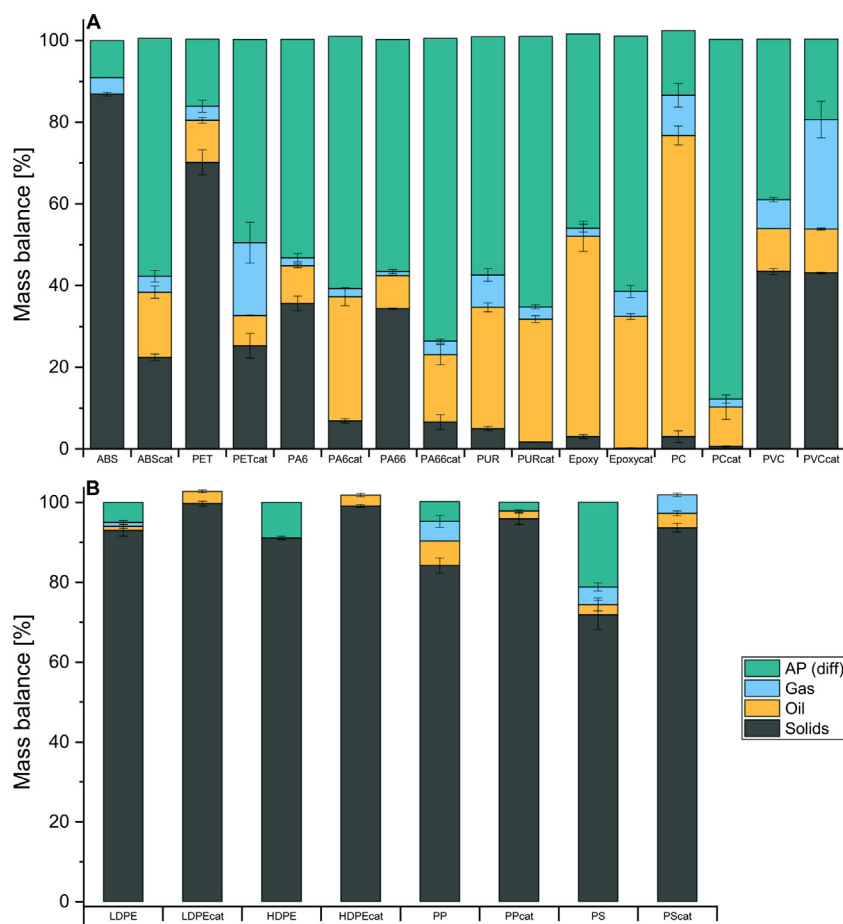


Fig. 1. Mass balances for polymers after HTL (cat = KOH catalyzed HTL). (a) Polymers prone to HTL conversion. (b) Polymers not prone to HTL treatment.

HTL conversion and (b) polymers which are not prone to conversion. For the polymers which do convert (Fig. 1a) the amount of material fractionating to the aqueous phase (AP) constitutes an important fraction of the mass balance for most polymers, particularly when alkali catalyst is present. Higher reaction rates for hydrolysis depolymerization mechanisms have previously been reported for PET in presence of alkali (Wan et al., 2001), which is confirmed in the current study for other polymers, as shown in Fig. 1a by markedly increased polymer conversions for all samples apart from PVC. Alkali reactions are responsible for breaking —O and N— structures into alcohols, carboxylic acids, amines or amides. (Singh and Sharma, 2008) In presence of alkali, hydrolysis reactions yield organic salts as well, which have higher water solubility. (Singh and Sharma, 2008) Hydrolysis reactions depend on a common characteristic of most polymers grouped into Fig. 1a: the presence of heteroatoms in their backbone structures.

The polymers subjected to HTL (see Table S1 for chemical structures) were grouped into the following topics for discussion according to important observations and characteristics during HTL processing:

- I) HDPE, LDPE, PP and PS: where the absence of heteroatoms in polymeric structures prevents HTL depolymerization mechanisms (Fig. 1b);
- II) ABS: a polymeric structure without backbone heteroatoms that shows increased depolymerization in alkali conditions;
- III) Epoxy and PC: comparison of two BPA-based polymers – one thermoset and one thermoplastic – evaluating how cross-linked polymers decompose differently;
- IV) PET: a polymer yielding a large amount of solid products;

- V) PA6 and PA66: where crystalline and amorphous polymer phases play a role on depolymerization mechanisms;
- VI) PUR: a thermosetting polymer containing both N and O heteroatoms;
- VII) PVC: process occurs in heavily acidic HTL conditions due to halogenated raw materials.

4.1. HDPE, LDPE, PP and PS

All of these polyolefins showed >90 % solid residue yields after HTL processing (see Fig. 1b). Additionally, when processing in the presence of alkali, solid residues increase for all four polymers. The main reason is that no heteroatoms or reactive sites are found in these materials, thus thermal cracking is the preferred depolymerization mechanism (Singh and Sharma, 2008). PE has been reported to decompose to oil products under supercritical water (450–480 °C), above its thermal cracking temperature (commonly around 435 °C) (Hai-feng et al., 2007; Su et al., 2004). When compared to pyrolysis, the presence of supercritical water prevents coke formation while increasing oil yield (Moriya and Enomoto, 1999). Subcritical water LDPE HTL, with hot release and condensation of vapours, has been reported once by Wong et al. (2005), showing an organic liquid yield of 28.42 % at 300 °C with residence time of 120 min. (Wong et al., 2016) As the temperature of 350 °C used in our experiments, is lower than the thermal cracking temperature of PEs in general, the reaction rate is too low for the time used in our experiments (20 min), leaving polymeric chains in solid state.

FTIR analysis of solid residues showed that some are partially oxidized (see Fig. 2S A–D). HDPE and LDPE non-catalyzed HTL resulted in oxidized materials containing = O bonds (1712 cm⁻¹).

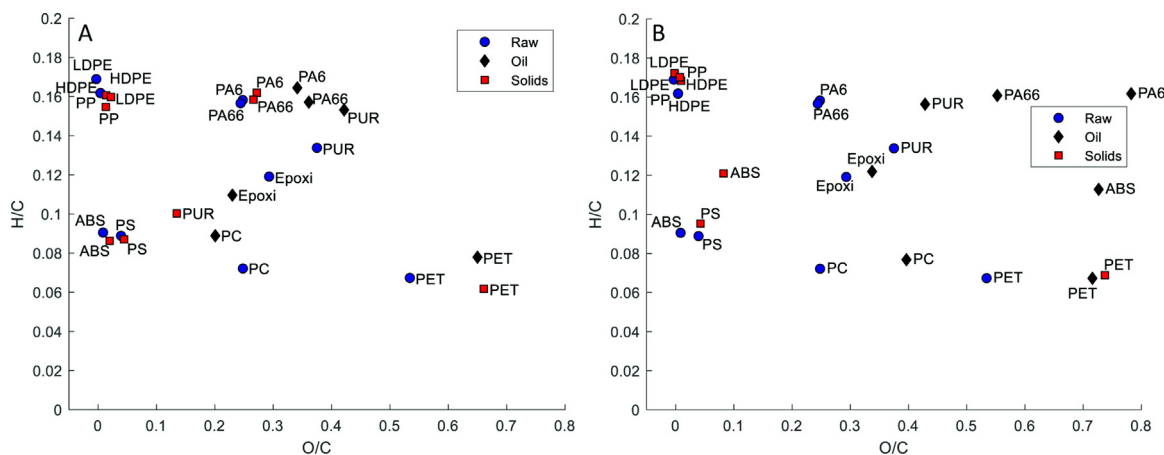


Fig. 2. Van Krevelen diagram of the different phases – without (A) and with catalyst (B).

Catalyzed reactions yielded a non-oxidized HDPE and a different type of oxidized LDPE, containing also C = C–O ($1648\text{--}1626$, 835 cm^{-1}) and CO ($1400\text{ cm}^{-1}\text{--}1256\text{ cm}^{-1}$) groups. PP solid products of non-catalyzed HTL also show C–O (1285 cm^{-1}), CO (1680 , 1714 cm^{-1}) and C = CH (934 , 841 , 732 cm^{-1}) groups, while catalyzed HTL of PP did not change the material according to the FTIR characterization.

HTL of PP has only been reported for long reaction times and low heating rate batch experiments. (Zhao et al., 2018b) For 1 h reaction time at $350\text{ }^{\circ}\text{C}$, 65 % solid residue yield was reported, with oil products containing cyclic alkanes and aliphatic alkenes. Similar products are also present in the small oil fraction recovered in our experiments, although at very low levels (see chromatograms in Fig. S5).

PS did not show any structural changes by HTL using FTIR analysis. A similar polymer to PS, a co-polymer of styrene with butadiene, has been reported to decompose in the presence of water at $350\text{ }^{\circ}\text{C}$ with depolymerization as high as 61 % for a reaction time of 60 min. (Park et al., 2001) Near supercritical HTL ($370\text{ }^{\circ}\text{C}$) was also reported to decompose PS into valuable chemicals in short residence times (Kwak et al., 2005), however, supercritical PS HTL (Kwak et al., 2005; Park et al., 2001) was recently found to have the most efficient condition at $490\text{ }^{\circ}\text{C}$ with carbon liquefaction efficiency as high as 80 %. (Bai et al., 2019) In the present study, the aromatic-containing polymer PS has shown to be stable under subcritical conditions.

The minor changes of H/C and O/C ratios change during HTL, presented in Fig. 2, indicate that HDPE, LDPE, PP and PS experience no measurable change in their chemical structures. The absence of heteroatoms in the polymer backbone structure prevents all depolymerization mechanisms that involve reactive water in the investigated HTL conditions. Hence it can be concluded that the inclusion of these polyolefin wastes should be avoided in HTL feedstocks for biocrude production in any future mixed waste application at subcritical conditions and supercritical conditions are favorable. A pyrolysis approach where higher temperatures, above the thermal cracking temperature, is employed or supercritical liquefaction are required conditions for the chemical recycling of these materials.

4.2. ABS

Even though the chemical structure of this polymer does not contain backbone heteroatoms to favor hydrolysis depolymerization reactions, ABS shows a positive effect on decreasing solid residues with alkali catalysis (Fig. 1a). This result is a consequence of the other reactive sites present in ABS, nitrile side group and

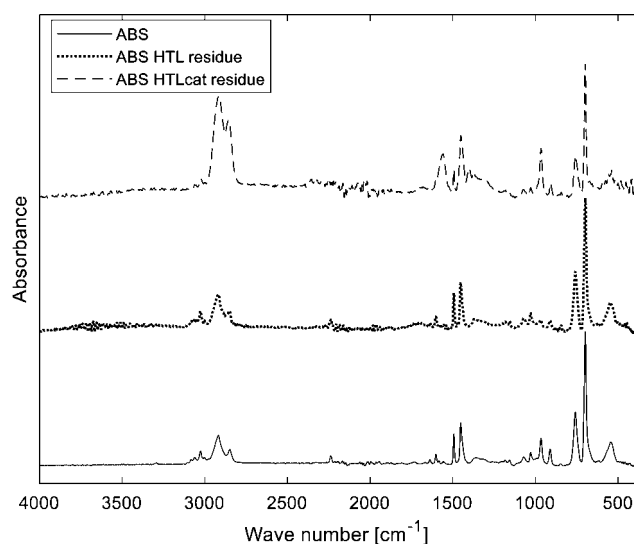


Fig. 3. FTIR of ABS solid residues in comparison to raw material.

the backbone double bond, becoming prone to depolymerization in alkali media.

The GC/MS analysis shows (Fig. S4 and S5) that aromatic $\equiv\text{N}$ molecules are present in non-catalyzed AP products, however, when alkali catalyst is present, only $-\text{NH}_2$ and $-\text{NH}-$ groups are detected. This indicates that alkali conditions stimulate depolymerization reactions by forcing nitrile hydrolysis. Principally, nitrile groups hydrolyze in presence of hot compressed water (Izzo et al., 1999) generating NH_3 and carboxylic acids with an amide intermediate ($-\text{CONH}_2$). (Izzo et al., 1997) Potassium hydroxide has been reported to catalyze this reaction at low temperatures (Sanli, 1990) ($20\text{--}80\text{ }^{\circ}\text{C}$). The same effect is observed here, by generating ammonia under HTL conditions, the depolymerization rate of the materials is increased.

Besides the ammonia generation path, as double bonds are present in butadiene units, direct addition of the amide intermediate (Sanli, 1990) to the alkene section (Mu et al., 2008) of butadiene units are possible. According to the FTIR data in Fig. 3, HTL without catalyst only changes the polymeric structure regarding the $-\text{C}=\text{C}-$ bonds, which is evident due to the disappearance of sharp peaks at 967 , 910 and 1638 cm^{-1} , meaning that such double bonds are either hydrogenated or substituted by rearrangement. On the other hand, the spectra found for the solid residue of catalyzed HTL suggests a rearranged structure containing more aliphatic sections and a $-\text{CNC}$ bond (1158 cm^{-1}), a derivative of amide addi-

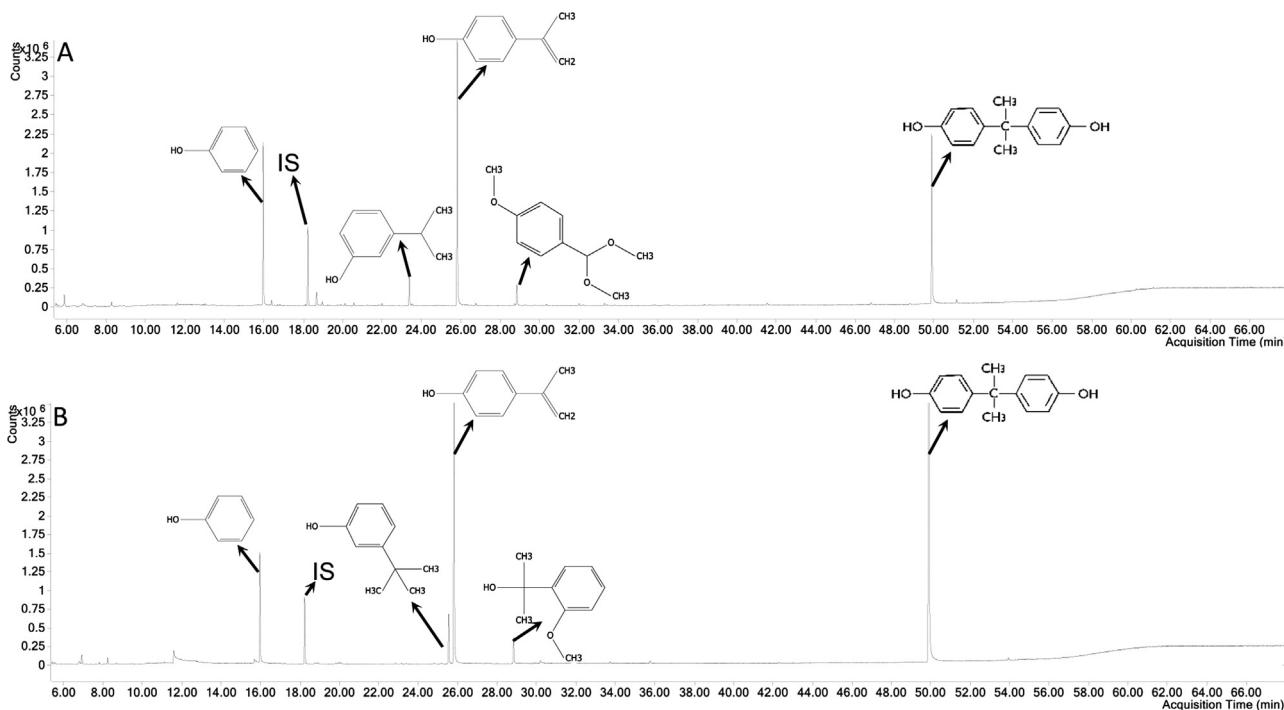


Fig. 4. Epoxy (A) and PC (B) oil products GC/MS. (IS = internal standard).

tion to butadiene units. Despite the evidence for a $-\text{CNC}=\text{C}-$ bond, the elemental analysis depicted in Table S3 shows that the solid residue only contains 0.31 % of N, a much lower value compared to the original content of 5.13 %.

Hence, KOH catalyzes nitrile hydrolysis, which generates reactive ammonia that interacts easily with butadiene and styrene units for depolymerization, generating oxygenated compounds that are more soluble in water. For the case of ABS, hydrolysis is not the main pathway for depolymerization, but the chain reaction started by a side group ($-\text{CN}\equiv$). The products generated by these reactions are hydrophilic – probably composed of oligomers due to the absence of small structures by GC/MS analysis – and only small amount of oil being generated.

4.3. Epoxy and PC

The two polymers have related chemical structures as epoxy is a thermoset composed of bis-phenol-A diglycidyl ester (BPA-DGE) and butandioldiglycidylether (BODGE) cross-linked by poly(oxypropylen)diamine and aminoethyl-3,5,5-trimethylcyclohexylamine, while PC is a thermoplastic of BPA. As both structures contain backbone oxygen heteroatoms, hydrolysis is the preferred depolymerization path. It is important to remark that one of the crosslinking reagents of Epoxy has significant nitrogen content (see Table S1 and S2), which reacts into NH_3 at HTL conditions, catalyzing depolymerization reactions.

Alkali effect on both reactions is qualitatively similar (Fig. 1a), as it increases the water-soluble products in different degrees. AP yield for PC increases from 15.9 % (no-cat) to 88.2 % (cat), while from 47.6 % (no-cat) to 62.5 % (cat) for Epoxy. The products obtained in both non-catalytic processes are typically alcohols, which can further react in presence of KOH into carboxylic acids or smaller alcohols, having higher water solubility.

The nitrogen content in Epoxy can explain the higher water-soluble products yield for the material in comparison to PC under non-catalytic HTL, as both oil-yielded reaction products are very similar (Fig. 4). Also in Fig. 4, it is possible to observe that even

though Epoxy is a heavily cross-linked polymer, it yielded very similar compounds as its thermoplastic counter-part (PC). Aqueous phase GC/MS analysis shows that phenol is present in both catalytic and non-catalytic HTL reactions. However, the phenol yield is more prominent when KOH is present (see Section 5 for further discussion).

For both Epoxy and PC, very low amounts of solids were obtained, showing that despite high levels of crosslinking in Epoxy, HTL conditions promoted severe depolymerization reactions as in PC. This fact corroborates that chemical structure (i.e. backbone heteroatoms) is more important than crosslinking for HTL treatment.

4.4. PET

This condensation polymer differs greatly in behavior to others, as one of its monomers – terephthalic acid (TA) – is an insoluble solid in both water and alcohols. Fig. 5 presents the FTIR spectra that shows clearly a high-purity TA as result of HTL procedure given the FTIR reference match. In this case, Fig. 1 shows an increase of AP for catalytic HTL, which demonstrates that alkali catalysis converts TA into its salts, increasing its solubility in water. Besides, the higher gas yield for catalytic HTL shows that decarboxylation reactions are favored, generating more CO_2 at the studied temperatures. This can be observed by the higher gas amount for catalytic HTL of PET in Fig. 1a and the GCMS findings in Fig. S6 and Fig. S7, which show direct decarboxylation products of TA.

Again, the presence of oxygen as heteroatoms contributes greatly to depolymerization reactions – mainly hydrolysis in this case. (Wan et al., 2001) PET depolymerization reactions have been studied before at lower temperatures (120–160 °C) than reported here, though also in presence of KOH. (Wan et al., 2001) Higher temperatures (190–307 °C) were also tested in a different study by Zenda and Funazukuri (2008) (Zenda and Funazukuri, 2008) in presence of other alkaline catalysts (ammonia and NaOH) yielding similar results. Both cases achieve very high terephthalic acid yields, as also shown in this study. Fig. 1a shows that PET HTL in

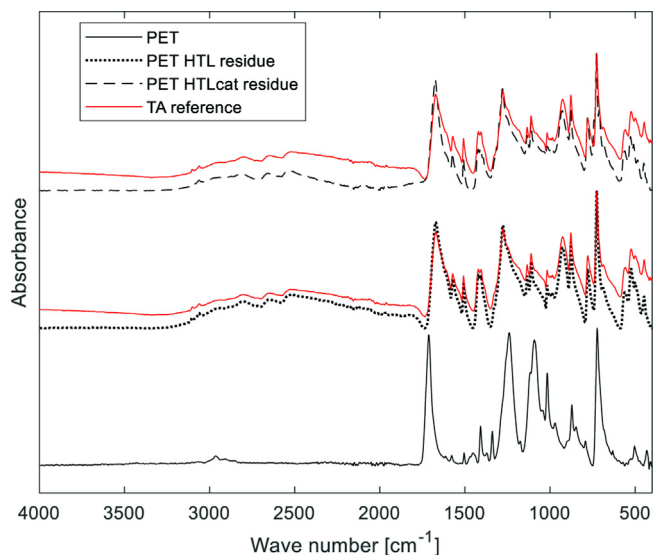


Fig. 5. FTIR of PET solid residues in comparison to raw material including TA reference.

presence of KOH exhibits a significantly higher gas yield, indicating catalytic decarboxylation of TA occurs at the temperature tested. For the case of catalytic PET HTL, the oil and water yields contain benzoic acid, a direct product of TA decarboxylation.

The presence of a valuable solid product raises an issue on PET HTL processing: how to deal with the solid streams in an application context. For the case of pure PET HTL, direct use of the solid stream is an advantage, however, if PET co-processing through HTL is desired, such valuable solid will be mixed with different byproducts. In this case, extraction and purification of the solid stream has to be considered as an essential step.

4.5. PA6 and PA66

Fig. 1a depicts a similar mass balance for PA6 and PA66 with slightly lower oil yield for catalyzed HTL of PA66 in comparison to catalyzed HTL of PA6, in both cases the addition of alkali approximately doubled the oil yield. For both PA6 and PA66, monomers, dimers and some variations of these compounds are the products identified in GC/MS analysis of the AP (see Fig. S8 and S9). Similar results were previously reported for non-catalyzed HTL (Iwaya et al., 2006), but surprisingly little effect on product distribution could be observed when KOH was present as catalyst despite the increase in oil yield.

The O/C ratio of PA6 oil products of catalytic HTL was higher than of the corresponding PA66 sample. Both were significantly different from the non-catalytic HTL products (see Fig. 2). The oxygen migration to the oil phase in PA6 when comparing non- and catalytic HTL is probably caused by a higher hydrolysis rate, which decomposes caprolactam (the main monomer) into further hydrolyzed products, which contain more oxygen.

Analysis of the FTIR spectra in Fig. 6 confirms that the amorphous phase of PA6 and PA66 (1145 cm^{-1}) (McKeen and McKeen, 2012) are depolymerized under non-catalytic HTL. For PA6, when alkali was used for HTL, the spectra show a significant difference between peaks at 665 cm^{-1} and 580 cm^{-1} , showing that α phase is the dominant type of PA present. i.e., γ phase was more prone for depolymerization, which is expected as α phases are the most stable for this type of polymer. (McKeen and McKeen, 2012) Here, the alkali again promotes higher rates of hydrolysis, however the crystalline structure dictates the depolymerization path.

4.6. PUR

Fig. 1a and Fig. 2 show that PUR does not exhibit major differences in mass balance nor in H/C and O/C ratios for catalytic HTL compared to non-catalytic HTL. The catalyst does have an effect of increasing quantified compounds, an observation which is discussed later. The lack of catalytic effect on H/C, O/C ratios for this polymer suggests that the amount of N present was already enough to generate sufficient *in situ* NH_3 , promoting hydrolysis by itself. This indicates that PUR is prone to catalyze degradation of other polymers under co-liquefaction, which opens up opportunities for positive synergistic processes for polymer or biomass combinations. PUR hydrolysis has been reported to yield mainly diamino toluene using long retention times and slow heating rate reactors. (Dai et al., 2002) Our study shows that for fast heating rate and short residence times, oligomers are the main products, with a clear phase separation. Fig. S10 presents the FTIR spectra of PUR oil, highlighting that secondary amines ($3400\text{--}3200\text{ cm}^{-1}$), NCO (1734 cm^{-1}) and CN (1222 cm^{-1}) characteristic bands are not present in both catalytic and non-catalytic HTL oil product. It also highlights that the C–OC band at 1089 cm^{-1} is present in all samples, indicating that the oil products also have ether groups, which corroborates that oligomers are the main components in this product stream.

Fig. S11 shows that N–H (3300 cm^{-1}) bonds are not present in the solid residues of non-catalyzed HTL, however aromatics are much more prominent (indicated by 700 , 757 , 1452 and 1495 cm^{-1}), which suggests that rearrangement of the polymer happened to yield a more stable structure. Even though aromatics are evident in these solid residues, they are present together with O heteroatoms (1089 cm^{-1}).

The AP yield increased from non-catalytic to catalytic HTL due to the reduction in gas yield, which indicates less decarboxylation and thus, more carbon retention in liquid products. The composition of this stream did not change significantly, as can be seen from the chromatogram in Fig. S12. The products identified in this phase are aromatics and polyaromatics containing O and N heteroatoms, however low match factors from the library search prevents reliable identification, due to characteristic branched compounds being identified.

4.7. PVC

The only halogenated polymer exhibited pronounced charring reactions rather than liquefaction reactions due to the acidic conditions. Addition of alkali resulted in no considerable differences in oil and solid yields (Fig. 1a), however, a major difference was measured on gas and AP yields. The higher gas yield in alkali conditions indicates that a greater portion of chlorine present was converted into Cl_2 , reducing the mass transfer to the AP. Despite this, the solid residues from catalyzed HTL have a lower carbon content (Table S1) compared to those from non-catalytic HTL, indicating that the catalyst lower the polymer–solid residue dechlorination effect.

HTL processing of PVC showed that it is capable of recovering a solid residue with much lower chlorine content, which could be an approach for solving incineration issues related to such contaminants. However, PVC should be avoided in HTL co-processing as acidification is undesired and unavoidably results in carbonization reactions.

5. Analysis of depolymerization products in oil phase

Fig. 7 shows the quantified compounds present in oil products for PC, Epoxy, PUR and PA66 HTL with and without catalyst. Of these, PC is the polymer with highest oil yield, which is com-

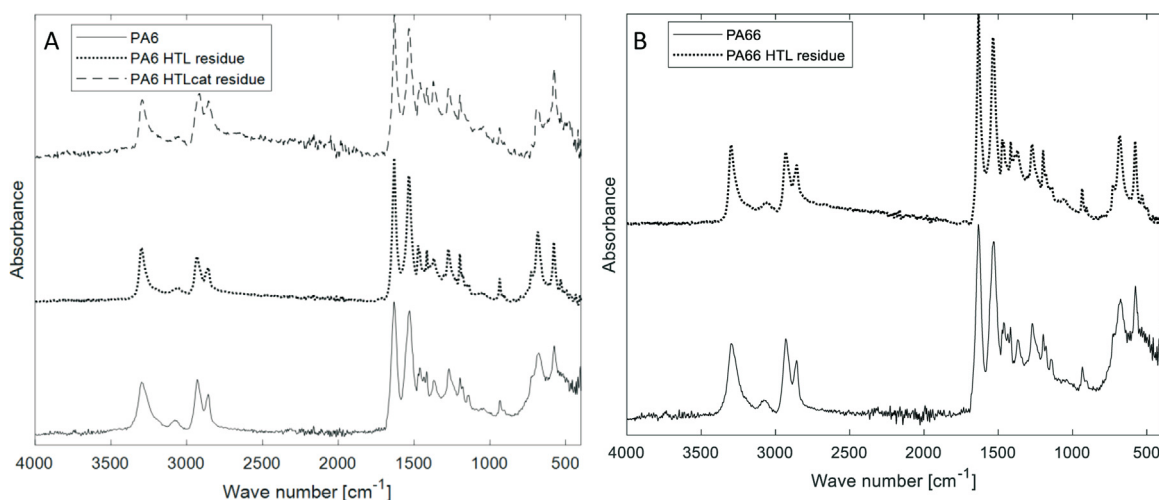


Fig. 6. FTIR PA6 (A) and PA66 (B) – Original polymer and solid residues of HTL with and without catalyst (KOH).

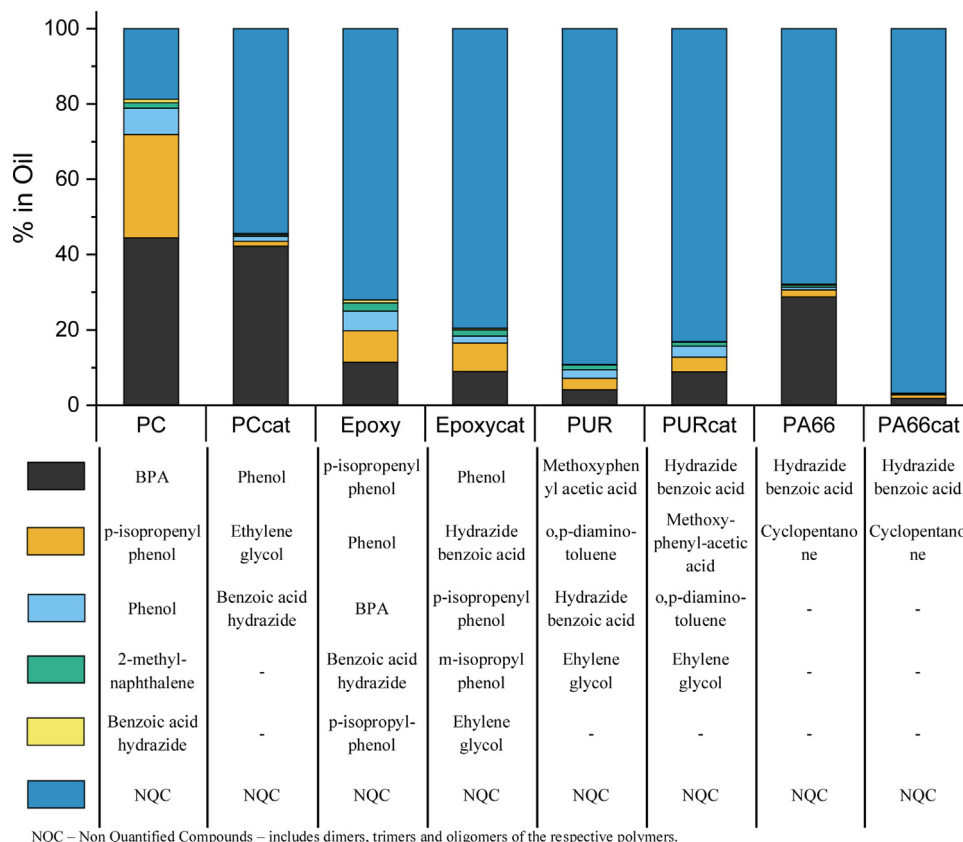


Fig. 7. Oil phase mass composition by quantitative GC/MS analysis.

posed of relatively few compounds, in particular its monomer, BPA, contributing 44.5 wt.% of the total oil yield. This means the total chemical recycling efficiency of PC to BPA is 32.8 wt.%, to p-isopropenyl phenol is 20.2 % and to phenol is 5.2 %. Part of the Epoxy oil yield is also composed of the same products as PC, however in lower concentrations, yielding a total chemical recycling efficiency of 5.6 % to p-isopropenyl phenol, 4.1 % to phenol and 2.6 % to BPA. Epoxy is a crosslinked thermoset and thus has a branched structure which leads to more complex depolymerization mechanisms and, by extension, more complex products. The presence of ether-like sections, generated by epoxy bonds in the original structure (see Table S1) leaves BPA attached to

branched alcohols, which contributes to the non quantified compounds (NQC).

PUR has been reported to hydrolyze in hot and compressed water (Brunner, 2014), however at the conditions tested, it seems that only partial decomposition is achieved. As shown in Fig. 7, the PUR oil only exhibits a minor amount of small organic compounds, suggesting that the NQC in this case are oligomers of the original structure. Full conversion of PUR can only generate water soluble compounds (Brunner, 2014), which would make it difficult for recovery of valuable compounds. Alkaline catalysis increases the concentration of identified oil products, which indicates that smaller compounds are produced. Thus, the HTL procedure sug-

gested here could be an option for high carbon recovery of waste PUR with the advantage of having a phase-separated product that can be further purified into an oil product or even individual chemicals.

Fig. 7 also shows that hydrazide benzoic acid is the main quantified oil product from PA66. When catalyzed with alkali, the products of PA66 HTL have higher concentrations of oxygen (Table S2 and S3) and lower of carbon, representing a more hydrolyzed product with lower value.

Besides the oil phases, AP products of polymer HTL are significant often making up over 50 % of the total mass yield. Their low concentrations represent an issue for recovery or valorization of chemicals and energy recovery via e.g. hydrothermal gasification is a more likely route (Elliott, 2011). Out of the polymers tested, the most favorable AP products are the ones resulting from PA6, PA66, Epoxy and PC HTL if chemical recovery from non mixed wastes is the objective. In the two former cases, the AP is reported (Iwaya et al., 2006) to be composed mostly by ϵ -caprolactam (approx. 80 % is converted of the original polymer), which could potentially be re-polymerized into new bulk polymers. For the two latter, phenol is the most abundant product in the alkali-catalyzed HTL of AP, constituting 5.3; 7.6; 29.9 and 11.0 % of the mass present for AP of Epoxy, Epoxycat, PC and PCcat, respectively.

For PET HTL, the solids recovered were the main product. They are composed of high purity TA, which is the monomer of PET. The decarboxylation observed when PET was processed with catalyst also yields useful platform chemicals that could be further processed in a HTL context where only PET is used as the feedstock. However we consider that this would be a downgrading of such a valuable monomer, as if PET is processed in its pure form (non-catalysed), the solid TA is recovered immediately. If co-processing is desired to eliminate the need of pure streams for HTL, a solid product represents a challenge for further separation.

The co-processing of different synthetic polymers in HTL for platform chemical recovery can offer advantages and disadvantages. In one hand, co-processing of selected polymers can offer synergies on specific recoveries, e.g. PC and Epoxy may be co-processed and the final oil phase will contain most of the BPA recovered for both, meanwhile the AP will comprise phenolics. On the other hand, the generation of certain products can interfere in the recovery of others, e.g. ethylene glycol generated in PET AP products can increase the solubility of organic compounds in other polymer's oil phase, which would increase separation costs. As valuable compounds are shown here, simple separation processes may be considered (liquid-liquid extraction, evaporation or distillation), however with the increase of mixture complexity in co-processing scenarios, increased cost may overcome such approaches' feasibility.

The processing of synthetic polymer waste in high thermal efficiency HTL reactors (Anastasakis et al., 2018) thus yields some ready-to-use platform chemicals which could be recovered if pure polymer streams are used, which can represent an advantage in comparison to other recycling strategies, such as mechanical recycling, as this approach is not limited by a number of recycling cycles. Overall, the results however also show that generally the composition of products is complex and would become even more if unsorted streams of synthetic wastes are used or mixed with biomass wastes. In this context it can be concluded that some of the polymers are beneficial in such approaches, as polyamides, PUR, epoxy and PC, yielding additional oil products, while others are uncertain, as ABS and PVC and their co-processing deserves additional attention. The polyolefins in general should be avoided, adding solid residue to the product mixture and little conversion at the subcritical conditions investigated here.

6. Conclusion

Subcritical HTL processing of synthetic polymers is a promising approach for certain types of polymers chemical recycling. Products identified and quantified for the case of suitable feedstock are valuable chemicals, thus this approach may contribute for a circular economy of the sector. The HTL process is intrinsically dependent on reactive sites for hydrolysis in the original chemical structures of the polymers and does not occur in absence of those. This creates a challenge for subcritical processing of polyolefins and polystyrene. On the other hand, for materials that present such reactive sites, a major part of the mass processed result in the AP, which creates difficulties in down-stream valorization. The alkali environment provided by the catalyst used in this study showed to favor a greater hydrolysis rate, generally decreasing solid residues and increasing AP yields.

For all other polymers evaluated in this study, particular process characteristics can be highlighted as follows:

ABS: alkali significantly increases depolymerization rates, however products are concentrated in the AP. The oil product generated is composed of oligomers of the original structure and requires purification and upgrading to recover platform chemicals;

Epoxy and PC: BPA and derived compounds are present in the oil products of HTL. Especially for PC, in which 80 % of the oil products from HTL without catalyst are readily available as off-the-shelf platform chemicals. For Epoxy, despite also having high-value chemicals present, its oil phase is more complex. This is due to its characteristic branched thermosetting chemical structure, which yields also branched products. In both cases, alkali increases hydrolysis rates yielding more AP products, mainly phenols.

PET: Solid TA is the main product of non-catalytic HTL. The AP is rich in identifiable chemicals and is increased in concentration by addition of KOH during HTL processing. The catalyst also favors decarboxylation of TA, resulting in by products in both solid and AP.

PA6 and PA66: Yields AP monomers that could be used for repolymerization if pure streams are processed. The concentration of such monomers is still of high importance for process feasibility and higher concentrations are desirable. The crystalline phases of these polymers decompose differently and KOH is capable of promoting total depolymerization in short residence times.

PUR: Yields a complex oil, composed of oligomers and a minor part of low boiling point compounds. KOH catalysis tends to increase the small compounds concentration, indicating more hydrolysis of the reactive sites. The small compounds identified and relatively high oil yield, show that PUR is a suitable feedstock for HTL processing.

PVC: HTL processing in the presence of alkali yields increased gas products due to Cl_2 release. PVC solid residues are highly dechlorinated, which indicates that this fraction can be further used as carbon source. The dechlorination of carbon in this case is especially valuable as HCl is the main product and is present solely in the AP.

Overall, each type of synthetic polymer presents its own depolymerization characteristics under HTL, which brings opportunities and challenges for future applications in pure and mixed streams. Low residence time subcritical HTL is not able to cope with polyolefins and PS, however it represents a very interesting approach on chemical recycling of heteroatom-containing synthetic polymers.

Declaration of Competing Interest

The authors declare that they have no known competing financial interests or personal relationships that could have appeared to influence the work reported in this paper.

Acknowledgments

This research was funded by the European Union's Horizon 2020 research and innovation program under grant agreement No. 764734 (HyFlexFuel—Hydrothermal liquefaction: Enhanced performance and feedstock flexibility for efficient biofuel production) and The Centre for Circular Bioeconomy (CBIO) of Aarhus University.

Appendix A. Supplementary data

Supplementary material related to this article can be found, in the online version, at doi:<https://doi.org/10.1016/j.psep.2020.04.040>.

References

- Anastasakis, K., Biller, P., Madsen, R.B., Glasius, M., Johannsen, I., 2018. Continuous hydrothermal liquefaction of biomass in a novel pilot plant with heat recovery and hydraulic oscillation. *Energies* 11, 1–23, <http://dx.doi.org/10.3390/en11102695>.
- Arai, R., Zenda, K., Hatakeyama, K., Yui, K., Funazukuri, T., 2010. Reaction kinetics of hydrothermal depolymerization of poly (ethylene naphthalate), poly (ethylene terephthalate), and polycarbonate with aqueous ammonia solution. *Chem. Eng. Sci.* 65, 36–41, <http://dx.doi.org/10.1016/j.ces.2009.03.023>.
- Bai, B., Jin, H., Fan, C., Cao, C., Wei, W., Cao, W., 2019. Experimental investigation on liquefaction of plastic waste to oil in supercritical water. *Waste Manag.*, <http://dx.doi.org/10.1016/j.wasman.2019.04.017>.
- Biller, P., Madsen, R.B., Klemmer, M., Becker, J., Iversen, B.B., Glasius, M., 2016. Effect of hydrothermal liquefaction aqueous phase recycling on bio-crude yields and composition. *Bioresour. Technol.* 220, 190–199, <http://dx.doi.org/10.1016/j.biortech.2016.08.053>.
- Biller, P., Johannsen, I., dos Passos, J.S., Ottosen, L.D.M., 2018. Primary sewage sludge filtration using biomass filter aids and subsequent hydrothermal co-liquefaction. *Water Res.* 130, 58–68, <http://dx.doi.org/10.1016/j.watres.2017.11.048>.
- Brunner, G., 2014. In: Elsevier, B.V. (Ed.), *Hydrothermal and Supercritical Water Processes*, v 5. ed, Hamburg, Germany.
- Castello, D., Pedersen, T.H., 2018. Continuous Hydrothermal Liquefaction of Biomass: A Critical Review., <http://dx.doi.org/10.3390/en11113165>.
- Castello, D., Haider, M.S., Rosendahl, L.A., 2019. Catalytic upgrading of hydrothermal liquefaction biocrudes: different challenges for different feedstocks. *Renew. Energy* 141, 420–430, <http://dx.doi.org/10.1016/j.renene.2019.04.003>.
- Cooperation, R.L., Birmingham, Alabama 1982. *An Investifation of Liquefaction of Wood*.
- Dai, Z., Hatano, B., Kadokawa, J.I., Tagaya, H., 2002. Effect of diaminitoluene on the decomposition of polyurethane foam waste in superheated water. *Polym. Degrad. Stab.* 76, 179–184, [http://dx.doi.org/10.1016/S0141-3910\(02\)00010-1](http://dx.doi.org/10.1016/S0141-3910(02)00010-1).
- Elliott, D.C., 2011. Hydrothermal processing. In: Brown, R.C. (Ed.), *Thermochemical Processing of Biomass: Conversion into Fuels, Chemicals and Power*. John Wiley & Sons Ltd, pp. 200–231, http://dx.doi.org/10.1002/9781119990840_ch7.
- Foudriaan, F., Peferoen, D.G.R., 1990. Liquid fuels from biomass via a hydrothermal process. *Chem. Eng. Sci.* 45, 2729–2734.
- Ghosh, S.K., Agamuthu, P., 2018. Circular Economy: the Way Forward., <http://dx.doi.org/10.1177/0734242X18778444>.
- Hai-feng, Z., Xiao-li, S.U., Dong-kai, S.U.N., Rong, Z., Ji-cheng, B.I., 2007. *Investigation on Degradation of Polyethylene to Oil in a Continuous Supercritical Water Reactor.*, pp. 35.
- Iwaya, T., Sasaki, M., Goto, M., 2006. Kinetic Analysis for Hydrothermal Depolymerization of Nylon, 6., pp. 1989–1995, <http://dx.doi.org/10.1016/j.polymdegradstab.2006.02.009>, 91.
- Izzo, B., Harrell, C.L., Klein, M.T., 1997. *Nitrile reaction in high-temperature water : kinetics and mechanism.* *AIChE J.* 43, 2048–2058.
- Izzo, B., Klein, M.T., LaMarca, C., Scrivner, N.C., 1999. Hydrothermal reaction of saturated and unsaturated nitriles: reactivity and reaction pathway analysis. *Ind. Eng. Chem. Res.* 38, 1183–1191, <http://dx.doi.org/10.1021/ie9803218>.
- Korhonen, J., Honkasalo, A., Seppälä, J., 2018. Circular economy: The concept and its Limitations. *Ecol. Econ.* 143, 37–46, <http://dx.doi.org/10.1016/j.ecolecon.2017.06.041>.
- Kwak, H., Shin, H., Bae, S., Kumazawa, H., 2005. Characteristics and Kinetics of Degradation of Polystyrene in Supercritical Water., pp. 1–6, <http://dx.doi.org/10.1002/app.23896>.
- Madsen, R.B., Jensen, M.M., Mørup, A.J., Houlberg, K., Christensen, P.S., Klemmer, M., Becker, J., Iversen, B.B., Glasius, M., 2016. Using design of experiments to optimize derivatization with methyl chloroformate for quantitative analysis of the aqueous phase from hydrothermal liquefaction of biomass. *Anal. Bioanal. Chem.* 408, 2171–2183, <http://dx.doi.org/10.1007/s00216-016-9321-6>.
- McKeen, L.W., McKeen, L.W., 2012. Polyamides (Nylons). *Film Prop. Plast. Elastomers.*, pp. 157–188, <http://dx.doi.org/10.1016/B978-1-4557-2551-9.00008-6>.
- Moriya, T., Enomoto, H., 1999. Characteristics of polyethylene cracking in supercritical water compared to thermal cracking. *Polym. Degrad. Stab.* 65, 373–386, [http://dx.doi.org/10.1016/S0141-3910\(99\)00026-9](http://dx.doi.org/10.1016/S0141-3910(99)00026-9).
- Mu, T.E., Hultzsich, K.C., Yus, M., Foubelo, F., Tada, M., 2008. *Hydroamination: Direct Addition of Amines to Alkenes and Alkynes.*, pp. 3795–3892.
- Park, Y., Hool, J.N., Curtis, C.W., Roberts, C.B., 2001. Depolymerization of Styrene - Butadiene Copolymer in Near-critical and Supercritical Water., pp. 756–767, <http://dx.doi.org/10.1021/ie0005021>.
- Pedersen, T.H., Conti, F., 2017. Improving the circular economy via hydrothermal processing of high- density waste plastics plastic waste value added. *Waste Manag.* 68, 24–31, <http://dx.doi.org/10.1016/j.wasman.2017.06.002>.
- Sanli, O., 1990. Homogeneous hydrolysis of polyacrylonitrile by potassium hydroxide. *Eur. Polym. J.* 26, 9–13.
- Singh, B., Sharma, N., 2008. Mechanistic implications of plastic degradation. *Polym. Degrad. Stab.* 93, <http://dx.doi.org/10.1016/j.polymdegradstab.2007.11.008>.
- Skaggs, R.L., Coleman, A.M., Seiple, T.E., Milbrandt, A.R., 2018. Waste-to-Energy bio-fuel production potential for selected feedstocks in the conterminous United States. *Renewable Sustainable Energy Rev.* 82, 2640–2651, <http://dx.doi.org/10.1016/j.rser.2017.09.107>.
- Su, X., Zhao, Y., Zhang, R., Bi, J., 2004. Investigation on Degradation of Polyethylene to Oils in Supercritical Water, 85., pp. 1249–1258, <http://dx.doi.org/10.1016/j.fuproc.2003.11.044>.
- Wan, B., Kao, C., Cheng, W., 2001. Kinetics of depolymerization of poly (ethylene terephthalate) in a potassium hydroxide solution. *Ind. Eng. Chem.* 40, 509–514, <http://dx.doi.org/10.1021/ie0005304>.
- Wong, S.L., Ngadi, N., Amin, N.A.S., Abdullah, T.A.T., Inuwa, I.M., Ngadi, N., Amin, N.A.S., Abdullah, T.A.T., Inuwa, I.M., 2016. Pyrolysis of Low Density Polyethylene Waste in Subcritical Water Optimized by Response Surface Methodology, 3330., <http://dx.doi.org/10.1080/09593330.2015.1068376>.
- Yildirim, E., Onwudili, J.A., Williams, P.T., 2015. Chemical recycling of printed circuit board waste by depolymerization in sub- and supercritical solvents. *Waste Biomass Valorization* 6, 959–965, <http://dx.doi.org/10.1007/s12649-015-9426-8>.
- Zenda, K., Funazukuri, T., 2008. DepolymerizaTion of Poly (Ethylene Terephthalate) in Dilute Aqueous Ammonia Solution Under Hydrothermal, 1386., pp. 1381–1386, <http://dx.doi.org/10.1002/jctb>.
- Zhao, X., Xia, Y., Zhan, L., Xie, B., Gao, B., Wang, J., 2018a. Hydrothermal treatment of E-Waste plastics for tertiary recycling: product slate and decomposition mechanisms. *ACS Sustain. Chem. Eng.* 7, 1464–1473, <http://dx.doi.org/10.1021/acscchemeng.8b05147>.
- Zhao, X., Zhan, L., Xie, B., Gao, B., 2018b. Products derived from waste plastics (PC, HIPS, ABS, PP and PA6) via hydrothermal treatment: Characterization and potential applications. *Chemosphere* 207, 742–752, <http://dx.doi.org/10.1016/j.chemosphere.2018.05.156>.

Chapter 3

Manuscript 1 - Hydrothermal liquefaction of polyolefins and polystyrene for chemical recycling: steam explosion as a pre-treatment step and the effects of combined supercritical processing.

Juliano Souza dos Passos^{a,b}, Monika Nowak^a, Patrick Biller^{a,b}

^a Department of Biological and Chemical Engineering, Aarhus University, Høngøvej 2, DK-8200 Aarhus N, Denmark

^b Aarhus University Centre for Circular Bioeconomy, DK-8830 Tjele, Denmark

Article history:

Manuscript draft to be submitted

Keywords:

Hydrothermal liquefaction

Chemical recycling

Circular economy

Polyolefins

3.1. Reflections

As identified in Chapter 2, addition polymers such as polyolefins, ABS and polystyrene are exceptionally difficult to depolymerize under subcritical water conditions due to their lack of reactive sites in the form of oxygen heteroatoms. Despite that, it is possible to find authors that claim this process as technically feasible.^{30,36,37} In particular, Sugano et al.³⁷ brings attention to a potential route for easing the depolymerization of polyolefins and polystyrene via a mechanical pre-treatment. The results describe that steam explosion pre-treatment decreases the molecular weight average of these materials, which has potential effect on triggering depolymerization under low temperature (down to 300 °C). Despite the promising approach, no literature was found evaluating further the strategy.

The technique would be of high interest for a co-processing approach of biomasses and polymers. The main assumption would be that lignocellulosic biomass can ease steam explosion processing of plastics by avoiding cluster formation, and the final product could be co-processed in HTL. That could increase the biocrude quality of lignocellulosics, given the products from polyolefins and polystyrene are carbon rich and oxygen poor, with elevated HHV.

The following chapter briefly describes our attempts to implement the approach described by Sugano et al.³⁷ and the results we gathered. It is also described how supercritical water seems to be needed for the decomposition of such materials, highlighting the depolymerization mechanism is still temperature dependent even after the suggested pretreatment step.

Abstract

The amount of plastic waste generated has been constantly increasing over past decades. The majority of this material is comprised of polyolefins and polystyrene. Currently, part of it accumulates in the natural environment leading to the pollution of the oceans, soil and air. Recently, hydrothermal liquefaction (HTL) is drawing attention as a strategy to take advantage of large quantities of waste synthetic material. The aim of this study is to investigate HTL of polyolefins – namely polypropylene (PP), polyethylene (PE) – and polystyrene (PS) using subcritical and supercritical water. The effects of a steam explosion pre-treatment for sub-critical HTL were evaluated. Steam explosion at 180 – 200 °C and 10 – 16 bar did not show any effect, leading to no conversion under subcritical HTL of all polymers tested. Supercritical conditions (420 °C) were needed for effective depolymerization and Polystyrene was found to be the easiest to be converted into synthetic oil among the polymers tested. PS resulted in an oil yield of 70.9% with HHV of 41 MJ.kg⁻¹. Also under supercritical HTL, mixing PS with PE and PP was shown to result in antagonistic effects regarding the oil yield, greatly affecting the final oil composition. In general, examined polymers are very challenging to decompose and supercritical conditions are required.

3.2. Materials and methods

Polystyrene (PS) was gathered as general shopping items such as plastic cutlery and cups. Polyethylene and polypropylene used are commercial pellets for extrusion (all BASF). All materials were milled in a Polymix® PX-MFC 90D knife mill with 2 mm sieve. The now powder polymers were steam exploded using an apparatus with boiler (steam max pressure and temperature of 20 bar, 220 °C), a 630 mL reactor and a fast pressure release valve. The procedure was carried out as a gas-gas steam explosion and started by loading the reactor with around 50 g of polymer per batch and then pressurizing with steam and heating at three specific conditions (180-200 °C; 10-16 bar). After a certain retention time (0-25 minutes), the fast pressure release valve was open to atmosphere allowing instantaneous depressurization. As reference, the three different conditions are listed in Table 1.

Table 1 – Steam explosion conditions

Experiment	T (°C)	P (bar)	Residence Time (min)
SE1	180	10	0
SE2	200	16	5
SE3	200	16	25

After steam explosion, the materials were dried (105 °C overnight) and milled using the same knife mill. HTL batch reactions were performed using 20 mL bomb-type custom Swagelok® reactors. In a typical subcritical reaction, 1 g of polymer was loaded together with 8 g of deionized water, the reactor closed, sealed and submerged in a fluidized sand bath at 350 °C. After 20-60 minutes (including heating time) the reactors were taken out of the sand bath and quenched in room temperature water. The reactors were vented and gas mass noted. Aqueous phase (AP) was decanted and the reactor washed with methanol to recover oil products. Methanol was chosen as solvent

because of its characteristic incapacity of solubilizing the synthetic raw polymers, but solubility in typical expected products.

Supercritical HTL batch experiments were performed in smaller (12 mL) bomb-type custom Swagelok® reactors. In a typical reaction, 0.5 g of synthetic polymers were loaded together with 2 g of water. The same procedure as for subcritical experiments was followed, though for supercritical conditions, 420 °C was chosen as temperature, resulting in an estimated water density of 0.167 g.mL⁻¹ and 278 bar pressure and rinsing solvent was acetone. Analytical methods such as CHNS-O, GC/MS and ATR-FTIR are listed in Chapter 2 Methods. Thermogravimetric analysis (TGA) was performed in a Mettler Toledo SDTA851. The TGA was operated using ceramic crucibles containing a minimum of 5 mg of sample, which was heated at constant rate of 10 K min⁻¹ from 50 to 900 °C under nitrogen followed by 10 min under air at constant temperature.

Synergistic effects were calculated as:

$$SE = \frac{Yield_{experiment}}{Yield_{expected}}$$

Where $Yield_{experiment}$ is the experimental yield and $Yield_{expected}$ is the weighted average yield from single HTL experiments. Thus, if $SE > 1$, positive synergies are observed; if $SE < 1$, antagonistic effects are present and; $SE = 1$ no synergies can be measured.

3.3. Results and discussion

3.3.1. Steam explosion

For both PE and PP, aqueous phases were clear in all steam explosion conditions, with no changes in TGA, FTIR or CHNS composition. The products of PS steam explosion (SE2) can be observed in Figure 3 A-B. For PS SE2 and SE3, the aqueous phase from steam explosion was clearly different, with darker aspect and smell of solvents. The solid products on the other hand did not seem changed in aspect or color. Styrene, benzaldehyde and acetophenone traces were found in GC/MS aqueous phase from steam explosion, which indicates minor decomposition of PS under these conditions. Sugano's work³⁷ describes steam explosion of such materials yields powdered solids, which was not observed in our attempts and may be a result of different steam explosion apparatus design.

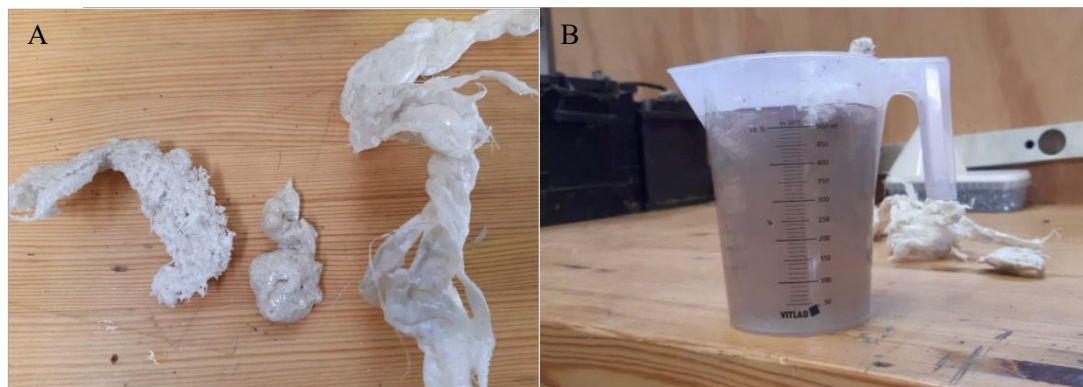


Figure 3 – Polystyrene solids (A), aqueous phase (B) and aqueous phase GC/MS (C) products of steam explosion (SE2)

Figure 4 depicts both FTIR spectra and DTG curves of PS steam explosion solid products. For PE and PP, products did not change in those two analysis, however PS shows a change in onset and maximum weight change in DTG, more pronounced in SE2. Even though DTG depicts clear change in thermal decomposition behavior of PS after steam explosion, FTIR spectra did not change with the process, showing the chemical structure – at least in the polymer surface – is unchanged. Thus, these two analysis point that the change may be related to change in molecular weight average of PS. Such observation agrees with Sugano’s group arguments and data³⁷, which encouraged us to proceed with PS SE2 products in subcritical HTL.

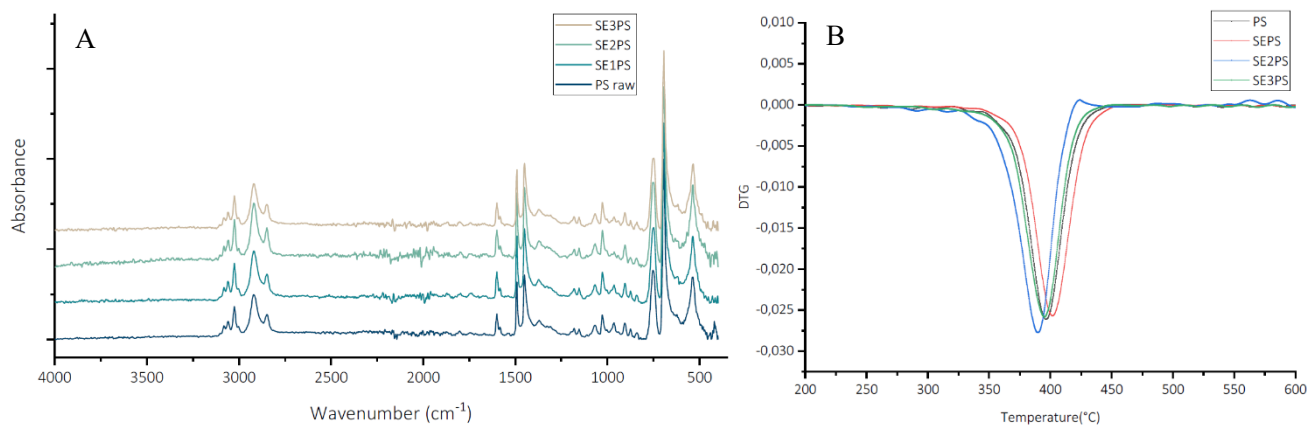


Figure 4 – PS steam explosion solid products FTIR and DTG

3.3.2. Subcritical HTL of steam exploded PS

Figure 5 depicts the mass balance of steam exploded PS, PP and PE subcritical HTL. The mass balance clearly shows no easing of depolymerization as a result of pre-treatment. Materials before and after HTL were also analyzed via FTIR and CHNS, both not having significant differences. For all experiments, the aqueous phase recovered was typically white and opaque, suggesting the first steps of polymer chain cleavage started for some molecules, however it did not affect the total mass balance. I.e. the decomposition did not occur because, despite some evidence of decrease in temperature required for depolymerization (as discussed about Figure 4), 350 °C is still too low of a temperature to provide the necessary energy for the carbon-carbon cleavage reactions.

Residence times up to 60 minutes were tested at 350 °C for PS to evaluate if residence time was hindering the total decomposition, given this material should decompose easier than PP and PE. The results were not significantly different from the ones presented in Figure 5 and, the solid residues also did not differ in CHNS-O nor FTIR results. In all cases, the results point that steam explosion is not an effective method to decrease depolymerization temperature under subcritical HTL.

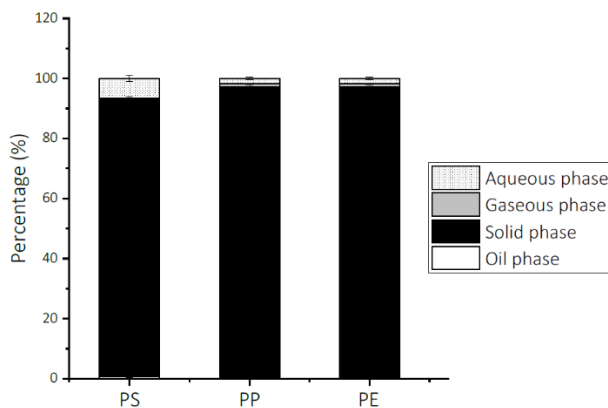


Figure 5 – Steam exploded materials subcritical HTL (350 °C, 20 minutes) mass balance

3.3.3. Supercritical co-HTL of polyolefins and PS

Despite a number of studies bringing attention to polyolefins and PS depolymerization under supercritical water have been reported dating back to the early 2000's^{35,38-40}, some even presenting promising results for the approach, the subject was not developed further than the microscale experiments at that time. With the development of supercritical HTL came together the opportunity of evaluating again this approach, which resulted in some studies reporting both subcritical^{30,41} and supercritical²⁵ excellent results for the depolymerization of PS.

Figure 6 depicts the mass balance for PS and polyolefins supercritical co-HTL at 420 °C. It is clear that PS is prone to depolymerization under these conditions and that PE and PP do not decompose at all. Up to 75% of oil yield from PS is achieved at 420 °C, leaving only 25% of the material not converted to this phase, mostly present as a solid residue by the end of the process. Only minor quantities of gas and aqueous phase yields were measured for all experiments.

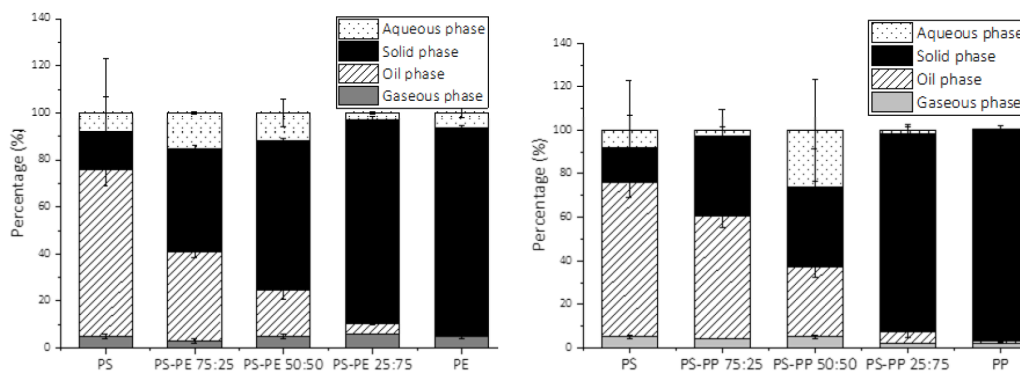


Figure 6 – PS:PE and PS:PP supercritical co-HTL (420 °C, 20 minutes) mass balance

In order to illustrate how oil yields of co-HTL of PS and polyolefins (Figure 6) behave in comparison to expected weighted average yields of those polymers (far left and right points of Figure 6 A and B), synergy effects are depicted in Figure 7. There is a remarkable resemblance of the two SE curves, both indicating that the more PS is present, the less antagonistic effects can be observed. It is also clear that PE is more prone to antagonistic effects than PP, the latter having almost neutral synergy when PS is 75% of the feed. Therefore, the results suggest that the small amount of molecules derived from both PE and PP under supercritical HTL at 420 °C are prone to recombine

with molecules from PS oil. Such recombination is likely to yield heavier products that are more likely to be found in the solid fraction of products, resulting in antagonist effects.

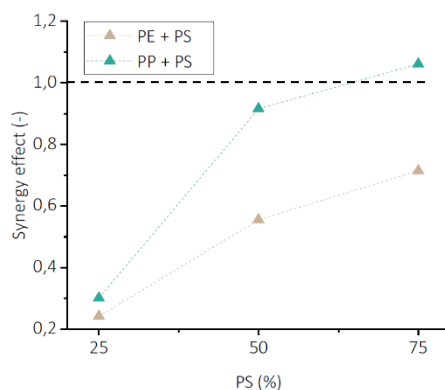


Figure 7 – Oil yield synergy effects of PS with PE and PP supercritical co-HTL

3.3.3.1. Supercritical HTL oil product elemental and molecular composition

The elemental composition of the PS and co-HTL oils depicts a very low oxygen concentration with >90% carbon content in all samples, as observed in Table 2. HHVs are all above 40 MJ · kg⁻¹, which represents a very high energy content in these oils, comparable to gasoline or diesel fractions of crude oil. Such energy density is typical for their feedstock materials, PS, PP and PE have respectively 40.2, 46.3 and 47.0 MJ kg⁻¹. The highest oil yield observed is 73.5% for PS at 420 °C, leading to a 75.7% carbon yield and 74.9% energy recovery. Comparing these values with the less antagonistic co-HTL experiments (PS:olefins 75:25) shows much lower values as shown in Table 2. For all co-HTL derived oils, it is also possible to see a lower oxygen content and higher hydrogen content, which can be a direct effect of these oil compositions.

In one of the most recent papers²⁵, optimal temperature for PS decomposition under supercritical water is reported as 500 °C with carbon recovery of 75%. Here, we present the same results at 420 °C, which can be an effect of HTL method discrepancy, with this specific paper²⁵ reporting values for thin quartz tube reactors, or the initial feedstock molecular weight average, which can also affect the oil recovery.

Table 2 – Supercritical synthetic oils CH-O analysis, HHV, Carbon Yield (CY) and Energy Recovery (ER) for PS and selected co-HTL with polyolefins

	C (wt%)	H (wt%)	O* (wt%)	HHV (MJ · kg ⁻¹)	Oil Yield (wt%)	CY (C%)	ER (%)
PS-400	90.3±1.8	7.7±0.1	2.0±2.0	41.3±1.2	34.7	35.3	35.6±1.0
PS-420	91.3±0.9	7.2±0.1	1.5±1.1	41.0±0.7	73.5	75.7	74.9±1.3
PS-PE 75:25	91.8±0.3	8.2±0.1	0.0±0.4	42.9±0.3	38.5	40.2	39.4±0.3
PS-PP 75:25	91.4±0.1	8.5±0.1	0.1±0.1	43.2±0.1	56.9	59.2	58.9±0.1

* - by difference

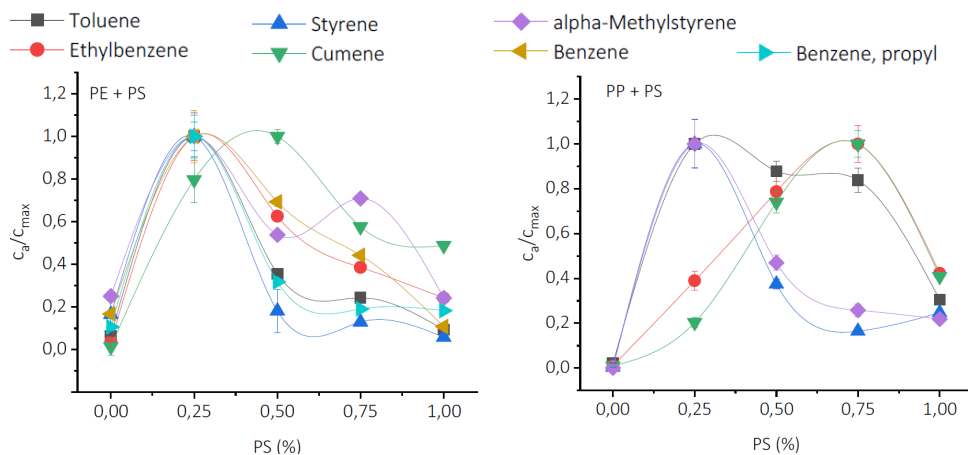


Figure 8 – PS:PE and PS:PP supercritical co-HTL (420 °C, 20 minutes) oil composition comparison via GC/MS

Figure 8 shows the change in concentration relative to the highest concentration found in different synthetic oils according to PS participating in co-HTL with polyolefins measured via GC/MS. Here we separated the styrene-like compounds, which comprises mono- or di-substituted single aromatics. It is remarkable that for PS-PE, the most antagonistic co-HTL, when PS is 25% of the feedstock (point with lowest synergy effect) most compounds present highest concentration. This can be interpreted as a lowering in quantities of other products, which tells us that mono or di-substituted aromatics are not the responsible for the antagonistic effects. No clear trend in other compounds analyzed by GC/MS could be found, indicating that such differences are present in compounds that cannot be analyzed by this technique, i.e. heavier compounds. Thus it is possible to hypothesize that when PS is decomposed down to small compounds, such as the ones shown in Figure 8, recombination is not as likely as when the process is occurring and chains are still in higher MW ranges. When in presence of small quantities of olefin-derived compounds, partially decomposed PS tends to react and form even longer molecules that yield more solids instead of oils. This hypothesis is in alignment with Table 2, where oxygen is not present in the co-HTL oils, which can signify that oxygenated end-groups of PS decomposition are capable of reacting with the polyolefin-derived compounds leading to the results observed here.

The solid residues from supercritical co-HTL of PS:PP (75:25) FTIR in Figure 9 corroborate further with the hypothesis of oxygen-containing compounds recombination. The broad peak around 3300 cm^{-1} is typical for O-H stretching, which matches with O-H bending with a sharp peak around 1300 cm^{-1} . Besides, the broad peak around 1000 cm^{-1} is an indication of typical C-O bonds in several forms, e.g. 1200 cm^{-1} for ester stretching, 1125 cm^{-1} for aliphatic ether or tertiary alcohols stretching, $1085\text{-}1125\text{ cm}^{-1}$ for secondary alcohol stretching, $1050\text{-}1085$ for primary alcohol stretching and, CO-O-C bending at 1000 cm^{-1} .

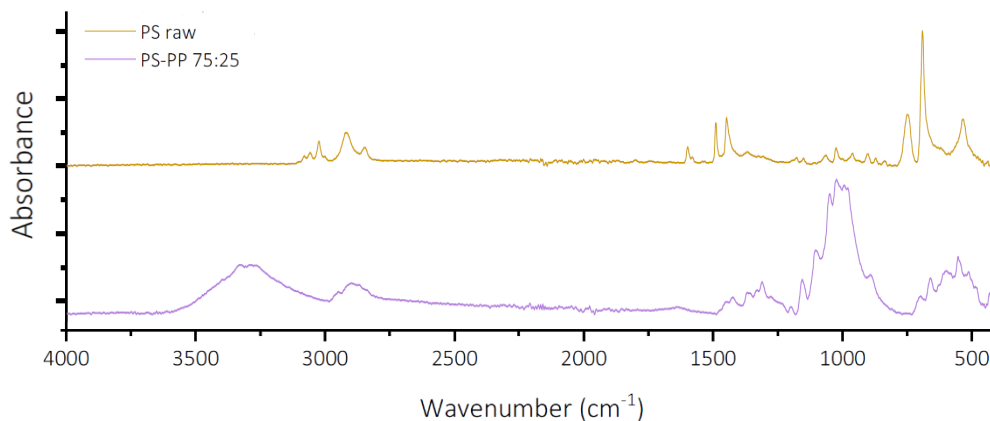


Figure 9 – PS:PP supercritical co-HTL (420 °C, 20 minutes) solid residues

3.4. Conclusion

The steam explosion pretreatment, despite showing effect in the TGA analysis of PS was not successful in promoting conversion of PS under subcritical water. The need for higher conversion temperatures is still present and little to no change in chemical analysis of the polymer was observed. It is thus, not advised to follow this approach, but rather seek new strategies to break carbon-carbon bonds present in polyolefins and polystyrene, which are responsible for inert characteristics of these materials under subcritical HTL.

As for the supercritical combined HTL processing approach, the addition of polyolefins to PS results in antagonistic effects, which hinder oil yields of PS in the conditions tested. With the data presented, it is possible to hypothesize oxygen containing intermediates and products of PS tend to react with minor quantities of polyolefin products of HTL to form heavy compounds, resulting in solids. That is, the oil phase of polystyrene is susceptible to reacting with contaminants, which causes concern for combined chemical recycling strategy, given such polymers are usually found together.

References Part I

- (1) Geyer, R.; Jambeck, J. R.; Law, K. L. Production, Use, and Fate of All Plastics Ever Made. *Sci. Adv.* **2017**, *3* (7), 25–29. <https://doi.org/10.1126/sciadv.1700782>.
- (2) Lebreton, L.; Andrady, A. Future Scenarios of Global Plastic Waste Generation and Disposal. *Palgrave Commun.* **2019**, *5* (1), 1–11. <https://doi.org/10.1057/s41599-018-0212-7>.
- (3) Jambeck, J. R.; Geyer, R.; Wilcox, C.; Siegler, T. R.; Perryman, M.; Andrady, A.; Narayan, R.; Law, K. L. Plastic Waste Inputs from Land into the Ocean. *Science (80-.)*. **2015**, *347* (6223), 768–771. <https://doi.org/10.1126/science.1260352>.
- (4) Vollertsen, J.; Anna Hansen, A. *Microplastic in Danish Wastewater: Sources, Occurrences and Fate*; 2017.
- (5) Machado, A. A. D. S.; Hempel, S.; Rillig, M. C.; Kloas, W.; Zarfl, C. Microplastics as an Emerging Threat to Terrestrial Ecosystems. **2017**. <https://doi.org/10.1111/gcb.14020>.
- (6) Weithmann, N.; Möller, J. N.; Löder, M. G. J.; Piehl, S.; Laforsch, C.; Freitag, R. Organic Fertilizer as a Vehicle for the Entry of Microplastic into the Environment. **2018**, 1–8.
- (7) Kane, I. A.; Kane, I. A.; Clare, M. A.; Miramontes, E.; Wogelius, R.; Rothwell, J. J.; Garreau, P.; Pohl, F. Seafloor Microplastic Hotspots Controlled by Deep-Sea Circulation. *Science (80-.)*. **2020**, *5899* (April), 1–11.
- (8) MacLeod, M.; Arp, H. P. H.; Tekman, M. B.; Jahnke, A. The Global Threat from Plastic Pollution. *Science (80-.)*. **2021**, *373* (6550), 61–65. <https://doi.org/10.1126/science.abg5433>.
- (9) Borrelle, S. B.; Ringma, J.; Law, K. L.; Monnahan, C. C.; Lebreton, L.; McGivern, A.; Murphy, E.; Jambeck, J.; Leonard, G. H.; Hilleary, M. A.; et al. Predicted Growth in Plastic Waste Exceeds Efforts to Mitigate Plastic Pollution. *Science (80-.)*. **2020**, *369* (6510), 1515–1518. <https://doi.org/10.1126/science.aba3656>.
- (10) European Council; Parliament, E. Directive (Eu) 2019/904 of the European Parliament and of the Council of 5 June 2019 on the Reduction of the Impact of Certain Plastic Products on the Environment. *Off. J. Eur. Union* **2019**, *2019* (March), 1–19.
- (11) The European Commission. *European Commission: Declaration of the Circular Plastics Alliance*; European Union: Brussels, Belgium, 2019.
- (12) UNEP - United Nations Environment Programme. Nations Commit to Fight Plastic Pollution Together during the UN General Assembly <https://www.unep.org/news-and-stories/press-release/nations-commit-fight-plastic-pollution-together-during-un-general> (accessed Aug 6, 2021).
- (13) World Economic Forum. Global Plastic Action Partnership <https://www.weforum.org/projects/global-plastic-action-partnership> (accessed Aug 6, 2021).
- (14) European Council; European Parliament. *A European Strategy for Plastics in a Circular Economy*; 2018.
- (15) Solis, M.; Silveira, S. Technologies for Chemical Recycling of Household Plastics – A Technical Review and TRL Assessment. *Waste Manag.* **2020**, *105*, 128–138. <https://doi.org/10.1016/j.wasman.2020.01.038>.
- (16) Cooperation, D. Dow and Mura Technology Announce Partnership to Scale Game-Changing New Advanced Recycling Solution for Plastics. **2021**.
- (17) RenewELP. A New Solution for Recycling Waste. RenewELP 2020.
- (18) Singh, N.; Hui, D.; Singh, R.; Ahuja, I. P. S.; Feo, L.; Fraternali, F. Recycling of Plastic Solid Waste: A State of Art Review and Future Applications. *Compos. Part B Eng.* **2017**, *115*, 409–422. <https://doi.org/10.1016/j.compositesb.2016.09.013>.
- (19) Schyns, Z. O. G.; Shaver, M. P. Mechanical Recycling of Packaging Plastics: A Review. *Macromol. Rapid Commun.* **2021**, *42* (3), 1–27. <https://doi.org/10.1002/marc.202000415>.
- (20) Hopewell, J.; Dvorak, R.; Kosior, E. Plastics Recycling: Challenges and Opportunities. *Philos. Trans. R. Soc. B Biol. Sci.* **2009**, *364* (1526), 2115–2126. <https://doi.org/10.1098/rstb.2008.0311>.
- (21) Anuar Sharuddin, S. D.; Abnisa, F.; Wan Daud, W. M. A.; Aroua, M. K. A Review on Pyrolysis of Plastic Wastes. *Energy Convers. Manag.* **2016**, *115*, 308–326. <https://doi.org/10.1016/j.enconman.2016.02.037>.
- (22) Grause, G.; Buekens, A.; Sakata, Y.; Okuwaki, A.; Yoshioka, T. Feedstock Recycling of Waste Polymeric Material. *J. Mater. Cycles Waste Manag.* **2011**, *13* (4), 265–282. <https://doi.org/10.1007/s10163-011-0031-z>.
- (23) Gholizadeh, M.; Li, C.; Zhang, S.; Wang, Y.; Niu, S.; Li, Y.; Hu, X. Progress of the Development of Reactors for Pyrolysis of Municipal Waste. *Sustain. Energy Fuels* **2020**, *4* (12), 5885–5915. <https://doi.org/10.1039/d0se01122c>.

- (24) Chen, W. T.; Jin, K.; Linda Wang, N. H. Use of Supercritical Water for the Liquefaction of Polypropylene into Oil. *ACS Sustain. Chem. Eng.* **2019**, *7* (4), 3749–3758. <https://doi.org/10.1021/acssuschemeng.8b03841>.
- (25) Bai, B.; Jin, H.; Fan, C.; Cao, C.; Wei, W.; Cao, W. Experimental Investigation on Liquefaction of Plastic Waste to Oil in Supercritical Water. *Waste Manag.* **2019**, *89*, 247–253. <https://doi.org/10.1016/j.wasman.2019.04.017>.
- (26) Jin, K.; Vozka, P.; Kilaz, G.; Chen, W. T.; Wang, N. H. L. Conversion of Polyethylene Waste into Clean Fuels and Waxes via Hydrothermal Processing (HTP). *Fuel* **2020**, *273* (March), 117726. <https://doi.org/10.1016/j.fuel.2020.117726>.
- (27) Elliott, D. C. Hydrothermal Processing. In *Thermochemical Processing of Biomass: Conversion into Fuels, Chemicals and Power*; Brown, R. C., Ed.; John Wiley & Sons Ltd, 2011; pp 200–231. <https://doi.org/10.1002/9781119990840.ch7>.
- (28) Iwaya, T.; Sasaki, M.; Goto, M. Kinetic Analysis for Hydrothermal Depolymerization of Nylon 6. **2006**, *91*, 1989–1995. <https://doi.org/10.1016/j.polyimdeggradstab.2006.02.009>.
- (29) Weiss, C. C. E.; Soudais, H. Y. Impact of Solvolysis Process on Both Depolymerization Kinetics of Nylon 6 and Recycling Carbon Fibers from Waste Composite. *Waste and Biomass Valorization* **2020**, *8* (8), 2853–2865. <https://doi.org/10.1007/s12649-017-9901-5>.
- (30) Zhao, X.; Zhan, L.; Xie, B.; Gao, B. Products Derived from Waste Plastics (PC , HIPS , ABS , PP and PA6) via Hydrothermal Treatment : Characterization and Potential Applications. *Chemosphere* **2018**, *207*, 742–752. <https://doi.org/10.1016/j.chemosphere.2018.05.156>.
- (31) Arai, R.; Zenda, K.; Hatakeyama, K.; Yui, K.; Funazukuri, T. Reaction Kinetics of Hydrothermal Depolymerization of Poly (Ethylene Naphthalate), Poly (Ethylene Terephthalate), and Polycarbonate with Aqueous Ammonia Solution. *Chem. Eng. Sci.* **2010**, *65* (1), 36–41. <https://doi.org/10.1016/j.ces.2009.03.023>.
- (32) Zenda, K.; Funazukuri, T. Depolymerization of Poly (Ethylene Terephthalate) in Dilute Aqueous Ammonia Solution under Hydrothermal. **2008**, *1386* (March), 1381–1386. <https://doi.org/10.1002/jctb>.
- (33) Liu, Y.; Wang, M.; Pan, Z. Catalytic Depolymerization of Polyethylene Terephthalate in Hot Compressed Water. *J. Supercrit. Fluids* **2012**, *62*, 226–231. <https://doi.org/10.1016/j.supflu.2011.11.001>.
- (34) Goto, M. Chemical Recycling of Plastics Using Sub- and Supercritical Fluids. *J. Supercrit. Fluids* **2009**, *47* (3), 500–507. <https://doi.org/10.1016/j.supflu.2008.10.011>.
- (35) Park, Y.; Hool, J. N.; Curtis, C. W.; Roberts, C. B. Depolymerization of Styrene - Butadiene Copolymer in Near-Critical and Supercritical Water. **2001**, 756–767. <https://doi.org/10.1021/ie000502l>.
- (36) Kwak, H.; Shin, H.; Bae, S.; Kumazawa, H. Characteristics and Kinetics of Degradation of Polystyrene in Supercritical Water. **2005**, 1–6. <https://doi.org/10.1002/app.23896>.
- (37) Sugano, M.; Komatsu, A.; Yamamoto, M.; Kumagai, M.; Shimizu, T.; Hirano, K.; Mashimo, K. Liquefaction Process for a Hydrothermally Treated Waste Mixture Containing Plastics. **2009**, 27–31. <https://doi.org/10.1007/s10163-008-0215-3>.
- (38) Su, X.; Zhao, Y.; Zhang, R.; Bi, J. Investigation on Degradation of Polyethylene to Oils in Supercritical Water. **2004**, *85*, 1249–1258. <https://doi.org/10.1016/j.fuproc.2003.11.044>.
- (39) Lilac, W. D.; Lee, S. Kinetics and Mechanisms of Styrene Monomer Recovery from Waste Polystyrene by Supercritical Water Partial Oxidation. *Adv. Environ. Res.* **2001**, *6* (1), 9–16. [https://doi.org/10.1016/S1093-0191\(00\)00066-6](https://doi.org/10.1016/S1093-0191(00)00066-6).
- (40) Fang, Z.; Koziski, J. A. A Comparative Study of Polystyrene Decomposition in Supercritical Water and Air Environments Using Diamond Anvil Cell. *J. Appl. Polym. Sci.* **2001**, *81* (14), 3565–3577. <https://doi.org/10.1002/app.1813>.
- (41) Seshasayee, M. S.; Savage, P. E. Oil from Plastic via Hydrothermal Liquefaction: Production and Characterization. *Appl. Energy* **2020**, *278* (March), 115673. <https://doi.org/10.1016/j.apenergy.2020.115673>.

Part II

Synthetic polymers and biomass co-HTL

Chapter 4

Introduction

4.1. Carbon, circular economy and materials

Demands for energy, materials and food are intrinsically connected to increasing world population, industrialization and modern life style. The current linear economic model based on extraction of natural resources and disposal of wastes (take-make-dispose) cannot cope with the societal demands in a sustainable manner.^{1,2} More specifically, carbon derived from fossil reserves is currently the basis for most energy-demanding economic sectors (mobility, electricity, industry) and synthetic materials. In short, we take carbon trapped in stable forms – such as crude oil, coal, natural gas – for thousands of years, oxidize it to make mostly energy, but also materials, and, as a result, we obtain residual CO₂, a gas that we dispose in earth's atmosphere, building up its concentration. The fact that CO₂ is also one of the major greenhouse gases and, thus, increases global average temperature, places the linear carbon-based economy as a threat to societies throughout the planet.³

The circular economy, and even more recently the circular bio-economy concept, has been gaining attention as it promises to alleviate this societal challenge. This approach relies on circling back to the economy materials used in any activities, creating a closed system that sustains itself. For instance, in a carbon-based circular economy, all production systems would focus on trapping most carbon in an indefinite short-time recycling loop, reducing amounts of intake and disposal to a minimum. Despite the promising concept, it lacks key engineering technologies to make it competitive over traditional linear activities and operable on the scale of today's societies.^{1,4,5}

Among carbon materials, biomass plays an important role on covering the carbon gap of future fossil-free systems. Special attention has to be brought to sustainable biomass resources, as the transformation of CO₂ into biomass is a crucial step in a carbon-based circular economy. In this sense, agricultural waste is preferred, e.g. straws, manure, plant stems, leaves. The preference for waste materials can also avoid food and energy crops competition for land use.⁶

Among the technologies that can perform the conversion of carbon materials into useful products are thermochemical processes. Thermochemical processes can be broadly divided into pyrolysis, gasification and hydrothermal liquefaction (HTL). The combination of different biomasses and synthetic materials in these processes has been studied for some of them, and a great knowledge gap is found in specific sectors of this field of research.

A number of studies bring attention to co-processing of plastics and biomasses in pyrolysis apparatus. As pyrolysis is typically inefficient in converting condensation polymers⁷, the combination with organic materials is usually reported for polyolefins and polystyrene conversion. Zhang et al., 2016⁸ reports a comprehensive review on specifically lignocellulosic-polyolefins interactions during catalytic pyrolysis. Overall, the technique enhances monocyclic aromatic hydrocarbons production and tends to reduce char formation, which is also described in other studies.⁹ Besides, the approach enhances gasification reactions, leading to more CO and H₂ formation.^{7,9} Overall, the co-pyrolysis

approach is limited to addition polymers and is not well suited for dealing with complex mixtures containing condensation polymers.

Another promising thermochemical process to enable carbon circularity, taking advantage of several different types of waste materials, is HTL. The process is able to convert carbon-based material streams into useful chemicals and liquid fuels with the aid of liquid compressed water.¹⁰ Biomass resources such as sugars, lipids, proteins, sewage sludge, wood-like materials, lipids, algae and food waste have been described in literature abundantly.^{11,12} However, there is still limited knowledge about how biological materials behave under hot and compressed water in presence of another major carbon-based material category: synthetic polymers. Synthetic polymers' perspectives towards HTL processing were described in Part I of this thesis. Next, recent developments of combined HTL of biological materials and different synthetic polymers are presented.

4.2. HTL of synthetic polymers and biological materials

4.2.1. Synthetic polymers and biomolecules under subcritical water

Basic knowledge on how simple molecules behave under HTL conditions plays an essential role on understanding the products of complex biomass processing. However, it was not until recently that simple molecules (e.g. pure sugars, lipids, proteins) were evaluated in presence of synthetic materials.^{13,14} The two studies are from Phillip E. Savage's group and bring attention to high synergistic effects for carbohydrates (cellulose, starch) and lignin in presence of a few types of plastics (PP, PET, PS and PC), while no synergies for the same plastics in presence of proteins or stearic acid are shown. In one of these studies¹⁴, it is reported that among the types of plastic tested, only PC shows synergistic effects for oil yields at 350 °C.

4.2.2. Algae and synthetic polymers

Algae are examples of biological materials generally composed of simple carbohydrates, lipids and proteins. Both macro and microalgae are of high interest as feedstock for HTL processing^{15,16}, and the co-HTL approach is the closest to model biomolecules due to their composition. The combination of microalgae and synthetic polymers in HTL was first reported in co-HTL with PP.¹⁷ The study reported very low synergistic effects with little to no conversion of the polyolefin under subcritical water. Nevertheless, the synthetic polymer presence influenced the oil product composition by reducing its organic acids content. Very recently, a study was published reporting the screening of several different synthetic polymers (PE, PP, PS, PET, PVC, PA6, PA66 and PC) co-HTL in presence of microalgae biomass.¹⁸ Results showed the type of microalgae with highest carbohydrate content presented also the best interaction with plastics for oil formation. More specifically, PS and PC were found to present the best co-HTL results with microalgae.

Four types of macroalgae have also been reported in co-HTL with plastics (PE, PP, PA6).¹⁹ Synergistic effects in biocrude formation were observed for all plastics, however for PA6 there was a decrease in energy recovery as biocrude. In this study¹⁹, the difference in ash content for the different macroalgae was hypothesized as the reason for the different behavior observed in co-

HTL results. In all cases, the synergistic effect observed was low in comparison to other studies already discussed.

4.2.3. Lignocellulosic biomass and synthetic polymers

Although other biomasses (e.g. algae, food waste) are also of great interest for synthetic polymer co-HTL, this thesis will focus on lignocellulosic biomasses, given an identified knowledge gap in current literature. Chapter 5 of this thesis discusses lignocellulosic biomass co-HTL with synthetic polymers by presenting our latest work on the topic, which contains a brief literature review about the subject in its introduction. Comments on very recent publications about the subject can also be found in the reflections section of Chapter 5.

Chapter 5

Paper 2 – Hydrothermal Co-Liquefaction of Synthetic Polymers and *Miscanthus Giganteus*: Synergistic and Antagonistic Effects

dos Passos, J. S.; Glasius, M.; Biller, P. Hydrothermal Co-Liquefaction of Synthetic Polymers and *Miscanthus Giganteus*: Synergistic and Antagonistic Effects. *ACS Sustain. Chem. Eng.* 2020. <https://doi.org/10.1021/acssuschemeng.0c07317>.

Article history:

Received: October 5th, 2020

Revised: November 10th, 2020

Published: December 11th, 2020

Keywords:

hydrothermal liquefaction

chemical recycling

depolymerization

circular economy

polymers

5.1. Reflections

With the knowledge gathered and described in Part I, a solid basis to investigate the co-HTL processing of synthetic polymers and lignocellulosic biomass is established. The present chapter describes the work to identify which synthetic polymers are most prone to act synergistically with lignocellulosic materials, here represented by *Miscanthus Giganteus*. The work highlighted the diversity of reactions involved in the co-HTL processing of different polymers. It not only investigated synergies, but also described molecular changes in each specific case. The results here reported were also presented in the Thermochemical Symposium of 2020 (October 5-7, 2020, Washington State University, Virtual Symposium) with very good acceptance of the scientific community and industry.

In the latest report by Seshayee, Stofanak & Savage¹³ about co-HTL of biomass and plastics, the results presented in this chapter are commented. The work¹³ proposes an additivity model for prediction of oil yields from plastics and biomass mixtures. The paper appended in the current chapter is cited in the context of testing the oil yield prediction capacity of the model described by their work as follows:

Another oil yield that was greatly overpredicted is from a recent study from Biller's lab (Souza Dos Passos et al., 2020). This mixture was 50 wt% PS, which gave an oil yield of 86 wt% at 350 °C in our earlier experimental work (Seshasayee and Savage, 2020). Even if the biomass in the other half of the mixture contributed nothing to the oil yield, we would expect an oil yield of 43 wt%. The experimental oil yield reported for the mixture was just 16 wt%. We used DCM to recover oil after HTL, whereas the Biller study (Souza Dos Passos et al., 2020) used methanol. To determine whether the different solvents were causing the widely different oil yields, we ran an experiment for HTL of PS at 425 °C, 30 min with methanol as the recovery solvent (following the recovery method of the Biller study (Souza Dos Passos et al., 2020)) and measured an oil yield of 13.32 ± 0.72 wt%. An analogous experiment with DCM as recovery solvent (following the recovery method of the Biller study (Souza Dos Passos et al., 2020)) for HTL of PS at 425 °C, 30 min gave an oil yield of 47.03 ± 0.13 wt%. The reason for this difference is the different solvents used to recover oil in the present work and in the Biller study.

Text from Seshayee, Stofanak & Savage¹³

References cited in the paragraph: Souza dos Passos et al., 2020 – The current chapter
Seshasayee and Savage, 2020 - Reference²⁰

The arguments raised by the report are valid and indeed concerning regarding the application of results. Dichloromethane (DCM) is the solvent of choice for recovery in most HTL literature, and it is for good reason, given for biomass-derived biocrudes it shows superior oil recovery.²¹ At the beginning of this thesis laboratory work, we also considered such arguments in favor of DCM, especially for allowing direct comparison with current literature.

An experimental selection of solvents was conducted at the time. In short, around 10 wt% mixtures of each type of raw polymers used in our studies (the list is available both in Chapter 2 and the present chapter's appended paper) with several different solvents (acetone, DCM, methanol, ethanol, ethyl acetate, hexane and toluene) were made in glass test tubes. The test tubes were closed and solubility observed for all polymers, considering single-phase or double-phase solution visual aspects. The only solvents to meet the criteria of not dissolving all raw synthetic polymers were methanol and ethanol. To ease solvent evaporation after extraction of oils, methanol was chosen due to lower boiling point.

DCM is considered a good solvent for PS, showing single phase aspect in mixtures for high solutions with concentrations (e.g. 80 wt% of PS), as shown in Figure 10A.²² Also, as depicted in Figure 10B²³ the solvent activity of DCM in PS is higher than 0.8 at a 30 wt% mass fraction, i.e. DCM dominates viscoelastic properties of the solution at low solvent weight fractions, giving a homogenous and low viscosity aspect to the mixture.²³ Thus, DCM is a recognized solvent for PS, which indicates that the high oil recovery reported by Seshayee, Stofanak & Savage's studies¹³ can be related to large oligomers or raw PS itself being transferred to the oil products. As also commented by the group¹³, understanding of the influence of solvents in the oil and carbon recoveries is still needed in the field.

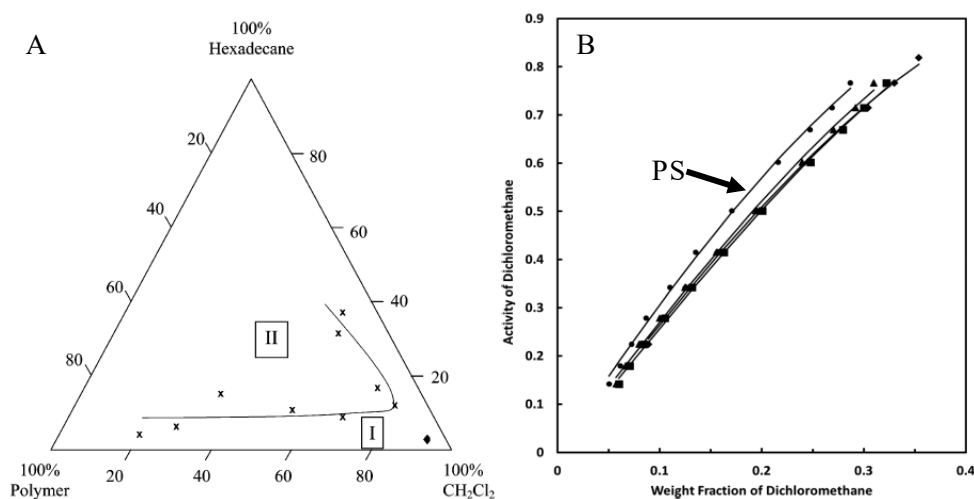


Figure 1 – (A) Ternary phase diagram for polystyrene (MW average 280 000 g mol⁻¹), dichloromethane and hexadecane²², where I indicates single phase and II two phase regions; (B) Experimental activities of dichloromethane in polystyrene (MW average 233 000 g mol⁻¹) and other co-polymers.²³

Hydrothermal Co-Liquefaction of Synthetic Polymers and *Miscanthus giganteus*: Synergistic and Antagonistic Effects

Juliano Souza dos Passos, Marianne Glasius, and Patrick Biller*

Cite This: *ACS Sustainable Chem. Eng.* 2020, 8, 19051–19061

Read Online

ACCESS |



Metrics & More



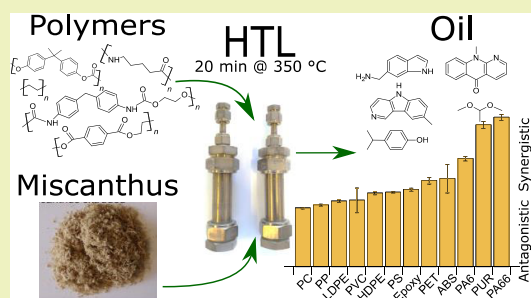
Article Recommendations



Supporting Information

ABSTRACT: Synthetic polymers constitute one of the main carbon-containing wastes generated nowadays. In this study, combined hydrothermal liquefaction (co-HTL) is evaluated for 1:1 mixtures of *Miscanthus giganteus* and different synthetic polymers—including poly-acrylonitrile-butadiene-styrene (ABS), bisphenol-A-based epoxy resin, high-density polyethylene (HDPE), low-density polyethylene (LDPE), polyamide 6 (PA6), polyamide 6/6 (PA66), poly(ethylene terephthalate) (PET), polycarbonate (PC), polypropylene (PP), polystyrene (PS), and polyurethane foam (PUR)—using batch HTL at 350 °C. Based on oil yields and composition, a comprehensive discussion of observed interactions is presented. The results show that even though polyolefins do not depolymerize under these conditions, the oil products depict that these materials interact with miscanthus biocrude changing its composition. Bisphenol-A-based polymers as PC and epoxy resins both contribute to the formation of monomer-like structures in the biocrude. PET increases the presence of carboxyl groups, while polyamides and PUR increase significantly the oil yield, modifying the biocrude composition toward nitrogen-containing molecules. PUR co-HTL was found to increase oil, carbon, and energy yields, leading to process improvement when compared to pure miscanthus processing.

KEYWORDS: hydrothermal liquefaction, chemical recycling, depolymerization, circular economy, polymers



INTRODUCTION

Out of 8300 million metric tons of virgin plastics produced up to 2017, a mere 7% was recycled and another 12% burned for energy recovery, leaving a little more than 6500 million metric tons of waste accumulated in the environment.¹ A large fraction of this waste accumulation takes place in an uncontrolled manner, leading to mixing of different waste streams with synthetic resins. Given the total synthetic polymer production is foreseen to double in the next 20 years accompanied by an increase of gross domestic product in developing countries,² accumulation of plastic waste is also expected to increase. Technologies that can recycle mixed wastes comprised of both synthetic and biological polymers are hence highly desired to reuse the fossil-derived carbon contained in plastic wastes, beyond incineration or landfilling.

Hydrothermal liquefaction (HTL) is a technology that uses the properties of near-critical water to depolymerize carbon-containing materials into a crude-like substance often referred to as biocrude.³ The technology has shown the potential to convert materials such as lignocellulosics, organic wastes,^{4,5} and algae⁶ both individually and mixed.^{7,8} Recently, co-liquefaction of wastes has been receiving increasing attention as researchers observe synergies in the liquefaction behavior of different organic wastes and biomass, depicting opportunities to ease processing and increase process efficiency. For instance, loblolly pine co-liquefaction with both manure and sewage

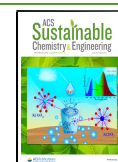
sludge has been reported to improve biocrude yields and quality.⁹ Furthermore, sewage sludge co-liquefaction with a variety of lignocellulosic materials has also shown the potential to improve the process efficiency.¹⁰

Synthetic polymers have received less attention in the HTL literature, partially because pyrolysis is often the preferred route for chemical recycling of polyolefins and polystyrene (PS). This technology is carried out above the thermal cracking temperature of these synthetic materials (~500 °C), which account for the majority of synthetic waste.¹ A recent study by the authors¹¹ on subcritical HTL of synthetic polymers (350 °C) has shown that only some polymer resins are suitable for oil or monomer recovery via HTL. Polyolefins and PS, for instance, were shown not to decompose at these conditions, while polymers with heteroatoms (N or O) in the backbone appeared more promising. Since different biomass fractions have previously shown synergies in HTL and avoided the need for catalysts, it is worth investigating if similar synergies exist between biomass and synthetic polymers. The

Received: October 5, 2020

Revised: November 10, 2020

Published: December 11, 2020



combination of biomass and synthetic wastes via HTL has the potential to improve the conversion of polymers and the overall carbon throughput and recovery, hence, broadening the application range of HTL technology. Given the current waste handling infrastructure worldwide, combined HTL (co-HTL) is of great interest due to its versatility and capacity to cope with the challenges posed. The combination of complex materials, such as commercial synthetic polymers and biomass, can result in unexpected interactions that must be explored and understood prior to full-scale applications. So far, previous research within this topic is limited and few polymers have been investigated.

The first study within this scope reported co-HTL of mixtures of lignite, wheat straw, and poly(ethylene terephthalate) (PET). It showed that at certain ratios, the total conversion to oils of mixed materials was higher than the single-component liquefaction calculated prediction.¹² Recently, a lignocellulosic biomass, *Prosopis juliflora*, was catalytically (activated bentonite) co-liquefied with non-identified polyolefin waste and reported to have the best oil yield (61.2%) using 3:1 (biomass/polyolefin) mixing ratio at 420 °C (supercritical conditions) and 60 min reaction time. The same study reports positive synergies for bio-oil production in sub- and supercritical water (340–440 °C).¹³ Using the same catalyst and biomass, co-HTL of paint sludge (described as containing synthetic polymer waste) was also reported to increase the oil yield significantly using a 2:1 ratio (biomass:paint sludge) for all investigated temperatures (340–440 °C).¹³

Subcritical (350 °C) co-HTL of pistachio hulls and individually polyethylene (PE), PET, polypropylene (PP), and nylon-6 (feed containing 10–20 wt % plastics) was reported to achieve synergy effects in oil yield as well. The biocrude higher heating value (HHV) increased in mixtures of 10 and 20% PE, while it was maintained for the other polymers tested. However, the only polymer to yield a higher chemical energy recovery when compared to the pure biomass (60%) was PET at 10–20% mix ratio (70%).¹⁴

The present study aims to expand the state of knowledge and critically evaluate the technical feasibility and efficiency of co-HTL of synthetic polymers and the model lignocellulosic *Miscanthus giganteus*. A systematic evaluation of 12 different synthetic polymers is presented, including previously unreported ABS, epoxy, PA66, polycarbonate (PC), PS, and polyurethane (PUR), and different mixture ratios than current literature are reported for all others. Unified process conditions, resembling those of continuous processing pilot reactors,^{15,16} were chosen to allow comparison among samples and identification of synergistic and antagonistic effects of different polymers with miscanthus. We also highlight how other important streams (aqueous phase, gas, and solids) of HTL processing behave under such conditions. The study clarifies the reaction pathways and product effects that we can expect to find upon co-HTL, highlighting opportunities and challenges of this approach.

EXPERIMENTAL SECTION

M. giganteus was harvested at Aarhus University's facilities (Foulum, Denmark), extruded using a twin-screw extruder (Xinda, 65 mm twin-screw extruder with 2000 mm barrel length), and dried for 24 h at 105 °C in a forced circulation oven. A total of 12 different commercial polymers were investigated: poly-acrylonitrile-butadiene-styrene (ABS, BASF, Terluran GP-22), bisphenol-A-based epoxy resin

(DowDuPont Airstone 760E/766H), high-density polyethylene (HDPE, INEOS HDPE T60-800-119), low-density polyethylene (LDPE, INEOS LDPE 23L430), noncolored plastic cable ties of polyamide 6 (PA6), Sigma-Aldrich polyamide 6/6 (PA66), poly(ethylene terephthalate) plastic bottles (PET), polycarbonate (PC, from transparent laboratory safety goggles), polypropylene plastic cups (PP), polystyrene plastic cups (PS), polyurethane chair foam (PUR), and Sigma-Aldrich poly(vinyl chloride) (PVC). Table S1 shows their molecular structures. Most polymers were milled individually using a Polymix PX-MFC 90D knife mill equipped with a 2 mm sieve prior to HTL, while PVC was used as acquired (powder).

HTL Procedure. Custom-made Swagelok bomb-type reactors were assembled as previously described¹⁷ with a total volume of 20 mL. Experiments were conducted using a mixture of miscanthus and synthetic polymers of ratio 1:1 (mass basis) for each individual polymer. Reactors were loaded with 0.50 g of miscanthus and synthetic polymer and 8.50 g of water and sealed and submerged in a preheated fluidized sand bath for a total of 20 min at 350 °C, including heating time. After reaction time, reactors were quenched in water, the mass of gas was determined gravimetrically by venting the room-temperature reactor, and the product workup procedure was followed. The aqueous phase (AP) was decanted into a centrifuge tube (spun for 5 min at 4000 rpm), while the remaining solids and viscous oil in the reactor were washed up with 30 mL of methanol and vacuum-filtered. Solids recovered from the bottom of the AP centrifuge tube were washed with methanol and filtered together with the reactor's content. Solids were collected and dried overnight in a 105 °C forced circulation oven. An aliquot of 1 mL out of the 30 mL of methanol used for washing the reactor was used for gas chromatography coupled with mass spectrometry (GC-MS) analysis, and the remainder was evaporated under light nitrogen flow to determine the biocrude weight after a minimum of 24 h. Yields are expressed in dry ash free basis (eq 1).

$$Y_{\text{experiment}} = \frac{W_{\text{phase}}}{W_{\text{feed}}} \quad (1)$$

Synergy effects (SE) were determined according to eq 2

$$\text{synergy effect} = \frac{Y_{\text{experiment}}}{X_{\text{polymer}} Y_{\text{polymer}} + X_{\text{miscanthus}} Y_{\text{miscanthus}}} \quad (2)$$

where $Y_{\text{experiment}}$ represents the mass yield in g/g_{feed} of a certain phase (oil, gas, or solids; aqueous by difference), X is the fraction of material in the feedstock (0.5), and Y is the yield from experiments with pure polymers¹¹ from previous data published by the authors or pure miscanthus.

Elemental Analysis. Using an Elementar vario Macro Cube elemental analyzer (Langensfeld, Germany), carbon, hydrogen, nitrogen, and sulfur (oxygen by 100% difference) contents were determined for all raw materials (see Table S1), solid residues, and oil products in duplicate, average values are reported. High heating value (HHV) of the fractions analyzed was estimated by the Channiwal-Parikh correlation (eq 3).¹⁸ The energy yield in the oil phase of each experiment was calculated according to eq 4, while the carbon yield was derived from eq 5.

$$\text{HHV} \left[\frac{\text{MJ}}{\text{kg}} \right] = 0.3491 \text{ C} + 1.1783 \text{ H} + 0.1005 \text{ S} - 0.1034 \text{ O} - 0.0151 \text{ N} - 0.0211 \text{ A} \quad (3)$$

$$\text{energy yield (\%)} = \frac{\text{HHV}_{\text{oil}} \left[\frac{\text{MJ}}{\text{kg}_{\text{oil}}} \right] \cdot \text{yield}_{\text{oil}} \left[\frac{\text{kg}_{\text{oil}}}{\text{kg}_{\text{feed}}} \right]}{\text{HHV}_{\text{feed}} \left[\frac{\text{MJ}}{\text{kg}_{\text{feed}}} \right]} \times 100 \quad (4)$$

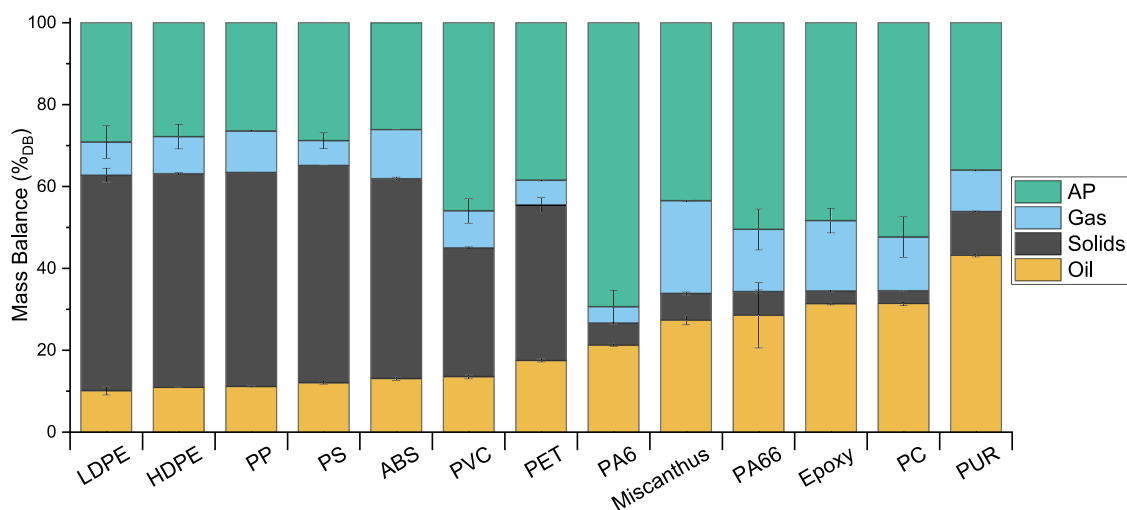


Figure 1. Mass balance of co-HTL of synthetic polymers and miscanthus (1:1 mixing ratio) [AP by difference].

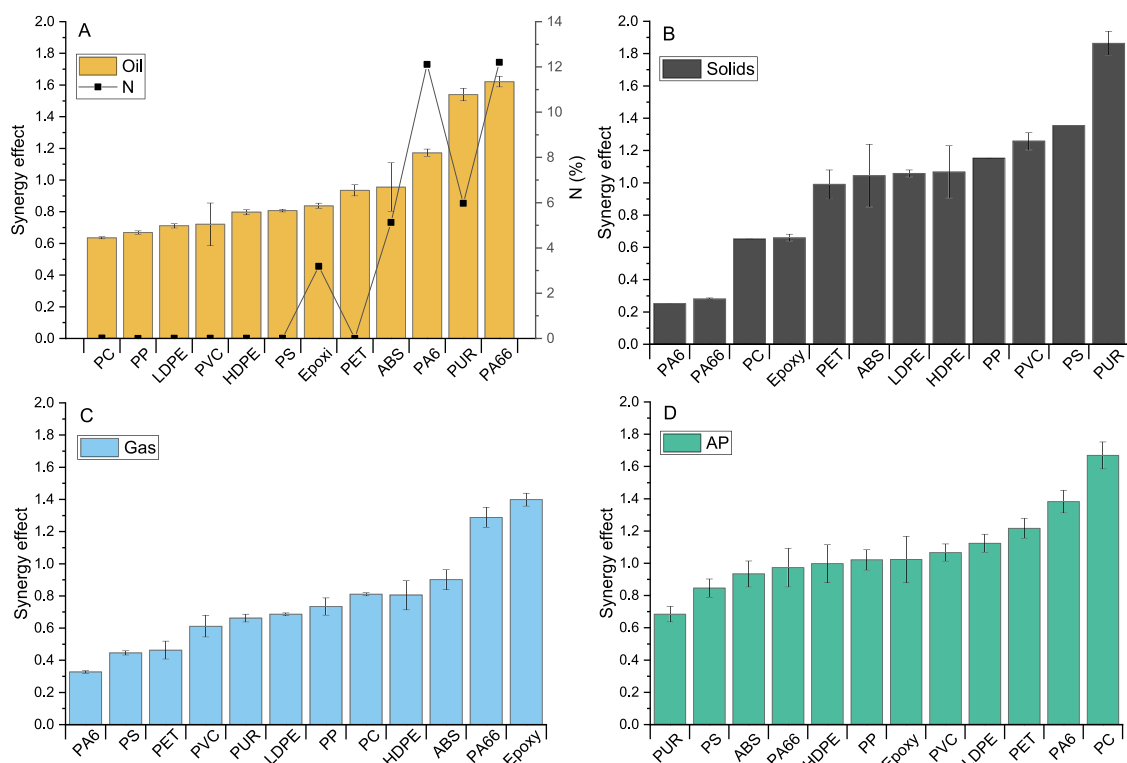


Figure 2. Weight yield-based synergy effects of synthetic polymers and miscanthus co-HTL (1:1 mixing ratio) for oil (A), solids (B), gas (C), and AP (D).

$$\text{carbon yield (\%)} = \frac{C_{\text{oil}} \left[\frac{\text{kg}_C}{\text{kg}_{\text{oil}}} \right] \cdot \text{yield}_{\text{oil}} \left[\frac{\text{kg}_{\text{oil}}}{\text{kg}_{\text{feed}}} \right]}{C_{\text{feed}} \left[\frac{\text{kg}_C}{\text{kg}_{\text{feed}}} \right]} \times 100 \quad (5)$$

GC–MS. An Agilent 7890B GC coupled to a quadrupole mass filter MS Agilent 5977A was used for all analyses. For oil analysis, the 1 mL methanol aliquot retrieved from the sample workup was diluted appropriately (from 1× to 8×), and the internal standard was added (4-bromotoluene) prior to direct injection (μL injection volume, inlet temperature of 280 °C, split ratio 20:1, helium flow 1 mL·min⁻¹). The GC column used was a VF-5ms column with dimensions 64.9 m × 0.25 mm × 0.25 μm , which experienced an oven temperature program initiated by 60 °C hold for 2 min, a ramp to 200 °C (5 °C·min⁻¹), another ramp to 320 °C (20 °C·min⁻¹), and a final hold of 5 min at

constant temperature. Compounds were identified with authentic standards, NIST17 mass spectra library, or based on literature references.

Equation 6 was used to estimate the change in oil composition of polymer and miscanthus blends in comparison to HTL of pure feedstock materials (pure miscanthus or pure polymer). $A_{i,\text{exp}}$ is the area of compound i identified in the GC–MS of a certain experiment (pure miscanthus, pure polymer, or blend), and it is used to discuss the change in oil composition and not the total conversion of the feedstock to a certain compound, as this would require complete quantification of each compound analyzed.

$$\frac{C_{i,\text{exp}}}{C_{i,\text{max}}} = \frac{A_{i,\text{exp}}}{A_{i,\text{max}}} \quad (6)$$

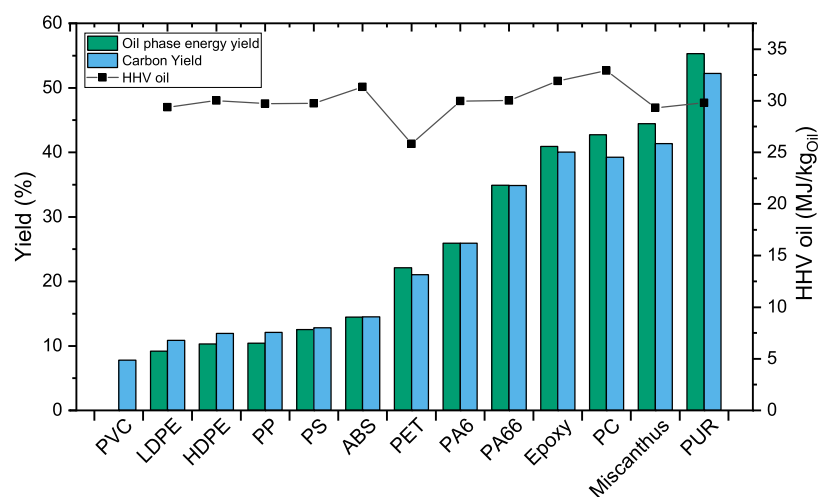


Figure 3. Oil-phase energy yield and HHV of synthetic polymers and miscanthus co-HTL (1:1 mixing ratio).

RESULTS AND DISCUSSION

Mass Balance. Figure 1 depicts the mass balance for all co-HTL experiments ordered by oil yield. Miscanthus' HTL is also included as reference for interpretation. Notably, oil yields vary from 10.1 to 43.2% for co-HTL of LDPE and PUR, respectively. Most co-HTL experiments show a significant decrease in the total oil yield, which is expected based on results previously published,¹¹ given most of them do not decompose into oil directly; namely, LDPE, HDPE, PP, PS, and ABS yield around 50% solid materials, essentially composed of unreacted or charred polymeric material and only about 10% oil. This indicates lack of depolymerization for the co-HTL conditions tested. As for PA66, epoxy, PC, and PUR, the oil yield improved, and generally, gas yields reduced, when compared to pure miscanthus HTL. It is noticeable that all polymers containing a significant amount of nitrogen in the form of amines are located on the right side of Figure 1, while ABS, which contains nitrogen in the form of nitrile, appears toward the left side, together with polyolefins and PS.

PC is the only material that does not contain nitrogen and is located on the right side of Figure 1. HTL of PC alone has shown the highest oil yield among all individual polymers tested at the same condition,¹¹ which can be the reason for its position among the highest oil yields of co-HTL as well. The mass balance shown in Figure 1 does not provide the information whether the co-liquefaction results in positive or negative synergies compared to what could be expected from their individual processing. Hence, mass yield synergy effects are depicted in Figure 2 to improve the understanding of all co-HTL experiments.

Synergy Effects. The co-liquefaction synergy effects, based on previously published data¹¹ and the data of this study, shown in Figure 2A–D depict several deviations from predicted results, demonstrating that products of miscanthus and synthetic polymers interact significantly during HTL processing. Figure 2A also depicts the nitrogen content of the raw synthetic polymer, showing a clear correlation between nitrogen presence and oil yield synergy effect. Polymers containing a larger amount of nitrogen tend to have positive synergy effects (>1, e.g., PUR at 1.54 and PA66 at 1.62), as nitrogen-containing organic molecules and ammonia under hydrothermal conditions act as catalysts of oil formation.¹⁹ Surprisingly, PC depicted the lowest synergy effect for oil

among all polymers tested, with a negative synergy of 0.63. This indicates that the products of PC HTL (mainly composed of bisphenol-A, *p*-isopropenyl phenol, and phenol¹¹) are reactive toward miscanthus-derived biocrude, yielding subsequent water-soluble compounds, evident from the large synergy of 1.65 for the aqueous yield (Figure 2D). PA6, PUR, and PA66 present the highest oil synergy effect while also having the highest nitrogen content among all polymers tested. PUR, however, presents a higher synergy effect than PA6, indicating that nitrogen is not the only factor interfering in oil formation for these materials. It is thus clear that even though nitrogen-containing polymers show a better chance to favor oil formation in the presence of miscanthus, the chemical characteristics of these materials play an important role in the result.

Figure 2B shows the synergy effects for solids. Antagonistic effects ($SE < 1$) for solids are observed for PA6, PA66, and epoxy, all feedstock materials depicting nitrogen concentrations higher than 4%, following the expectation of increased reactivity by ammonia formation. PC also has a similar antagonistic effect for solid formation as epoxy (its thermosetting counterpart), even though it does not contain significant amounts of nitrogen, which again shows that the nitrogen content is not the only parameter affecting the reactions. PUR showed the highest solid synergy effect among all polymers tested, with a total solid yield of 10.7% for the co-liquefaction experiment (Figure 1), despite containing significant amounts of nitrogen. Given these observations, it can be concluded that the chemical reactivity of nitrogen (determined by its conformation in the synthetic polymer) is more important than the presence of nitrogen for the synergistic effects observed. PVC does not exhibit the highest synergy effect on solid yield, which could be expected due to acidification of the media by HCl formation and consequent carbonization.^{11,20} Despite PVC showing a positive solid synergy effect, PS and PUR are more prone to increase the solid content upon interaction.

Figure 2C shows the gas-phase synergy effects, which are generally negative (<1) for most polymers, being positive only for PA66 and epoxy. PA6 and PA66 differ in gas synergy effect by 0.96, the former depicting an antagonistic effect and the latter synergistic, which may be related to differences in nitrogen reactivity depending on the type of molecular

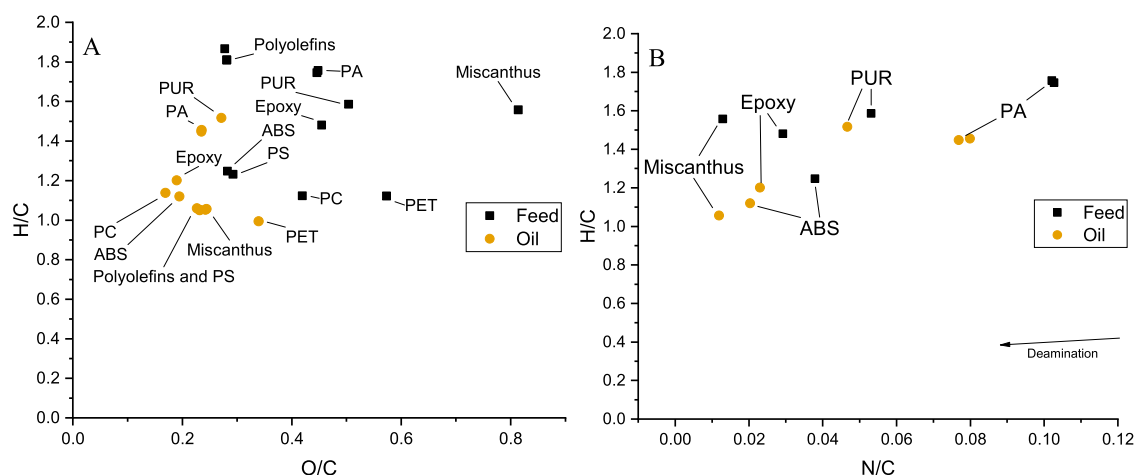


Figure 4. H/C–O/C (A) and H/C–N/C (B) van Krevelen diagrams of synthetic polymers and miscanthus co-HTL (1:1 mixing ratio feed and oil product) (PA6 and PA66 label as PA).

structure.¹⁹ PA6 HTL yields mainly secondary amides, while PA66 results in amines and amides.¹¹ It is possible that the higher reactivity of the latter results in an increase of gas yield via interactions with miscanthus-derived components. PA66 and epoxy are the only co-HTL experiments with positive synergy effects for gas yields (PA66 and epoxy), both containing amines as single-polymer HTL products.¹¹

PET has a negative synergy effect for gas formation (Figure 2C), which indicates that the carboxyl groups present in biomass prone to gas formation tend to recombine into other products in the presence of PET. This can also be verified in Figure 4A, where PET oil is depicted having a higher O/C in comparison to pure miscanthus oil, which indicates an oil containing more carboxyl groups.

Figure 2D depicts the synergy effects for AP yield, which for most polymers is neutral. PUR shows a negative effect, and PET, PA6, and PC show a positive synergy effect. The negative synergy effect for PUR AP and gas products indicates migration of the products to oil and solid phases, both having pronounced positive synergy effects. As PET only presents deviation from neutral synergy in the gas phase, being negative, and in the AP, being positive, the data indicates that PET products (mainly composed of terephthalic acid and ethylene glycol¹¹) tend to release less carbon in the form of CO₂ when miscanthus products are present in the media, giving preference for AP yields.

Oil Yields and Atomic Composition. Figure 3 shows the oil energy yield, oil carbon yield, and HHV for all experiments, plotted in an ascending order. The HHV of PVC was not calculated, as oxygen content was determined by difference, and in PVC samples the difference is composed of both chlorine and oxygen. The figure shows that both oil energy and carbon yields have a very similar trend, ranging from 9.2% (LDPE co-HTL) to 55.3% (PUR co-HTL) and from 7.8% (PVC co-HTL) to 52.2% (PUR co-HTL), respectively. The HHV for miscanthus biocrude was calculated to be 29.3 MJ/kg. Among the co-HTL oils, LDPE, HDPE, PP, PS, PA6, PA66, and PUR are within 2.5% of the miscanthus biocrude HHV, while ABS, epoxy, and PC present values increased by 6.9, 8.8, and 12.3%, respectively. PET HHV is the only co-HTL oil to present a lower HHV than miscanthus biocrude, being 12.0% lower. PUR is the only synthetic polymer in co-HTL that increases oil energy and carbon yields in comparison

to pure miscanthus HTL. This effect is observed not only because this polymer has one of the highest synergy effects for oil formation (Figure 2A) but also due to an increase in H/C ratio (see Figure 4A). It is also possible to see that PC and epoxy are positioned side by side, with very similar energy and carbon yields to miscanthus, but higher HHV for both. The similar molecular structures of these two materials (see Table S1) result in similar HHV and energy yield in co-HTL, indicating that the overall interactions among lignocellulosic- and PC-like-derived biocrude are equivalent, even though synergy effects for the different product streams differ greatly (Figure 2A–D).

All polyolefins, PS, and ABS depict very low energy and carbon yields due to the increase of both HHV_{feed} and C_{feed} without a reciprocal increase in co-HTL oil yield (see eqs 4 and 5 as reference). ABS has a higher HHV than other products due to lower O/C (Figure 4A), which can be linked to the appearance of aromatic-like compounds in the oil composition (presented in the Composition of Co-HTL Oils section).

The already discussed increase of O/C ratio in PET co-HTL oil is the reason for its HHV being lower than pure miscanthus biocrude, which also contributes to lower energy yield in comparison to other polymers. In the literature, PET co-HTL with pistachio hulls (10–20% w/w PET in feed) has been reported to increase both oil-phase energy yield and HHV;¹⁴ however, our observations with miscanthus co-HTL show the opposite, indicating that feed composition can be optimized.

Co-HTL of PA6 gives a lower energy yield than PA66, even though both biocrudes have equal HHV. The difference in oil synergy effects of PA6 and PA66 components with miscanthus biocrude indicates that primary amines from PA66¹¹ tend to contribute to oil-phase compounds, increasing the energy yield while maintaining the H/C, O/C, and N/C ratios very similar (see Figure 4), resulting in a similar HHV for both.

Figure 4A shows the van Krevelen diagrams (H/C versus O/C) for all oil and feedstock samples, while Figure 4B shows the H/C versus N/C data for experiments with a significant amount of nitrogen in the feed composition. The polymer feed ratios plotted in the graph are based on a 1:1 mixture of polymer with miscanthus. When comparing the co-HTL feed mixture with pure miscanthus, it is possible to see that O/C and H/C ratios are very similar for all polyolefins and PS,

indicating little contribution of the synthetic materials to biocrude formation. As for H/C ratios, PUR, PA6, and PA66 (labeled as PA in Figure 4 as points are too close to one another) have higher values than pure miscanthus, while PC, ABS, and epoxy also have higher values, though less pronounced.

With miscanthus biocrude as reference, it is possible to observe that PET is the only co-HTL oil product that gives both an increase in O/C ratio and a slight decrease in H/C ratio, which indicates that PET products of HTL tend to carry a large portion of oxygen into the oil phase in co-HTL with miscanthus. This conclusion is in agreement with the HHV observations previously discussed. Polyolefins and PS seem not to interfere in H/C and O/C ratios, which is not surprising, as they do not contribute to oil formation. ABS, PC, and epoxy show a decrease in O/C and an increase in H/C slightly. Both PA and PUR maintain the same O/C while increasing H/C compared to pure miscanthus biocrude. These observations, in combination with the results of oil-phase synergy effects (Figure 2), show that not only oil yields are increased but their quality regarding H/C is also improved.

Figure 4B shows only experiments involving nitrogen-containing synthetic polymers. It is possible to observe a decrease in N/C ratio for all oil products when compared to the original co-HTL feed. Generally, the higher the feed N/C ratio, the higher is the oil product N/C ratio. This does not occur when comparing epoxy to ABS. This last observation may be attributed to the type of nitrogen group present in both raw materials, the former being a secondary or tertiary amine and the latter being a nitrile group. It seems, thus, that nitrogen in the form of nitrile groups is not as prone as amines to migrate to biocrude in co-HTL with lignocellulosics. This observation follows the lack of reactivity of ABS when processed via HTL by itself.¹¹

The N/C ratios of PUR and PA oils (Figure 4B) are closer to those of their respective feeds than to pure miscanthus biocrude. This indicates the high efficiency of transfer of nitrogen from feedstock to biocrude during co-HTL. In Figure 2A, PUR and PA oil-phase positive synergy effects are prominent; thus, it seems that nitrogen in the form of amines contributes to oil yield increase, possibly participating in the formation of more hydrophobic products partitioning to the oil phase.

This observation is corroborated with results indicating the increase of oil yield for the co-HTL of nitrogen-containing biomass and low-nitrogen lignocellulosics.^{7–10,21} Previous results show that co-HTL of different lignocellulosics—including miscanthus—with sewage sludge, manure, or algae has the effect of improving biocrude yields.^{10,22} Similar effect has been observed with co-HTL of algae and wood.²³ Lignin and *Spirulina platensis* co-HTL using a feed ratio of 2:1 also results in positive synergy effects for oil yield,⁸ as well as *Enteromorpha clathrata* and rice husk.⁷ In another study using model compound mixtures, all protein-containing co-HTL processes with cellulose or lignin-derived materials showed higher biocrude yields than expected.²¹ In all literature examples, biomasses containing a significant amount of nitrogen in the form of amines result in an increase of biocrude yield. The present study reports for the first time similar findings for synthetic polymers. However, two of the materials studied here are examples of nitrogen-containing polymers that do not result in significant positive synergy effects for oil formation: ABS and epoxy. Both also do not

contain nitrogen in the form of primary or secondary amines but rather as nitrile groups or tertiary amines. Thus, the chemical conformation of nitrogen is important for synergy effects to be positive in co-HTL processing of lignocellulosics and nitrogen-containing materials, with higher synergy effects for oil formation occurring in the presence of nitrogen in the form of secondary or primary amines in the oil phase.

Composition of Co-HTL Oils. The changes in relative concentration of specific compounds measured by GC–MS can help understand how the composition of the volatile fraction of biocrude changes according to the feedstock used. It is worth noting that the following section does not refer to the amount of a certain compound that can be recovered from a certain blend, rather it explores how concentrations of compounds change in the presence of synthetic and lignocellulosic materials. For a better understanding, the following sections are grouped according to the similarity of the synthetic polymers used in co-HTL experiments.

LDPE, HDPE, PP, PS, and ABS. Figure S1 shows that selected methoxylated compounds are found at higher concentrations when miscanthus is co-liquefied with polyolefins. At the same time, Figure S2 shows that *o*-methoxyphenols relative concentrations are not changed, while alkyl *o*- and *p*-phenolics are increased when HTL takes place in the presence of polyolefins. This indicates that the presence of polyolefins favors the formation of alkyl phenols, though it does not interfere significantly in the formation of methoxyphenols. This observation points out that alkyl groups are more prone to be added to phenolic structures derived from lignocellulosic biocrude when polyolefins are present in HTL media. Table S2 depicts that even though phenolics are still the major components found in co-HTL of HDPE and LDPE, ethers and acids become more prominent for those in comparison to pure miscanthus biocrude. The same data for PP shows a high prominence of tetrahydrofuran (21.46%) together with aromatic compounds (e.g., 1,2,3-trimethoxy-5-methyl-benzene, 1.91%; 7-methoxy-1-naphthol, 1.60%). PP and pistachio hulls co-HTL has been described to change the bio-oil composition significantly,²⁴ however, not specifically identifying the compounds involved in this change. The observations above indicate that the compounds formed in co-HTL of PP are more likely to change the composition of the biocrude in comparison to HDPE and LDPE.

PS and ABS also do not significantly affect biocrude yields, though the presence of phenolics in the product is increased (except for 2-methoxy-phenol), together with several different single-substituted aromatics (see Figures S3 and S4). For all five polymers (LDPE, HDPE, PP, PS, and ABS) meta-alkyl-substituted compounds were not present. This is directly linked to the reactivity of phenolic compounds derived from lignocellulosic biomass, which gives preference for ortho and para alkyl substitutions.²⁵ The GC–MS area-based composition of biocrude from co-HTL of ABS shows a high presence of styrene, ethyl benzene, and benzene-butanenitrile, structures very similar to the monomers of ABS (Tables S1 and S2). For PS, Table S2 shows a distinct presence of 3-(2-cyclopentenyl)-2-methyl-1,1-diphenyl-1-propene and similar isomers, also to a lesser extent of styrene, ethyl benzene, and other polyaromatics. The presence of these compounds with a similar structure in comparison to the monomers of the synthetic resins used in co-HTL is interesting for the valorization of biocrude as a source not only of fuels but possibly as a source of platform chemicals.

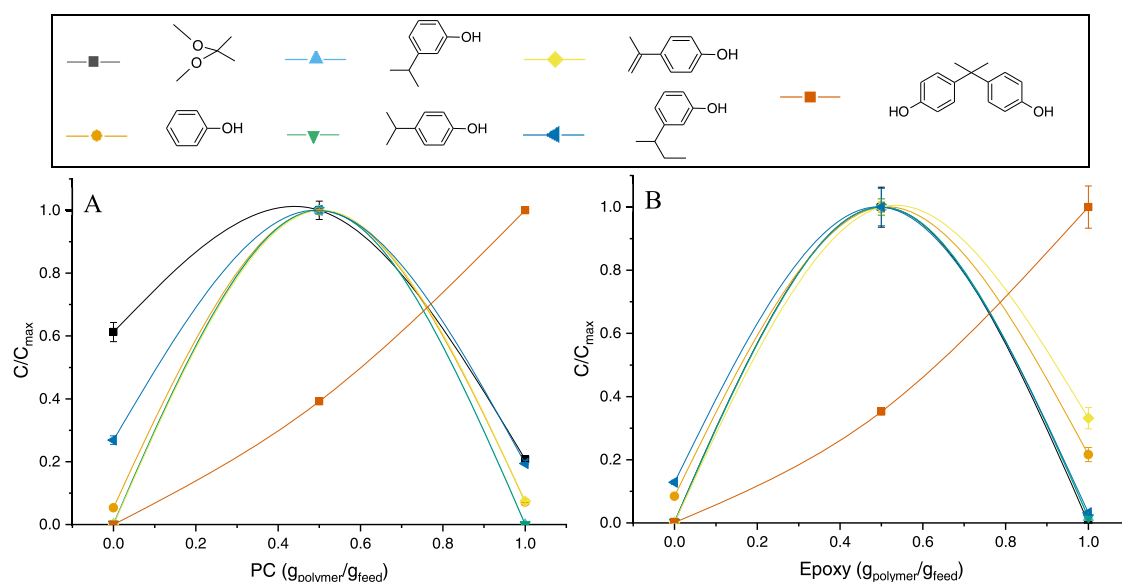


Figure 5. Relative concentration change in PC (A) and epoxy (B) co-HTL oil for selected compounds (—■—, 2,2-dimethoxy-propane; —●—, phenol; —▲—, 2-(1-methylethyl)-phenol; —▼—, 3-(1-methylethyl)-phenol; —◀—, 3-(1-methylpropyl)-phenol; —■—, 4,4'-(propane-2,2-diyl)diphenol).

The observations above indicate that synthetic resins without backbone heteroatoms affect the quality of miscanthus biocrude, despite not depolymerizing into oil products under these conditions, corroborating the van Krevelen diagram findings discussed previously (Figure 4). This change in quality occurs mainly due to the addition of alkyl groups in biocrude volatile molecules. The occurrence of such alkyl groups in the backbone of the polyolefins co-processed creates a potential opportunity for biocrude quality improvement with this co-HTL strategy despite the lack of oil yield increase.

PVC. Comparison of PVC co-HTL-derived oil with miscanthus biocrude (Table S2) shows a remarkably higher presence of carboxylic acids, aromatics, and polyaromatics. This is expected based on acid-catalyzed reactions in lignocellulosic biomass HTL. Chlorine released from the polymer side group hydrolyzes into HCl, acidifying the media and promoting dehydration reactions of the phenolic compounds, yielding aromatics. For PVC, hydrothermal processing instead yields a Cl poor solid phase, concentrating much of the chlorine into the aqueous phase.²⁰ Low-temperature hydrothermal co-processing of PVC and lignocellulosic biomass has been proven to be an effective method for dechlorination.²⁰ Higher subcritical temperatures, such as that tested in this study (350 °C), do not provide advantages regarding the generation of a valuable oil phase.

PC and Epoxy. The co-HTL oils produced from PC and epoxy have very similar trends, as shown in Figure 5. The concentration comparison shows very clearly that phenolic compounds are more prominent in co-HTL oil than in miscanthus or synthetic polymers alone. Phenolic compounds have partial solubility in water and are formed from HTL of both pure PC and epoxy, which indicates that these are attracted to biocrude (a nonpolar phase) when present in the reaction media, increasing the oil quality. The observation can also indicate that co-processing favors these compounds. The improvement in oil quality by co-processing is also depicted in Figure 4A by the decrease of O/C ratio in comparison to pure miscanthus HTL biocrude.

4,4'-(Propane-2,2-diyl)diphenol (bisphenol-A) follows the opposite curve, indicating a lower concentration than that expected upon co-HTL. This fact partially explains the higher concentration of the other compounds, which are direct byproducts of bisphenol-A cracking or hydrolysis. Even though this is the case, it cannot fully explain the significant concentration increase of the other compounds, which may result from the rearrangement of both miscanthus and PC (or epoxy) components. We suggest two possible pathways to explain this observation. First, it is possible that bisphenol-A is relatively stable toward the media; thus, the increase in the presence of other compounds is due to rearrangements involving products of both feedstock materials. Another possibility is that oligomers yielded from PC and epoxy HTL are more easily converted into bisphenol-A in the presence of miscanthus HTL products, compensating the consumption of this compound in the formation of byproducts and keeping concentrations proportional. The latter option follows chemical equilibrium principles, and recently published kinetics²⁶ suggests that bisphenol-A is present in a high concentration around 20 min reaction time; thus, the hypothesis explains the increase in byproducts of bisphenol-A hydrolysis.

PET. PET co-HTL experiments yield an oil richer in phenols, ketones, and carboxylic acids (Figure S5). The terephthalic acid from the synthetic resin seems to contribute to this formation; however, only a minor part of this component has reacted into different products, as its majority is present in the solid products and PET synergy effect for this phase is neutral (Figure 2). A significant conversion of terephthalic acid into oil components would be indicated by a negative synergy effect on solids, which is not the case.

The second major product of PET HTL is located primarily in the aqueous phase,¹¹ ethylene glycol. However, it is also partially found in the oil phase due to partitioning. It appears not to interact with the products of miscanthus liquefaction, as shown in Figure S5. The lack of reactivity of ethylene glycol toward lignocellulosic products of HTL has been reported before.²⁷ However, PET co-HTL oil has a very different

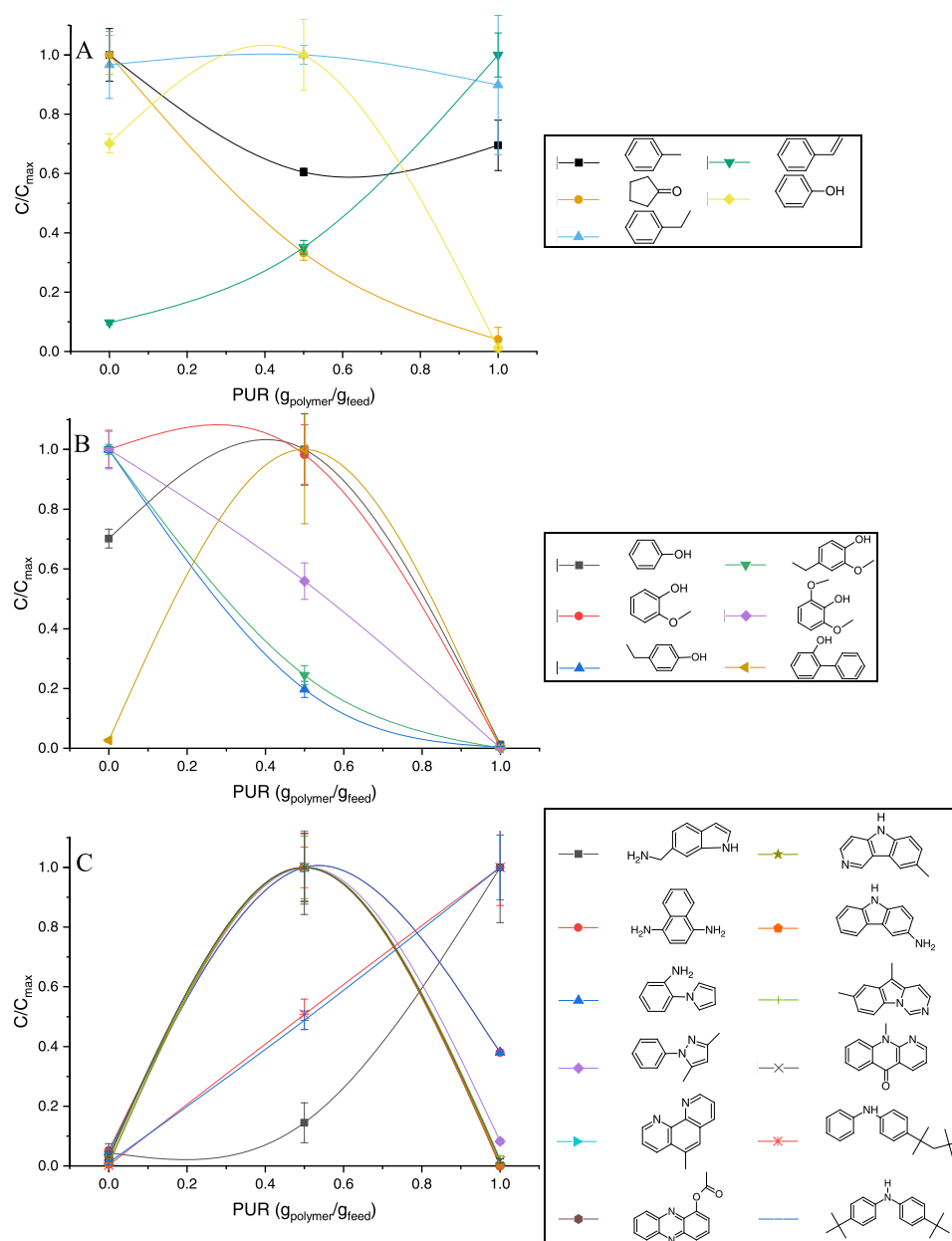


Figure 6. Relative concentration change in PUR co-HTL oil for selected aromatic (A), phenolic (B), and nitrogenated (C) compounds. ((A) → —■—: toluene; —●—: cyclopentanone; —▲—: ethyl benzene; —▼—: styrene; —◆—: phenol); ((B) → —■—: phenol; —●—: 2-methoxy-phenol; —▲—: 4-ethyl-phenol; —▼—: 4-ethyl-2-methoxy-phenol; —◆—: 2,6-dimethoxy-phenol; —◆—: *o*-hydroxybiphenyl); ((C) → —■—: 1H-indol-6-ylmethanamine; —●—: 1,4-naphthalenediamine; —▲—: 1-(2-aminophenyl)pyrrole; —◆—: 3,5-dimethyl-1-phenyl-1H-pyrazole; —▼—: 5-methyl-1,10-phenanthroline; —●—: acetate (ester) 1-phenazinol; —◆—: 8-methyl-5H-pyrido[4,3-*b*]indole; —●—: 3-aminocarbazole; —◆—: 5,7-dimethylpyrimido-[3,4-*a*]indole; —×—: 10-methyl-benzo[*b*]-1,8-naphthyridin-5(10H)-one; —*—: *tert*-octyldiphenylamine; — —: 4,4'-di-*tert*-butyl-diphenylamine).

volatile composition, as shown in Table S2. Here, we can observe a more pronounced presence of acids, methoxy- and carboxyl-containing compounds. This is in agreement with the findings of Figure 4. Despite lowering the energy content in the oil phase, such compounds may be of use for direct applications, being more valuable than their energy use.

PA6 and PA66. Besides resulting in an increased oil yield, both PA6 and PA66 also change the oil composition significantly (see Figures S6 and S7). On the one hand, the presence of PA6 increases the concentration of cycloketones and mono-substituted phenols while not changing double-substituted phenols. Given PA6 products of HTL are mostly composed of amines,¹¹ it is unlikely that those would form

phenolic or cyclic compounds without the presence of nitrogen in the composition if known mechanisms are followed.²⁵ Thus, it seems the media provides a better chance for the miscanthus-derived compounds to react into phenolics that are incorporated into the oil phase. On the other hand, PA66 seems to have the opposite effect for 2-methyl-2-cyclopenten-1-one and mono-substituted phenols. Even so, PA66 still promotes positive oil synergies and superior carbon yield when compared to PA6. This could be derived from larger compounds being formed from PA66- and miscanthus-derived compounds in comparison to PA6.

Table S2 provides the comparison between miscanthus biocrude and the co-HTL oil composition of PA6 and PA66.

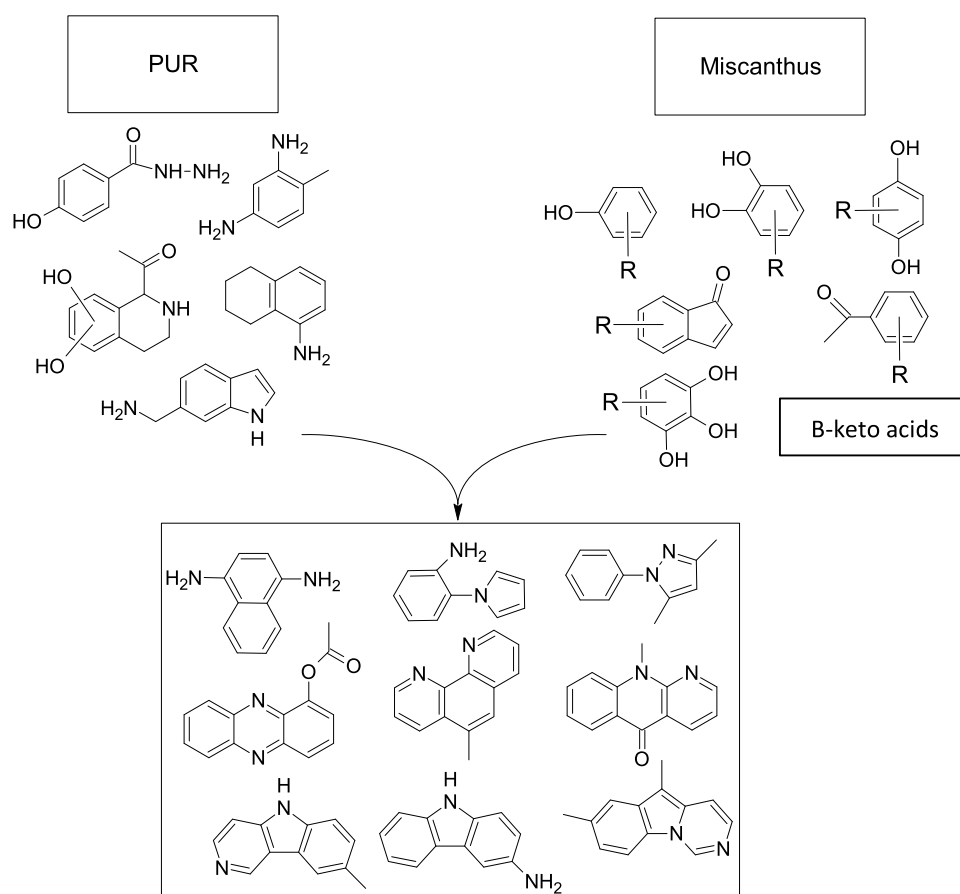


Figure 7. Reaction scheme for PUR- and miscanthus-derived HTL products.

The PA-derived oils contain significantly more compounds with nitrogen, including the dimer 1,8-diazacyclotetradecane-2,7-dione, clearly derived from PA structures. Hexadecanoic acid, which is one of the monomers for PA66 production, is also present in these samples. Given the composition of volatiles in the oil, it is possible to assert that the biocrude of co-HTL with PA is rich in monomer-like compounds that can possibly be recovered through co-HTL.

PUR. PUR co-HTL with miscanthus had the most promising oil synergistic effect identified, being the only combination to increase both energy and carbon yields. The GC–MS discussion will try to suggest the reasons behind the superior yields. Figure 6 depicts the concentration changes for selected compounds measured by GC–MS. It is possible to observe in Figure 6A a similar concentration for ethyl benzene in all experiments, also only modest deviations for cyclopentanone and styrene. Cyclopentanone presents the highest concentration in miscanthus HTL, while styrene in pure PUR, though both have slightly lower concentrations than that expected in the co-HTL oil. On the other hand, phenol seems to be more prevalent in the co-HTL than in the single HTL oil.

Figure 6B depicts changes in concentration of phenolics. Despite the presence of phenol being favored in co-HTL, followed by *o*-hydroxybiphenyl and, to a less extent, 2-methoxy-phenol, di-substituted phenols (4-ethyl-phenol and 4-ethyl-2-methoxy-phenol) have the opposite behavior. The tri-substituted 2,6-dimethoxy-phenol seems to be present proportionally in the co-HTL oil (around 0.5 in Figure 6B). Figure 6C depicts a group of compounds found with relatively small areas (the highest being 6.1% for 8-methyl-5H-pyrido[4,3-

b]indole—see Table S2), however, in great abundance. These compounds are all heterocyclic aromatic containing nitrogen within the rings and all seem to be formed only in the presence of both PUR and miscanthus.

Table S2 also shows that the presence of 5 heterocyclic nitrogen-containing aromatics within the 20 most prominent identified compounds is the major difference between PUR co-HTL oil and miscanthus. The presence of such compounds indicates that the positive synergies and higher yields discussed before are connected to the reaction between PUR- and miscanthus-derived compounds, yielding this class of chemicals. Interestingly, Table S2 also shows that there are none of such compounds found within the 20 most prominent for all other nitrogen-containing tested materials (namely PA6, PA66, epoxy, and ABS).

It is possible to observe by the nucleophilic reactivity of amines²⁸ and amides²⁹ that aromatic compounds with amine side groups are much more prone to react with phenolic compounds than organic molecules containing amides or nitriles. The latter two are the form of nitrogen present in the HTL products of PA6, PA66, epoxy, and ABS, while the former is present in PUR.¹¹ This observation corroborates the discussion around Figure 2A, pointing toward the nature of the nitrogen-containing compounds being responsible for oil synergies. Figure 7 depicts a reaction scheme for PUR- with lignocellulosic-derived compounds, yielding products due to nucleophilic combinations, which is corroborated by other hypotheses previously described.²⁵ This is the first time nitrogen compounds from synthetic polymers are observed to be having a behavior similar to proteins in HTL conditions

and interacting significantly with lignocellulosic-derived compounds. However, in the case of PUR, the oil formation effect is more pronounced due to the reactivity of the nitrogen species involved.

CONCLUSIONS

Co-HTL of 12 different polymers with miscanthus resulted in different synergy effects and yields depending on the original synthetic polymers' chemical structures. A summary of the observations made through the present study is presented below:

- Positive oil yield synergy effects were observed from co-HTL of PA6, PA66, and PUR with miscanthus.
- Only PUR co-HTL with miscanthus increased carbon and energy oil yields when compared to single HTL of miscanthus. PC and epoxy maintained equivalent carbon and energy yields in the same comparison, while all other polymers showed a decrease in both parameters.
- HHVs of co-HTL oils from LDPE, HDPE, PP, PS, PA6, PA66, and PUR are within 2.5% of the miscanthus biocrude. ABS, epoxy, and PC, on the other hand, present increased values by 6.9, 8.8 and 12.3% respectively. PET HHV is 12.0% lower than miscanthus biocrude, due to the presence of more oxygenated molecules.
- ABS, despite having a small synergistic effect, changed significantly the oil composition, increasing the biocrude quality, even though the transfer of degradation products of these materials to the oil phase is limited.
- PVC promotes severe carbonization reactions and the resulting acidic media leads to the formation of aromatics and polyaromatics in the oil phase.
- PC and epoxy co-HTL yields an oil rich in monomer-like structures of the original materials.
- PA6 and PA66 co-HTL oil is rich in nitrogen and contains monomer-like structures, however to a lower extent.
- The type of nitrogen group in the synthetic polymer dictates the synergy effects. Amines connected to aromatics are more prone to recombine with lignocellulosic biocrude than alkyl amines, amides, and nitriles. PUR, PA6, PA66, and ABS co-HTL synergies and oil compositions illustrate the findings.

ASSOCIATED CONTENT

Supporting Information

The Supporting Information is available free of charge at <https://pubs.acs.org/doi/10.1021/acssuschemeng.0c07317>.

Reference chemical structure and elemental analysis of synthetic polymers used; relative concentration changes of selected compounds in HDPE, LDPE, PP, ABS, PS, PET, PA6 and PA66; and relative composition of oil phase characterized via GC/MS for all co-HTL experiments and *Miscanthus giganteus* (PDF)

AUTHOR INFORMATION

Corresponding Author

Patrick Biller – Biological and Chemical Engineering, Aarhus University, DK-8200 Aarhus N, Denmark; Aarhus University Centre for Circular Bioeconomy, DK-8830 Tjele, Denmark;

orcid.org/0000-0003-2982-6095; Email: pbiller@eng.au.dk

Authors

Juliano Souza dos Passos – Biological and Chemical Engineering, Aarhus University, DK-8200 Aarhus N, Denmark; Aarhus University Centre for Circular Bioeconomy, DK-8830 Tjele, Denmark; orcid.org/0000-0001-5345-3669

Marianne Glasius – Department of Chemistry, Aarhus University, DK-8000 Aarhus C, Denmark; Aarhus University Centre for Circular Bioeconomy, DK-8830 Tjele, Denmark; orcid.org/0000-0002-4404-6989

Complete contact information is available at: <https://pubs.acs.org/10.1021/acssuschemeng.0c07317>

Notes

The authors declare no competing financial interest.

ACKNOWLEDGMENTS

This project has received funding from the European Union's Horizon 2020 research and innovation grant agreement No. 764734 (HyFlexFuel – Hydrothermal Liquefaction: enhanced performance and feedstock flexibility for efficient biofuel production) and the Aarhus University Centre for Circular Bioeconomy (CBIO).

REFERENCES

- (1) Geyer, R.; Jambeck, J. R.; Law, K. L. Production, Use, and Fate of All Plastics Ever Made. *Sci. Adv.* **2017**, *3*, No. e1700782.
- (2) Lebreton, L.; Andrady, A. Future Scenarios of Global Plastic Waste Generation and Disposal. *Palgrave Commun.* **2019**, *5*, No. 6.
- (3) Brunner, G. *Hydrothermal and Supercritical Water Processes*; Elsevier B.V.: Hamburg, Germany, 2014; Vol. 5.
- (4) Zheng, J. L.; Zhu, M. Q.; Wu, H. Alkaline Hydrothermal Liquefaction of Swine Carcasses to Bio-Oil. *Waste Manage.* **2015**, *43*, 230–238.
- (5) Thomsen, L. B. S.; Carvalho, P. N.; dos Passos, J. S.; Anastasakis, K.; Bester, K.; Biller, P. Hydrothermal Liquefaction of Sewage Sludge; Energy Considerations and Fate of Micropollutants during Pilot Scale Processing. *Water Res.* **2020**, *183*, No. 116101.
- (6) Biller, P.; Ross, A. B. Potential Yields and Properties of Oil from the Hydrothermal Liquefaction of Microalgae with Different Biochemical Content. *Bioresour. Technol.* **2011**, *102*, 215–225.
- (7) Yuan, C.; Wang, S.; Cao, B.; Hu, Y.; Abomohra, A. E. F.; Wang, Q.; Qian, L.; Liu, L.; Liu, X.; He, Z.; et al. Optimization of Hydrothermal Co-Liquefaction of Seaweeds with Lignocellulosic Biomass: Merging 2nd and 3rd Generation Feedstocks for Enhanced Bio-Oil Production. *Energy* **2019**, *173*, 413–422.
- (8) He, Z.; Wang, B.; Zhang, B.; Feng, H.; Kandasamy, S.; Chen, H. Synergistic Effect of Hydrothermal Co-Liquefaction of *Spirulina Platensis* and Lignin: Optimization of Operating Parameters by Response Surface Methodology. *Energy* **2020**, *201*, No. 117550.
- (9) Saba, A.; Lopez, B.; Lynam, J. G.; Reza, M. T. Hydrothermal Liquefaction of Loblolly Pine: Effects of Various Wastes on Produced Biocrude. *ACS Omega* **2018**, *3*, 3051–3059.
- (10) Biller, P.; Johannsen, I.; dos Passos, J. S.; Ottosen, L. D. M. Primary Sewage Sludge Filtration Using Biomass Filter Aids and Subsequent Hydrothermal Co-Liquefaction. *Water Res.* **2018**, *130*, 58–68.
- (11) dos Passos, J. S.; Glasius, M.; Biller, P. Screening of Common Synthetic Polymers for Depolymerization by Subcritical Hydrothermal Liquefaction. *Process Saf. Environ. Prot.* **2020**, *139*, 371–379.
- (12) Wang, B.; Huang, Y.; Zhang, J. Hydrothermal Liquefaction of Lignite, Wheat Straw and Plastic Waste in Sub-Critical Water for Oil: Product Distribution. *J. Anal. Appl. Pyrolysis* **2014**, *110*, 382–389.

- (13) Jayakishan, B.; Nagarajan, G.; Arun, J. Co-Thermal Liquefaction of *Prosopis juliflora* Biomass with Paint Sludge for Liquid Hydrocarbons Production. *Bioresour. Technol.* **2019**, *283*, 303–307.
- (14) Hongthong, S.; Raikova, S.; Leese, H. S.; Chuck, C. J. Co-Processing of Common Plastics with Pistachio Hulls via Hydrothermal Liquefaction. *Waste Manage.* **2020**, *102*, 351–361.
- (15) Anastakis, K.; Biller, P.; Madsen, R. B.; Glasius, M.; Johannsen, I. Continuous Hydrothermal Liquefaction of Biomass in a Novel Pilot Plant with Heat Recovery and Hydraulic Oscillation. *Energies* **2018**, *11*, No. 2695.
- (16) Castello, D.; Pedersen, T. H.; Rosendahl, L. A. Continuous Hydrothermal Liquefaction of Biomass: A Critical Review. *Energies* **2018**, *11*, No. 3165.
- (17) Biller, P.; Madsen, R. B.; Klemmer, M.; Becker, J.; Iversen, B. B.; Glasius, M. Effect of Hydrothermal Liquefaction Aqueous Phase Recycling on Bio-Crude Yields and Composition. *Bioresour. Technol.* **2016**, *220*, 190–199.
- (18) Channiwal, S. A.; Parikh, P. P. A Unified Correlation for Estimating HHV of Solid, Liquid and Gaseous Fuels. *Fuel* **2002**, *81*, 1051–1063.
- (19) Lu, J.; Li, H.; Zhang, Y.; Liu, Z. Nitrogen Migration and Transformation during Hydrothermal Liquefaction of Livestock Manures. *ACS Sustainable Chem. Eng.* **2018**, *6*, 13570–13578.
- (20) Huang, N.; Zhao, P.; Ghosh, S.; Fedyukhin, A. Co-Hydrothermal Carbonization of Polyvinyl Chloride and Moist Biomass to Remove Chlorine and Inorganics for Clean Fuel Production. *Appl. Energy* **2019**, *240*, 882–892.
- (21) Lu, J.; Liu, Z.; Zhang, Y.; Savage, P. E. Synergistic and Antagonistic Interactions during Hydrothermal Liquefaction of Soybean Oil, Soy Protein, Cellulose, Xylose, and Lignin. *ACS Sustainable Chem. Eng.* **2018**, *6*, 14501–14509.
- (22) Zhu, Y.; Jones, S. B.; Schmidt, A. J.; Billing, J. M.; Santosa, D. M.; Anderson, D. B. Economic Impacts of Feeding Microalgae/Wood Blends to Hydrothermal Liquefaction and Upgrading Systems. *Algal Res.* **2020**, *51*, No. 102053.
- (23) Jarvis, J. M.; Billing, J. M.; Corilo, Y. E.; Schmidt, A. J.; Hallen, R. T.; Schaub, T. M. FT-ICR MS Analysis of Blended Pine-Microalgae Feedstock HTL Biocrudes. *Fuel* **2018**, *216*, 341–348.
- (24) Hongthong, S.; Leese, H. S.; Chuck, C. J. Valorizing Plastic-Contaminated Waste Streams through the Catalytic Hydrothermal Processing of Polypropylene with Lignocellulose. *ACS Omega* **2020**, *5*, 20586–20598.
- (25) Madsen, R. B.; Zhang, H.; Biller, P.; Goldstein, A. H.; Glasius, M. Characterizing Semivolatile Organic Compounds of Biocrude from Hydrothermal Liquefaction of Biomass. *Energy Fuels* **2017**, *31*, 4122–4134.
- (26) Jin, H.; Bai, B.; Wei, W.; Chen, Y.; Ge, Z.; Shi, J. Hydrothermal Liquefaction of Polycarbonate (PC) Plastics in Sub-/Supercritical Water and Reaction Pathway Exploration. *ACS Sustainable Chem. Eng.* **2020**, *8*, 7039–7050.
- (27) Demirbas, A. Liquefaction of Biomass Using Glycerol. *Energy Sources, Part A* **2008**, *30*, 1120–1126.
- (28) Brotzel, F.; Chu, Y. C.; Mayr, H. Nucleophilicities of Primary and Secondary Amines in Water. *J. Org. Chem.* **2007**, *72*, 3679–3688.
- (29) Breugst, M.; Tokuyasu, T.; Mayr, H. Nucleophilic Reactivities of Imide and Amide Anions. *J. Org. Chem.* **2010**, *75*, 5250–5258.

Chapter 6

Paper 3 – Combined Hydrothermal Liquefaction of Polyurethane and Lignocellulosic Biomass for Improved Carbon Recovery

dos Passos, J. S.; Chiaberge, S.; Biller, P. Combined Hydrothermal Liquefaction of Polyurethane and Lignocellulosic Biomass for Improved Carbon Recovery. *Energy and Fuels* **2021**, *35* (13), 10630–10640. <https://doi.org/10.1021/acs.energyfuels.1c01520>.

Article history:

Received: May 17th, 2021

Revised: May 28th, 2021

Published: June 15th, 2021

Keywords:

Hydrothermal liquefaction

chemical recycling

circular economy

polymers

polyurethane

6.1. Reflections

The high synergy effect identified in *Miscanthus Giganteus* and polyurethane co-HTL encouraged us to investigate if there is an optimal mixing ratio that can enhance even further the recovery of carbon as a synthetic oil using this process. As the attention of polyurethanes' chemical recycling processes throughout literature rises and HTL enters the pool of options, understanding deeply the suggested process is of highly importance.

The paper attached in this chapter shows large synergies in batch experiments are successfully validated in a continuous HTL pilot plant. The overall carbon and energy efficiencies of the process are thoroughly discussed and depict that the combination of PUR and lignocellulosic biomass can be a very attractive processing route for this type of polymer waste. The resulting oil is characterized in detail and its composition is rich in nitrogen-containing heteroaromatics and polyols. The approach suggested here can be a promising route to synthesize nitrogen-containing aromatics based on sustainable feedstock materials. The results showed that the synergistic HTL reaches 71% carbon and 75% energy yields in synthetic oil basis. These results are superior to most reports on continuous HTL yields in literature.^{12,24,25} Besides, as the strategy depicted here used fresh water for slurry preparation, further efficiency enhancement may be achieved if aqueous phase recirculation is applied.²⁶

Synthetic oils were characterized via high resolution mass spectroscopy by ENI, Italy, our collaborator in this paper. The results here reported were also presented in the Thermochemical Symposium of 2020 (October 5-7, 2020, Washington State University, Virtual Symposium) with very good acceptance from industry and scientific community.

Combined Hydrothermal Liquefaction of Polyurethane and Lignocellulosic Biomass for Improved Carbon Recovery

Juliano Souza dos Passos, Stefano Chiaberge, and Patrick Biller*

Cite This: *Energy Fuels* 2021, 35, 10630–10640

Read Online

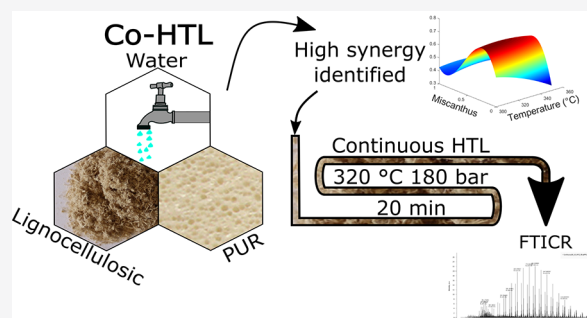
ACCESS |

Metrics & More

Article Recommendations

Supporting Information

ABSTRACT: Due to the high versatility of polyurethane (PUR), its share among synthetic polymers to manufacture consumer goods is increasing. This study proposes, tests, and validates through pilot processing a highly efficient method for the conversion of PUR to an oil phase concentrated in carbon using hydrothermal liquefaction (HTL) aided by lignocellulosic biomass. Hot liquid water mixed with PUR residues and a lignocellulosic material (two species of *Miscanthus*) were treated at subcritical water temperatures, generating an oil phase rich in hydrocarbons. A high-synergistic effect in the coliquefaction was observed, leading to carbon and chemical energy recovery to the oil of 71 and 75%, respectively. Pilot plant processing, using optimized process parameters, yielded a total process efficiency accounting for heating utilities of 61% and resulting in a 3.2 ratio of energy return over investment. By using spectroscopic and high-resolution mass spectrometry analysis, the oil revealed a high content of nitrogen hetero aromatic and polyol compounds. The high synergy observed for the coliquefaction of PUR and *Miscanthus* is attributed to recombination of synthetic and biological materials, specifically due to highly active nitrogen-containing intermediate compounds that recombine with lignocellulosic-derived molecules. During continuous processing, around 58% of the nitrogen contained in the feed is transferred to the oil produced, resulting in a 4 wt % nitrogen concentration in the oil. The results show that HTL can be an efficient method for the mass, carbon, and energy recovery of PUR aided by biomass.



1. INTRODUCTION

Polyurethanes (PURs) are a group of extremely versatile synthetic polymers. Their applications range from automobile seats, chairs, sofas, footwear, and carpets to refrigerators, insulation boards, medical applications, coatings, binders, and many others.¹ Such a variety of applications and continuous innovations have resulted in a PUR yearly production of around 26.4 Mton worldwide, with a production growth rate of 6.25% per year [2013–2018].^{1,2} PUR is usually divided into flexible and rigid foams, coatings, adhesives, sealants, and elastomers.^{1,3} The main difference between these groups are the polyols' composition and ratios of isocyanides and polyols used in production. PUR manufacturing plants are known to be wasteful, generating a considerable amount of trims and scrap, reaching 10% of the total PUR production.^{2,3} Despite the fact that part of the waste material produced has recycling opportunities that yield secondary products (carpets, inferior quality insulation boards), the amount diverted to such applications does not alleviate waste handling, particularly for postconsumer products,² and hence, innovation is still needed for PUR recycling.

The variety of PUR applications also brings challenges upon general recycling methods that can cope with all kinds of inputs. The most common recycling methods are mechanical (regrinding, rebinding, adhesive pressing, injection molding,

and compression molding), mainly yielding lower quality products than the initial feedstock source. These processes can cope with mixed flexible PUR, though the preference is usually for pure inputs. Nevertheless, mechanical recycling cannot handle rigid PUR. All of the mechanical recycling methods, besides adhesive pressing, have limitations regarding recycled feedstock, as it tends to decrease product quality.^{2,3}

Chemical recycling methods for PUR are known and can be divided into pyrolysis, gasification, hydrogenation, and solvolysis (hydrolysis, aminolysis, and glycolysis). Pyrolysis typically produces a considerable amount of HCN, NO, and CO in the gas phase² together with volatiles that include methane, ethylene, benzene, and others.⁴ The process usually yields (at >450 °C) 5–25%_{wt} char, 10–45%_{wt} liquids, and >40%_{wt} gases. Due to the undesired products present in the gas phase, pyrolysis is not preferred when dealing with PUR. A recent catalytic gasification report shows that hydrogen-rich

Received: May 17, 2021

Revised: May 28, 2021

Published: June 15, 2021



gases (up to 80% hydrogen fraction) are achievable, with gas yields around 70% at 1100 °C.⁵ Gasification also entails the issue of generating pollutants, such as NO, HCN, and other nitrogen-containing gases. Hydrogenation, on the contrary, as it is conducted in a reductive media, tends to produce NH₃ from the feedstock nitrogen. This process generates comparable amounts of volatiles as pyrolysis, with greater energy content due to the hydrogen saturation toward hydrocarbons.^{2,6}

The most used and developed solvolysis method for PUR recycling is glycolysis, with existing examples of pilot plants and industrial scale facilities.³ As the glycol reactant attaches to urethane bonds *via* transesterification reactions, the polyols from the feedstock are released and become available for further use.³ Several catalysts have been tested for this approach; however, amines are typically employed, though their presence in products is undesired.² Many research groups and patents have described PUR glycolysis employing different glycols as reactants for different PURs and a range of catalysts, generally with a high recovery of polyols, sometimes with two phase separation.^{2,3,7} Despite this method being the most developed, with pilot and industrial scale plants around the world, the complexity of the products obtained restrict their use to rigid foam manufacturing at limited contribution to virgin feedstock.³

The hydrolysis of PUR is usually described as employing dry superheated steam at mild temperatures and low pressures (190–250 °C, 10–20 bar) for relatively long residence times (>30 min).³ The products obtained are complex and difficult to separate, hindering process development so far to laboratory and pilot scale. We have described before that hydrothermal liquefaction (HTL) using 350 °C liquid water successfully depolymerizes PUR, generating an oil rich in polyols and amines free from urethane bonds.⁸ HTL is a comparable process to hydrolysis; however, HTL has the advantage of not using steam as a water source—i.e., avoiding evaporation energy spent on steam generation—and recovering products in a separated oil phase. Typically, HTL processing has been developed for dealing with organic wastes—e.g., sewage sludge,^{9–11} manure,¹² food waste,¹³ lignocellulosic materials¹⁴ and algae.¹⁵ Currently, several pilot plants are operational,^{14,16} and the technology readiness level of HTL is considered to be 5.

The combined HTL (co-HTL) of synthetic polymers and different materials has been suggested before, for instance on reports about microalgae co-HTL with polypropylene,¹⁷ macroalgae with polyethylene, polypropylene, and polyamides,¹⁸ lignocellulosic materials with polypropylene, polyethylene, PET, and polyamides,¹⁹ and, more recently, the catalytic processing of lignocellulosic materials and polypropylene.²⁰ All studies have found synergies and antagonistic effects for selected mixtures and materials, which indicates that co-HTL is an interesting approach for processing polymers together with biomasses due to the increase in efficiency and the flexibility of HTL processes. Combined liquefaction can also improve the pumpability needed for the continuous processing of slurries containing plastics, which otherwise would be difficult to achieve due to density differences and slurry instability. Recently, we have reported that *Miscanthus giganteus*—a model for lignocellulosic biomass—presents significant synergy effects in co-HTL with PUR foam at a 1:1 biomass to synthetic polymer resin feedstock mixing ratio.²¹

Those findings encouraged the objective of the present study: to investigate batch experiments using different temperatures (300–350 °C) and mixing ratios of PUR and *Miscanthus giganteus* in order to develop a predictive model for oil, carbon, and energy yields and to validate the models in continuous HTL processing using a continuous flow pilot plant. We further employ Fourier-transform ion cyclotron resonance mass spectrometry (FTICR-MS) analysis and use this information to elucidate possible reaction mechanisms that yield the observed synergistic effects on the basis of molecular level characterization.

2. MATERIALS

Miscanthus giganteus (used in batch experiments) and *Miscanthus lutarioriparius* (used in continuous experiments), hereby referred to as M, were harvested at Aarhus University's facilities at Foulum, Denmark. PUR foam utilized in batch experiments was taken from a disposed chair, while the PUR foam utilized in continuous experiments was kindly provided by Dan-Foam ApS (Tempur Denmark). Both types of PUR and M utilized in batch and continuous experiments were characterized *via* thermogravimetric analysis (TGA), FTIR, and compositional analysis (comparison available in Figures S1 and S2 and Table S2). Two different types of PUR and *Miscanthus* were used due to sample quantity availability. When comparing *Miscanthus giganteus* and *Miscanthus lutarioriparius*, a higher fixed carbon content was found present in the former, shown in the TGA measurements depicted in Figure S1. This difference likely arises from lignin content variations between the two species. Nevertheless, the other characterizations (Figure S2 and Table S2) are considered sufficiently similar for the direct comparison of results.

3. METHODS

3.1. Batch HTL. Batch experiments were conducted using 20 mL bomb-type reactors using the procedure previously described elsewhere.²² Table S1 depicts the set of experiments conducted in batch mode to screen blends of M and PUR from pure M to pure polyurethane in steps of 25% change within the temperature range 300–350 °C. In each experiment, an appropriate amount of each material summing 1.00 g of dry matter was added to the reactor together with 8.00 g of water, performing a 1:8 feedstock to water ratio. Reactors were sealed and inserted in a preheated fluidized sand bath at the desired temperature, reaching reaction set point in around 4 min.²³ After 20 min of reaction time (including heating), reactors were immediately quenched in water to room temperature. Gases were vented, and the mass of gas loss was recorded. The aqueous phase was decanted from the reactor, and the solids and oil mixture were separated *via* solvent-assisted vacuum filtration (methanol). The oil mass was weighed after solvent evaporation under nitrogen flow. Gas, solid, and oil yields are based on initial feed mass, according to eq 1, while the aqueous phase yield was calculated by the difference.

$$\text{yield}_{\text{component}} = \frac{m_{\text{component}}}{m_{\text{feed}}} \quad (1)$$

Predictive models for the oil, carbon, and energy yields were derived from the data set (acquired according to Table S1) using the eq 2 regression.¹³ As the mixtures tested were binary, i.e., PUR + M = 1 (where PUR is the dry basis polyurethane concentration in feed and M is the dry ash free basis M concentration in feed), the model was shortened for a single variable on feed material concentration, M, for simplification. Temperature (*T*) is expressed in °C.

$$\text{yield}(T, M) = a_0 + \sum_{i=1}^2 b_i T^i + \sum_{i=1}^3 c_i M^i + \sum_{i=2, j=1}^{i=2, j=3} d_{i,j} T^i M^j \quad (2)$$

The Bayesian information criterion (BIC) was used to exclude terms in an iterative manner, simplifying the model without losing

significance. The analysis of variance (ANOVA) was also conducted for the final predictive models.

3.2. Elemental Analysis. The CHNS-O (oxygen by difference) was determined for solid and oil fractions of both batch and continuous experiments using an Elemental vario Macro Cube elemental analyzer (Langensfeld, Germany). The Channiwala–Parikh correlation (eq 3) was used to estimate the HHV for oils.²⁴ Energy and carbon yields were calculated using eqs 4 and 5, respectively.

$$\text{HHV} \left[\frac{\text{MJ}}{\text{kg}} \right] = 0.3491C + 1.1783H + 0.1005S - 0.1034O - 0.0151N - 0.0211A \quad (3)$$

$$\text{energy yield } (\eta_{th})\% = \frac{\text{HHV}_{oil} \left[\frac{\text{MJ}}{\text{kg}_{oil}} \right] \cdot \text{yield}_{oil} \left[\frac{\text{kg}_{oil}}{\text{kg}_{feed}} \right]}{\text{HHV}_{feed} \left[\frac{\text{MJ}}{\text{kg}_{feed}} \right]} \times 100 \quad (4)$$

$$\text{carbon yield \%} = \frac{C_{oil} \left[\frac{\text{kg}_C}{\text{kg}_{oil}} \right] \cdot \text{yield}_{oil} \left[\frac{\text{kg}_{oil}}{\text{kg}_{feed}} \right]}{C_{feed} \left[\frac{\text{kg}_C}{\text{kg}_{feed}} \right]} \times 100 \quad (5)$$

3.3. Attenuated Total Reflectance-Fourier Transformed Infrared (ATR-FTIR). Selected solid and oil samples were analyzed using a Bruker Alpha Platinum ATR FTIR spectrometer (24 spectra collected from 4000 to 400 cm^{-1}) with resolution of 2 cm^{-1} . In between analyzes, 96% ethanol was used for cleaning the diamond crystal before baseline collection. Solid samples were compressed against the crystal, and oil samples were rubbed on top for measurements.

3.4. Thermogravimetric Analysis (TGA). A TGA Mettler Toledo SDTA851 was used to analyze raw materials, oil, and solid products. The TGA was operated using a constant heating rate of 10 K min^{-1} from 50 to 900 $^{\circ}\text{C}$ under nitrogen followed by 10 min under air at constant temperature. A minimum of 5 mg of mass sample was placed in the TGA ceramic crucibles.

3.5. Fourier Transform Ion Cyclotron Resonance Mass Spectrometry (FTICR MS). Biocrude samples were diluted with a mixture of chloroform and acetonitrile (1:20) to a final concentration of 0.4 mg/mL. Mass spectrometry analysis were performed on a 7T FTICR MS (LTQ-FT Ultra Thermo Scientific) equipped with an atmospheric pressure chemical ionization (APCI) ion source. The mass spectra were collected in positive ion mode. The samples were infused at a flow rate of 100 $\mu\text{L min}^{-1}$ using the following typical APCI (+) conditions: source heater 380 $^{\circ}\text{C}$, source voltage 5 kV, capillary voltage 7 V, tube lens voltage 60 V, capillary temperature at 275 $^{\circ}\text{C}$, sheath gas 60 arbitrary units, auxiliary gas 10 arbitrary units. The mass spectra were acquired in positive mode with a mass range of m/z 100–1400. The resolution was set to 200 000 (at m/z 400). The ion accumulation time was defined by the automatic gain control (AGC), which was set to 10^6 . Three hundred and sixty scans were acquired for each analysis to improve the signal-to-noise ratio using a Booster Elite system (Spectroswiss), which allowed us to directly register the transient data. Transients were then processed by the software Peak by Peak-Petroleomic version (Spectroswiss). The 360 transients were averaged and then Fourier transformed into a single averaged mass spectrum. The resulting spectrum was further processed to remove noise (thresholding set to 6 σ of the background noise) and internally recalibrated through the unwrapping method.²⁵ Around 10 000 different peaks were then obtained. The final attribution of these peaks was conducted using the composing function of the software Peak by Peak with an error limit of ± 2 ppm.

Molecular formulas were categorized according to different parameters, such as the number of heteroatoms (N and O) and number of unsaturations expressed as double bond equivalents (DBE).²⁶ For each molecular formula, the DBE was calculated according to eq 6 (for $\text{C}_c\text{H}_h\text{N}_n\text{O}_o\text{S}_s$).

$$\text{DBE} = c - \frac{h}{2} + \frac{n}{2} + 1 \quad (6)$$

Classes of compounds were assigned according to the heteroatoms present in each molecule, and their relative abundances were used for building class distribution plots. The more abundant classes were then plotted in double bond equivalent (DBE) versus carbon number plots according to their carbon number, DBE value, and relative abundance in the mass spectrum.

3.6. Continuous HTL. PUR waste and raw M were milled using a modified twin screw extruder (Xinda, 65 mm twin screw extruder with 2000 mm barrel length) and mixed in the optimal proportion identified from the batch experiments. Fresh water and carboxymethyl cellulose (0.5% total slurry weight) were added to prepare the slurry using a 2 m^3 paddle mixer together with a Microcut MCH-D 60 A wet mill to ensure homogeneity and pumpability. The slurry was fed in the continuous HTL pilot plant located at Aarhus University, Foulum, as described by our group previously.¹⁴ Figure 1 depicts the temperature

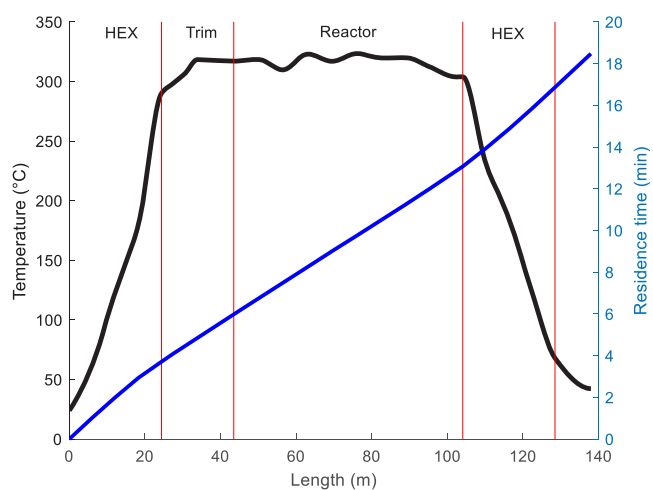


Figure 1. Pilot plant temperature profile during campaign.

profile over the pilot plant during the production campaign. The reactor section temperature was kept at 316.4 ± 6.2 $^{\circ}\text{C}$, and the slurry feed mass flow was 55.1 ± 0.6 kg/h . The campaign ran for 5 h, and the results presented are based in thermal steady state operation, as highlighted in Figure S3. The thermal steady state was verified using the logarithmic mean temperature difference in the heat exchanger. Steady state was determined when this value change was less than 5%, which was achieved after 2 h of continuous operation for a total steady state period of approximately 3 h (see Figure S3).

The synthetic oil product was separated gravimetrically from water, and 10 g raw oil aliquots were diluted in methanol and vacuum filtered to determine solid content. Water content in the raw oil was determined via Karl Fischer titration. The total energy efficiency (η_{tot}) and the energy return over investment (EROI) for continuous processing were calculated using eqs 7 and 8, respectively.¹⁴

$$\eta_{tot} = \frac{E_{oil}[\text{kW}_{oil}]}{(E_{feed} + E_{pump} + E_{trim\ heat} + E_{reactor\ heat})[\text{kW}_{total\ input}]} \times 100 \quad (7)$$

$$\text{EROI} = \frac{E_{oil}[\text{kW}_{oil}]}{(E_{pump} + E_{trim\ heat} + E_{reactor\ heat})[\text{kW}_{external\ input}]} \quad (8)$$

4. RESULTS AND DISCUSSION

4.1. Batch HTL and Yield Predictive Models. Figure S4 depicts the mass balance for all mixing ratios and temperatures tested. A high-synergy effect for oil production can be observed for coliquefaction, especially for 75/25 (PUR/M) mixing

ratios. Further, it is shown that solids yields are the highest for 2S/75S mixing ratios for all temperatures. AP mass yields are higher for pure components (PUR or M), while gas yields vary with both temperature and mixing ratio.

Equations 9–11 show the oil, carbon, and energy yield predictive models, respectively, derived from eqs 4 and 5 results regressed for eq 2 and simplified stepwise using the BIC. ANOVA correspondents to these models are found in Tables S3–S5, respectively, for oil, carbon, and energy yields. Statistically significant p -values still present in the models were allowed to comply with a lower BIC, enhancing prediction efficiency. Other statistical tests were performed to test the model for bias and are depicted in Figure S5–S7 for oil, carbon, and energy yield models, respectively. The data shows all models being highly capable of predicting yields with a relatively low bias. Generally, the empirical terms presented are within the same orders of magnitude.

$$\begin{aligned} \text{oil}_{\text{yield}} = & -7.3701 + 5.222110^{-2}T + 10.712M - 8.621610^{-5}T^2 \\ & - 7.114610^{-2}TM + 0.15073M^2 + 3.474710^{-5}T^2M - 1.2577 \\ & 10^{-2}TM^2 + 2.2617M^3 \end{aligned} \quad (9)$$

$$\begin{aligned} \text{carbon}_{\text{yield}} = & -1.9371 + 1.847410^{-2}T - 2.1977M + 1.27010^{-2}TM \\ & - 3.42110^{-5}T^2 - 1.3397M^2 - 9.508310^{-3}TM^2 \\ & + 2.4806M^3 \end{aligned} \quad (10)$$

$$\begin{aligned} \text{energy}_{\text{yield}} = & 1.7772 - 4.084310^{-3}T - 2.5976M + 1.430810^{-2}TM \\ & - 1.0344M^2 - 1.112010^{-2}TM^2 + 2.5693M^3 \end{aligned} \quad (11)$$

Parts A–C of Figure 2 show, respectively, the oil, carbon, and energy yields heat maps based on respective models (eqs 9–11). It is possible to identify the maximum oil yield with 65.7% at 314 °C and M 0.225 $\text{g}_{\text{Miscanthus}}/\text{g}_{\text{DM}}$. Temperatures between 300 and 325 °C and M between 0.175 and 0.30 $\text{g}_{\text{Miscanthus}}/\text{g}_{\text{DM}}$ all depict oil yields higher than 64%. When compared to pure feedstock materials (PUR and M), where oil yields range from 35 to 45%, there is a remarkable 30–40% increase. Within the range tested, the effects of M are more pronounced than temperature, as can be observed in Figure 2, indicating that lower temperatures may be used as long as feedstock mixture is optimized for maximum oil production. The carbon yield peaks at 70.8% at 308 °C and M 0.25 $\text{g}_{\text{Miscanthus}}/\text{g}_{\text{DM}}$ while the energy yield maximum reaches 75.0% at the same M but at 300 °C. Overall, temperatures between 300 and 325 °C should be preferred, while M mixtures in PUR of 0.20–0.28 yield the best results in all three parameters mapped.

The surface responses depicted in Figure 2A–C are clearly similar, confirming that the superior oil yield carries carbon and chemical energy to this product fraction. Usually the HTL of common biomass-derived feedstock materials does not reach such high efficiencies for oil yields, particularly when not using lipid-rich biomaterials or oil recycling strategies; yields of up to 50% have been reported.^{16,27} For example, co-HTL synergies of lignocellulosic materials and sewage sludge are reported to increase oil yields to up to 47.1%,¹⁰ while the co-HTL of lignocellulosic biomass and manure can reach 30%.²⁸ The synergistic effect previously reported for *Miscanthus giganteus* and PUR²¹ was significantly improved from 43% oil, 52% carbon, and 55% energy yields at a 50:50 mix ratio and 350 °C to the aforementioned optimal conditions upon reaction parameters optimization. This indicates that a specific stoichiometric relation is present, which will be clarified further

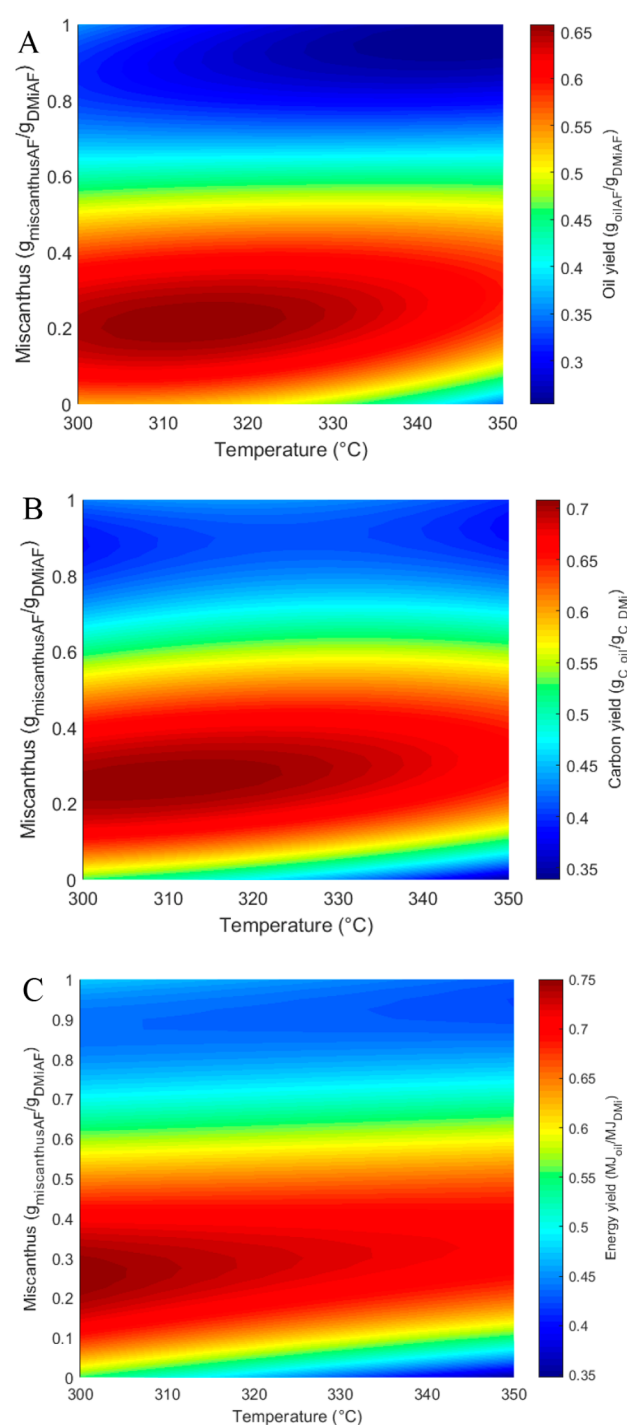


Figure 2. (A) Oil, (B) carbon, and (C) energy yields prediction model heatmaps.

upon oil composition discussion. Controlling the presence of lignocellulosic materials and PUR in HTL media can clearly enhance the chemical recycling opportunities of PUR.

In the literature, batch bomb-type reactor models have been developed to investigate HTL because of their characteristic fast heating rates, which are very similar to the heating profiles observed in continuous HTL plants.^{29,30} In the following section, the models described here, on the basis of batch reactor results, are validated using a continuous HTL reactor.

4.2. Continuous HTL. The feedstock preparation for the continuous campaign, using the ratio of M and PUR identified

in the predictive models, was successful, and pumpability was achieved. This was not the case for PUR/water slurries alone; thus, the addition of lignocellulosic biomass to PUR also facilitates the formation of a pumpable slurry. The resulting slurry exhibited clear signs of non-Newtonian behavior by syringe tests performed *in situ*. The slurry was successfully pumped using helical rotor pumps and a Graco Check-Mate positive displacement pump. No clogs or significant pressure difference over the pilot plant components (heat exchanger hot and cold sections, reactor, and takeoff system) were observed during the entire run, which indicates that the slurry is stable upon pressurized heating, and the products do not tend to cross-link.

Table 1 depicts a summary of the continuous campaign results, including feed slurry mass and energetic character-

Table 1. Continuous Production Campaign Data Summary and Results^a

property	value	±	unit
feed slurry			
Miscanthus concentration in feed	0.22		$g_{\text{miscanthus}}/g_{\text{feed}}$
PUR concentration in feed	0.78		$g_{\text{PUR}}/g_{\text{feed}}$
PUR/M ratio in feed	3.52		$g_{\text{PUR}}/g_{\text{miscanthus}}$
mass flow rate	55.1	0.6	kg/h
dry matter content	13.77%	0.01	wt %
energy in feedstock	57.5	0.2	$kW_{\text{feed, dry}}$
product aqueous phase			
total organic carbon	8824	48	mg/L
total inorganic carbon	20	2	mg/L
aqueous phase carbon yield	9.8%		$kg_{\text{C AP}}/kg_{\text{C input}}$
total nitrogen	1123	4	mg/L
aqueous phase nitrogen yield	16.2%		$kg_{\text{N oil}}/kg_{\text{N input}}$
product biocrude			
biocrude yield (dry solids free)	65.6%		$kg_{\text{oil}}/kg_{\text{input}}$
biocrude carbon content (dry basis)	63.1%	0.11	$kg_{\text{C}}/kg_{\text{oil}}$
biocrude carbon yield (dry solids free)	71.2%		$kg_{\text{C oil}}/kg_{\text{C input}}$
biocrude nitrogen content (dry basis)	3.95%	0.14	$kg_{\text{N}}/kg_{\text{oil}}$
biocrude nitrogen yield (dry solids free)	57.9%		$kg_{\text{N oil}}/kg_{\text{N input}}$
HHV biocrude (dry solids free)	31.1	0.5	MJ/kg_{oil}
energy in biocrude (dry solids free)	43.1	0.2	$kW_{\text{oil, dry}}$
external energy input			
trim heater energy requirements	7.9	0.4	kW
reactor energy requirement	5.0	0.0	kW
main pump energy requirement	0.48		kW
energy efficiency			
energy yield (η_{th})	75.0%		$kW_{\text{oil}}/kW_{\text{feed}}$
total efficiency (η_{tot})	60.7%	0.2	$kW_{\text{oil}}/kW_{\text{total input}}$
EROI	3.2	0.2	$kW_{\text{oil}}/kW_{\text{external input}}$

^aPressure = 161.6 ± 8.8 bar; Reactor temperature = 315.6 ± 5.1 °C.

ization over the analyzed time frame of steady state operation, together with the products aqueous phase and biocrude and the energy utilities. The mass flow rate was around 55.1 kg·h⁻¹, giving a total residence time of approximately 18.5 min, following the temperature profile depicted in Figure 1 at 161.6 ± 8.8 bar. This mass flow carried into the reactor was 32.1 kg_{carbon}·h⁻¹, of which 71.2% was found in the oil phase, 9.8% in the aqueous phase and, by difference, the remaining 19% was

converted either to gas or solid products. These results are superior when compared to pure miscanthus HTL, high-nitrogen biomasses such as *Spirulina*, or sewage sludge using the same pilot plant.¹⁴

The nitrogen balance shows that, out of the 2.46 kg_N·h⁻¹ fed to the reactor, 57.9% was found in the oil phase, which contained 3.95% nitrogen by weight, while 16.2% was collected in the aqueous phase, which contained 1123 mg_N·L⁻¹. Even though there is a negative contribution of N to the HHV, the oil phase still presented a relatively high value of 31.1 MJ·kg⁻¹. The nitrogen content in oil is comparable to biomass-derived biocrudes, even though its yield is higher.^{9,14,31} The total nitrogen in the aqueous phase and its yield to this fraction are lower than biomass HTL processing results, especially compared to manures and sewage sludge.^{32,33}

The chemical energy fed to the pilot plant was 57.5 kW, which was heated using 7.9 kW in the trim heater and 5 kW in the reactor section. The oil product carried 43.1 kW of energy, which is 75.0% of the initial feedstock slurry. Accounting the utilities, the total energy efficiency is 60.7%, with an energy return over investment (EROI) of 3.2. This data leads PUR/M co-HTL to be an attractive strategy to recover carbon from used materials in an oil form.

4.3. Oil analysis. **4.3.1. Thermogravimetric Analysis (TGA).** The batch sample acquired at 325 °C, with a mixing ratio of 75:25 (PUR/M), was selected as the most representative in comparison to the already mentioned sample collected from the continuous campaign. Figure 3 compares the TGA and DTG results from batch oils of M, PUR, and co-HTL, together with the continuous oil campaign. It is clear that the co-HTL oil, either from batch or continuous, is much more similar to the PUR oil than the M biocrude. The co-HTL oils and the PUR one all have a sharp main weight loss around 400 °C. This DTG peak is slightly above the 360–390 °C main decomposition peak found in the raw PURs (Figure S1), which is related to the polyalcohols' thermal degradation.^{4,34,35} Both batch and continuous co-HTL oils have a different behaviors at temperatures <400 °C. The former loses around 8% of its weight, while the latter reaches 20% weight loss, both yielding minor broad peaks at 200 and 280 °C, respectively. After the 400 °C peak, the batch co-HTL oil still holds around 15% of its initial weight, while the continuous campaign oil behaves similarly to the pure batch PUR, both with <5%. This could be caused due to the higher amount of lignin in the M species used in batch (indicated *via* the TGA solid residue amount in Figure S1).

Overall, the TGA and DTG results point out that the oil derived from co-HTL of PUR and M is more similar to pure PUR oil than to pure M. The findings are partially surprising, given that the M addition significantly increases the oil phase recovery. However, the amount of PUR participation in the initial mixtures is indeed higher and so the characteristics measured by TGA and DTG follow.

4.3.2. ATR-FTIR. Figure 4 depicts an ATR-FTIR comparison of batch biocrudes from *Miscanthus giganteus*, PUR, one sample of 75:25 (PUR/M, 325 °C), and the continuous campaign biocrude (filtered using methanol, water free). The M biocrude presents its typical peaks related to phenolics, aliphatics, acids, ketones, and alcohols.^{36,37} Hydroxyl groups are located between 3030 and 3660 cm⁻¹ with a broad peak, while C—O bonds can also be identified at 1110 and 1205 cm⁻¹ and C=O at 1690 cm⁻¹. Characteristic C—H bonds can be verified at 2928 (—CH₂), 2846 (—CH₃), 1460–1350 cm⁻¹,

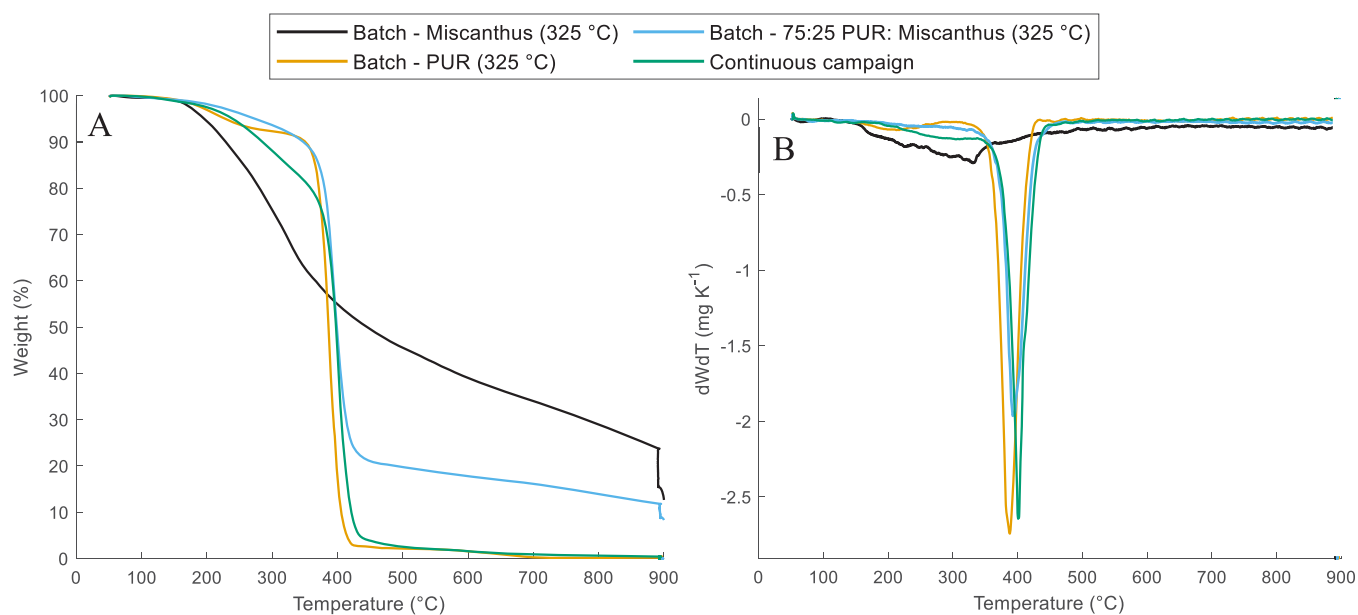


Figure 3. TGA and DTG of oil from HTL experiments in batch and continuous. Batches: *Miscanthus giganteus*, PUR, 75:25 (PUR/M), 325 °C.

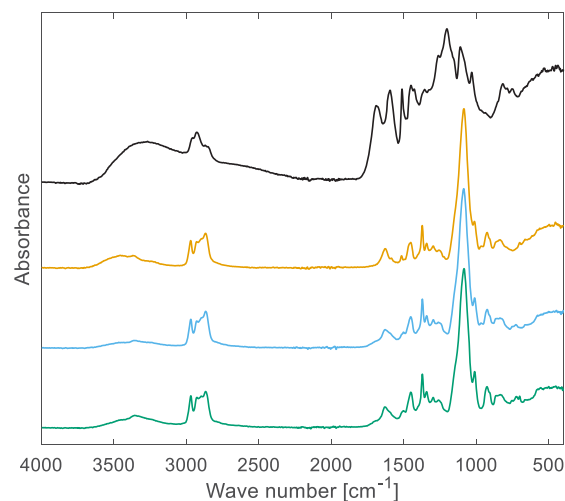


Figure 4. ATR-FTIR spectra of oil from HTL experiments in batch and continuous campaign. Batches: *Miscanthus giganteus*, PUR, 75:25 (PUR/M 325 °C).

and 740–830 cm^{-1} . Lastly, C=C bonds are shown at 1603 and 1512 cm^{-1} .

The PUR oil FTIR spectra depicted in Figure 4 share a significant resemblance to those of raw PUR (Figure S2). However, the oil does not contain the characteristic urethane bonds at 1223 (C(=O)O) and 1533 (C–N) cm^{-1} , rather presenting a clear N–H peak at 1624 cm^{-1} and a much broader peak in the 3030–3600 cm^{-1} region, related to OH presence together with primary and secondary amines. It is worth noticing a shift from 3291 to 3358 cm^{-1} (from raw feedstock to oil) peak, indicating a change from secondary to primary amines. Other peaks, present in both the oil and the raw material, are an ether C–O (1090 cm^{-1}), double bonded C=C (1590–1630 cm^{-1}), and characteristic C–H bonds around 2800–3000 cm^{-1} .

It is clear the biocrude yielded from the 75:25 (PUR/M, 325 °C) batch is more similar to the PUR oil than the M biocrude. The only differences observed are the broad peaks between

3030 and 3660 cm^{-1} related to OH and NH groups and, also, a broadening of the 1624 cm^{-1} N–H peak. When comparing both oils, it is possible to see that the PUR oil has a wider 3030–3660 cm^{-1} peak, indicating a higher occurrence of OH groups. The peak at 3358 cm^{-1} , connected to the presence of primary amines, can be observed in both oils spectra. The continuous campaign and batch (75:25 PUR/M, 325 °C) oils do not present differences, indicating that they share very similar chemical groups and structures in comparable proportion.

4.3.3. FTICR MS Analysis. The FTICR mass spectra contain over ten thousand different molecular ion peaks (mainly protonated molecular ions); thus, some data representation choices were made to clarify the composition, including the classification of the elemental formulas of the detected ions on the basis of N and O numbers, C number, DBE, and H/C, O/C, and N/C ratios. The spectra collected for the continuous campaign oil are shown in Figure S12 as a sample of the results.

Figure S8 shows the DBE versus C number for all classes detected in the M batch oil (325 °C). No compounds with nitrogen were detected, as shown in Figure 5, thus families were divided only according to oxygen number (which were identified from 2 to 7). The results depict an oil that contains molecules with 8–68 carbons, with relatively more presence from C₅ to C₄₀ and a generally increasing average C number directly proportional to oxygen number. The DBE values of the most intense species are between 5 and 20; therefore, most of the compounds likely belong to aromatic oxygen-containing species. Despite not detecting nitrogen-containing compounds, the analysis presented here is in good agreement to those of other lignocellulosic materials' HTL biocrudes characterized using similar techniques.^{38,39}

Figure 5 depicts the PUR batch (325 °C) oil compound families according to their abundance. It is possible to observe the most prominent abundances in Figure 5A, where only compounds without nitrogen are located. A bell-shaped curve can be seen, peaking around family O₁₅ and tailing toward lower O numbers. These compounds can be best observed in

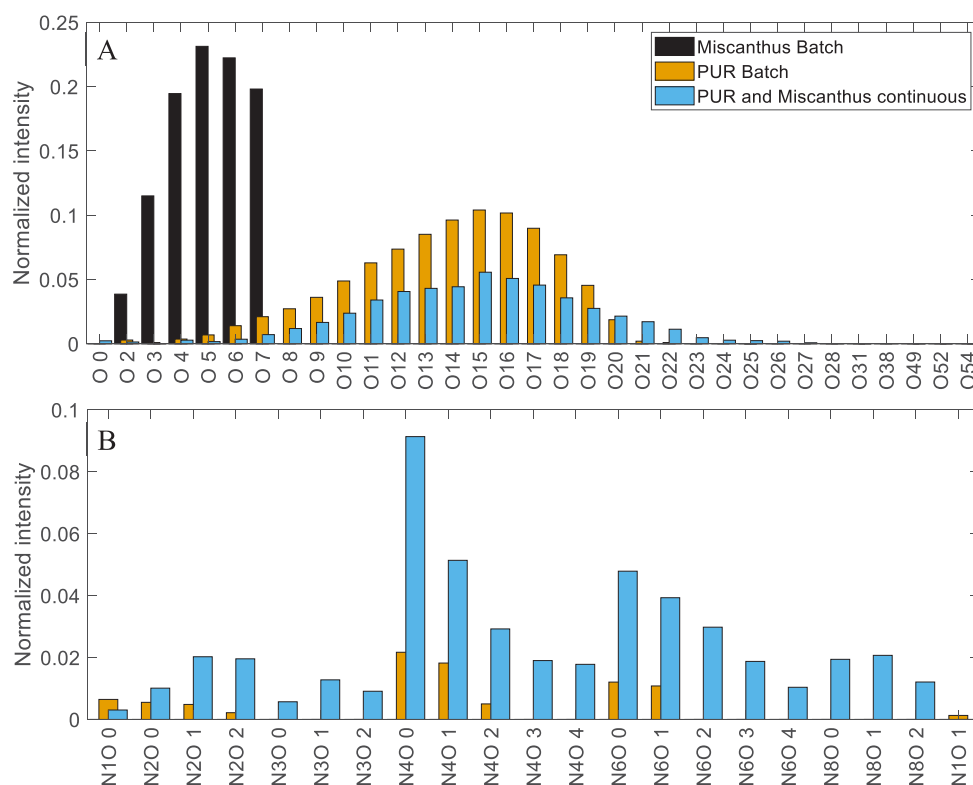


Figure 5. Normalized intensity for all compounds in each N_xO_x family for M batch biocrude (325 °C), PUR batch (325 °C), and continuous oil: (A) N = 0 and (B) N ≥ 1.

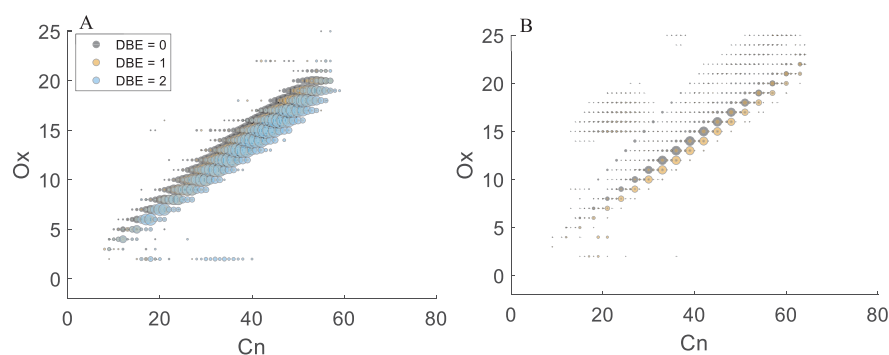


Figure 6. Number of carbon vs oxygen atoms for O_x ≥ 1 families (for DBE 0, 1, and 2). The size of each dot is related to the relative abundance of the FTICR mass peak: (A) PUR batch at 325 °C and (B) continuous oil.

Figure 6A, where the carbon number is plotted over oxygen for all DBE compounds found. This observation is very characteristic of oligomers or polymers. In this case, they are clearly derived from the polyol group of PUR resins.^{34,35} Thus, the PUR oil has a main fraction characterized by the water insoluble fraction of the polyols present in the original feedstock. The remaining identified compounds have either 1, 2, 4, or 6 N atoms (predominantly 4) accompanied by up to 3 O atoms. Overall the synthetic oil derived from PUR alone differs greatly from nitrogen-rich biomass-derived biocrudes, which may present families with up to 4 N atoms accompanied by up to 3 O atoms, especially with regards to relative abundance and DBE.^{33,39}

In the PUR and M continuous oil, the most intense peaks according to their accurate mass values belong to the classes C_(5+n)H_(12+2n)O_(1+m), C_(5+n)H_(10+2n)O_(1+m), and C_(5+n)H_(8+2n)O_(1+m)—with *n* from 0 to 80 and *m* from 0 to 40. A constant gap of C₃H₆O was found for the most intense

species, being compatible with polyol (polypropylenglycols) structures. When comparing these polyols *via* a C_n over O_x plot, as depicted in Figure 6A, it is possible to verify a linear relation that also shows monomer addition as the molecular difference between compounds. The polyols identified in the co-HTL oil (Figure 6B) are similar to the ones identified in the pure PUR oil (Figure 6A), however the former are present in relatively smaller quantities—also shown in Figure 5A.

Parts A and B of Figure 5 depict that, despite the fact that the polyols in the co-HTL oil are distributed similarly to pure PUR oil (but with smaller relative intensities), both oils differ greatly in the nitrogen-containing species. The continuous oil presents a higher occurrence of species with nitrogen, especially N₄, N₆, and N₈ classes (as shown also in Figure S11). Interestingly, no compounds containing N₅, nor N₇ were identified both in the co-HTL or pure PUR oil. The oil elemental composition presented in Table S2 also corroborates these results, depicting a low nitrogen content for M oil in

comparison to co-HTL oil, which has similar compositions for both batch and continuous processing.

Figure S9 depicts the Van Krevelen diagram for all nitrogen species identified in pure PUR and co-HTL oil. All oils demonstrated consistently a lower than 0.2 O/C ratio, while also depicting H/C mostly below 2, commonly with 1 as the median. The comparison between oils demonstrates that the co-HTL oil is more complex, tending to have a greater number of nitrogen families than pure PUR oil. For all oils, compounds of the same family tend to group around a short range of O/C ratios and relatively greater ratios of H/C.

The increase of O/C according to a family maintaining similar H/C ratios indicates that the molecular difference may be explained by the addition of hydroxyl side groups in these molecules. The atomic ratios of families that do not contain nitrogen are depicted in Figure 7, for batch PUR (A), M (B),

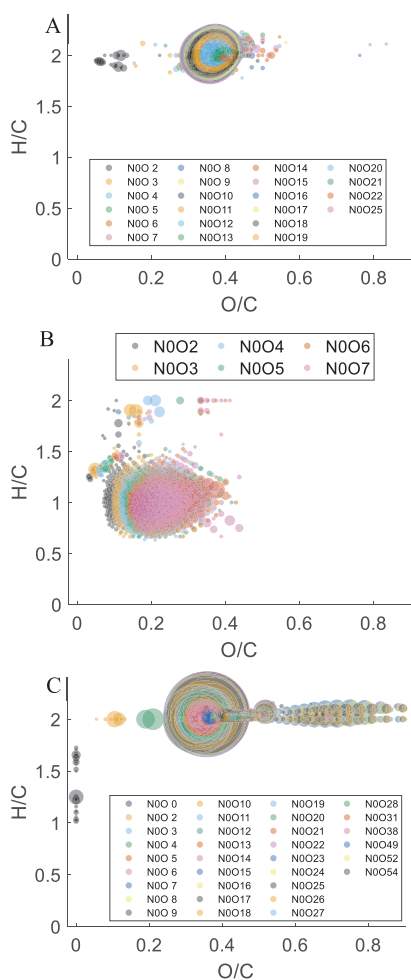


Figure 7. Van Krevelen diagram for O_x families: (A) PUR batch at 325 °C, (B) M batch at 325 °C, and (C) continuous oil.

and continuous (C) oils. Here, a very high H/C ratio for molecules with more than 1 oxygen atom was found both for PUR and the continuous oil in comparison to M biocrude. For both PUR-derived oils, a broad range of O/C ratios was identified, particularly in Figure 7C. The absence of compounds around a H/C of 1 in Figure 7C thus indicates that biomass-derived molecules rearrange in the presence of PUR-derived compounds.

A modified version of the Van Krevelen diagram, showing a N/C ratio in the x -axis, can be found in Figure S10. Here again, only the oils containing significant groups of N-containing structures are depicted. The difference between PUR batch and continuous oil indicates a clear recombination of molecules derived from M and PUR liquefaction, more specifically with a much greater variety of species with higher peak intensities, showing N/C ratios of up to 0.2. A greater number of nitrogen families is also depicted in Figure S11, where the DBE is plotted versus C number. PUR oil presents irregular distributions in DBE plots, very different from those of the continuous oil. The latter contains classes that are grouped around an area in the C_n vs DBE plot with species showing the highest relative intensities. These peaks vary according to family from 20 to 40 C numbers, generally increasing the DBE with N and O contents. Such results are very indicative of the nitrogen-containing species being connected to aromatic structures, which increase the DBE drastically when comparing to biologically derived HTL biocrude with high nitrogen content.³³

In general, the complex oil derived from the continuous processing of PUR and M is more aromatic than common biomass-derived biocrudes yet still containing thousands of compounds. Furthermore, its composition includes molecules attached to polyol groups and short chain polyols as depicted in Figure 5 A. It is likely that the aromaticity favors the attachment of amine groups in pairs, given the families identified.

4.4. Overall Reactions for High-Synergy Effects.

Maillard reactions are the main contributor to synergistic effects in the hydrothermal liquefaction of biomass-derived protein in combination with sugars and other oxygen-containing compounds.³¹ Usually the recombination of monosaccharides and amino groups leads to the formation of pyrazines, indoles, pyrrolines, pyridines, pyrimidines, and pyrazoles. Such heterocyclic compounds can also be a product of amino acids reacting in HTL media, but their formation is enhanced by the presence of sugars or other structures containing oxygen, for instance furans, ketones, organic acids, etc.⁴⁰

Figure 8 depicts a possible reaction pathway for the observed high-synergistic effect between PUR and M. Maillard reactions involving amines attached to aromatic groups occur faster than amino acids-like ones would,⁴¹ which can explain the high-synergy effect observed in the co-HTL of PUR and M. The imine intermediates known in Maillard pathways³³ are formed, and its consequent cyclization increases aromaticity and stability for molecules. After dehydration or hydrogenation, reactions can follow leading to stable nitrogen heteroaromatics connected to alkyl side groups. However, a second reaction path can involve the still reactive sites present in the form of hydroxyl, ketone, or acidic groups near hetero aromatic structures. In this case, the recombination of these with other imine intermediates or amines adds aromaticity and leads to more stable compounds with more hetero aromatic nitrogen atoms. Such participation of the nitrogen species in the oil formation during PUR and M processing can also be observed in Table S2 by comparing the nitrogen content of PUR batch oil and the co-HTL product of 75:25 PUR/M, which is twice as high as the latter.

The nitrogen-containing families described in Section 4.3.3 depict a nitrogen atomic addition of 2, with a major presence of N_4 , N_6 , and N_8 structures. This may indicate that imines or

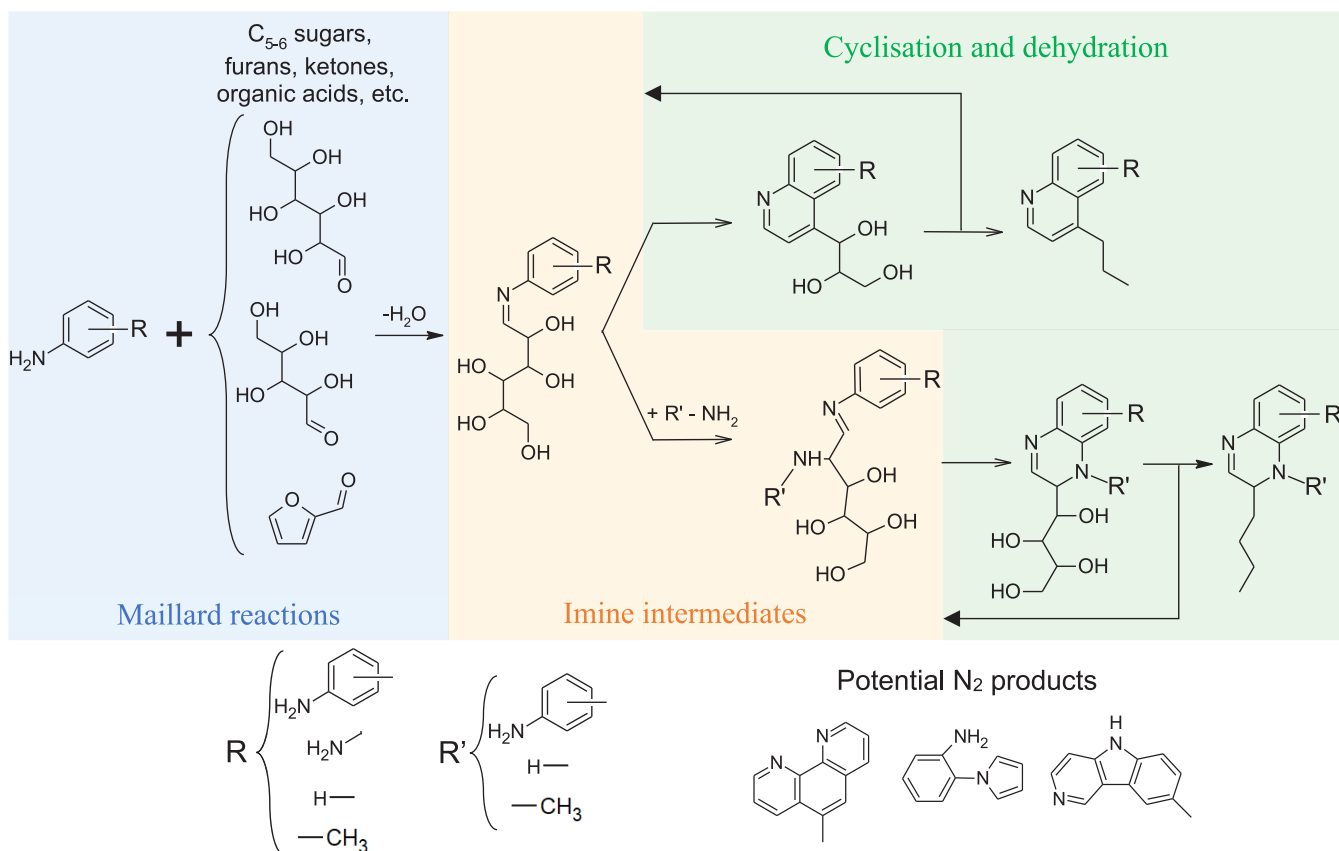


Figure 8. Possible reaction pathway for high-synergistic effect.

other compounds containing two nitrogens tend to recombine with the same family of intermediates, leading to very stable and highly aromatic structures. Overall, the reaction pathway proposed is very similar to biomass-derived nitrogen reactions, but as the amino groups are more active due to aromatic proximity and the synergy effects observed upon HTL processing are also more pronounced. Besides, the generation of compounds containing high levels of nitrogen (up to 8 atoms) differs from that of previously described biocrudes, despite similar oil elemental compositions.^{31–33}

5. CONCLUSION

The chemical recycling method presented can successfully enhance carbon and energy recovery in the form of an oil phase from lignocellulosics and PUR *via* combined HTL. From individual HTL carbon and energy recovery ranges of 35–45 and 35–55%, respectively, the co-HTL models predicted in batch experiments a maximum of 70.8% for carbon and 75.0% for energy recovery. The model predictions were successfully validated *via* continuous HTL in a pilot plant operating at 316.4 °C and 55 kg·h⁻¹ slurry intake, which contained 78% of PUR and 22% of *Miscanthus L.*, yielding 75% of energy and 71.2% carbon in the form of oil. Using the described pilot plant, a total energy efficiency of 60.7% was achieved (including utility requirements), leading to an EROI of 3.2.

The biocrude produced in batch experiments at the specific ratio of 75:25 PUR/M (325 °C) is considered very similar to the biocrude produced in the continuous campaign on the basis of TGA and FTIR results. The biocrude derived from the co-HTL processing of PUR and lignocellulosic material was characterized as containing a significant portion of aromatic

hydrocarbons with nitrogen heteroatoms, particularly with even numbers of those. Urethane bonds were fully hydrolyzed, generating primary amines, ethers, alcohol, aromatics, and others, which recombined with biomass-derived compounds into nitrogen-containing species. Maillard reactions combining oxygen-containing molecules with amino groups attached to aromatics are probably the main reason for the superior performance observed in these trials in comparison to pure biomass HTL. The characteristics lead to the formation of indoles and pyrazines, very stable compounds with high aromaticity, which contribute to the maintenance of chemical energy in the form of oil product.

The results have demonstrated that HTL is a technically attractive method to recover carbon from synthetic resins aided by biomass. The combination of synthetic and biological materials can provide a new platform for circular economy by using the feedstock flexibility depicted here in favor of carbon recovery. The oil product depicted in this work can be considered a potential feedstock for refineries, which can be a pathway for including thermosetting resins in circular loops.

■ ASSOCIATED CONTENT

Supporting Information

The Supporting Information is available free of charge at <https://pubs.acs.org/doi/10.1021/acs.energyfuels.1c01520>.

Tables of Batch experimental plan, feedstock composition, and oil, carbon, and energy yield prediction models' ANOVA and figures of TGA curves, FTIR spectra, continuous reactor average temperature and power consumption over time, PUR/*Miscanthus* batch HTL mass balance results, prediction and experimental

comparison, residual histogram, normal probability plots, DBE versus carbon number for miscanthus biocrude, Van-Krevelen diagram for all nitrogen-containing compounds identified using FTICR, DBE over carbon number according to nitrogen and oxygen number, and APC1(+) FTICR mass spectrum (PDF)

AUTHOR INFORMATION

Corresponding Author

Patrick Biller – Department of Biological and Chemical Engineering, Aarhus University, DK-8200 Aarhus N, Denmark; Aarhus University Centre for Circular Bioeconomy, DK-8830 Tjele, Denmark; orcid.org/0000-0003-2982-6095; Email: pbiller@bce.au.dk

Authors

Juliano Souza dos Passos – Department of Biological and Chemical Engineering, Aarhus University, DK-8200 Aarhus N, Denmark; Aarhus University Centre for Circular Bioeconomy, DK-8830 Tjele, Denmark; orcid.org/0000-0001-5345-3669

Stefano Chiaberge – Eni s.p.a. Renewable Energy & Environmental R&D, 28100 Novara, Italy

Complete contact information is available at:
<https://pubs.acs.org/10.1021/acs.energyfuels.1c01520>

Notes

The authors declare no competing financial interest.

ACKNOWLEDGMENTS

The authors would like to thank Dan-Foam ApS (Tempur Denmark) for providing the sample for continuous flow processing. This project has received funding from the European Union's Horizon 2020 research and innovation grant agreement No. 764734 (HyFlexFuel – Hydrothermal Liquefaction: enhanced performance and feedstock flexibility for efficient biofuel production) and the Aarhus University Centre for Circular Bioeconomy (CBIO).

REFERENCES

- (1) Akindoyo, J. O.; et al. Polyurethane types, synthesis and applications-a review. *RSC Adv.* **2016**, *6*, 114453–114482.
- (2) Nikje, M. M. A. *Recycling of Polyurethane Wastes*; De Gruyter: Berlin/Boston, 2019.
- (3) Simón, D.; Borreguero, A. M.; de Lucas, A.; Rodríguez, J. F. Recycling of polyurethanes from laboratory to industry, a journey towards the sustainability. *Waste Manage.* **2018**, *76*, 147–171.
- (4) Font, R.; Fullana, A.; Caballero, J. A.; Candela, J.; García, A. Pyrolysis study of polyurethane. *J. Anal. Appl. Pyrolysis* **2001**, *58–59*, 63–77.
- (5) Guo, X.; Song, Z.; Zhang, W. Production of hydrogen-rich gas from waste rigid polyurethane foam via catalytic steam gasification. *Waste Manage. Res.* **2020**, *38*, 802–811.
- (6) Zia, K. M.; Bhatti, H. N.; Ahmad Bhatti, I. Methods for polyurethane and polyurethane composites, recycling and recovery: A review. *React. Funct. Polym.* **2007**, *67*, 675–692.
- (7) Simón, D.; García, M. T.; De Lucas, A.; Borreguero, A. M.; Rodríguez, J. F. Glycolysis of flexible polyurethane wastes using stannous octoate as the catalyst: Study on the influence of reaction parameters. *Polym. Degrad. Stab.* **2013**, *98*, 144–149.
- (8) dos Passos, J. S.; Glasius, M.; Biller, P. Screening of common synthetic polymers for depolymerization by subcritical hydrothermal liquefaction. *Process Saf. Environ. Prot.* **2020**, *139*, 371–379.
- (9) Thomsen, L. B. S.; et al. Hydrothermal liquefaction of sewage sludge; energy considerations and fate of micropollutants during pilot scale processing. *Water Res.* **2020**, *183*, 116101.
- (10) Biller, P.; Johannsen, I.; dos Passos, J. S.; Ottosen, L. D. M. Primary sewage sludge filtration using biomass filter aids and subsequent hydrothermal co-liquefaction. *Water Res.* **2018**, *130*, 58–68.
- (11) Faeth, J. L.; Valdez, P. J.; Savage, P. E. Fast hydrothermal liquefaction of nannochloropsis sp. to produce biocrude. *Energy Fuels* **2013**, *27*, 1391–1398.
- (12) Conti, F.; et al. Valorization of animal and human wastes through hydrothermal liquefaction for biocrude production and simultaneous recovery of nutrients. *Energy Convers. Manage.* **2020**, *216*, 112925.
- (13) Aierzhati, A.; et al. Experimental and model enhancement of food waste hydrothermal liquefaction with combined effects of biochemical composition and reaction conditions. *Bioresour. Technol.* **2019**, *284*, 139–147.
- (14) Anastasakis, K.; Biller, P.; Madsen, R. B.; Glasius, M.; Johannsen, I. Continuous Hydrothermal Liquefaction of Biomass in a Novel Pilot Plant with Heat Recovery and Hydraulic Oscillation. *Energies* **2018**, *11*, 2695.
- (15) Biller, P.; Ross, A. B. Potential yields and properties of oil from the hydrothermal liquefaction of microalgae with different biochemical content. *Bioresour. Technol.* **2011**, *102*, 215–225.
- (16) Castello, D.; Pedersen, T. H.; Rosendahl, L. A. Continuous hydrothermal liquefaction of biomass: A critical review. *Energies* **2018**, *11* (11), 3165.
- (17) Xu, D.; et al. Co-hydrothermal liquefaction of microalgae and sewage sludge in subcritical water: Ash effects on bio-oil production. *Renewable Energy* **2019**, *138*, 1143–1151.
- (18) Raikova, S.; Knowles, T. D. J.; Allen, M. J.; Chuck, C. J. Co-liquefaction of Macroalgae with Common Marine Plastic Pollutants. *ACS Sustainable Chem. Eng.* **2019**, *7*, 6769–6781.
- (19) Hongthong, S.; Raikova, S.; Leese, H. S.; Chuck, C. J. Co-processing of common plastics with pistachio hulls via hydrothermal liquefaction. *Waste Manage.* **2020**, *102*, 351–361.
- (20) Hongthong, S.; Leese, H. S.; Chuck, C. J. Valorizing Plastic-Contaminated Waste Streams through the Catalytic Hydrothermal Processing of Polypropylene with Lignocellulose. *ACS Omega* **2020**, *5*, 20586–20598.
- (21) dos Passos, J. S.; Glasius, M.; Biller, P. Hydrothermal Co-Liquefaction of Synthetic Polymers and Miscanthus giganteus: Synergistic and Antagonistic Effects. *ACS Sustainable Chem. Eng.* **2020**, *8* (51), 19051.
- (22) Biller, P.; et al. Effect of hydrothermal liquefaction aqueous phase recycling on bio-crude yields and composition. *Bioresour. Technol.* **2016**, *220*, 190–199.
- (23) Gollakota, A.; Savage, P. E. Fast and Isothermal Hydrothermal Liquefaction of Polysaccharide Feedstocks. *ACS Sustainable Chem. Eng.* **2020**, *8*, 3762–3772.
- (24) Channiwala, S. A.; Parikh, P. P. A Unified Correlation for Estimating HHV of Solid, Liquid and Gaseous Fuels. *Fuel* **2002**, *81*, 1051–1063.
- (25) Kozhinov, A. N.; Zhurov, K. O.; Tsybin, Y. O. Iterative method for mass spectra recalibration via empirical estimation of the mass calibration function for fourier transform mass spectrometry-based petroleomics. *Anal. Chem.* **2013**, *85*, 6437–6445.
- (26) Pellegrin, V. Molecular formulas of organic compounds: the nitrogen rule and degree of unsaturation. *J. Chem. Educ.* **1983**, *60*, 626.
- (27) Gollakota, A. R. K.; Kishore, N.; Gu, S. A review on hydrothermal liquefaction of biomass. *Renewable Sustainable Energy Rev.* **2018**, *81*, 1378–1392.
- (28) Saba, A.; Lopez, B.; Lynam, J. G.; Reza, M. T. Hydrothermal Liquefaction of Loblolly Pine: Effects of Various Wastes on Produced Biocrude. *ACS Omega* **2018**, *3*, 3051–3059.

- (29) Qian, L.; Wang, S.; Savage, P. E. Fast and isothermal hydrothermal liquefaction of sludge at different severities: Reaction products, pathways, and kinetics. *Appl. Energy* **2020**, *260*, 114312.
- (30) Elliott, D. C.; Biller, P.; Ross, A. B.; Schmidt, A. J.; Jones, S. B. Hydrothermal liquefaction of biomass: Developments from batch to continuous process. *Bioresour. Technol.* **2015**, *178*, 147–156.
- (31) Leng, L.; et al. Nitrogen in bio-oil produced from hydrothermal liquefaction of biomass: A review. *Chem. Eng. J.* **2020**, *401*, 126030.
- (32) Wu, B.; Berg, S. M.; Remucal, C. K.; Strathmann, T. J. Evolution of N-Containing Compounds during Hydrothermal Liquefaction of Sewage Sludge. *ACS Sustainable Chem. Eng.* **2020**, *8*, 18303–18313.
- (33) Lu, J.; Li, H.; Zhang, Y.; Liu, Z. Nitrogen Migration and Transformation during Hydrothermal Liquefaction of Livestock Manures. *ACS Sustainable Chem. Eng.* **2018**, *6*, 13570–13578.
- (34) Lattimer, R. P.; Polce, M. J.; Wesdemiotis, C. MALDI-MS analysis of pyrolysis products from a segmented polyurethane. *J. Anal. Appl. Pyrolysis* **1998**, *48*, 1–15.
- (35) Esperanza, M. M.; García, A. N.; Font, R.; Conesa, J. A. Pyrolysis of varnish wastes based on a polyurethane. *J. Anal. Appl. Pyrolysis* **1999**, *52*, 151–166.
- (36) Madsen, R. B.; Anastakis, K.; Biller, P.; Glasius, M. Rapid Determination of Water, Total Acid Number, and Phenolic Content in Bio-Crude from Hydrothermal Liquefaction of Biomass using FT-IR. *Energy Fuels* **2018**, *32*, 7660–7669.
- (37) Pretsch, E.; Bühlmann, P.; Badertscher, M. *Structure Determination of Organic Compounds*; Springer: Berlin Heidelberg, 2009. DOI: 10.1007/978-3-540-93810-1.
- (38) Sudasinghe, N.; et al. High resolution FT-ICR mass spectral analysis of bio-oil and residual water soluble organics produced by hydrothermal liquefaction of the marine microalga *Nannochloropsis salina*. *Fuel* **2014**, *119*, 47–56.
- (39) Jarvis, J. M.; et al. FT-ICR MS analysis of blended pine-microalgae feedstock HTL biocrudes. *Fuel* **2018**, *216*, 341–348.
- (40) Zhang, C.; Tang, X.; Sheng, L.; Yang, X. Enhancing the performance of Co-hydrothermal liquefaction for mixed algae strains by the Maillard reaction. *Green Chem.* **2016**, *18*, 2542–2553.
- (41) Brotzel, F.; Chu, Y. C.; Mayr, H. Nucleophilicities of primary and secondary amines in water. *J. Org. Chem.* **2007**, *72* (10), 3679–3688.

References Part II

- (1) Ghosh, S. K.; Agamuthu, P. Circular Economy : The Way Forward. **2018**.
<https://doi.org/10.1177/0734242X18778444>.
- (2) Keijer, T.; Bakker, V.; Slootweg, J. C. Circular Chemistry to Enable a Circular Economy. *Nat. Chem.* **2019**, *11* (3), 190–195. <https://doi.org/10.1038/s41557-019-0226-9>.
- (3) Masson-Delmotte, V., P. Zhai, A. Pirani, S.L. Connors, C. Péan, S. Berger, N. Caud, Y. Chen, L. Goldfarb, M.I. Gomis, M. Huang, K. Leitzell, E. Lomny, J. B. R.; Matthews, T.K. Maycock, T. Waterfield, O. Yelekçi, R. Yu, and B. Z. eds. *Climate Change 2021: The Physical Science Basis. Contribution of Working Group I to the Sixth Assessment Report of the Intergovernmental Panel on Climate Change*; 2021.
- (4) Stahel, W. R. Circular Economy. **2016**.
- (5) Korhonen, J.; Honkasalo, A.; Seppälä, J. Circular Economy : The Concept and Its Limitations. *Ecol. Econ.* **2018**, *143*, 37–46. <https://doi.org/10.1016/j.ecolecon.2017.06.041>.
- (6) Henrich, E.; Dahmen, N.; Dinjus, E.; Sauer, J. The Role of Biomass in a Future World without Fossil Fuels. *Chemie-Ingenieur-Technik* **2015**, *87* (12), 1667–1685. <https://doi.org/10.1002/cite.201500056>.
- (7) Block, C.; Ephraim, A.; Weiss-Hortala, E.; Minh, D. P.; Nzihou, A.; Vandecasteele, C. Co-Pyrogasification of Plastics and Biomass, a Review. *Waste and Biomass Valorization* **2019**, *10* (3), 483–509.
<https://doi.org/10.1007/s12649-018-0219-8>.
- (8) Zhang, X.; Lei, H.; Chen, S.; Wu, J. Catalytic Co-Pyrolysis of Lignocellulosic Biomass with Polymers: A Critical Review. *Green Chem.* **2016**, *18* (15), 4145–4169. <https://doi.org/10.1039/c6gc00911e>.
- (9) KUMAGAI, S.; FUJITA, K.; TAKAHASHI, Y.; KAMEDA, T.; SAITO, Y.; YOSHIOKA, T. Impacts of Pyrolytic Interactions during the Co-Pyrolysis of Biomass/Plastic: Synergies in Lignocellulose-Polyethylene System. *J. Japan Inst. Energy* **2019**, *98* (9), 202–219. <https://doi.org/10.3775/jie.98.202>.
- (10) Elliott, D. C. Hydrothermal Processing. *Thermochem. Process. Biomass Convers. into Fuels, Chem. Power* **2011**, No. 2011, 200–231. <https://doi.org/10.1002/9781119990840.ch7>.
- (11) Brunner, G. *Hydrothermal and Supercritical Water Processes*, V 5.; Elsevier B.V.: Hamburg, Germany, 2014.
- (12) Elliott, D. C.; Biller, P.; Ross, A. B.; Schmidt, A. J.; Jones, S. B. Hydrothermal Liquefaction of Biomass: Developments from Batch to Continuous Process. *Bioresour. Technol.* **2015**, *178*, 147–156.
<https://doi.org/10.1016/j.biortech.2014.09.132>.
- (13) Seshasayee, M. S.; Stofanak, R.; Savage, P. E. Component Additivity Model for Plastics—Biomass Mixtures during Hydrothermal Liquefaction in Sub-, near-, and Supercritical Water. *iScience* **2021**, *24* (12), 103498.
<https://doi.org/10.1016/j.isci.2021.103498>.
- (14) Seshasayee, M. S.; Savage, P. E. Synergistic Interactions during Hydrothermal Liquefaction of Plastics and Biomolecules. *Chem. Eng. J.* **2021**, *417* (March), 129268. <https://doi.org/10.1016/j.cej.2021.129268>.
- (15) Biller, P.; Ross, A. B. Potential Yields and Properties of Oil from the Hydrothermal Liquefaction of Microalgae with Different Biochemical Content. *Bioresour. Technol.* **2011**, *102* (1), 215–225.
<https://doi.org/10.1016/j.biortech.2010.06.028>.
- (16) Anastasakis, K.; Ross, A. B. Hydrothermal Liquefaction of the Brown Macro-Alga *Laminaria Saccharina*: Effect of Reaction Conditions on Product Distribution and Composition. *Bioresour. Technol.* **2011**, *102* (7), 4876–4883. <https://doi.org/10.1016/j.biortech.2011.01.031>.
- (17) Wu, X.; Liang, J.; Wu, Y.; Hu, H.; Huang, S.; Wu, K. Co-Liquefaction of Microalgae and Polypropylene in Sub-/Super-Critical Water. *RSC Adv.* **2017**, *7* (23), 13768–13776. <https://doi.org/10.1039/c7ra01030c>.
- (18) Guo, B.; Yang, B.; Su, Y.; Zhang, S.; Hornung, U.; Dahmen, N. Screening and Optimization of Microalgae Biomass and Plastic Material Coprocessing by Hydrothermal Liquefaction. *ACS ES&T Eng.* **2021**.
<https://doi.org/10.1021/acsestengg.1c00261>.
- (19) Raikova, S.; Knowles, T. D. J.; Allen, M. J.; Chuck, C. J. Co-Liquefaction of Macroalgae with Common Marine Plastic Pollutants. *ACS Sustain. Chem. Eng.* **2019**, *7* (7), 6769–6781.
<https://doi.org/10.1021/acssuschemeng.8b06031>.
- (20) Seshasayee, M. S.; Savage, P. E. Oil from Plastic via Hydrothermal Liquefaction: Production and Characterization. *Appl. Energy* **2020**, *278* (March), 115673. <https://doi.org/10.1016/j.apenergy.2020.115673>.
- (21) Watson, J.; Lu, J.; de Souza, R.; Si, B.; Zhang, Y.; Liu, Z. Effects of the Extraction Solvents in Hydrothermal

- Liquefaction Processes: Biocrude Oil Quality and Energy Conversion Efficiency. *Energy* **2019**, *167*, 189–197. <https://doi.org/10.1016/j.energy.2018.11.003>.
- (22) Dowding, P. J.; Atkin, R.; Vincent, B.; Bouillot, P. Oil Core - Polymer Shell Microcapsules Prepared by Internal Phase Separation from Emulsion Droplets . I . Characterization and Release Rates for Microcapsules with Polystyrene Shells. **2004**, No. 22, 11374–11379.
- (23) Wong, H. C.; Campbell, S. W.; Bhethanabotla, V. R. Sorption of Benzene, Dichloromethane, and n -Propyl Acetate by Poly(Methyl Methacrylate)/ Polystyrene Copolymers at 323.15 K Using a Quartz Crystal Balance. *J. Chem. Eng. Data* **2018**, *63* (8), 2753–2757. <https://doi.org/10.1021/acs.jced.8b00094>.
- (24) Castello, D.; Pedersen, T. H.; Rosendahl, L. A. Continuous Hydrothermal Liquefaction of Biomass: A Critical Review. *Energies* **2018**, *11* (11). <https://doi.org/10.3390/en11113165>.
- (25) Marrone, P. A.; Elliott, D. C.; Billing, J. M.; Hallen, R. T.; Hart, T. R.; Kadota, P.; Moeller, J. C.; Randel, M. A.; Schmidt, A. J. Bench-Scale Evaluation of Hydrothermal Processing Technology for Conversion of Wastewater Solids to Fuels. *Water Environ. Res.* **2018**, *90* (4), 329–342. <https://doi.org/10.2175/106143017x15131012152861>.
- (26) Biller, P.; Madsen, R. B.; Klemmer, M.; Becker, J.; Iversen, B. B.; Glasius, M. Effect of Hydrothermal Liquefaction Aqueous Phase Recycling on Bio-Crude Yields and Composition. *Bioresour. Technol.* **2016**, *220*, 190–199. <https://doi.org/10.1016/j.biortech.2016.08.053>.

Part III

HTL of mixed organic wastes

Chapter 7

Introduction

7.1. Assessment of potential energy in agricultural waste streams for fossil fuel replacement

A broad energy-basis estimate is reported here to show the potential benefits of the technologies discussed in this thesis and the need to improve energy conversion of biomass to biofuels. The full assessment of this topic is not the objective of this chapter. Instead, it is considered in this discussion a wide-ranging global energy balance. Henrich et al.¹ reported a full order of magnitude analysis of the available energy worldwide, including the biomass-derived contributions, concluding that the amount of energy needed in a future (year 2100) without fossil-derived carbon seems possible to be harvested globally through several different methods. However, the current 600 EJ year⁻¹ worldwide energy consumption rate – of which 474 EJ year⁻¹ are fossil-derived – will deplete known fossil reserves (around 9500 EJ) by year 2068.

The combustion of those fossil fuels generates greenhouse gases that build up concentration in atmosphere and, by consequence, further deepens the current climate crisis. If in the near future we do not develop sufficiently efficient processes to produce materials and liquid fuels from sustainable feedstock sources, coal reserves will kick-in to substitute crude oil in most fossil-dependent economical sectors. Even considering that economically feasible fossil reserves double during the next few decades due to development of new extraction technologies, worldwide energy consumption will lead to the exhaustion of these materials within the next 150 years. Long before that, if fossil reserves keep business-as-usual consumption rates, by mid-21st century the current climate crisis will further deteriorate, leading to the exacerbation of catastrophic events and their economic consequences.²

According to the latest estimates of the International Energy Agency (IEA), 110 out of 121 EJ of energy used in 2019 only for transportation came from crude oil. In 2019, biofuels contributed with 4 EJ worldwide for the sector.³ It is historical that we depend on crude oil products for transportation, and this is well illustrated by Figure 1, where contributions of renewable biofuels and electricity (which may or may not be renewable) are barely observable given the massive scale of fossil-derived fuels. According also to IEA⁴, motor gasoline consumption worldwide in 2018 and 2019 was respectively 1131 and 1143 Mton, which correspond to around 53 EJ given an approximate 46 MJ.kg⁻¹ heating value. That is, out of the 121 EJ year⁻¹ of energy spent in transportation currently, heavy duty transport (trucks, trains and marine) and aviation consume around 68 EJ. Henrich et al.¹ and other various studies suggest electrification of small vehicles will lead to the need of liquid biofuels being concentrated in heavy duty and aviation transport, i.e. jet fuel, diesel and marine primarily. However, the current scenario of biofuels utilization could not be more distant than the need for applying them in heavy transport.

The fraction of renewables in the transportation energy is very unequal among countries, ranging from 0 to 24.9%, and averaging in the world at around 4.6%.³ Figure 2 shows the fraction of renewables by country in 2019, and it is possible to verify that, according to IEA global energy

balance estimates³, only two countries have a higher percentage than 15% - Sweden and Brazil. In both, the introduction of ethanol in common gasoline blend in higher fractions than other countries is the main reason for the relative success in biofuel deployment when compared to their peers.

In Sweden, around 50% of the ethanol production is domestic, while the remaining fraction mainly comes from European Union countries, both productions being based primarily on cereal (e.g. wheat, corn). Besides ethanol, biodiesel (mainly fatty acids methyl esters, FAME, derived from rapeseed and tall oil) also contributes to the Swedish success on implementing an environmental-based approach to transportation sector.⁵

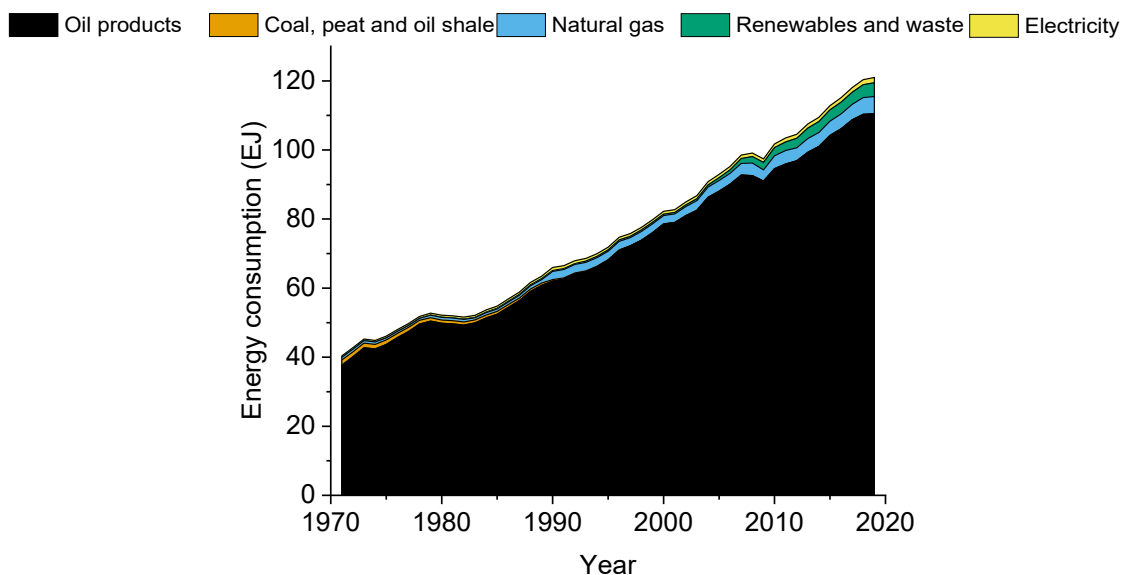


Figure 1 – Global energy consumption in transportation by source. (adapted from IEA³)

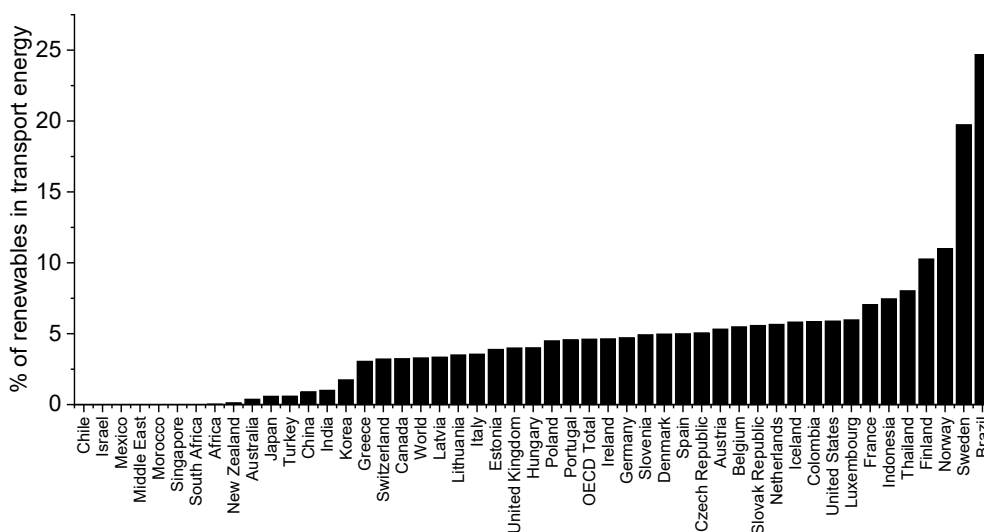


Figure 2 – Percentage of renewable energy sources in the respective transportation sector by country in 2019. (elaborated by the author based on IEA³)

The Brazilian biofuel strategy started with the “Pro-Álcool” program in 1975, which was implemented not for environmental reasons, but rather as an energy security practice due to the 1970-1980 crude oil crises.⁶ It ensured reliable supply of ethanol throughout the country that lasts until today, with pure bioethanol fuel pumps in almost all gas stations. The program has also introduced flex-fuel vehicles by the end of 1990’s, which today still are the standard car

manufacturing practice in Brazil. Most ethanol production is domestic and based on sugar extracted from sugar cane. Even though cellulosic ethanol has been gaining market space lately, its contribution is still insignificant compared to the amount of biofuel consumed in the country.⁷ Biodiesel has also entered the Brazilian energy mix with FAME of vegetable oils (mainly soy). The 24.9% renewable fraction in the Brazilian transportation sector is composed of 19.4% bioethanol and 5.5% biodiesel.⁸ Therefore, most biofuels utilized are running small vehicles.

In short, both success cases in biofuel utilization worldwide did not manage to supply more than a quarter of their fuel needs through this route and still rely on food-competing feedstock materials for their transportation energy matrixes. Their substitution of crude oil products is concentrated in small size vehicles, which are prone to be electrified in the near future. Therefore, if future global food security is to be assured, the current practices regarding biofuel production cannot continue¹, and the introduction of new renewable alternatives must focus on heavy duty and aviation biofuels.

Henrich et al.¹ estimates that cropland waste generation is currently at a 78 EJ year⁻¹ rate, of which 50% – or 39 EJ year⁻¹ – is composed of crop straw. The processing of cropland wasted materials into biofuels is a logic next step on bioenergy utilization, given their carbon rich nature and abundance. In the context of diversifying biofuel production feedstock materials away from food-competing sources, other typical agricultural wastes can be of great value, such as animal faeces.

According to Berendes et al.⁹ the estimated mass of recoverable faeces produced globally in 2014 was 3.9 Gton. Out of that, approximately 3.25 Gton are domestic animal faeces, while the rest is human. This estimate is in fresh basis, which results in around 520-845 Mton of dry faeces given a range of 16-26 wt% dry matter content.¹⁰ Ash contents of this dry matter ranges from 20 to 25%, resulting in around 390-676 Mton of organic matter with a range of 15-20 MJ kg⁻¹ HHV for animal manures.¹¹ Thus, the global energy potential in animal faeces is estimated to be around 5.9-13.5 EJ. A conservative 10 EJ year⁻¹ will be considered in the discussion.

As stated above, the predicted demand for biofuels to cover liquid fuel-dependent economic sectors is at least 68 EJ year⁻¹. Consider a theoretical energy efficiency of 50% from biomass to fuel (specifically jet fuel and diesel) for all world's biomass-to-biofuel processes combined. In this scenario, the total energy input required as biomass is doubled to 136 EJ year⁻¹. This illustrates that any gain in conversion efficiency can be paramount, where 1% of efficiency increase represents a potential energy global savings of 2.8 EJ year⁻¹.

Crop straw (39 EJ) and recoverable animal faeces (10 EJ) sum yearly around 49 EJ and the need for heavy duty transport and aviation biofuels is currently 68 EJ year⁻¹, meaning both agro wastes alone cannot supply the current demand. If the whole crop land residue estimate¹ is considered (78 EJ year⁻¹), the waste agribusiness biomass energy available yearly is 88 EJ, requiring an overall process energy efficiency conversion worldwide of 78% from biomasses to biofuels for it to be sole energy source of a fossil free transportation sector. This scenario proves unlikely that agricultural residual biomass alone can provide the biofuel need in the near future, meaning there will be a need for supplementary biomass sources. However, the currently available 78 EJ year⁻¹ in this form of organic matter is undeniably attractive due to its low or negative cost and availability. Apart from crop straw, agribusiness waste materials are considerably wet, ranging from 5 to 20 wt% dry matter contents, depending which material is considered (e.g. from diluted manure to plant stalks).

As expanding cropland by clearing other ecological systems is counter-productive in efforts to reduce greenhouse gas emissions¹², the utilization of agricultural waste should be the first method explored when trying to reach a carbon neutral global economy. Besides, when comparing the energy available as agricultural wasted materials (88 EJ) with the current contribution of biofuels (4 EJ) to the global transportation energy mix (a total of 121 EJ), it becomes evident that there is a great opportunity to support this sector if conversion processes are up to the task. As discussed, energy efficiency of such processes must be as high as possible for the technical and economic feasibility to be attained.

7.2. Energy considerations of thermochemical processes for biomass waste conversion to biofuels

Agricultural waste materials are mostly rich in lignocellulosic components, also containing proteins, short chain carbohydrates, lipids and salts. Often these materials are wet – e.g. manure, plant stalks and leaves – ranging from 70 to 95 wt% moisture, though considerably drier options are available in the form of crop straw (< 20 wt% moisture). The organic components of waste can potentially be converted into biofuels, carrying the waste energy into the transportation sector, avoiding increase in land requirements. While biofuel conversion can be conducted using biological methods, the energetic considerations in the current topic will be limited to thermochemical processes. These can be divided into pyrolysis, gasification and HTL depending on the conversion conditions.

Pyrolysis is a process that may be conducted in several different types of reactors¹³ and can be generally divided into regular, fast and flash pyrolysis, depending on the reactor residence time, which ranges from seconds to minutes. Processes aiming at producing bio-oil intermediates to biofuels are usually conducted using fast or flash pyrolysis strategies.¹³ The process operates at moderate temperatures around 500 °C in atmospheric pressure and inert atmosphere. Occasionally, feedstock oxidation is used to provide energy to the process, practice known as autothermal pyrolysis, which tends to decrease the biomass-to-fuel energy conversion by using biomass as thermal energy source and generating CO₂ instead.¹⁴ In any case, high feedstock moisture contents can drastically reduce process efficiency due water evaporation and parallel water-feedstock interactions, often requiring pre-drying to increase process bio-oil yields.¹⁵

Gasification processes are similar to pyrolysis, though in this case temperatures are higher, 700-1500 °C, depending on reactor constructions¹⁶, with the objective of producing gaseous products such as syngas, mostly composed of CO and H₂. Depending on CO:H₂ ratio, syngas may be used in classic liquid production processes such as Fischer-Tropsch, methanol synthesis, hydroformylation or even (if H₂ concentration is high enough) the Haber-Bosch process.¹⁷ Due to the high temperature needed, excessive moisture contents in feedstock are also avoided in gasification processes, as water severely damages both process energy balances and product yields.¹⁸ Moisture content limits in feedstock for gasification depend on reactor construction type, varying from 25 to 50%. The moisture limits are typically higher than pyrolysis because at such high temperatures conversion of CO and water into hydrogen may be beneficial in case hydrogen production is the aim of the process, though overall increasing tar generation. Condensable hydrocarbons generated during gasification are often referred to as tar, an undesired product in all pilot and demonstration gasification facilities.¹⁸

For both pyrolysis and gasification processing, the presence of water is damaging for process efficiency due to high energy expenses in drying procedures. Other effects are also observed, such as decrease in bio-oil generation and increase in char quality for pyrolysis and decrease in gas HHV for gasification. Taking only the drying expenses in consideration, it is already possible to estimate the difference in overall energy efficiency feedstock drying can make in thermochemical processing. Figure 3 compares the energy required to dry one kilogram of water compared to the energy needed to heat the same mass under pressure (220 bar). The amount of energy required to dry one kilogram of water is the same amount of energy required to heat compressed water until it reaches 394 °C, crossing the supercritical water state (373 °C). The potential energy savings to heat water to typical subcritical HTL conditions (around 350 °C) under pressure compared to drying it is around 1 MJ kg⁻¹. Moreover, despite evaporated water at 100 °C can potentially be used as steam, during drying processes the addition of dry air is required, leading to water dilution and consequent disposal as a gaseous byproduct, in practice losing the energy spent. On the other hand, liquid water heated under pressure can potentially serve as a heat source if proper heat exchanging equipment can handle it together with possible impurities.

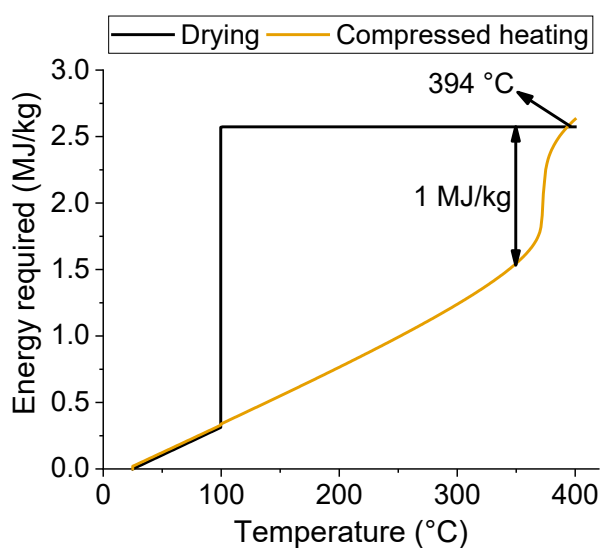


Figure 3 – Energy required to handle water during drying and compressed heating (220 bar).
(elaborated by the author based on NIST WebBook¹⁹)

With the exception of crop straw, agricultural waste materials – e.g. plant leaves, stalks, animal manure – typically have high moisture contents, meaning water handling must be one of the main parts of process design when dealing with thermochemical routes. As an example to illustrate the effect of drying energy expenses, consider cattle faeces or plant stalks. In these materials, moisture content is around 80 wt%, while the 20 wt% organic matter has typically 18 MJ kg⁻¹. The HHV per kg of slurry is actually 3.6 MJ kg⁻¹ due to the water presence. If the moisture content present is to be dried, the energy needed is 2.57 MJ kg_{water}⁻¹, or 2.06 MJ kg_{slurry}⁻¹. By difference, the harvestable energy would be 1.5 MJ kg_{slurry}⁻¹ instead of the initial 3.6 MJ kg_{slurry}⁻¹. Thus, if drying processes can be avoided while converting this 20 wt% dry matter agricultural waste into biofuels, such effort will pay out by saving around 58% of the slurry energy.

In HTL technologies water is heated under pressure which means that it is kept under liquid state at all times.²⁰ In practice, this circumvents feedstock drying, making HTL an attractive

process for wet materials processing. During HTL process, water aids the thermochemical conversion of organic matter into a crude-like substance called biocrude, which is equivalent to pyrolysis bio-oil or syngas and acts as an intermediate to biofuel production. The biocrude separates from aqueous phase right after processing due to its non-polar characteristics. Using this technique, prior drying of the feedstock materials is therefore not necessary for thermochemical conversion to take place.

Considering this processing strategy, the full $3.6 \text{ MJ kg}_{\text{slurry}}^{-1}$ from cattle faeces or plant stalks is potentially available when drying processes are circumvented. Thus, the only step determining total efficiency is HTL. If HTL processing reaches $>42\%$ energy efficiency, it is more favorable than any other processes that require a drying step for 20 wt% dry matter feedstock materials. In other words, if HTL has an energy efficiency higher than 42%, even if other thermochemical processes manage to achieve 100 % energy efficiency post-drying, HTL is overall more effective.

Subcritical HTL operates in temperatures ranging from 300 to 360 °C, which is considerably lower than pyrolysis or gasification requirements. Thus, when considering reactor heat loss and its main driving force (the difference between ambient temperature and reaction conditions), HTL also has an advantage when comparing to other thermochemical processes. This may be counter balanced by the known higher processing complexity required by HTL when compared to pyrolysis or gasification. The two latter are typically based in single reaction vessels, meaning HTL utilities may require more energy.

Overall, there is great appeal to HTL processing of agribusiness wet waste materials due to potential energy savings through this route. In HTL processing pure dry feedstock is to be avoided due to the need of a slurry as reaction media. On the other hand, diluted streams may carry too little energy into the system, damaging the overall energy efficiency. Thus, their combination may be beneficial for the technology. The results of this combination must be assessed, and one way of doing so is applying mathematical modelling.

Both mass- and carbon-based biocrude yields are very good indicatives of where materials processed energy ends up. Thus, HTL yield prediction is a great assessment tool to verify potential benefits of combining different molecule groups (e.g. lipids, carbohydrates, proteins). As agribusiness waste is composed of several different biomolecules, it is crucial to predict the potential benefits of different mixtures under HTL.

7.3. Combined HTL models based on biomolecules and their applicability

Combined biomolecules HTL yield prediction via modelling is a topic of interest due to its correlation to practical waste materials, as the latter is composed of fractions of large heterogeneous groups, e.g. carbohydrates, lipids, proteins. Model compounds were used to construct linear addition non-interactive models to predict algae liquefaction biocrude yields in singular conditions by Biller and Ross, 2011.²¹ Their work used biomasses biochemical composition and relate it to potential yields for HTL processing according to model compounds behavior. The same type of linear model was reported by Leow et al., 2015²² using microalgae feedstock composition analysis instead of model compounds, showing reasonable agreement with the dataset collect. However, the interaction of biomolecules and cross reactions between their groups during HTL processing changes to a great extent the resulting products, requiring more refined modelling for its prediction to be

reliable, such as the addition of iterative elements among biomolecules²³ or conducting surface-response-based modelling.²⁴ Overall, temperature and reaction time can also affect the HTL products, leading to the need of more elaborated models for reliable prediction.

Efforts to elaborate kinetic models based in reaction rates of biomolecule groups to enhance prediction capacity and account for reaction parameters such as temperature and time have been reported also for microalgae.²⁵⁻²⁷ Results show that biocrude yields from microalgae can be predicted with sufficient accuracy, however solid formation and aqueous phase products do not show correlation to models. In other cases, for example when applying these models (based on carbohydrates, lipids and proteins) to food waste, their accuracy is severely decreased.²⁸ Results show that waste-specific modelling provides higher accuracy, capturing feedstock-specific HTL behavior with greater reliability.

Very recently, modelling of HTL process for oil and energy yield optimization have advanced towards machine learning techniques, which can aid predictions by taking in account multiple possible interactions. These models may take in account the composition of materials (carbohydrates, lipids, proteins, ash and elemental composition) and reaction conditions, creating a multivariable predictor that iteratively determines the best feedstock and processing characteristics correlated to desired HTL products. To do so, several different computational approaches may be considered and a great number of specific algorithms are available. In one study²⁹, this technique has been reported for several different biomasses (micro and macro algae and lignocellulosic materials) and liquefaction solvents (ethanol, water and acetone) taking into account only feedstock elemental composition, oil yields and biocrudes HHVs. Results show sufficient accuracy of the model for specific experiments, however the discussion of combined effects is limited due to the data input available. Another research group has recently reported two studies: one dedicated machine learning model for micro and macroalgae based on biochemical and elemental composition³⁰ and; another model that includes, besides both types of algae, food waste, manure and sewage sludge.³¹ In both studies, results were experimentally validated using model biomolecules with success, depicting the potential of this technique.

Nevertheless, datasets used in the construction of these models did not account for combined waste materials, so it is still unclear how capable they are to predict real waste streams HTL performance. Overall, the importance of initial dataset still plays the major contribution for model construction, independent of modelling technique. That is, models based on real waste tend to perform better than model compounds.

7.4. Real waste HTL predictive models

Literature on combined real waste HTL is limited, however modelling studies using real waste samples have been reported.³²⁻³⁴ The first study conducted by Deniel et al, 2017³² reports both model compounds and real waste mixtures in an effort to understand HTL performance in subcritical conditions (fixed temperature and residence time - 300 °C, 60 min) by separating the feedstock composition into carbohydrates, lignin, proteins and lipids. The elaborated model took in account interactions of these biomolecule groups and it was shown to have a better correlation than previous models reported²¹⁻²³, though accepting >20% deviation. That³² is one of the few studies to report a model including lignin content of feedstock materials. When applying it to real organic waste

(blackcurrant pomace, raspberry achenes, brewer's spent grain and grape pomace), it could not evaluate the effect of lignin contents as the feedstock materials tested had low concentration of this biomolecule group.

Aierzhati et al., 2019³³ used food waste and its main components (carbohydrates, proteins and lipids) to construct a model including varying HTL operation conditions (temperatures from 280 to 360 °C, residence times of 10-60 min). This model performs much better than the biomolecules-based models discussed before²¹⁻²³, reaching a R² coefficient of 0.983 within the dataset collected. In both models proposed^{32,33}, the biocrude prediction is correlated with the lipid content in the initial feedstock. As lipids' carbon yields in HTL are usually >90%, the contribution is likely not interactive with other components. The only synergistic interaction of feedstock components reported in this study³³ was between lipids and carbohydrates, though the effect is much less prominent than the lipid content itself.

Li et al., 2021³⁴ merges an extensive dataset containing several types of algae, manure, food waste mixtures, food industry wastes, yeast biomasses and different types of sewage sludge to train a machine learning-based model that performs very well compared to aforementioned studies. The model presented elects the feedstock lipid content, the HTL processing temperature and retention time as the most important processing parameters for biocrude yield and energy recovery prediction. So far, this seems to be the most extensive effort to predict yields based on advanced modelling techniques. The predicted optimal mixture for HTL processing was a feedstock with 28% protein, 48% lipids and 21% carbohydrates, leading to an 80% energy recovery in biocrudes. Nevertheless, the interaction of feedstock components was not evaluated and this effect is still a variable to be optimized in further studies.

Overall, the use of real waste feedstock materials for biocrude and energy recovery prediction in HTL processing seems to be a field to be expanded on current literature. As it was discussed in Part II of this thesis, the interaction between feedstock compounds in real lignocellulosic and other feedstock materials during HTL may lead to improved yields and superior carbon and energy recoveries. This was also reported in the co-HTL processing of sewage sludge and lignocellulosic materials.³⁵ Besides the chemical advantages gained by superior carbon and energy recoveries as biocrude, engineering processing aspects, such as increase in slurry concentration via filtration, also play an important role in co-HTL strategies. Therefore, the study of real waste combined HTL is of utmost interest to understand the consequences of co-processing waste materials.

As a case study, one wet and one dry agribusiness waste feedstock materials – namely cow manure and wheat straw, respectively rich and poor in nitrogen content – were selected for a detailed investigation of the possible benefits of co-HTL. In the following chapters, the conversion from biomass to biofuels of cow manure and wheat straw will be discussed in two steps: 1 – the combined processing of both during HTL and the optimization of biocrude carbon and energy recoveries and; 2 – the effects of co-HTL biocrudes hydrotreatment under industrially common conditions. The objective of the present section is to elucidate benefits and drawbacks of co-HTL of wet and dry agricultural waste, using the case study of wheat straw and manure as basis for discussion.

Chapter 8

Manuscript 2 – Enhanced biocrude and carbon recovery from cow manure and wheat straw combined hydrothermal liquefaction via mixed feedstock optimization: from batch to continuous processing

Juliano Souza dos Passos^{a,b}, Aisha Matayeva^a, Patrick Biller^{a,b}

^a Department of Biological and Chemical Engineering, Aarhus University, Høngøvej 2, DK-8200 Aarhus N, Denmark

^b Aarhus University Centre for Circular Bioeconomy, DK-8830 Tjele, Denmark

Article history:

Manuscript to be submitted.

Keywords:

Hydrothermal liquefaction

Waste valorization

Manure

Wheat straw

Biofuel

8.1. Reflections

After the study of synthetic polymers and lignocellulosic materials' synergistic effects, the study of agribusiness waste material shows how the discussions of Part II of this thesis can be extended to other waste streams. The selection of cow manure as a representative of a wet waste was based on its composition, with a considerable amount of protein residues, and thus nitrogen. Wet waste materials tend to have a higher amount of residual protein than dry ones, which can cause severe change in HTL behavior and may provide similar synergies to PUR and lignocellulosic materials. Though in the case of wet and dry wastes the nitrogen groups will be less active than a benzo-amino group of PUR.

It was surprising to realize manure is greatly diluted during its management for reasons such as hygiene, pumping and relative low water cost. These slurries reach less than 5 wt% dry matter content, which may not be a problem for biological treatment, but dilutes greatly the stream energy potential. As currently most manure is treated via anaerobic digestion, the water added during faeces handling ends up in the biogas digestate byproduct, which is spread in agricultural fields returning nutrients in a diluted form. For the study presented in this chapter, we collected fresh cow manure after being washed in a barn, which is the most concentrated form possible to obtain this waste.

One of our group's latest reports³⁶ has shown nutrients such as phosphorus concentrate in the solid residues during HTL processing, however with reduced nutrient bioavailability. The phosphorus bioavailability can be achieved when reclaiming P as struvite, a solid with concentrated

nutrients that may be used as fertilizer in agriculture.^{37,38} In this context, the strategy presented here not only enhances carbon and energy recovery in the form of biocrude, but may also have positive effects on nutrient recovery.

The following manuscript describes the co-HTL strategy focusing in maximizing biocrude production, carbon and energy recoveries. The chemical pathways are briefly discussed, as well as the practical implementation of the strategy using a continuous HTL pilot plant.

Enhanced biocrude and carbon recovery from cow manure and wheat straw combined hydrothermal liquefaction via mixed feedstock optimization: from batch to continuous processing

Juliano Souza dos Passos^{a,b}, Aisha Matayeva^a, Patrick Biller*^{a,b}

^a Department of Biological and Chemical Engineering, Aarhus University, Høngøvej 2, DK-8200 Aarhus N, Denmark

^b Aarhus University Centre for Circular Bioeconomy, DK-8830 Tjele, Denmark

Key words: Hydrothermal liquefaction; waste valorization; manure; wheat straw; biofuel

ABSTRACT

Agribusiness crop and animal residues constitute some of the major waste streams worldwide. Among them, wheat straw and cow manure are large contributors to the quantities generated. Both materials can be converted using hydrothermal liquefaction (HTL) for recovery of biocrude and here we investigate how combined HTL processing can be of great interest to boost biocrude production and carbon recovery. This study presents batch HTL experiments using individual and blended feedstock mixtures to build predictive models for biocrude, carbon and energy recovery. These models are validated using a continuous HTL pilot plant. The combined approach led to the nitrogen-containing compounds present in cow manure to react with lignocellulosic-derived compounds from wheat straw and divert carbon into the oil phase, the reason for which biocrude, carbon and energy yields were drastically improved. Continuous HTL pilot plant campaigns successfully demonstrated increased carbon yields from 40 to 60% when using optimal feedstock ratios. Continuous data also shows the great benefits of increasing the organic matter concentration input with combined processing, resulting in total energy efficiencies larger than 50% and energy return over investment of 2.6, compared to 1.3-1.9 for individual feedstock processing.

1. INTRODUCTION

Crop waste materials are present all around the world as a result of agribusiness activities and summed up an enormous 3600 MT_{DM} of residue only in 2013¹, with wheat straw constituting around 30% of this amount. Such crops, besides feeding humans, also feed animal livestock, which unavoidably generates waste. Around 3120 MT_{DM} of animal faeces was estimated to be generated worldwide in 2014 alone.² The greatest contributor for this number is cattle livestock manure with around 41.6% of the total generation.² Both wheat straw and cattle manure are present in agricultural regions and, thus, co-processing strategies for waste handling become attractive due to such proximity.

Wheat straw is a dry lignocellulosic material with usually high ash content, often unsuitable or undesirable for combustion processes, however used in this application in some heat and power plants.³ Manure is a wet biological waste, often directly employed as fertilizer to soils, but more recently used for biogas production prior to field application.⁴ The energy-related applications of wheat straw and manure typically result in heat and electricity

production, converting carbon directly into CO₂ or going through methane as an intermediate.

An alternative product from the conversion of these biomasses could be liquid hydrocarbons that can be used both in the chemical industry and as aviation, heavy duty or marine liquid fuel.⁵ Hydrothermal liquefaction (HTL) is a technology that has shown appropriate flexibility to deal with several types of biomasses, including plant straw and manure. Wheat straw HTL has first been reported in combination with lignite coal and plastic residue, potentially showing synergistic effects with the other components.⁶ Other studies have described attractive oil yields within subcritical region for plant straw^{7,8}, including a recent comparison of wheat straw supercritical (400 °C) versus subcritical (350 °C) HTL, depicting higher carbon, energy and oil yields for the lower temperature option.⁹

Swine manure HTL was first described in the year 2000¹⁰, HTL being considered as a process to convert this type of waste, reducing its accumulation. Since then, several studies have described cattle^{11,12}, swine¹³⁻¹⁶ and both

manures¹⁷⁻¹⁹ HTL. Studies employing batch Parr reactors for subcritical HTL of swine manure found maximum biocrude yields varying from 24% (at 340 °C)^{13,15} to 48% (in presence of CO₂ at 310 °C)¹¹ with HHV of around 35 MJ/kg. A recent study comparing subcritical and supercritical processing of swine and cow manure has shown that subcritical processing (at 350 °C) results in higher biocrude, carbon and energy recovery when compared to supercritical.¹⁹ It's also shown in literature that HTL successfully decomposes different micro-contaminants usually present in manure.¹⁶ In addition, heavy metals present in livestock manure tend to primarily migrate into the solid residues of HTL (70.0%–98.0%).¹⁷

As manure waste is commonly a wet stream (dry matter of 2-10 wt.%) and wheat straw can be found considerably dryer (>80 wt.%), slurries combining both feedstock materials would save clean water consumption compared to if straw is used individually and increases the slurry dry matter compared to using manure alone, thereby taking advantage of existing livestock industry practice where excess water is used to wash out manure from the stables. Additionally, both proposed feedstock materials are found in rural areas, leading to further co-processing advantages with regards to logistics. The combination of manure and a lignocellulosic material has been shown to increase biocrude yield and quality before¹², nonetheless, the full extend and maximum biocrude, carbon and energy yields of the combined process has never been explored. Thus, to fully understand and take advantage of this co-HTL strategy, we map the best mixing ratio of wheat straw and manure, evaluate the biocrude composition and the chemical mechanisms of its synthesis and show continuous processing data in a pilot plant. This study aims at unveiling the opportunities and process advantages of combined HTL using manure and wheat straw.

2. MATERIALS

2.1. Materials used

Wheat straw (from here referred to as simply straw) used in batch and continuous experiments was harvested at Aarhus University's facilities at Foulum, Denmark. For batch processing, the material was milled using a Polymix® PX-MFC 90D knife mill with a 2 mm sieve. As for continuous processing, the milling process took place using a modified twin screw extruder (Xinda, 65 mm twin screw extruder with 2000 mm barrel length). Cow manure (from

here referred to as simply manure) was collected at the Danish Cattle Research Centre (DKC) at Foulum, Denmark. Both samples were dried in a forced circulation oven overnight at 105 °C and their elemental composition is shown in Table S1.

3. METHODS

3.1. Batch hydrothermal liquefaction

Batch HTL was carried out in 20 mL bomb-type custom made reactors. The procedure was previously described elsewhere.²⁰ A typical reaction condition was tested by adding 1.00 g of total dry matter in the desired ratio of each biomass, and 8.00 g of deionized water to the reactor, which was then sealed and submerged into pre-heated fluidized sand at setpoint temperature. After 4 minutes, the reactor already reaches the desired temperature²¹ and is kept at it for 20 minutes (including heating time). Reactors are then quenched to room temperature in water, cleaned, dried, weighed, vented and weighed again for generated gas mass determination. The aqueous phase is decanted from the reactor and the organic material remaining is washed and filtered using dichloromethane. Solids are weigh from the filtration, liquid organics are found together with the solvent, which is evaporated under nitrogen flow overnight. Aqueous phase mass yield is determined by difference from gas, solids and oil yields, which are all calculated using Equation 1.

Synergistic effects were calculated as show in Equation 2, where manure (x_1) and wheat straw (x_2) single batch experiments at a certain temperature (z) are merged into a weighted average and compared to the yield of the co-HTL batch at the same temperature ($yield_z$) and mixing ratios.²²

$$\text{Equation 1} \quad yield_{component} = \frac{m_{component}}{m_{feed}}$$

$$\text{Equation 2} \quad Synergistic\ effect = \frac{yield_z}{x_{1,z} yield_{1,z} + x_{2,z} yield_{2,z}}$$

3.2. Continuous hydrothermal liquefaction

For pure wheat straw biocrude production, a slurry was prepared using fresh water and extruded wheat straw, fully homogenized using a Microcut MCH-D 60 A wet mill in combination with a 2 m³ paddle mixer. For pure manure biocrude production, the material was processed as collected, in the form of an aqueous slurry with 8.1% dry

matter content. The co-HTL continuous experiment was conducted using a slurry prepared with the manure slurry as received added by milled wheat straw (~95% dry matter) until optimal ratio. 1%_w carboxymethyl cellulose was added to all slurries containing wheat straw to achieve satisfactory pumpability. The slurries pumpability was tested *in-situ* via a syringe test, which all passed after the preparation procedure above.

The slurries were fed in three different campaigns to the continuous HTL pilot plant (Aarhus University, Foulum, Denmark). The pilot plant detailed design²³ and

$$\text{Equation 3} \quad \eta_{tot} = \frac{E_{oil} [kW_{oil}]}{(E_{feed} + E_{pump} + E_{Trim\ heat} + E_{Reactor\ heat}) [kW_{total\ input}]} \times 100$$

$$\text{Equation 4} \quad EROI = \frac{E_{oil} [kW_{oil}]}{(E_{pump} + E_{Trim\ heat} + E_{Reactor\ heat}) [kW_{external\ input}]}$$

3.3. Analytical methods

Carbon, hydrogen, nitrogen, sulphur and oxygen (by difference) were determined using an Elementar vario Macro Cube elemental analyser (Langensfeld, Germany). To estimate higher heating value (HHV), the Channiwalla-Parikh correlation²⁶ was used as depicted in Equation 5. Energy recovery and carbon yields were calculated according to Equation 6 and Equation 7, respectively.

ATR-FTIR was conducted with a Bruker Alpha Platinum spectrometer using 24 spectra from 4000 to 400 cm⁻¹ in 2 cm⁻¹ resolution. Samples were rubbed on the diamond crystal and cleaned with appropriate solvent. Spectra were analyzed using principal component analysis

$$\text{Equation 5} \quad HHV \left[\frac{MJ}{kg} \right] = 0.3491 C + 1.1783 H + 0.1005 S - 0.1034 O - 0.0151 N - 0.0211 A$$

$$\text{Equation 6} \quad \text{Energy Recovery } (\eta_{th}) \% = \frac{HHV_{oil} \left[\frac{MJ}{kg_{oil}} \right] \cdot Yield_{oil} \left[\frac{kg_{oil}}{kg_{feed}} \right]}{HHV_{feed} \left[\frac{MJ}{kg_{feed}} \right]} \times 100$$

$$\text{Equation 7} \quad \text{Carbon yield } \% = \frac{C_{oil} \left[\frac{kg_C}{kg_{oil}} \right] \cdot Yield_{oil} \left[\frac{kg_{oil}}{kg_{feed}} \right]}{C_{feed} \left[\frac{kg_C}{kg_{feed}} \right]} \times 100$$

3.4. Experimental design and data analysis

A simplex-lattice mixture design (SLD) of two feedstock materials, namely manure (x_1) and wheat straw (x_2), coupled with a process variable, reaction temperature (z), was determined and interior points were added to augment the prediction capacity.²⁷ For the modelling of this data system, given fixed levels of the process variable, the cubic polynomial model (Equation 8) for the mixture of manure x_1 and wheat straw x_2 and a quadratic term (Equation 9) of the process variable z , temperature, results

operation²⁴ is described elsewhere. Temperature profiles and residence times are shown in Figure S1. All campaigns ran for at least 5 hours, achieving heat transfer steady state in 2h²⁵ and using the following 3 hours of steady state for heat efficiency calculations. All produced biocrudes were analyzed for solid content (using DCM), water content (Karl-Fischer titration) and CHNS analysis (Elementar vario Macro Cube elemental analyser). Total energy efficiency (η_{tot}) was calculated using Equation 3 and the energy return over investment (EROI) was calculated using Equation 4.

(PCA) for insights on which wavelengths most differ among samples, and thus, which chemical bonds can be assigned as characteristic changes.

Gas chromatography coupled with mass spectrometry (GC-MS) was measured using an Agilent 7890B GC and a quadrupole mass filter MS Agilent 5977A. Around 10 mg of biocrude were diluted in 1 mL DCM with 4-bromotoluene internal standard and injected on a VF-5ms column (65 m x 0.25 mm x 0.25 μ m). The analysis sequence was described elsewhere.²² All molecules assignments were based on NIST mass spectra database 2017.

in the integrated Equation 10. Where $f(x)$ is the Scheffé cubic mixture model for 2-component mixture, $g(z)$ is the quadratic model and $\beta_i(z) = \beta_i \cdot (\alpha_0 + \alpha_1 z + \alpha_2 z^2)$. By multiplication of the terms the equation could be defined as Equation 11.

Equation 8

$$f(x) = \beta_1 x_1 + \beta_2 x_2 + \beta_{12} x_1 x_2 + \beta_{12(1-2)} x_1 x_2 (x_1 - x_2)$$

Equation 9

$$g(z) = \alpha_0 + \alpha_1 z + \alpha_2 z^2$$

Equation 10

$$\eta_{zx} = \beta_1(z)x_1 + \beta_2(z)x_2 + \beta_{12}(z)x_1x_2 + q_{12}(z)x_1x_2(x_1-x_2) + \beta_1(z^2)x_1 + \beta_2(z^2)x_2 + \beta_{12}(z^2)x_1x_2 + q_{12}(z^2)x_1x_2(x_1-x_2)$$

Equation 11

$$\eta_{zx} = \gamma_1^0 x_1 + \gamma_2^0 x_2 + \gamma_{12}^0(z)x_1x_2 + \gamma_{12(1-2)}^0 x_1x_2(x_1-x_2) + \gamma_1^1 x_1 z + \gamma_2^1 x_2 z + \gamma_{12}^1 x_1 x_2 z^2 + \gamma_{12(1-2)}^1 x_1 x_2 (x_1 - x_2) z + \gamma_1^2 x_1 z^2 + \gamma_2^2 x_2 z^2 + \gamma_{12}^2 x_1 x_2 z^2 + \gamma_{12(1-2)}^2 x_1 x_2 (x_1 - x_2) z^2$$

where $\gamma_i^0 = \beta_i \cdot \alpha_0$, $\gamma_i^1 = \beta_i \cdot \alpha_1$, $\gamma_i^{12} = \beta_i \cdot \alpha_2$.

In Equation 11 the first four terms represent the linear, quadratic and cubic blending of the mixtures. The last eight terms represent the changes in these linear, quadratic and blending effects caused by the temperature. The quadratic term γ_{12}^i is called nonlinear blending term and represent the synergistic effect if it is positive.²⁷ Correspondingly, it represents antagonistic effect if it is negative. The cubic term $\gamma_{12(1-2)}^i$ represent both synergistic and antagonistic effects existing between mixture components.

In the present study five ratios of manure to wheat straw (0/1, 0.25/0.75, 0.5/0.5, 0.75/0.25 and 1/0) was crossed with four-level of one process variable of temperature (300, 325, 350, 365 °C). For each level of the process variable, the experimental design contains 2 vertices, 1 center of edges, 2 thirds of edges with 2 replicates for all points, resulting in total 40 runs. The temperature was coded for statistical calculations (-1, -0.23, 0.54 and +1 for 300, 325, 350, 365 °C, respectively). The biocrude yield, energy recovery and carbon yield have been selected as the response variables. The SLD mixture design for the co-HTL of manure and wheat straw coupled with the process variable (temperature) has been carried out using R software. The regression quality assessment included analysis of variance (ANOVA) and residuals.

4. RESULTS AND DISCUSSIONS

4.1. Biocrude yield, elemental analysis and HHV

Mixing ratio of different wastes in co-liquefaction processing is an important factor to be considered and affects oil, carbon and energy recovery, depicting synergistic and antagonistic interactions.²⁵ Such effects must be understood for best implementation of different strategies combining feedstock materials. Figure S2 depicts the full mass balance for the experiments. In Figure 1A it is possible to observe higher oil yields are found in co-HTL for most temperatures tested. The effect can be better observed in Figure 1B, where synergistic effects are shown, depicting up

to 1.45 times the oil yield when compared to the weighted average of co-HTL using single HTL experiments. Straw biocrude yield increased from 23.3% to 28.6% with an increment of temperature from 300 to 325°C and 350 °C, slightly decreasing at 365 °C to 26.9%. Similarly, the highest manure biocrude yield was 29% at 325°C, though elevating temperature increased also production of water soluble polar and gaseous compounds. Both manure and wheat straw contain significant fractions of cellulose and hemicellulose, which are known to undergo retro-aldol cleavage reactions at higher temperatures, which can explain the observed behavior.²¹

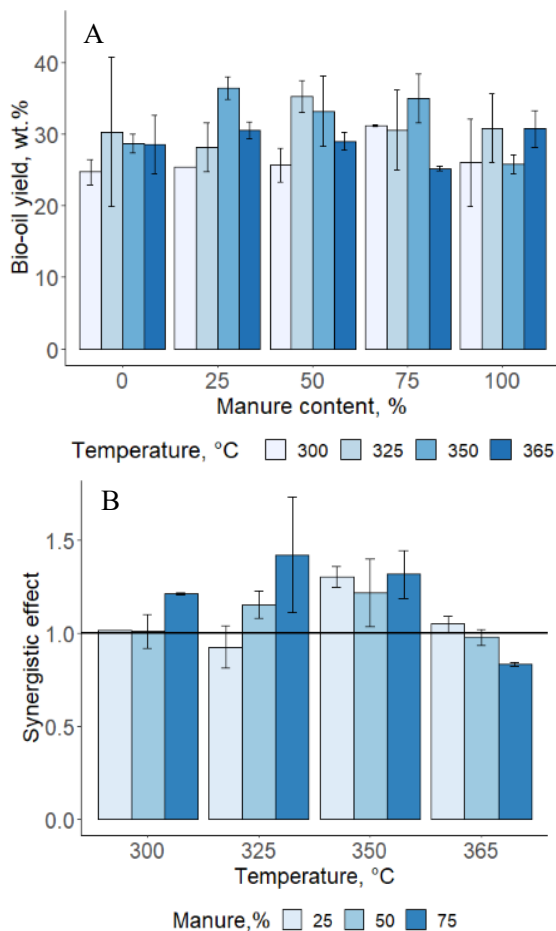


Figure 1 - a) Biocrude yields and b) synergies for biocrude from co-liquefaction of manure and wheat straw with different mixing ratios

Based on the observed synergy of manure and straw co-HTL (Figure 1B), it can be assumed that higher content of manure gives rise in biocrude yields due to the higher alkalinity resulted from protein degradation. However, oil yields obtained from the supplementary experiments performed on the wheat straw HTL using 1% KOH (Supporting information Figure S3) did not show significant changes at 300 and 325 °C, increasing only by 5% the oil yield at 350 °C. Thus, the improved biocrude yields from the co-liquefaction of manure and wheat straw are not only due to the alkaline environment, but also from the chemical interactions between manure and wheat straw products.

4.2. Element analysis and HHV

Both manure and wheat straw are feedstock materials characterized by significant oxygen content of 28 and 46%, respectively, resulting in higher heating values (HHV) of 17.3 and 14.8 MJ/kg (Table S1). The CHNS-O and HHV values of the biocrude products are presented in Table 1. As

expected judging by feedstock composition, with an increment of manure fraction in initial feed, the nitrogen content of biocrudes increased for all temperatures tested. On the other hand, oxygen content varied from 14.6 to 26.9% depending on the temperature and mixing ratios. The only trend found in oxygen content was at 365°C, where it decreased and carbon content increased with the increment of manure content. Therefore, HHV values of biocrude products were higher at higher temperatures. In comparison, at 325°C the oxygen content decreased with the manure content from 0.25 to 0.75, but the carbon content did not change significantly, while at 300 and 350 °C the carbon content decreased as well. This shows that an increase in biocrude yields occurred due to the incorporation of more O and N containing species into the oil components. It is important to highlight that an increase in oil yields is not always beneficial in terms of their quality, as this phenomenon could occur due to the undesirable migration of oxygen and/nitrogen atoms to the oil components.

Table 1 - Element analysis and HHV values of biocrude products

T, °C	M**, %	Element analysis					HHV, MJ . kg ⁻¹
		C	N	H	S	O*	
300	0.00	68.3 ± 0.6	0.8 ± 0.0	6.7 ± 0.1	0.1 ± 0.0	24.1 ± 0.6	29.2 ± 0.6
300	0.25	68.6 ± 1.2	1.8 ± 0.6	7.1 ± 0.1	0.2 ± 0.0	22.3 ± 0.6	30.0 ± 0.6
300	0.50	65.4 ± 0.4	2.2 ± 0.3	7.7 ± 0.3	0.4 ± 0.0	24.3 ± 0.5	29.3 ± 0.5
300	0.75	62.3 ± 1.1	2.7 ± 0.1	7.6 ± 0.0	0.4 ± 0.0	26.9 ± 1.1	27.9 ± 1.1
300	1.00	67.0 ± 2.2	3.2 ± 0.0	8.1 ± 0.1	0.7 ± 0.1	21.0 ± 0.5	30.8 ± 0.5
325	0.00	70.9 ± 0.4	0.9 ± 0.1	7.1 ± 0.3	0.2 ± 0.1	20.9 ± 0.1	31.0 ± 0.1
325	0.25	70.3 ± 0.2	1.8 ± 0.1	7.6 ± 0.0	0.2 ± 0.0	20.1 ± 0.6	31.4 ± 0.6
325	0.50	65.4 ± 1.6	2.3 ± 0.1	7.8 ± 0.1	0.4 ± 0.1	24.1 ± 1.0	29.5 ± 1.0
325	0.75	69.6 ± 1.8	2.9 ± 0.1	8.2 ± 0.2	0.8 ± 0.6	18.4 ± 0.8	32.2 ± 0.8
325	1.00	65.6 ± 1.5	3.0 ± 0.1	8.2 ± 0.3	0.7 ± 0.2	22.4 ± 1.2	30.2 ± 1.2
350	0.00	72.6 ± 0.4	1.1 ± 0.1	8.5 ± 1.1	0.1 ± 0.1	17.7 ± 1.7	33.5 ± 1.7
350	0.25	69.4 ± 2.5	1.8 ± 0.1	8.2 ± 1.0	0.4 ± 0.2	20.3 ± 2.1	31.7 ± 2.1
350	0.50	68.9 ± 3.7	2.6 ± 0.1	7.9 ± 0.3	0.3 ± 0.0	20.3 ± 1.4	31.2 ± 1.4
350	0.75	65.7 ± 2.0	2.9 ± 0.2	9.1 ± 0.8	0.6 ± 0.3	21.7 ± 0.8	31.3 ± 0.8
350	1.00	70.7 ± 1.7	3.2 ± 0.2	8.2 ± 0.1	1.5 ± 0.8	16.4 ± 1.0	32.8 ± 1.0
365	0.00	70.7 ± 2.8	0.9 ± 0.1	7.1 ± 0.4	0.3 ± 0.2	20.9 ± 0.8	30.9 ± 0.8
365	0.25	70.1 ± 1.8	1.5 ± 0.1	7.6 ± 0.3	0.4 ± 0.1	20.4 ± 1.5	31.3 ± 1.5
365	0.50	69.8 ± 1.8	2.2 ± 0.1	7.8 ± 0.5	1.5 ± 1.3	18.7 ± 1.7	31.7 ± 1.7
365	0.75	72.4 ± 3.4	2.7 ± 0.1	8.2 ± 0.2	1.3 ± 0.3	15.4 ± 0.2	33.4 ± 0.2
365	1.00	73.2 ± 0.4	2.9 ± 0.1	8.4 ± 0.3	0.9 ± 0.2	14.6 ± 0.6	33.9 ± 0.6

*Calculated by difference

**Manure content

4.3. Predictive model for co-liquefaction

In co-liquefaction experiments we have identified synergistic and antagonistic effects, which can be exploited to produce higher biocrude yield with improved characteristics. The quantification of these effects were performed using typical temperature range for subcritical HTL (300-365 °C) and residence time compatible to that of modern HTL continuous plants (20 min). The mixture design coupled with the process variable model (temperature) was conducted for the co-HTL of manure and wheat straw for the biocrude yield, energy recovery (ER), carbon recovery (CR) (Table S2) and the simplified models including only significant terms ($p < 0.05$) are provided in Equation 11, Equation 12 and Equation 13, where x_1 is Manure content, x_2 is Wheat Straw content and, z is the HTL batch setpoint temperature.

$$\begin{aligned} \text{Equation 12} \quad BC_{\text{yield}}\% &= 27.16 x_1 + 24.12 x_2 + 32.16 x_1 x_2 - 26.73 x_1 x_2 (x_1 - x_2) z - 30.10 x_1 x_2 z^2 \\ \text{Equation 13} \quad ER_{\text{yield}}\% &= 42.30 x_1 + 46.73 x_2 + 58.31 x_1 x_2 + 5.61 x_1 z + 5.7 x_2 z - 61.07 x_1 x_2 z^2 \\ \text{Equation 14} \quad CR_{\text{yield}}\% &= 38.94 x_1 + 40.69 x_2 + 53.97 x_1 x_2 + 4.9 x_1 z - 57.68 x_1 x_2 z^2 \end{aligned}$$

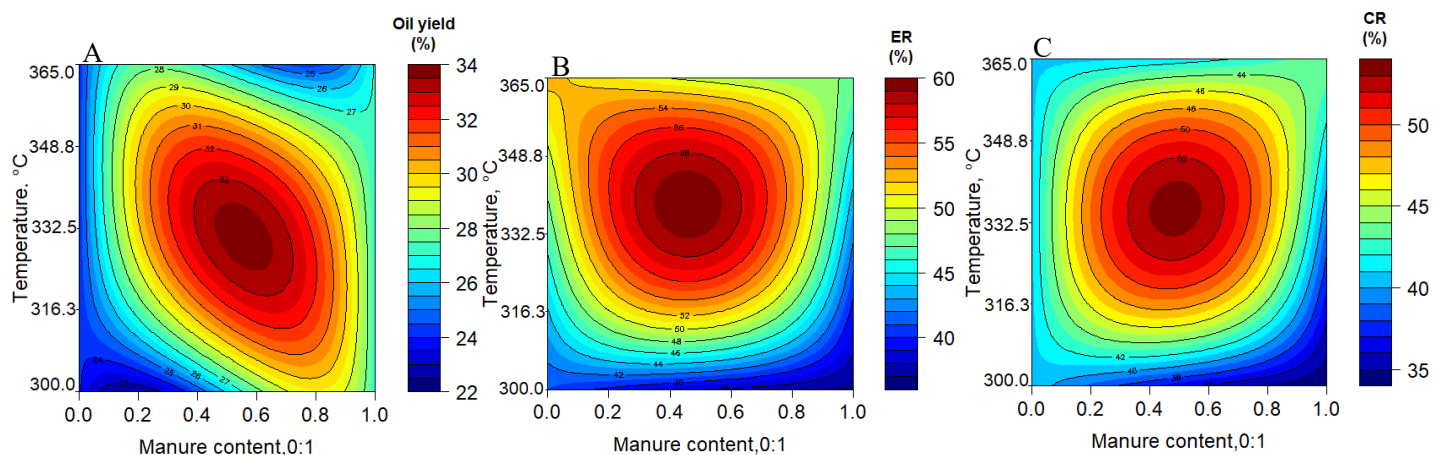


Figure 2 - Contour plots of the biocrude yield wt.% (A), ER % (B) and, CR % (C).

For all equations, the quadratic term was significant and its positive value indicates a parabola with defined maximum, i.e. that the x_1 and x_2 components act synergistically on the biocrude yield, ER and CR. On the other hand, the cubic mixing term of two feeds $x_1 x_2 (x_1 - x_2)$ combined with temperature z indicates that both synergistic and antagonistic effects are present on the biocrude yield depending on mixing ratio and temperature at the same time. For the ER, additional interactions of the linear terms x_1 , x_2 and quadratic term $x_1 x_2$ with the temperature z emphasize the role of temperature on the individual fractions as well as their different mixing ratios.

The developed prediction models were further employed to generate contour plots to illustrate the optimal operating parameters that maximize the biocrude yield, ER

and CR (Figure 2). It is possible to observe that for a manure content of around 0.45-0.65, a maximum biocrude yield of 34% can be obtained in the co-HTL at 325-335 °C. In general, with increase in the manure content, lower temperature is required to get higher biocrude yield. Similarly, the CR of about 55% can be achieved at the mixing ratio of 0.4-0.6 and at 325-335 °C. For ER it is also possible to observe that pure wheat straw and high temperatures are needed for ER > 50%, whereas when the synergistic effects of manure co-HTL are exploited, processing temperature can be reduced significantly. ER of 60 % can be achieved with manure concentration in feed around 0.35-0.55 and temperatures of 330-345 °C.

Similar patterns observed for all three models indicate that a strong synergistic effect exists between manure and

wheat straw at the mixing ratio of 0.4-0.6. The literature could provide some insights into potential causes of this synergistic effect. For instance, Zhang et al.²⁸ reported that the highest biocrude yield was obtained with the ratio of glucose to protein of 3/1. To explore these observations further, biocrude analysis is discussed in the following sections.

4.4. Biocrude characterization

4.4.1. GC-MS

Figure 3 depicts clustered GC-MS compound areas in four groups, namely phenols, carboxylic acids, N-compounds and alcohols, ketones and aldehydes over straw fraction. There seems not to be an effect on identified phenols according to straw participation on feed, as observed in Figure 3A. Similarly, in Figure 3D, alcohol, ketones and aldehydes do not depict a clear trend, despite having a much lower presence in pure straw HTL biocrude. It is however clear in Figure 3B and Figure 3C that the lower straw, and consequent higher manure, in feed composition increases the carboxylic acid presence along with nitrogen-containing molecules. The latter can be explained by the increase of N in feed, as manure has a considerable protein content. The former seems to follow results reported elsewhere⁸ where carboxylic acids are favored by higher lignin contents. The description goes against expectations that alkalinity caused by higher amounts of nitrogen in feed would increase pH not favoring formation of carboxylic acids, as would be expected following previous literature, which describe carboxylic acids as prone to reacting with nitrogen compounds in the migration of nitrogen during HTL.¹⁸

Figures S5, S6, S7 and S8 show selected phenolics, carboxylic acids, nitrogen-containing and alcohols, ketones and aldehydes compounds separately. It is possible to see in Figure S5 that some compounds tend to increase their presence with decreasing straw participation in feed, such as phenol, p-cresol, 4-propyl-phenol, 2-methoxy, 4-propyl-phenol. It is surprising that increasing the feed participation of the component with most lignocellulosic material in its composition decreases phenolic production for specific compounds. However, it is not all compounds that follow the same trend. This could indicate that some of the reported compounds are more prone to recombine when in presence of manure-derived molecules.

Observing both Figure 3 and Figure S6 it is clear that the majority of carboxylic acids are more prone to appear in

the oil phase when manure participation in the feed is higher. This could be an effect of lipid-derived molecules, such as undecanoic acid, creating a more favorable non-polar phase for organic acids to be partitioned in. As for nitrogen compounds depicted in Figure S7 and following Table S1, the more nitrogen in the feed, the more nitrogen compounds. The majority of those found by GC-MS are heterocyclics, which contribute with non-polar phase stability.

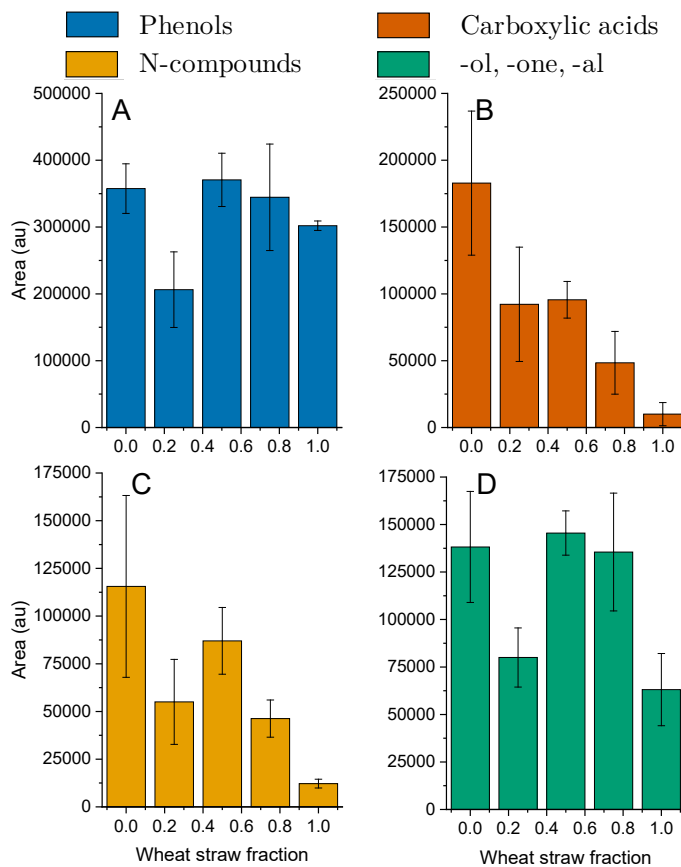


Figure 3 – GC/MS grouped areas for A) phenolics; B) carboxylic acids; C) nitrogen-containing compounds; D) alcohols, ketones and aldehydes (Temperature of 325 °C)

4.4.2. ATR-FTIR

The PCA using ATR-FTIR data revealed distinct peaks explaining most variance in the sample group, as shown in Figure 4. PC1 explains >70% of the total variance in the dataset and depicts that the region between 1700 and 500 cm^{-1} is remarkably diverse. Within this region, sharp peaks are found at 1586 and 1075 cm^{-1} , the latter with clear shoulders. The first, together with a minor 1515 cm^{-1} peak, are related to C=C stretching, indicating the degree of unsaturation plays an important role in differentiating biocrudes, while the second is connected to C–O from primary alcohols derived both from lignocellulosics and

protein groups. Simultaneously, broad contributions with several minor peaks are found within 1460 to 900 cm^{-1} and 720 to 400 cm^{-1} . Both are remarkably filled with minor deviating peaks, such as 1420, 1354, 1320, 1205 and 925 cm^{-1} in the first region and 582, 525 and 460 cm^{-1} . Within these

regions, each biocrude fingerprint diverges due to several chemical groups, including C–O, C–C, C–N groups. Finally, the typical CH_3 and CH_2 sharp peaks are clearly found both in PC1 and PC2 at 2918 and 2850 cm^{-1} , right by the side of a broad O–H contribution in PC1 peaking at 3340.

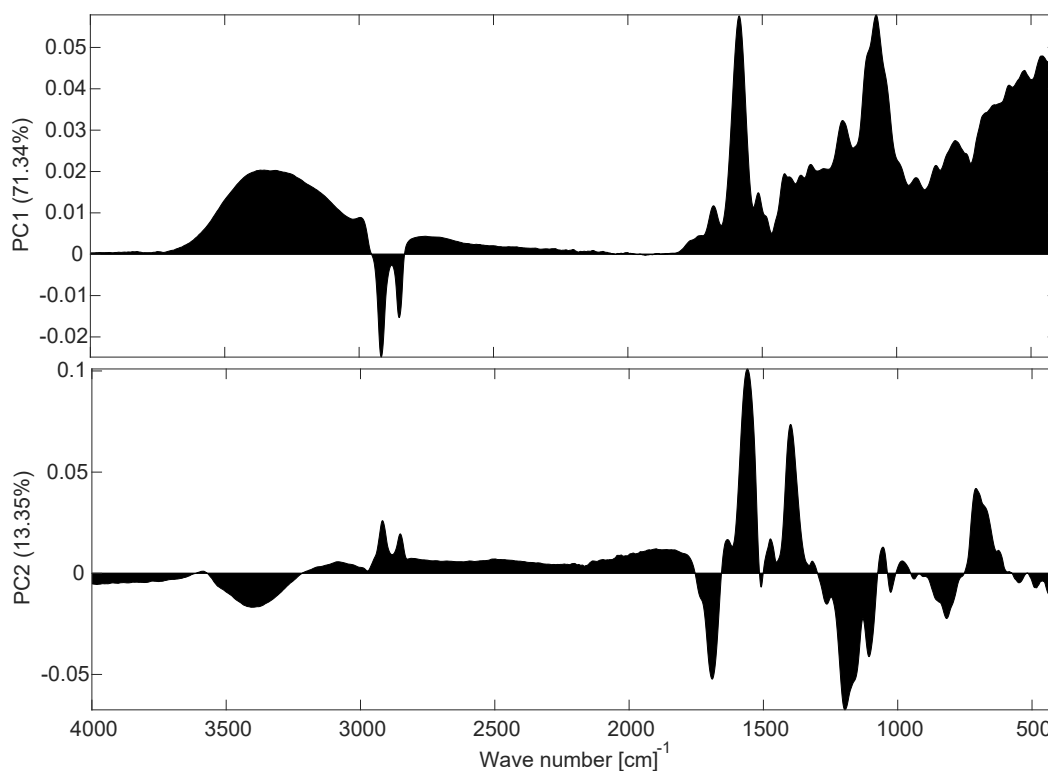


Figure 4 – Principal Components 1 (71.34%) and 2 (13.35%) GC/MS grouped areas for A) phenolics; B) carboxylic acids; C) nitrogen-containing compounds; D) alcohols, ketones and aldehydes

PC2 on the other hand has much lower interferences in the form of prominent baselines in the fingerprint region ($< 1500 \text{ cm}^{-1}$), with distinct sharp peaks both positive and negative. 708 cm^{-1} can be related to C–H bending in C_6 aromatic groups, while the 818 cm^{-1} is connected to C=C alkene bending (stretching also at 1560 cm^{-1}). Both of them again indicate that saturation and aromaticity are distinctive within biocrude samples. Ether and ester groups are also present as dissimilar features in 1106, 1196, 1400 cm^{-1} . At 1633 cm^{-1} it is possible to see a small peak which can be related to N–H side groups. On the left side of the spectra, a remarkable separation of the 3000–3200 cm^{-1} positive peak and the 3200–3590 cm^{-1} negative one depicts that the related amino-groups (former) and alcoholic groups (latter) are identified as dissimilar characteristics among biocrudes. In the 3200–3590 cm^{-1} region, around 3530 and small shoulder is present, possibly due to primary amines, while the rest can be related to secondary amines and heterocyclic nitrogen. Heterocyclic nitrogen compounds

containing nitrogen are especially important in synergistic processes²⁵, given its typical stability. The more N-containing heterocycles are formed, the more biocrude yield will follow, as the nitrogen present in manure will be prone to carrying carbon to a more non-polar phase. Figure S9 depicts straw, manure and mixed 325 °C biocrudes FTIR spectra for observation.

The PCA score plot of PC1 versus PC2 depicted in Figure 5 shows partial separation of biocrudes according to mixing ratio of feedstock. Pure straw is positioned in upper section and mixtures are spread in the descending diagonal from right to left according to manure feedstock contribution. This means the peaks depicted and discussed before (Figure 4) successfully tells apart biocrudes according to their initial feedstock composition.

Accordingly, PC1 arguably focuses in C=C, C–O, C=O groups, while PC2, despite having the same groups in its peak description, also takes in account nitrogen-related subgroups. Bearing this in mind, we can say that, besides

nitrogen content and form (also depicted in Table 1), aromaticity and oxygenated groups are distinctive traces of these biocrudes. The more manure content in the feedstock, the lesser the aromaticity and oxygenated groups, however the higher amino group are present. This means wheat straw contributes, as expected⁸, to aromatics and oxygen heteroatoms in the biocrude compounds.

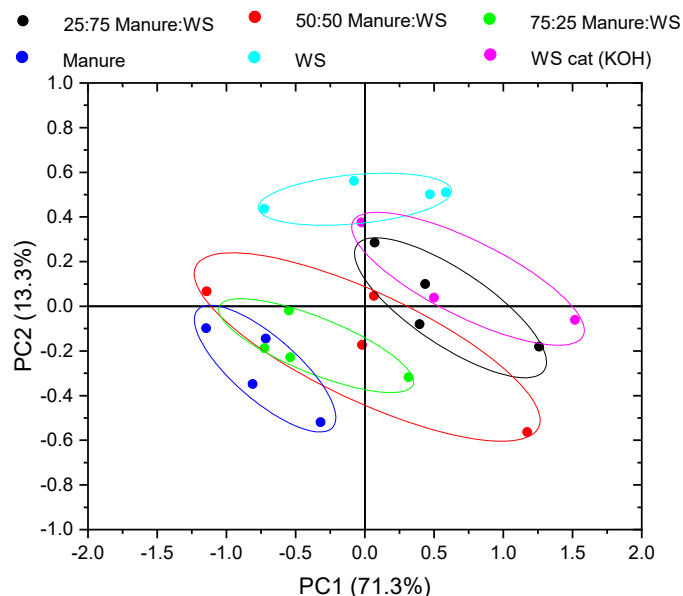


Figure 5 – Principal component 1 versus 2 score plot

4.5. Continuous processing

Due to relative low dry matter content, slurry pumpability of manure was optimal with feedstock as received. However, for both two slurries containing straw (pure straw and combined with manure), the addition of 1% slurry basis of CMC enhanced largely the slurry flowing properties and provided conditions for successful continuous processing. The wet-milling procedure also increased pumpability of slurries containing straw, which shows the importance of slurry handling when dealing with lignocellulosic biomasses. Such observations are in good agreement with HTL continuous processing experience reported elsewhere.^{23,24,29}

As shown in Table 2 and Figure S1, flow rates and residence times for all campaigns were within 9 kg/h and 1.5 minutes, which are considered here sufficiently similar for yields and energy balance comparisons. The increase in dry matter content achieved with addition of straw to manure slurry (from 8.1% to 14.7%) resulted in significant increase of energy input in the pilot plant through feedstock from 24.5 kW to 47.2 kW. The latter being even higher than pure

straw slurry, which was 41.9 kW (Table 2). This shows a benefit of straw and manure continuous co-processing just by making energy balances more favorable through the increase of energy carried into the HTL process per unit of plant activity time.

The predicted biocrude yields and respective confidence intervals (90%) to the operating conditions shown in Table 2 using Equation 11 are for straw 24% (20-28%), manure 27% (25-30%) and combined processing 33% (26-38%), and the continuous results show straw with 26.9%, manure 35.2% and combined processing yielding 38.5%. The model, thus, seems to successfully predict all biocrude yields within confidence intervals. For ER, Equation 12 predicts 47% (39-54%), 43% (36-44%) and 55% (42-65%), while continuous data shows 44.7%, 59.8%, 63.8% for straw, manure and combined processing respectively. This shows that ER was underestimated for manure and estimated correctly for straw and combined processing. Finally, the carbon recovery predicted for straw, manure and combined processing by Equation 13 was 41% (34-47%), 44% (35-47%) and 53% (40-63%), while continuous data show 39.7%, 56.2% and 60.2% respectively. In this case, the model successfully predicts straw and combined processing, while underestimates manure.

Biocrudes prepared via continuous processing presented HHV comparable with batch results (see Table 1 and Table 2), which indicates atomic composition similarity as expected. The total efficiency (η_{tot}) of the HTL processes was, respectively 36.3%, 40.8%, 51.4% for straw, manure and combined processing i.e. the amount of energy recovered from biocrude, compared to the amount of energy put in the system, combined heating, pumping utilities and feedstock carried energy, was at least a third and at best half. The best η_{tot} was achieved with combined processing, which not only benefits from chemical synergistic effects, but also by the increased energy in feedstock to be superior than the alternative single feedstock processing.

The EROI, which shows how much energy is recovered as biocrude for every unit of energy spent in electrical utilities (pumping and heating), values are respectively 1.9, 1.3 and 2.6, for straw, manure and combined processing. Manure value approaches unitary as energy input via feedstock was diminished given its dry matter content, which means more energy was spent pumping water rather than convertible feedstock. The number increases for straw processing and doubles for combined processing. For straw this happens because, even though its ER is lower than manure (as shown in Table 2),

its slurry was more concentrated in dry matter and thus carried more energy to be converted. As for combined processing, besides the slurry dry matter concentration, the

synergistic effects discussed were capable of increasing the amount of energy recovered as biocrude.

Table 2 – Continuous processing results

Property	Value	±	Value	±	Value	±	Unit
Feed slurry properties	Straw		Manure		Straw + manure		
Manure concentration in feed	0.00	-	1.00	-	0.52	-	$\text{g}_{\text{Manure}}/\text{g}_{\text{Feed}}$
Wheat straw concentration in feed	1.00	-	0.00	-	0.48	-	$\text{g}_{\text{Wheat Straw}}/\text{g}_{\text{Feed}}$
Manure : Wheat Straw ratio in feed	-	-	-	-	1.07	-	$\text{g}_{\text{Manure}}/\text{g}_{\text{Wheat Straw}}$
Mass flow rate	54.2	0.1	60.2	0.1	63.1	0.1	kg/h
Dry matter content	16.1%	0.3%	8.1%	0.2%	14.7%	0.4%	(wt.%)
Average reactor temperature	329.8	8.3	319.7	9.3	319.0	9.6	°C
Energy in Feedstock	41.9	0.1	24.5	0.1	47.2	0.1	(kW, dry)
Bio-crude							
Bio-crude yield (dry ash free)	26.9%	-	35.2%	-	38.5%	-	($\text{kg}_{\text{oil}} / \text{kg}_{\text{input}}$)
Bio-crude carbon yield (dry ash free)	39.7%	-	56.2%	-	60.2%	-	($\text{kg}_{\text{C oil}} / \text{kg}_{\text{C Input}}$)
Bio-crude Nitrogen yield (dry ash free)	38.5%	-	36.4%	-	41.2%	-	($\text{kg}_{\text{N oil}} / \text{kg}_{\text{N Input}}$)
HHV bio-crude (dry ash free)	28.7	0.4	30.6	0.4	30.4	0.3	(MJ/kg)
Energy in Bio-crude (dry ash free)	18.7	0.2	14.6	0.3	30.1	0.0	(kW, dry)
Energy Recovery (η_{th})	44.7%	-	59.8%	-	63.8%	-	(%)
Trim heater energy requirements	5.2	1.3	6.1	0.2	6.1	0.5	(kW)
Reactor energy requirement	4.0	0.0	4.8	0.0	4.8	0.0	(kW)
Main pump energy requirement	0.7	-	0.7	-	0.7	-	(kW)
Total efficiency (η_{tot})	36.1%	0.2	40.6%	0.0	51.2%	0.1	(%)
EROI	1.9	0.3	1.3	0.2	2.6	0.2	$\text{kW}_{\text{Oil}} / \text{kW}_{\text{Electric input}}$

5. CONCLUSION

Combined processing of straw and manure showed high synergistic effects in batch and continuous processing. The biocrude composition of these depicted that incorporation of nitrogen in biocrudes from combined processing was higher than in manure processing, which indicates nitrogen acted as a carbon carrier to the biocrude fraction. The form in which this nitrogen was incorporated in biocrude is amino groups connected to carbon chains and aromatic heterocyclic nitrogen. The latter is of importance to understand the synergistic effect given its typical stability. In summary, the more heterocyclic nitrogen-containing compounds are formed, the more stable the biocrude will be and, thus, the more biocrude in the end of the process.

The predicting models developed based on batch data mainly underestimated the results obtained via continuous pilot processing. Nevertheless, it gave understanding of optimal mixing ratios and temperature for straw and

manure conversion. The predicted optimal carbon yield and energy recovery were estimated within confidence intervals. Such results are encouraging, as estimates were within 10% of continuous processing results.

The continuous processing described here depicted that advantages can be taken from combined HTL not only from the chemical perspective of increasing carbon yield and energy recovery, but also for overall energy balances. In specific, the fact that manure is found as a diluted biomass slurry can be corrected by the addition of straw, resulting in a more favorable energy recovery (from 44.7% to 63.8%) and total efficiency (from 40.6% to 51.2%).

ACKNOWLEDGEMENTS

This research was funded. This project has received funding from the European Union's Horizon 2020 research and innovation grant agreement No. 764734 (HyFlexFuel), the

European Research Council (ERC) under the European Union's Horizon 2020 research and innovation program grant No. 849841 (REBOOT) and the Aarhus University Centre for Circular Bioeconomy (CBIO).

REFERENCES

- (1) Cherubin, M. R.; Oliveira, D. M. D. S.; Feigl, B. J.; Pimentel, L. G.; Lisboa, I. P.; Gmach, M. R.; Varanda, L. L.; Morais, M. C.; Satiro, L. S.; Popin, G. V.; et al. Crop Residue Harvest for Bioenergy Production and Its Implications on Soil Functioning and Plant Growth: A Review. *Sci. Agric.* **2018**, *75* (3), 255–272. <https://doi.org/10.1590/1678-992x-2016-0459>.
- (2) Berendes, D. M.; Yang, P. J.; Lai, A.; Hu, D.; Brown, J. Estimation of Global Recoverable Human and Animal Faecal Biomass. *Nat. Sustain.* **2018**, *1* (11), 679–685. <https://doi.org/10.1038/s41893-018-0167-0>.
- (3) Miles, T. R.; Miles Jr, T. R.; Baxter, L.; Bryers, R. W.; Jenkins, B. M.; Oden, L. L. Alkali Deposits Found in Biomass Power Plants: A Preliminary Investigation of Their Extent and Nature. *NREL/TP* **1995**, *1*. <https://doi.org/10.1163/156852403322849323>.
- (4) HE, Z.; PAGLIARI, P. H.; WALDRIP, H. M. Applied and Environmental Chemistry of Animal Manure: A Review. *Pedosphere* **2016**, *26* (6), 779–816. [https://doi.org/10.1016/S1002-0160\(15\)60087-X](https://doi.org/10.1016/S1002-0160(15)60087-X).
- (5) Henrich, E.; Dahmen, N.; Dinjus, E.; Sauer, J. The Role of Biomass in a Future World without Fossil Fuels. *Chemie-Ingenieur-Technik* **2015**, *87* (12), 1667–1685. <https://doi.org/10.1002/cite.201500056>.
- (6) Wang, B.; Huang, Y.; Zhang, J. Hydrothermal Liquefaction of Lignite, Wheat Straw and Plastic Waste in Sub-Critical Water for Oil: Product Distribution. *J. Anal. Appl. Pyrolysis* **2014**, *110* (1), 382–389. <https://doi.org/10.1016/j.jaap.2014.10.004>.
- (7) Zhu, Z.; Rosendahl, L.; Toor, S. S.; Yu, D.; Chen, G. Hydrothermal Liquefaction of Barley Straw to Bio-Crude Oil: Effects of Reaction Temperature and Aqueous Phase Recirculation. *Appl. Energy* **2015**, *137*, 183–192. <https://doi.org/10.1016/j.apenergy.2014.10.005>.
- (8) Tian, Y.; Wang, F.; Djandja, J. O.; Zhang, S. L.; Xu, Y. P.; Duan, P. G. Hydrothermal Liquefaction of Crop Straws: Effect of Feedstock Composition. *Fuel* **2020**, *265* (2001). <https://doi.org/10.1016/j.fuel.2019.116946>.
- (9) Seehar, T. H.; Toor, S. S.; Shah, A. A.; Pedersen, T. H.; Rosendahl, L. A. Biocrude Production from Wheat Straw at Sub and Supercritical Hydrothermal Liquefaction. *Energies* **2020**, *13* (12). <https://doi.org/10.3390/en13123114>.
- (10) He, B. J.; Zhang, Y.; Funk, T. L.; Riskowski, G. L.; Yin, Y. Thermochemical Conversion of Swine Manure: An Alternative Process for Waste Treatment and Renewable Energy Production. *Am. Soc. Agric. Eng.* **2000**, *43* (6), 1827–1833.
- (11) Yin, S.; Dolan, R.; Harris, M.; Tan, Z. Subcritical Hydrothermal Liquefaction of Cattle Manure to Bio-Oil: Effects of Conversion Parameters on Bio-Oil Yield and Characterization of Bio-Oil. *Bioresour. Technol.* **2010**, *101* (10), 3657–3664. <https://doi.org/10.1016/j.biortech.2009.12.058>.
- (12) Saba, A.; Lopez, B.; Lynam, J. G.; Reza, M. T. Hydrothermal Liquefaction of Loblolly Pine: Effects of Various Wastes on Produced Biocrude. *ACS Omega* **2018**, *3* (3), 3051–3059. <https://doi.org/10.1021/acsomega.8b00045>.
- (13) Xiu, S.; Shahbazi, A.; Shirley, V.; Cheng, D. Hydrothermal Pyrolysis of Swine Manure to Bio-Oil: Effects of Operating Parameters on Products Yield and Characterization of Bio-Oil. *J. Anal. Appl. Pyrolysis* **2010**, *88* (1), 73–79. <https://doi.org/10.1016/j.jaap.2010.02.011>.
- (14) Vardon, D. R.; Sharma, B. K.; Scott, J.; Yu, G.; Wang, Z.; Schideman, L.; Zhang, Y.; Strathmann, T. J. Chemical Properties of Biocrude Oil from the Hydrothermal Liquefaction of Spirulina Algae, Swine Manure, and Digested Anaerobic Sludge. *Bioresour. Technol.* **2011**, *102* (17), 8295–8303. <https://doi.org/10.1016/j.biortech.2011.06.041>.
- (15) Xiu, S.; Shahbazi, A.; Wallace, C. W.; Wang, L.; Cheng, D. Enhanced Bio-Oil Production from Swine Manure Co-Liquefaction with Crude Glycerol. *Energy Convers. Manag.* **2011**, *52* (2), 1004–1009. <https://doi.org/10.1016/j.enconman.2010.08.028>.
- (16) Pham, M.; Schideman, L.; Sharma, B. K.; Zhang, Y.; Chen, W. T. Effects of Hydrothermal Liquefaction on the Fate of Bioactive Contaminants in Manure and Algal Feedstocks. *Bioresour. Technol.* **2013**, *149*, 126–135. <https://doi.org/10.1016/j.biortech.2013.08.131>.
- (17) Li, H.; Lu, J.; Zhang, Y.; Liu, Z. Hydrothermal Liquefaction of Typical Livestock Manures in China: Biocrude Oil Production and Migration of Heavy Metals. *J. Anal. Appl. Pyrolysis* **2018**, *135* (September), 133–140. <https://doi.org/10.1016/j.jaap.2018.09.010>.
- (18) Lu, J.; Li, H.; Zhang, Y.; Liu, Z. Nitrogen Migration and Transformation during Hydrothermal Liquefaction of Livestock Manures. *ACS Sustain. Chem. Eng.* **2018**, *6* (10), 13570–13578. <https://doi.org/10.1021/acssuschemeng.8b03810>.
- (19) Conti, F.; Toor, S. S.; Pedersen, T. H.; Seehar, T. H.; Nielsen, A. H.; Rosendahl, L. A. Valorization of Animal and Human Wastes through Hydrothermal Liquefaction for Biocrude Production and Simultaneous Recovery of Nutrients. *Energy Convers. Manag.* **2020**, *216* (February), 112925. <https://doi.org/10.1016/j.enconman.2020.112925>.
- (20) Biller, P.; Madsen, R. B.; Klemmer, M.; Becker, J.; Iversen, B. B.; Glasius, M. Effect of Hydrothermal Liquefaction Aqueous Phase Recycling on Bio-Crude Yields and Composition. *Bioresour. Technol.* **2016**, *220*, 190–199. <https://doi.org/10.1016/j.biortech.2016.08.053>.
- (21) Gollakota, A.; Savage, P. E. Fast and Isothermal Hydrothermal Liquefaction of Polysaccharide Feedstocks. *ACS Sustain. Chem. Eng.* **2020**, *8* (9), 3762–3772. <https://doi.org/10.1021/acssuschemeng.9b06873>.
- (22) dos Passos, J. S.; Glasius, M.; Biller, P. Hydrothermal Co-Liquefaction of Synthetic Polymers and Miscanthus Giganteus: Synergistic and Antagonistic Effects. *ACS Sustain. Chem. Eng.* **2020**, *acssuschemeng.0c07317*. <https://doi.org/10.1021/acssuschemeng.0c07317>.
- (23) Johannsen, I.; Kilsgaard, B.; Milkevych, V.; Moore, D. Design, Modelling, and Experimental Validation of a Scalable Continuous-Flow Hydrothermal Liquefaction Pilot Plant. *Processes* **2021**, *9* (2), 1–18. <https://doi.org/10.3390/pr9020234>.
- (24) Anastasakis, K.; Biller, P.; Madsen, R. B.; Glasius, M.; Johannsen, I. Continuous Hydrothermal Liquefaction of Biomass in a Novel Pilot Plant with Heat Recovery and Hydraulic Oscillation. *Energies* **2018**, *11* (10), 1–23. <https://doi.org/10.3390/en1102695>.
- (25) dos Passos, J. S.; Chiaberge, S.; Biller, P. Combined Hydrothermal Liquefaction of Polyurethane and Lignocellulosic Biomass for Improved Carbon Recovery. *Energy and Fuels* **2021**, *35* (13), 10630–10640. <https://doi.org/10.1021/acs.energyfuels.1c01520>.
- (26) Channiwala, S. A.; Parikh, P. P. A Unified Correlation for Estimating HHV of Solid, Liquid and Gaseous Fuels. *Fuel* **2002**, *81* (8), 1051–1063. [https://doi.org/10.1016/S0016-2361\(01\)00131-4](https://doi.org/10.1016/S0016-2361(01)00131-4).
- (27) Cornell, J. A. *Experiments with Mixtures*; Wiley Series in Probability and Statistics; Wiley, 2002. <https://doi.org/10.1002/9781118204221>.
- (28) Zhang, C.; Tang, X.; Sheng, L.; Yang, X. Enhancing the Performance of Co-Hydrothermal Liquefaction for Mixed Algae Strains by the Maillard Reaction. *Green Chem.* **2016**, *18* (8), 2542–2553. <https://doi.org/10.1039/c5gc02953h>.

(29) Elliott, D. C.; Schmidt, A. J.; Hart, T. R.; Billing, J. M. Conversion of a Wet Waste Feedstock to Biocrude by Hydrothermal Processing in a Continuous-Flow Reactor: Grape Pomace. *Biomass*

Convers. Biorefinery **2017**, 7 (4), 455–465.
<https://doi.org/10.1007/s13399-017-0264-8>.

Chapter 9

Manuscript 3 – Upgrading of hydrothermal liquefaction biocrudes from mono- and co-liquefaction of cow manure and wheat straw via hydrotreating followed by distillation

Juliano Souza dos Passos^{a,b}, Petr Straka^c, Miloš Auersvald^c, Patrick Biller^{a,b}

^a Department of Biological and Chemical Engineering, Aarhus University, Høngøvej 2, DK-8200 Aarhus N, Denmark

^b Aarhus University Centre for Circular Bioeconomy, DK-8830 Tjele, Denmark

^c Department of Petroleum Technology and Alternative Fuels, University of Chemistry and Technology Prague, Technická 5, 166 28 Prague, Czech Republic

Article history:

Manuscript draft not submitted to any journal.

Keywords:

Hydrothermal liquefaction
Biocrude upgrading
Hydrotreating
Waste valorization
Biofuel

9.1. Reflections

The HTL biocrudes produced from cow manure, wheat straw and their optimized co-HTL are an opportunity to understand how the Maillard-like reactions that result in most synergistic effects during the process affect the follow-up upgrading. Hydrogenation of heavy oils is a common practice in the crude oil refining business, however HTL biocrude characteristics are very different from a heavy crude. For instance, the heteroatom content in the form of oxygen and nitrogen have a severe effect on hydrotreatment processing, and it does seem that more complex oils derived from the co-HTL route are harder to upgrade due to recalcitrant nitrogen species. In any case, investigating the hydrotreatment severity effect on biocrudes from mono- and co-HTL shows the ramifications of the gain in carbon and energy recovery during HTL.

Nevertheless, the very recent work published by a team of researchers from the Biofuel Engine Research Facility (BERF, Australia)³⁹ shows that high nitrogen content diesel-like fuels tend not to increase so drastically the NO_x emissions. When testing these diesel-like fuels containing up to 4 wt% nitrogen, the researchers reported that there is no significant loss in energy power, nor changes in CO or particulate matter emissions. At the same time, SO₂ emissions increase together with hydrocarbons at specific nitrogen and sulfur fuel contents.

These observations corroborate with the manuscript appended in this chapter in the sense that the distillate cuts produced may be considered applicable biofuels, even though outside current fossil standards. The current standards and legislation for liquid hydrocarbon fuels are based on virtually nitrogen-free fossil-derived fuels. Nevertheless, it is of great interest that no infrastructure

has to be modified to handle advanced biofuels and those are treated as “drop-in” solutions in fossil fuel equipment. It could be the case for less strict biofuels (such as regular diesel or marine bunker fuel) that the addition of specific units to handle slightly higher nitrogen gas outputs can broaden the biofuel specifications and enable < 4 wt% nitrogen hydrocarbon mixtures to be used. Despite being outside the scope of this thesis’ investigation, the BERF report³⁹ indicates that relatively high nitrogen contents are not necessarily an inconvenience for HTL biofuel implementation. As discussed in Chapter 7, the alternative high CO₂ footprint left by fossil fuels and its consequences are a much harder problem to solve, and HTL can greatly help in this feat.

The work presented in this chapter was conducted in partnership with the Department of Petroleum Technology and Alternative Fuels of the University of Chemistry and Technology (UCT) Prague, in Czech Republic. The work was part of my stay abroad period, when I worked with the Green Catalysts research group at UCT.

Upgrading of hydrothermal liquefaction biocrudes from mono- and co-liquefaction of cow manure and wheat straw via hydrotreating followed by distillation

Juliano Souza dos Passos ^{a,b}, Petr Straka ^c, Miloš Auersvald ^c, Patrick Biller* ^{a,b}

^a Department of Biological and Chemical Engineering, Aarhus University, Høngøvej 2, DK-8200 Aarhus N, Denmark

^b Aarhus University Centre for Circular Bioeconomy, DK-8830 Tjele, Denmark

^c Department of Petroleum Technology and Alternative Fuels, University of Chemistry and Technology Prague, Technická 5, 166 28 Prague, Czech Republic

* Corresponding author – pbiller@bce.au.dk

Key words: Hydrothermal liquefaction; biocrude upgrading; hydrotreating; waste valorization; manure; wheat straw; biofuel

ABSTRACT

Liquid hydrocarbons from agriculture wet waste can be a strategy to greatly reduce CO₂ emissions worldwide. This study presents the effect of upgrading via catalytic hydrotreatment of hydrothermal liquefaction (HTL) biocrudes derived from cow manure, wheat straw and a biocrude derived from their co-liquefaction (co-HTL). Four different temperatures are tested (340, 360, 380 and 400 °C) at constant hydrogen feed and weight hourly space velocity. The most severe hydrotreating condition ran for an extended time to produce hydrotreated products for experimental distillation. The co-liquefied biocrude showed to have a higher concentration of recalcitrant nitrogen-containing molecules towards hydrotreatment. Increase in hydrotreatment temperature increases also physicochemical quality of oil products, leading to generally higher yields of gasoline and kerosene and decreasing on average 8.5 wt% of bottom residues for every 20 °C of temperature increase. Nitrogen-containing molecules tend to have a relatively lower concentration in the gasoline distillation cuts for all three upgraded samples. Bottom residues derived from single feedstock HTL biocrudes showed to be totally miscible in fossil-derived vacuum gas oil at room temperature, while the co-HTL derived one needed increase in temperature. A carbon balance from biomass to fuel cuts for all three processing concepts shows that the co-HTL approach leads to a higher production of hydrotreated products by increasing the bottom residue fraction. Overall, single feedstock HTL leads to a carbon efficiency from biomass to upgraded oils of 34 and 38% respectively for wheat straw and cow manure, while the co-HTL approach increases this value to 43%. The combination of agribusiness waste for HTL processing is shown here to be an attractive solution for wet waste processing and carbon recovery towards advanced biofuels.

1. INTRODUCTION

Liquid hydrocarbons are consumables of upmost importance for the world's current economies, playing the role of energy carriers.¹ Today, such liquids are derived in almost its entirety from fossil reserves – namely crude oil, coal and natural gas – causing an increase in greenhouse gas concentration in earth's atmosphere by linearly converting carbon-based materials into its oxidized form (CO₂). As the natural process of converting CO₂ back to a fossil reserve takes orders of magnitude longer than their extraction and emission, the increase in concentration of CO₂ will not cease until fossil reserves use becomes obsolete. The consequences of CO₂ build-up in the atmosphere are severe and the global climate crisis will further worsen if no action is taken towards a carbon neutral economy.²

The aviation and heavy-duty transportation sectors are particularly impacted by its dependency on liquid fuels composed of hydrocarbons.³ Fortunately, not all carbon-based liquid hydrocarbons have to be fossil derived. Converting wet agricultural waste into liquid fuels could greatly alleviate greenhouse gas emissions by using photosynthetic-reduced carbon.⁴ Estimates are that globally 1080 M_{TonDM} of wheat straw was generated in 2013 alone.⁵ That, combined with around 1300 M_{TonDM} of cow manure⁶ in 2014 would sum up almost 2400 Mton of underutilized agricultural residue. Several routes of conversion for these materials are available, however wet wastes conversion into liquid hydrocarbons by the hydrothermal liquefaction technology has been gaining attention, as it avoids energy-

demanding drying processes and is able to convert otherwise wasted carbon into an intermediate oil product usually referred to as biocrude.⁷ The combination of different agricultural wastes has been proven to be beneficial to biocrude production, which can be also beneficial regarding logistics by enlarging the amount of feedstock materials available for direct processing.⁸

When HTL processes straw and manure, this biocrude intermediate oil product composition is around 62-73% carbon, 6-9% hydrogen, 0-3% nitrogen and 15-24% oxygen, with a higher heating value (HHV) of 28-34 MJ.kg⁻¹.⁸ Biocrudes from lignocellulosic and agricultural waste are typically composed of phenolics, ketones, alcohols, heteroatom-containing aromatics, amines and other molecules, increasing the nitrogen-containing aromatics with the blend of protein rich and lignocellulosic feedstock materials in HTL.^{9,10} Such oil has a high viscosity derived from its molecular composition, which combined with its lower HHV compared to typical liquid fuels makes upgrading a necessary step before final consumption of fuel-like products.

The first efforts for catalytic upgrading via hydrotreatment of HTL biocrudes were reported in the early 80's and are summarized in a publication by Elliott, D.¹¹, using both model compounds and HTL biocrudes from the Albany Biomass Liquefaction Pilot Plant. Cobalt-Molybdenum (CoMo) and Nickel-Molybdenum (NiMo) sulfided catalysts supported in alumina were identified as promising approaches for deoxygenation of this type of oil at that time, and given their classic use in fossil refining processes for denitrogenation¹², these catalysts are until today the preferred choice for bio-oil upgrading via hydrotreatment. Since then, several reports have used similar catalysts for upgrading of HTL biocrudes in batch and continuous processing apparatus from algae¹³⁻¹⁸, lignocellulosic materials^{18,19} and sewage sludge^{18,20} and pyrolysis bio-oils²¹⁻²⁵. While fast pyrolysis bio-oils have been reported to deactivate NiMo catalysts when processed via hydrotreating²³, recently, HTL biocrude hydrotreating using a two-stage catalyst bed of CoMo and NiMo with temperature gradient over the reactor was shown to have extended lifetime for upgrading of wet waste biocrude (up to 1500 h of steady-state operation).²⁶

The aim of the study is to investigate whether there is a difference in hydrotreating behavior and final distillate fuel quality if biocrudes are produced by synergistically co-liquefaction versus their individual counterparts. To do so, the influence of temperature in the hydrotreatment of three

different biocrudes is presented, one from wheat straw, one from cow manure and a third one from the optimized mixing ratio of both feedstock materials combined hydrothermal processing. Physicochemical properties of the upgraded oil product from different hydrotreatment temperatures are evaluated and discussed. Biocrudes were produced in a continuous HTL pilot plant and the hydrotreatment of those was also conducted in a continuous apparatus, mimicking expected conditions in large scale operations. Products from the most severe condition tested in the hydrotreatment experiments were individually distilled and their composition is discussed regarding its compatibility with fossil-derived products. By evaluating the quality of upgraded oils and distillate cuts and estimating the biomass to biofuel carbon efficiency, we highlight here the potential benefits and drawbacks of the approach for production of biobased hydrocarbon mixtures to be applied as biofuels.

2. MATERIALS AND METHODS

2.1. Hydrothermal liquefaction

Three separate production campaigns were conducted with wheat straw (hereafter referred to as straw), cow manure (hereafter referred to as manure) and an optimized mixture (1.1:1.0 Manure:Straw mix ratio) of both feedstock materials (hereafter referred to as co-HTL) in a continuous HTL pilot plant²⁷ located at Aarhus University's facilities in Foulum, Denmark. The HTL mixture ratio optimization is described elsewhere⁸, together with other details about the continuous biocrude production, carbon and energy balances. Part of the biocrude product from HTL was then filtered using acetone as solvent in a 20 µm paper filter. The solvent was then evaporated in a rotary evaporator and around 2.5 kg of each biocrude was taken for each hydrotreatment experiment. Acetone residual concentration was determined to be lower than 0.5 wt% by GC/MS analysis. To adjust sulfur content in the straw biocrude, dimethyl disulfide was added to this biocrude, achieving the same concentration as in other feedstock materials.

2.2. Hydrotreatment of biocrudes

The hydrotreatment took place in a co-current, downflow, assumed trickle bed reactor with hydrogen (99.9 %) flowing at a rate of 45 NL.h⁻¹ and 80 bar of pressure. The catalyst packing was selected based in previous studies^{26,28}, which show extended time on stream of a double-bed

catalyst approach with temperature gradient in the first section of the reactor for upgrading of HTL biocrudes. Here, we use also a double-bed catalyst approach of crushed (590 to 1000 μm) CoMo (35 g of 7.7 wt% Co and 28.4 wt% Mo in Al_2O_3) and NiMo (50 g of 6.6 wt% Ni and 31.8 wt% Mo in Al_2O_3) catalysts. The two catalyst zones were separated by a layer of 3 mm glass balls. The simplified process flow diagram and reactor packing details are shown in Figure S1.

Catalysts were sulfided *in situ* with 4.4 wt% dimethyl disulfide in hydrotreated gasoil flowing at a rate of 60 $\text{g}\cdot\text{h}^{-1}$, with hydrogen flow at 70 $\text{NL}\cdot\text{h}^{-1}$, pressure of 40 bar and temperature ramped from ambient to 330 $^\circ\text{C}$ in the whole reactor at 15 $^\circ\text{C}\cdot\text{min}^{-1}$, holding the final temperature for a minimum of 4 hours. After sulfided, catalysts' activity was stabilized for a minimum of 24 h running with straight run gas oil at 60 $\text{g}\cdot\text{h}^{-1}$, hydrogen flow rate of 30 $\text{NL}\cdot\text{h}^{-1}$, pressure of 40 bar and temperature of approximately 290 $^\circ\text{C}$ before biocrude was fed.

The three biocrude upgrading campaigns were conducted using freshly *in-situ* sulfided catalysts with constant biocrude weight hourly space velocity (WHSV) of 0.7 h^{-1} for CoMo and 0.5 h^{-1} for NiMo (biocrude flow rate of 25 $\text{g}\cdot\text{h}^{-1}$). The CoMo zone was heated at around 150 $^\circ\text{C}$ in the intake and temperature rose up to around 340 $^\circ\text{C}$ by the end of the first bed due to the typical exothermic reactions and setpoint temperature in the following reactor section. Four different temperatures were tested for the NiMo bed, starting with the least severe (340 $^\circ\text{C}$) and stepping up (20 $^\circ\text{C}$) to the most severe condition (400 $^\circ\text{C}$). At each temperature (340, 360 and 380 $^\circ\text{C}$), sampling started after a minimum of 4 hours stabilization and lasted for approximately 3 hours. For the last temperature (400 $^\circ\text{C}$) the sampling continued until the biocrude feedstock ran out and it was divided into two equal aliquots (hereafter referred to as 400I and 400II). Figure S2 A-C depicts the temperature, pressure and gas flows for all three campaigns. At all times the reactor pressure drop was observed not to be higher than 1 bar in all experiments. Figure S3 A-C shows the reactor average temperature profiles for each temperature tested in all three campaigns, from which the reactor temperature average was calculated using the first 4 thermocouples of the NiMo zone. After collection, the hydrotreated products showed two phases, which are further

referred to as aqueous and oil phases. Yield determination was conducted after product centrifugation to ensure complete phase separation.

2.3. Distillation of hydrotreated products

The oil phase of the three hydrotreated products collected at 400 $^\circ\text{C}$ (both 400I and 400II) in each campaign were distilled separately in a batch distillation apparatus Fischer® Scientific with a SPALTROHR HMS 500 spiral column with 90 theoretical plates. Distillation cuts are labeled here as gasoline (< 150 $^\circ\text{C}$), kerosene (150-250 $^\circ\text{C}$), diesel (250-360 $^\circ\text{C}$) and bottom residue (BR) (> 360 $^\circ\text{C}$). All distillations took place with reflux ratio of 1 and adequate pressures, avoiding distillation feedstock temperatures higher than 250 $^\circ\text{C}$.

Bottom residue fractions were tested individually for solubility in vacuum gas oil (VGO) distillate (boiling points of around 350-540 $^\circ\text{C}$). In short, 25/75, 50/50, 75/25 %wt. mixtures of bottom residues with VGO were mixed in a 5 mL vial, homogenized and spread in microscope glass slides. Microscope observation aimed at identifying the presence or not of biphasic regions in the mixture.

2.4. Analytical methods

Carbon, hydrogen, nitrogen, sulfur and oxygen (by difference) were determined using combustion analysis (Elementar Vario EL Cube). Analysis were performed according to according to ASTM D5291 for CHN and DIN 51724-3 for sulfur. To estimate higher heating value (HHV), the Channiwala-Parikh correlation²⁹ was used (Equation 1). Carbon and nitrogen yields were calculated according to Equation 2.

Gas chromatography coupled with mass spectrometry (GC/MS) was carried out with an Agilent 7890B GC and a quadrupole mass filter MS Agilent 5977A. Typically, 10 mg of sample was diluted in 1 mL DCM with 4-bromotoluene internal standard. The column used was a VF-5ms column (65 m x 0.25 mm x 0.25 μm) and the analysis sequence is described elsewhere.³⁰ Spectra was compared with NIST mass spectra database 2017 for molecular identification.

$$\text{Equation 1} \quad \text{HHV} \left[\frac{\text{MJ}}{\text{kg}} \right] = 0.3491 C + 1.1783 H + 0.1005 S - 0.1034 O - 0.0151 N - 0.0211 A$$

$$\text{Equation 2} \quad \text{Elemental yield \%} = \frac{\text{yield}_{\text{phase}} \left[\frac{\text{g}_{\text{phase}}}{\text{g}_{\text{biocrude}}} \right] \cdot \text{Element content}_{\text{phase}} \left[\frac{\text{g}_{\text{Element}}}{\text{g}_{\text{phase}}} \right]}{\text{Element content}_{\text{biocrude}} \left[\frac{\text{g}_{\text{Element}}}{\text{g}_{\text{biocrude}}} \right]} \times 100$$

Simulated distillation was conducted according to ASTM D2887 standard in an Agilent 6890 GC equipped with a capillary column DB-HT-SIMDIS, 55 m × 530- μ m id × 0.15- μ m and flame ionization detector. Standards and oil samples were diluted in DCM and calculations were performed using Agilent's Chemstation software.

ATR-FTIR spectra was collected using a Bruker Alpha Platinum spectrometer (collection of 24 spectra from 4000 to 400 cm^{-1} in 2 cm^{-1} resolution). Typically, one drop sample was placed on the diamond crystal during the measurement and cleaned with appropriate solvent in-between analysis. Principle component analysis (PCA) was conducted after spectra were smoothed with first order Savitzky-Golay filtering using 20 cm^{-1} frame length and the noise-dominant 2820-1810 cm^{-1} signals retrieved from dataset. Water content in oil phases was measured via Karl Fischer titration. Density, dynamic and kinetic viscosities were measured using an Anton Paar Stabinger SVM 3000 viscometer at 40 °C. Total acid number (TAN) and basic nitrogen in hydrocarbons were measured using an 888 titranda (Metrohm). For biocrude TAN, the last turning point among the typically 5 was considered for measurement, while for upgraded products typically only one turning point was observed. Basic nitrogen in hydrocarbons was measured according to UOP method 269-10. Micro carbon residue (μ MCR) was determined by Conradson micro method using a Normalab Analysis NMC 420 according to ASTM D4530.

3. RESULTS AND DISCUSSION

3.1. Hydrotreatment yields

The hydrotreated liquid products were typically composed of a dark oil phase and a clear aqueous phase. Usually the two phases separated without centrifugation, though the lower the temperature the more difficult the two phase formation was. Interestingly, the oil phase collected from manure at 400 °C (400I) had an orange color, clearly differing from all other collected samples. The temperature control for the upgrading campaigns of single-feedstock biocrudes were more stable, as depicted by Figure S2C reactor temperature average standard deviation, which is higher than the ones in Figure S2A-B and Figure S3. It was not possible to close the mass balance for 400II in the co-HTL biocrude campaign, thus yields are omitted in the dataset presented in Figure 1. Mass yields presented in Figure S4 correlate well with wheat straw pyrolysis upgrading with a similar catalyst bed construction, and so

does the oil-water separation ease with temperature increase.²⁴

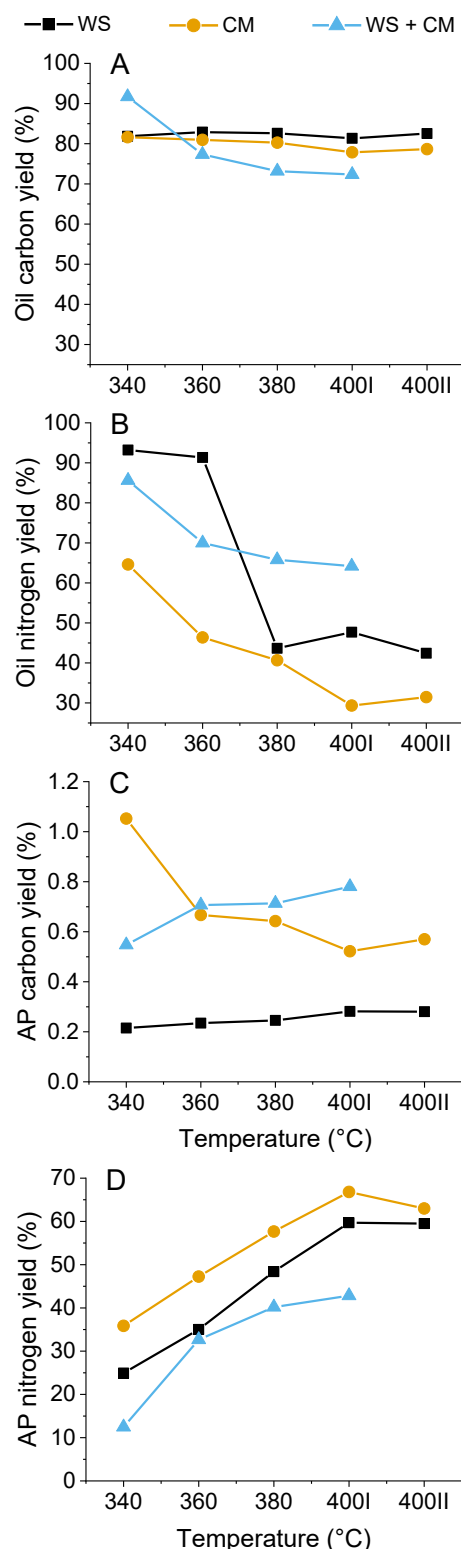


Figure 1 – Oil (A, B) and aqueous phase (AP) (C, D) carbon (A, C) and nitrogen (B, D) weight-based yields over temperatures tested for wheat straw (WS), cow manure (CM) and co-HTL biocrude of wheat straw and cow manure (WS + CM)

Figure 1A-B shows the effect of temperature in the oil carbon and nitrogen yields. For biocrudes from single feedstock, the effect is minimal and the oil carbon yield is on average 81 wt%. As for the co-HTL biocrude, the effect of temperature in the oil carbon yield is pronounced, dropping from 92 wt% at 340 °C to 73 wt% at 400 °C. Such an effect can be a sign of small sections of carbon (e.g. derived from carboxylic acids, ketones, aldehydes) attached to larger N-containing hydrocarbon structures during the co-HTL process⁸, which may be released with higher hydrotreatment temperatures. The oil carbon yields are generally higher than lignocellulosic-derived pyrolysis hydrotreated products using similar strategies^{11,22}, but fall within the range of carbon yields from hydrotreated HTL biocrudes of algae^{17,20}, sewage sludge^{20,31} or lignocellulosic³¹ materials.

Oil nitrogen yields in general decreased with increase in temperature depending on biocrude sample (Figure 1B). Manure and straw biocrudes yield less nitrogen at high temperatures in the oil phase (< 50%). However, the co-HTL biocrude shows a lesser effect of temperature in denitrogenation, decreasing the yield only from 86% to 64%. This shows the nitrogen-containing molecules in the co-HTL biocrude are more resistant to hydroprocessing and are more prone to resulting in the oil phase. As these molecules are derived from Maillard-like reactions typically followed by cyclization⁸, it is very likely N-containing heterocyclic aromatics (both pyridines and pyrroles) are responsible for these observations.

Figure 1C-D depicts the aqueous phase carbon and nitrogen yields. For carbon, yields were in general lesser than 1%, showing that most carbon retrieved from the oil phase ended-up in the gas phase instead of forming water-soluble molecules, as expected based on catalyst selection for hydro-deoxygenation.¹¹ Nitrogen aqueous phase yields generally sum up to 100% together with oil yields, showing that denitrogenation reactions tend to form water-soluble molecules, mostly ammonia, not yielding significant gaseous products.

3.2. Hydrotreatment products physicochemical characteristics

Figure 2 depicts physicochemical characteristics of biocrudes and oil phases from hydrotreated products. Figure 2A-B shows that both dynamic and kinematic viscosities decrease significantly, from 100-420 mPa.s and 90-350 mm².s⁻¹ for the biocrudes, in which the co-HTL biocrude

sample was the most viscous, to 2-5 mPa.s and 2-6 mm².s⁻¹ for hydrotreated products at 400 °C. Increasing the temperature from 340 °C to 400 °C decreased in one order of magnitude viscosity values, illustrating that deoxygenation (shown in Table S1) significantly impacts viscosities in such biocrudes. Figure 2C shows the density decrease from biocrudes (> 1.02 g.cm⁻³) to hydrotreated oil products (down to 0.85 g.cm⁻³), where the lowest density in all temperatures tested was observed for cow manure biocrudes. The characteristics of hydrotreated products prepared at high temperature are compatible to the ones from sewage sludge and food waste HTL biocrude in terms of viscosity and density.²⁶

The water content decreases to values under 1 wt% (Figure 2D) for all hydrotreated products irrespective of temperature, which illustrates the severe loss of polar compounds from biocrudes to upgraded products, making the oil phase less prone to water incorporation. This is corroborated by the previously commented enhancement in phase separation, relative high deoxygenation (Table S1) and corresponds well to hydrotreated products previously reported.²⁰ Figure 2E-F depicts that the carbon residue and TAN were decreased significantly after upgrading. The high temperature upgraded samples have only slightly higher MCR and TAN values than some types of crude oil, showing that further refining of these oils would not require major modifications to current refinery setups regarding material construction of reactors.³² A TAN lesser than 1 mg_{KOH}/g decreases the corrosion of these biocrudes, enhancing material durability in long term operation of refining processes.³² Simultaneously, a low carbon residue is desired for liquid fuels and the decrease from 25-27 wt% biocrude values to < 5 wt% depicts that the hydrotreatment was successful in eliminating most coke-prone structures present in the biocrude. Even so, there is a sensible increase in μ MCR with temperature for the co-HTL biocrude upgraded products, which can be related to N-containing aromatics leading to coking structures, indicating that at least in some degree there is a change in species with temperature increase for this group of molecules.

Figure 2G-H show the basic nitrogen and total nitrogen contents. The fraction of basic nitrogen species in the total nitrogen content (Figure S5A) of biocrudes is around 30-41%, the lowest being for the co-HTL biocrude, and the highest for the wheat straw one. For the hydrotreated products, this fraction is higher for the low temperature scenario, reaching 56% for cow manure and the co-HTL biocrude. With the increase of temperature, the

fraction tends to decrease, reaching 28-42% at high temperatures, this time with the highest being the combined biocrude and the lowest the wheat straw derived one. The increase in basic nitrogen fraction from biocrudes to low temperature hydrotreated products depicts that the non-basic N compounds are more easily hydrotreated. On the other hand, with the increase of temperature there is a decrease in basic nitrogen fraction, showing that more severe conditions make basic nitrogen species as prone to hydrotreating as non-basic ones. Thus, at least part of the basic and non-basic nitrogen species contained in all

biocrudes are recalcitrant in hydrotreatment, however, it seems the co-HTL oil maintains the highest fraction of basic nitrogen in the total content. I.e. the basic nitrogen species of the co-HTL biocrude are less reactive, correlating well with expected larger molecules containing nitrogen in this biocrude⁸ and a μMCR increase with temperature during hydrotreatment. So, the larger the nitrogen-containing molecule, the less prone it is to be hydrotreated due to aromatic stability and more prone to coking reactions.

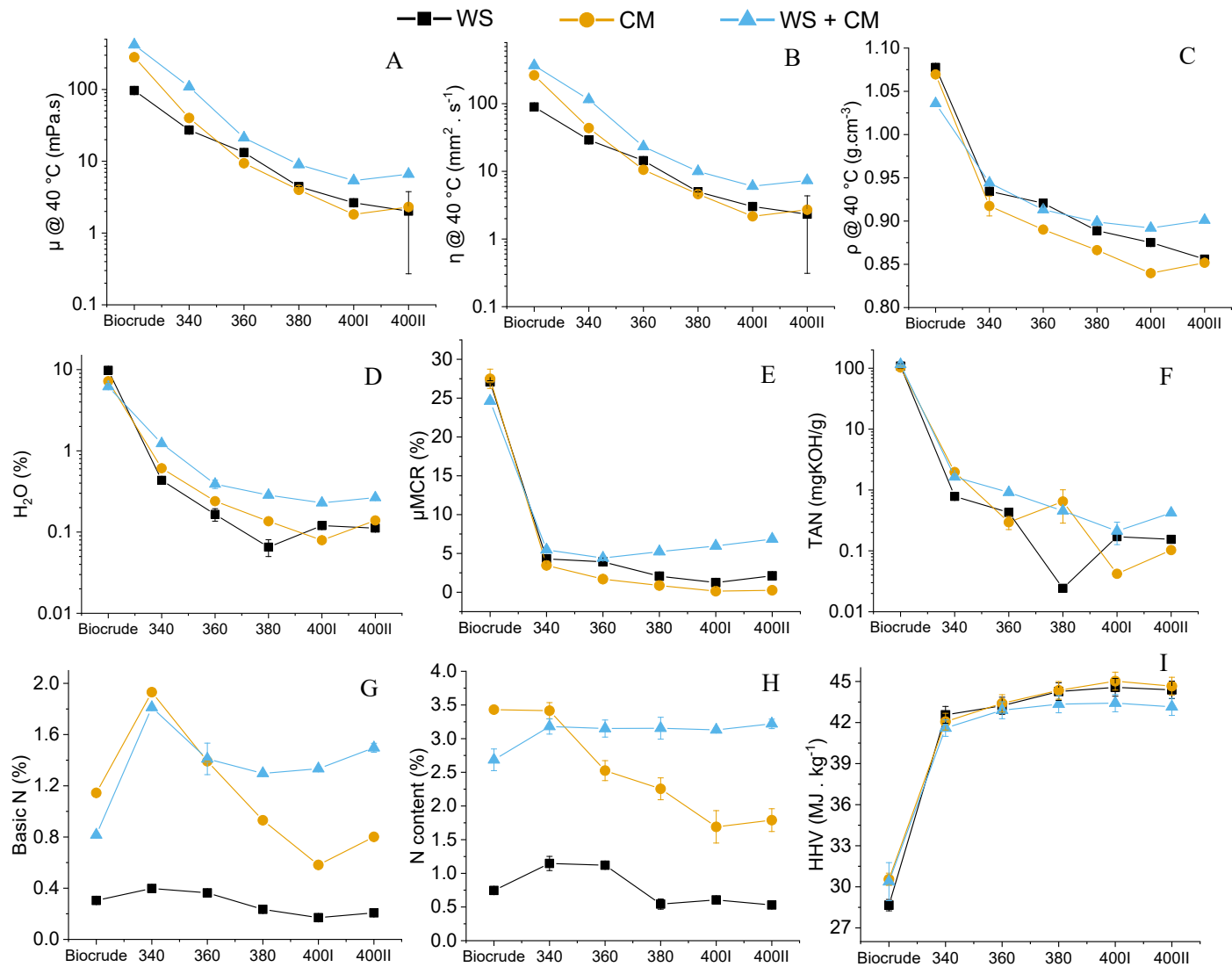


Figure 2 – Dynamic viscosity (μ) (A); kinematic viscosity (η) (B); density (ρ) (C); water content (D); micro carbon residue (μMCR) (E); Total Acid Number (TAN) (F); basic nitrogen in hydrocarbons (G); nitrogen content (H) and; high heating value (HHV) (I) of wheat straw (WS), cow manure (CM) and combined biocrude of wheat straw and cow manure (WS + CM) hydrotreated oil products

As shown also in Figure 1B, the yield of nitrogen of co-HTL biocrude is larger than the one for single feedstock

biocrudes. Interestingly, the only hydrotreated oil nitrogen content that does not change with temperature is the co-

HTL derived samples. Such an effect can be associated with more complex molecules containing nitrogen in the co-HTL sample, as discussed in our previous study.⁸ I.e. the basic nitrogen in the manure biocrude is mostly comprised of amines, prone for easier hydrotreatment, while for the co-HTL biocrude pyridines are likely the basic N compounds present, which being aromatic are more difficult for hydrodenitrogenation. Thus, the manure hydrotreated products decrease in basic N and N content illustrates that the co-HTL biocrude N compounds require a more aggressive approach for total denitrogenation. Figure 2I shows that all hydrotreated products have HHV higher than 42 MJ.kg⁻¹, but only single feedstock biocrudes reach >44 MJ.kg⁻¹ values for high temperature hydrotreated samples, given the negative contribution of nitrogen content for HHV (Equation 2) and the co-HTL biocrude products N content.

Table S1 shows the elemental composition of biocrudes and their respective hydrotreated products. The hydrotreatment process is successful in fully deoxygenating all biocrudes, however the denitrogenation does not follow. As already discussed about Figure 1B, the combined biocrude shows most yield of nitrogen in the hydrotreated oil, and the concentration of this element showed in Table S1 follows, being even higher than the biocrude itself due to oxygen mass loss and following concentration effect. Hydrogen consumption is also shown in Table S1 and much lower values are verified for the co-HTL biocrude (11-18 $g_{H_2}/kg_{oil\ DB}$) than the single feedstock ones (18-36 $g_{H_2}/kg_{oil\ DB}$). This, together with the low denitrogenation values for co-HTL oil compared to others, indicates the components of this biocrude do not react as much with hydrogen as other biocrudes. I.e. the co-HTL biocrude has nitrogen-containing recalcitrant compounds that difficult hydrotreating, and by preventing saturation decrease hydrogen consumption.

As already reported by PNNL's upgrading research team²⁶, there is a high correlation between nitrogen contents and density of upgraded products. We report here the same observation (Figure S5B), though the correlation is feedstock-dependent and cannot be verified for the combined biocrude, as its nitrogen content did not change significantly.

The combined HTL biocrude shows slightly inferior physicochemical characteristics among the ones measured here. Its most distinguishing characteristic is the nitrogen content, which seems to be in forms of recalcitrant molecules towards hydrotreatment. This could affect severely the application of combined feedstock in HTL setups, however

the gain in carbon recovery is a major factor to be considered, as described later.⁸

In general, the increase of temperature increases also the hydrotreated product quality in terms of its physicochemical properties. Remarkably, dynamic viscosity, kinematic viscosity, density, water content, μ MCR, TAN and HHV reach numbers close to crude oil specifications for direct refining. Despite that, the nitrogen contents for manure and co-HTL biocrude derived products are still an issue for direct applications as fuel and require further processing. The straw derived products have similar nitrogen contents to crude oils with high amounts of this element, depicting a similar scenario as other HTL hydrotreated biocrudes from lignocellulosic materials.^{33,34} As described elsewhere²⁰, lower WHSV (around 0.1 h⁻¹) can achieve total denitrogenation from biocrudes with similar initial N content using similar catalyst strategies as we described here, although typical crude oil hydrotreatment processes use 0.7-12 h⁻¹ WHSV.¹² Thus, given the results shown here, it is likely that such HTL biocrudes need specific units in refining setups for deep denitrogenation to occur, even though deoxygenation and reasonable physicochemical properties are achieved with 0.5 h⁻¹ WHSV. As the nitrogen content can be related to specific molecular weights present in these hydrotreated products, a following distillation step can assist on decreasing even further the contents and concentrating those in more specific and less volumetric byproducts.

3.3. GC/MS of hydrotreated products

GC/MS total ion chromatograms are shown in Figure 3A-C normalized to highest count. Only the sample volatile and semivolatiles fractions eluted are shown in these chromatograms, however it is still possible to see the classic biocrude components³⁵ for lignocellulosic feedstock materials in Figure 3A-C, such as substituted phenolics, ketones, alcohols and nitrogen-containing small heterocyclics. As for the upgraded products, a range of C4-C18 hydrocarbons was observed. Among those, cyclics, aromatics, alkanes and alkenes. The deoxygenation was particularly efficient for this fraction and it was not possible to identify oxygenated compounds in the upgraded samples. These results are in good agreement with the Van Krevelen diagram in Figure S6.

The main difference between upgraded products was the relative presence of long linear chain hydrocarbons derived from lipids in comparison to branched C4-C9

hydrocarbons. The C12-C18 class compounds increases from straw, manure and combined upgraded products respectively. These results can indicate that either the combined approach increases their concentration by converting also straw derived carbon into long chain alkanes or that the amount of small branched hydrocarbons decreases in comparison to the lipid-derived class. According to results of simulated distillation and distillates physicochemical characteristics to be discussed in the

following section, what happens is the decrease in light hydrocarbons.

The light hydrocarbons (C4-C10) identified in the hydrotreated samples are all compatible to gasoline-range hydrocarbons and have similar H/C ratio to the ones identified in the experimental distillate sample Van Krevelen diagram (Figure S6). This corroborates further the quality of the gasoline fraction derived from all hydrotreated biocrudes, suggesting that addition of this fraction to crude-oil derived gasoline can be an option for its application.

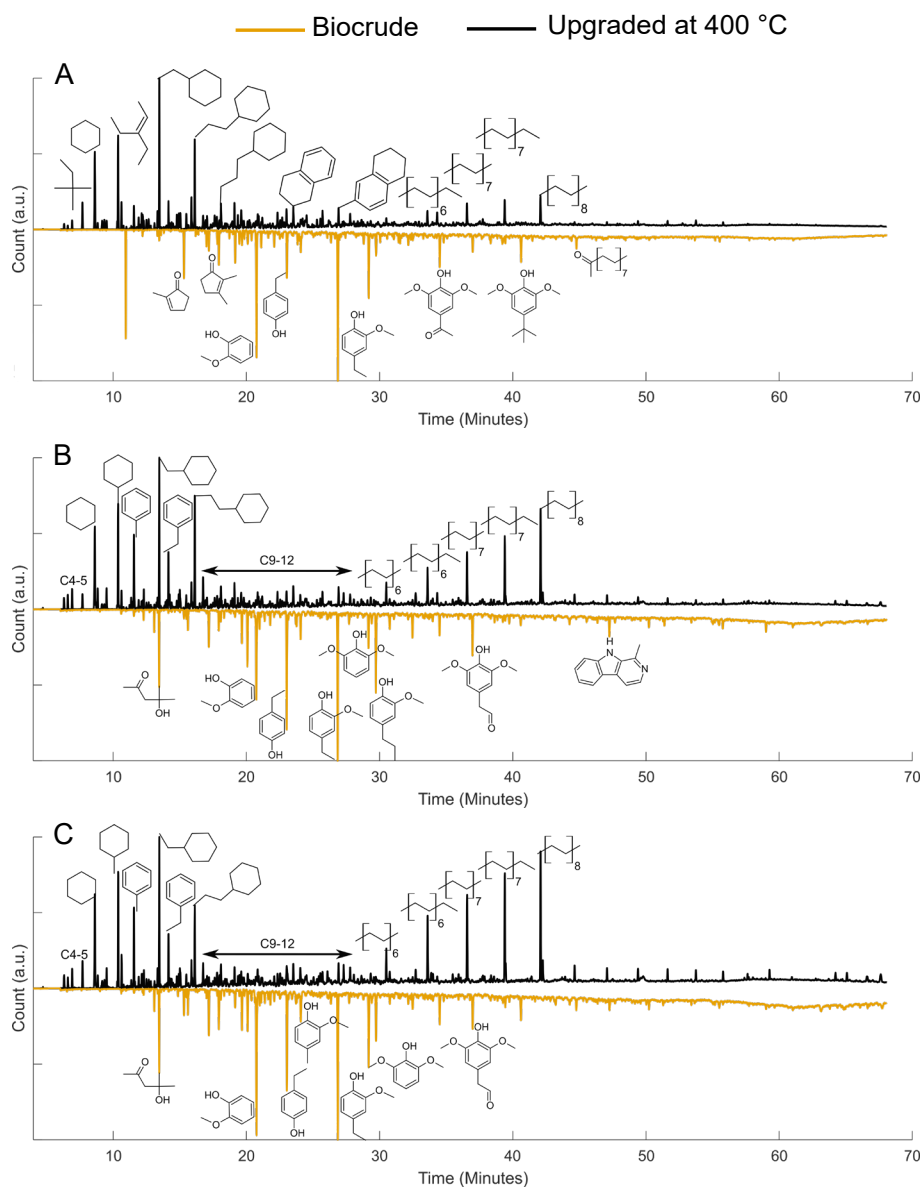


Figure 3 – GC/MS of biocrudes and hydrotreated products (400 °C). (A) Wheat straw; (B) Cow manure; (C) combined biocrude wheat straw and cow manure

3.4. Distillation of hydrotreated products

Gasoline, kerosene, diesel and bottom residue (BR) distillation cuts are shown in Figure 4A-D. Experimental distillation cuts were determined within $\pm 3.5\%$ for all 400 °C hydrotreated products simulated distillation. Thus, simulated distillation values will be considered for further discussion on the effect of temperature on the distillate cut yields. For the experimental distillation cuts, all gasoline and kerosene fractions were transparent upon immediate recovery, while diesel cuts had light yellow color and BR were dark and viscous appearance. The highest experimental distillation cut was the BR for straw and co-HTL upgraded products, while for manure biocrude upgraded products it was the diesel fraction. This is related to the relative higher amount of lipids in manure in comparison to the other feedstock tested. The lipid fraction of the feedstock tends to form oils with carbon range compatible with diesel specifications.⁸

Figure 4A shows that for straw biocrude upgrading, the increase of hydrotreating temperature from 340 to 400 °C resulted in a 3.6% gain in gasoline yield, while for manure and co-HTL biocrudes, the gain was 13.5 and 10.7% respectively. The highest gasoline yield observed experimentally was for manure biocrude hydrotreatment (20.7%). Figure 4B shows that the hydrotreatment temperature increased kerosene yield from 17.2, 17.4% and 15.6% at 340 °C to 24.1, 22.2, 18.6% at 400 °C for straw, manure and co-HTL biocrudes respectively. This means the temperature effect on the increase of this cut was higher for single feedstock biocrudes than for the combined one. The highest experimental kerosene yield observed was for straw with 23.7%.

The diesel distillation cuts shown in Figure 4C depict only increase of around 3 wt% in this fraction with the increase of temperature for all biocrudes tested. No significant change was observed in all upgraded products from the increase of 380 to 400 °C in hydrotreating temperature. However, Figure 4D depicts that there is a very high effect of decreasing BR with the increase of temperature. The yields from this fraction decrease from 54.4, 56.5 and 62.3% at 340 °C to 34.9, 24.3, 37.6% at 400 °C, respectively for straw, manure and co-HTL biocrude products. The decrease in BR is highest for manure biocrude, though on average there is an $8.5 \pm 1.1\%$ decrease in BR yield for every 20 °C increase in hydrotreatment temperature. Such observations point that the increase of temperature in hydrotreating tends to decrease BR

components, which corroborates with the increase of gasoline and kerosene fractions.

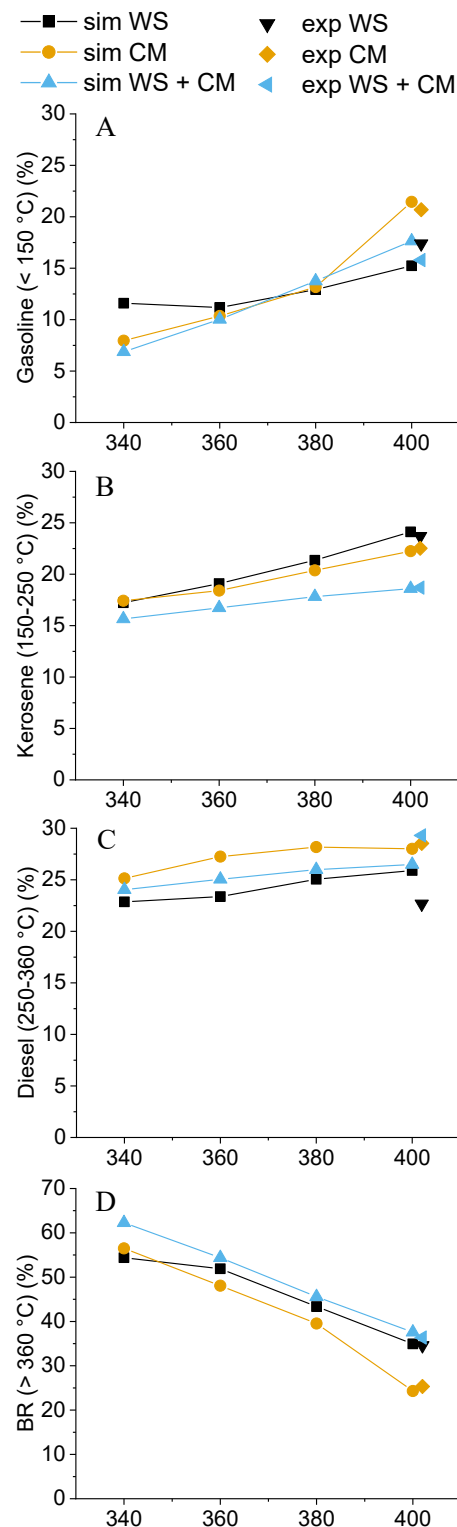
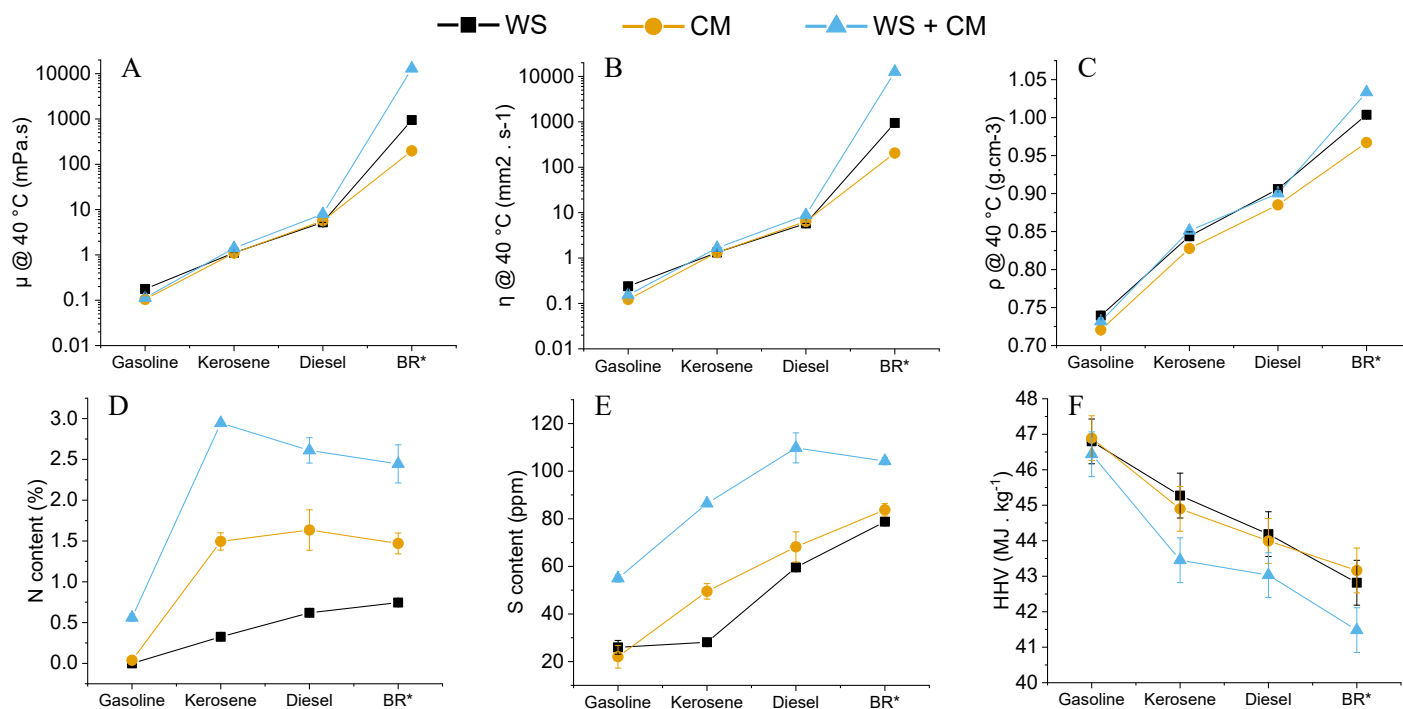


Figure 4 – Simulated and experimental distillation cuts for gasoline (A), kerosene (B), diesel (C) and bottom residue (BR) (D). (sim – simulated distillation GC analysis; exp – experimental 400 °C hydrotreated oil products distillation; WS – wheat straw; CM – cow manure)

Surprisingly, the diesel fraction does not change as significantly, which suggests that either the components consumed from BR are transferred directly to kerosene and gasoline or that the increase in temperature also increases cracking reactions in the diesel fraction, which equilibrates material gain from the BR. Nevertheless, increasing temperature clearly increases light hydrocarbons yields, benefiting mostly gasoline for manure and co-HTL biocrude and kerosene for straw.

Figure 5A-F depicts physicochemical characteristics of the 400 °C hydrotreated biocrudes distilled fractions. Density and viscosities (Figure 5A-C) of gasoline, kerosene and diesel fractions are similar among the different hydrotreated products, however the BR viscosities of the combined biocrude is much higher, to the point it was not possible to measure it at 40 °C, so values are shown at 50 °C. These viscosities are one order of magnitude apart, being

manure, straw and combined products respectively from lowest to highest viscosities and density. The gasoline nitrogen content is almost zero for straw and manure, though for the combined biocrude it reaches around 0.5 wt%. For straw, the heavier the fraction, the higher the nitrogen content. For manure, nitrogen contents of kerosene, diesel and BR are around 1.5 wt%. As for the combined biocrude products, kerosene has the highest nitrogen content with almost 3.0 wt%, while diesel and BR from this fraction have only around 2.5 wt%. Thus, the nitrogen containing molecules tend not to be present in the lightest distillate fraction, showing that the smaller the molecule, the more prone it is for denitrogenation processes. Such observation opens the possibility for heavier fractions to be further refined in specific processes targeting nitrogen containing molecules.



* - BR = Bottom Residue; viscosities of WS + CM BR were measured at 50 °C due to equipment limitations

Figure 5 – Dynamic viscosity (μ); kinematic viscosity (η); density (ρ); nitrogen content; sulfur content and; high heating value (HHV) of distilled products from hydrotreatment at 400 °C of biocrudes from wheat straw (WS), cow manure (CM) and combined wheat straw and cow manure (WS + CM)

It is however important to realize that the nitrogen contents showed in kerosene and diesel distillation cuts are high compared to fossil-derived fuels. Engines tested with similar fuels, containing comparable nitrogen contents, viscosities, HHVs and densities, show that motor efficiency does not suffer with this elemental compositions. Furthermore, the emissions of NO_x for engines working in

high loads increase only marginally.³⁶ That is, despite the fuel composition showed here, practical applications may still be within reach for the future fossil-free transportation sector.

Figure 5E shows that the S content of distillates is between 20 and 110 ppm, which is higher than current fuel standards and highlights the need of further upgrading or blending with low S content alternatives. The S content for

the combined HTL biocrude distilled products in particular seem consistently higher than others, ranging from gasoline at 52 ppm to diesel at 108 ppm. HHV of products depicted in Figure 5F fall within close range for single feedstock products and lower for kerosene, diesel and BR from combined biocrude. This is derived from the higher nitrogen content and unsaturated compounds of the latter (see also Figure S6 where lower H/C ratios point to increase of aromatics and unsaturated compounds). Despite that, HHV are relatively high and within fuel standards.

The Van Krevelen diagram of all biocrudes, upgraded and distilled samples (Figure S6 A-D) shows that biocrudes O/C ratio are around 0.25-0.35, typical values, however the upgraded products are all <0.03 . Even though O/C ratios are that low, there is still a trend for the higher the temperature, the lower the O/C ratio is verified H/C values for upgraded products are around 1.6-1.8, while the distillates have clear separation for gasoline, kerosene, diesel and BR showing H/C ranges of >2.0 , 1.75-1.80, 1.60-1.65 and 1.25-1.45 respectively. Gasoline and kerosene samples are generally within crude oil derived H/C and O/C limits, however diesel presents a lower H/C. This indicates gasoline H/C values are compatible with C6-C15 alkanes, as for kerosene, diesel and BR alkenes, unsaturated cyclic hydrocarbons and polyaromatics H/C ratios are more likely to be present in high concentrations. A lesser content of alkanes in heavier fractions decreases H/C values and is in agreement with the type of catalyst used, selected based on deoxygenation potential rather than saturation.¹¹ Still, the observation highlights the lighter the molecules, the more prone they are to be deoxygenated, denitrogenated and saturated via hydrotreatment.

The solubility in vacuum gas oil distillate (boiling points of around 350-540 °C) of all bottom residue fractions was tested. The selected crude oil fraction is representative of a common hydrocracking unit feed. Bottom residues from single feedstock biocrudes did not present phase separation when observed at room temperature. The co-HTL derived bottom residue fraction presented two phases in the form of an emulsion when in presence of all ratios of VGO tested. Increasing the temperature to 45 °C eliminated the biphasic separation for the mixture containing 75% of bottom residue, showing that increase in temperature can be an effective way to enhance their miscibility. Thus, co-processing of the BR distillate product with fossil VGO can be considered as a possible approach to increase biofuel light hydrocarbon yields.

Figure 6 shows that the gasoline distillation product is mostly composed of cycloalkanes for all feedstock biocrudes processed, even though CoMo and NiMo catalysts are typically used due to their deoxygenation activity. While straw generated relatively more cycloalkanes than the other two biocrudes, n-alkanes were present in higher quantities for manure products. This is related to a higher amount of lipids in these feedstock materials, leading to n-alkane formation during hydrotreatment. Aromatics sum 7.7 wt% for straw products and 10.4 wt% for both manure and co-HTL biocrude hydrotreatment products. The typical higher amount of lignin/cellulose in manure lignocellulosic components can be connected with the difference for single-feedstock biocrudes, while for the co-HTL biocrude, a higher amount of aromatics in the biocrude⁸ also yields higher amounts of aromatics in the gasoline distillation cut. Isoalkanes concentration in co-HTL oil is around the average of that on both single-feedstock biocrude upgraded products. This shows this class of compounds likely derives from molecules not involved in the synergistic effects of co-HTL, which may be short chain ketones and aldehydes.⁸ Due to the high presence of cycloalkanes, the calculated octane number for straw, manure and co-HTL biocrude hydrotreated products were respectively 63, 61 and 64. The much lower octane number than the 95 of fuel-grade petrol (BS EN 228:2008) hydrocarbons shows the need of further treatment via isomerization and reforming, even though limits (BS EN 228:2008) of olefin ($<18\%$), aromatics ($<35\%$), benzene ($<1.0\%$), oxygen ($<2.7\%$) are all met.

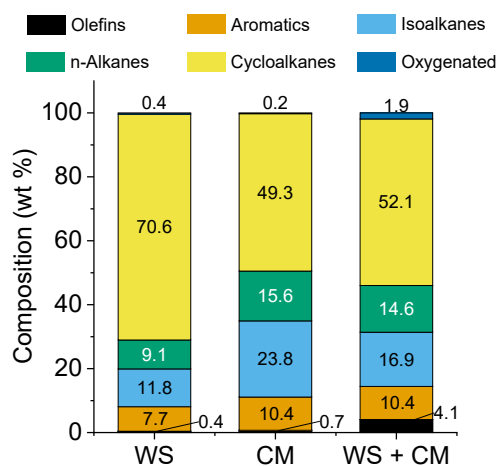


Figure 6 – Composition analysis of distilled gasoline fraction ($<150\text{ °C}$)

3.5. ATR-FTIR

The PCA conducted with all oil samples results in three main principal components, explaining 90.5, 6.9 and 1.7% of all spectra variation respectively, summing up to 99.1%. PC1 (90.5%) accounts all main oil characteristics with large loadings in the 1800-400 cm^{-1} region, distinctive CH_3 and CH_2 negative loadings at 2850 and 2920 cm^{-1} and a broad $-\text{OH}$ vibration at 3030-3690 cm^{-1} (Figure S7A). Methyl and methylene groups are typically connected with oil quality, given they can be associated with long chain alkanes and their respective end-of-chain terminations. The $-\text{OH}$ vibration is associated with phenols, alcohols, water and carboxylic acids. Oxygen containing groups can also be observed in peaks such as 1220, 1360 and 1700 cm^{-1} , all related to ethers, esters and aromatic ketones and, 1270 cm^{-1} of $-\text{OH}$ bend. Given the loadings of the 1800-400 cm^{-1} and the respective chemical groups identified in the peaks within the region, PC1 can easily separate oils based on their respective quality. The more the oxygen-containing chemical groups are present, the higher the PC1 score for a specific sample, which is clearly observed in Figure 7A where biocrudes are to the right of upgraded and distilled products.

PC2 (6.9%) depicts much more specific wave numbers for high loadings than PC1, showed as peaks in Figure S7B. The sequence of negative loading peaks at 723, 777, 875 and 934 cm^{-1} is related to carbon-carbon bonds. The first three are signs of $=\text{C}-\text{H}$ aromatics and the last one alkene $\text{C}=\text{C}$. The positive 1220 and 1360 cm^{-1} loadings are shared with PC1 identifying also oxygenated groups, while 1286 (negative) and 1706 (positive) cm^{-1} peaks depict respectively O-H and $=\text{O}$ groups. Remarkably, a sharp negative loading at 1671 cm^{-1} identifies $\text{C}=\text{N}$ from amides and aromatic heterocyclic compounds. The typical 2850 and 2920 CH_3 and CH_2 peaks are also present as negative loadings, while the broad $-\text{OH}$ group around 3120 and 3630 cm^{-1} is a positive contribution. Thus, the lower the PC2 score, the higher the carbon-carbon single, double and aromatic bonds, indicating alkanes, alkenes and aromatics characteristic groups for the sample are present. Despite this tendency, a high presence of N groups such as heterocyclic aromatics and amides can interfere in final scores also contributing to low PC2. Simultaneously, high PC2 scores can be related to high presence of oxygenated groups in the forms of alcohols, ketones and aldehydes. The loading scatter of PC1 versus PC2 is depicted in Figure S7C.

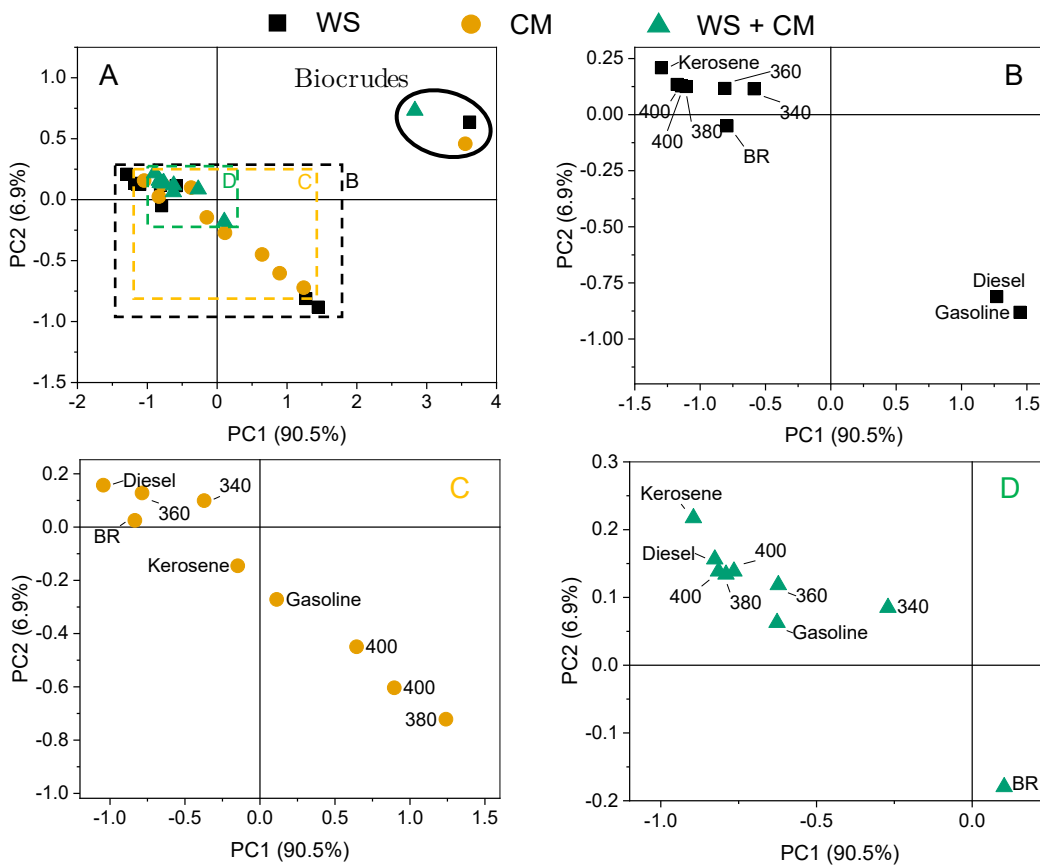


Figure 7 – PCA scores for all samples. (A) All samples; (B) Wheat straw; (C) Cow manure; (D) combined biocrude wheat straw and cow manure

Figure 7A shows that PC1 and PC2 successfully cluster biocrude samples and, separately, upgraded and distilled ones. All upgraded and distilled samples form a line tendency going from the upper left quadrant to the lower right one, meaning differences are connected to the increase of PC1 while decreasing PC2 scores. For straw biocrude upgraded samples, as shown in Figure 7B, only PC1 differs, even though to a lower degree, upgraded samples at different temperatures. Distillates on the other hand are scattered, with gasoline and diesel in the lower right quadrant and kerosene and bottom residue in the upper left. As N contents are generally low for these distillate samples ($< 0.5\%$), the difference can be attributed either to a lower presence of oxygenates in the gasoline and diesel fraction or a higher unsaturation of those. Manure upgraded biocrude products also are not as clustered as others (Figure 7C), with high temperature samples in the lower right quadrant. The lipid presence in the HTL feedstock can be associated with larger concentrations of aliphatics, which would both decrease PC2 and increase PC1. Lastly, the combined upgraded biocrude samples were the least differentiated by both PC1 and PC2, with most of them located in the upper left quadrant, except for BR in the lower right one. This can be related to the N groups of these samples and is an indicative that the N heterocyclic compounds formed during HTL are recalcitrant towards the upgrading approach showed here.

Figure S8 depicts both PC3 loading plot and PC2 versus PC3 scores. Similar to PC2, PC3 also shows generally sharp loading coefficients. A positive duplet in 752 and 804 cm^{-1} shows the importance of aromatic C-H deformations and a negative peak at 933 cm^{-1} shows C=C alkene separation. A very sharp negative peak at 1681 cm^{-1} shows that PC3 is able to differentiate samples based on N containing heterocyclics (C=N), however the typical 2845 and 2910 methyl and methylene groups contribute positively to the final score. As observed in Figure S8B, the hydrotreated products are generally clustered, with a decrease of PC3 with temperature. It is possible to observe that most distillates are separated from their original hydrotreated products, except for manure and combined biocrude diesel.

The FTIR spectra analyzed here shows that the chemical groups that differ most from the samples analyzed are also related to their respective quality, depicting ATR-FTIR as a powerful and reliable technique for rapid assessment of biocrude quality. The most important chemical groups identified in each principal component as best explanatory of differences were oxygenates in PC1,

carbon bond types in PC2 and a mix of carbon bond types and nitrogen containing species in PC3. Coupling density measurements and ATR-FTIR analysis can be a promising approach to instantly evaluate not only biocrude properties³⁷, but also hydrotreated products.

3.6. Process carbon balance

In order to compare the benefits of combined processing of manure and straw via HTL followed by hydrotreatment and distillation, a carbon balance of the entire approach – 1000 kg of carbon biomass to biofuels – is shown in Figure 8A-C with results presented elsewhere for HTL⁸ and here with the upgrading of biocrudes. The most significant carbon loss for all approaches is in the HTL-derived aqueous phase, ranging from 365 kg for wheat straw to 392 kg for manure. The combined approach yields 369 kg of carbon in this fraction, being more similar to straw than manure. Treatment of aqueous phase compounds can be considered a resource rather than waste handling³⁸, when gasification³⁸, wet oxidation³⁹ or electro-oxidation⁴⁰ technologies are applied. Thus, this aqueous phase carbon is not necessarily a carbon loss, depending on the approach to be considered.

Solids from HTL carry around 100 kg of carbon from single feedstock processing, however this number is reduced to 56 kg in the combined approach. The synergistic effect of combined HTL can be associated with this decrease, and so can be related to the reduction in gaseous carbon. The solids from HTL of agricultural waste streams are rich in phosphorus⁴¹, and further processing is needed to retrieve fertilizer-grade forms of this element.⁴² Thus, the reduction of carbon yielded as solids in the HTL process can also be beneficial for the handling and valorization of this fraction, greatly benefiting agricultural management of land and soil nutrient circularity.

For every 1000 kg of carbon entering a HTL unit in the form of wheat straw, manure or a combination of both, 410, 440 and 531 kg of carbon end-up as biocrude respectively. If the process was non-synergistic, the combination of feedstock materials would result in 425 kg, as oppose to the experimental 531 kg, which represents a 25% gain. In the hydrotreatment step, the combined HTL biocrude yields a greater gas fraction, leading 100 kg of carbon to this byproduct, though still maintaining a larger overall efficiency by generating 427 kg of carbon as upgraded oil as opposed to 338 or 380 kg of carbon for single feedstock approaches. That is, despite losing more carbon for the gas

fraction, the combined HTL approach still achieves a greater carbon efficiency for upgraded oils (almost 43%). Overall, light hydrocarbons (boiling points < 360 °C) have a total carbon yield from feedstock of 21.6, 27.2 and 26.5% respectively from wheat straw, cow manure and the combined biocrude. That is, the co-HTL approach does not enhance carbon yields compared to pure manure, however it does act synergistically towards the production of light hydrocarbons.

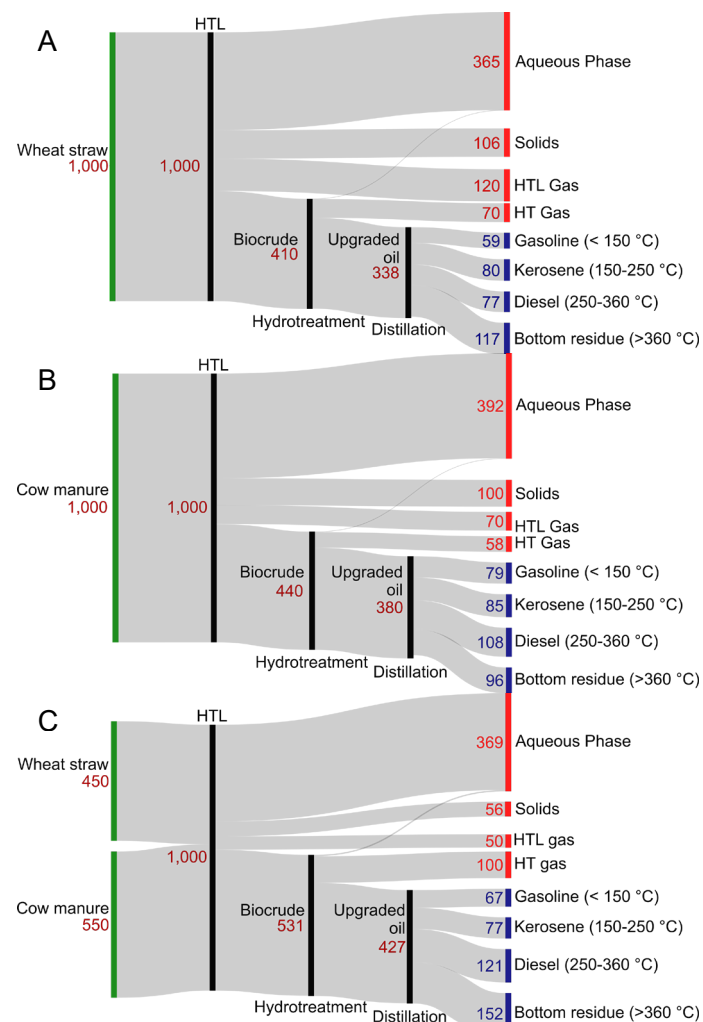


Figure 8 – HTL, hydrotreatment and distillation total carbon balance for all three feedstock slurries starting with 1000 kg of carbon. (A) Wheat straw; (B) Cow manure; (C) combined wheat straw and cow manure

The distillation step illustrates further benefits and drawbacks of combining waste materials in the HTL process. On one hand, gasoline and kerosene did not gain much with the approach regarding carbon yields. On the other hand, it seems the gain in upgraded oil carbon was entirely transmitted to diesel and bottom residues, which increase to

121 kg and 152 kg of carbon from the single feedstock 77-108 and 117-96 kg respectively for straw and manure. The increase in BR production highlights the need of further processing of this fraction, which can take place via hydrocracking. The miscibility of BR and VGO can ease handling of these highly viscous products.

4. CONCLUSION

In a broad processing perspective, the combined HTL of agricultural waste materials can increase the amount of hydrocarbons available for upgrading, generating gains in carbon efficiency from biomass to hydrocarbon products. However, the denitrogenation steps required to produce biofuel-grade hydrocarbons through hydrotreating are reduced by the presence of the same compounds that generated gain in HTL efficiency. Thus, a more aggressive approach targeting specifically these compounds have to be considered as a further refining step.

All hydrotreated products obtained through the route proposed here using typical industrial catalysts have attractive physicochemical characteristics and should easily fit within modern refining facilities and equipment. Low TAN, oxygen content, viscosities, density and μMCR , together with crude-like HHV illustrate these findings. Besides, distillate products obtained show good correlation to biofuel specifications, meaning the upgrading approach chosen here significantly enhances liquids quality and aggregates value. Even all heavy fractions obtained through distillation show good solubility in less viscous fossil-derived VGO, which opens great possibilities in combined processing of those in current refinery infrastructure.

The nitrogen-containing recalcitrant molecules from these hydrocarbon mixtures may be acceptable in future fossil-free transportation sector, and only isomerization is needed in the case of gasoline for biofuel applications. Therefore, the combination of agribusiness waste for HTL processing is shown here to be an attractive solution for wet waste processing and enhanced carbon and energy recovery towards advanced biofuels.

ACKNOWLEDGEMENTS

This project has received funding from the European Union's Horizon 2020 research and innovation grant agreement No. 764734 (HyFlexFuel), the European Research Council (ERC) under the European Union's Horizon 2020 research and innovation program grant No.

849841 (REBOOT), the Aarhus University Centre for Circular Bioeconomy (CBIO) and the Aarhus University Graduate School of Technical Sciences (GSTS).

REFERENCES

- (1) Singh, D.; Sharma, D.; Soni, S. L.; Sharma, S.; Kumar Sharma, P.; Jhalani, A. A Review on Feedstocks, Production Processes, and Yield for Different Generations of Biodiesel. *Fuel* **2020**, *262* (November 2019), 116553. <https://doi.org/10.1016/j.fuel.2019.116553>.
- (2) Masson-Delmotte, V.; Zhai, P.; Pirani, A.; Connors, S. L.; Péan, C.; Berger, S.; Caud, N.; Chen, Y.; Goldfarb, L.; Gomis, M. I.; et al. *IPCC, 2021: Climate Change 2021: The Physical Science Basis. Contribution of Working Group I to the Sixth Assessment Report of the Intergovernmental Panel on Climate Change*; Cambridge, 2021.
- (3) Gegg, P.; Budd, L.; Ison, S. The Market Development of Aviation Biofuel: Drivers and Constraints. *J. Air Transp. Manag.* **2014**, *39*, 34–40. <https://doi.org/10.1016/j.jairtraman.2014.03.003>.
- (4) Henrich, E.; Dahmen, N.; Dinjus, E.; Sauer, J. The Role of Biomass in a Future World without Fossil Fuels. *Chemie-Ingenieur-Technik* **2015**, *87* (12), 1667–1685. <https://doi.org/10.1002/cite.201500056>.
- (5) Cherubin, M. R.; Oliveira, D. M. D. S.; Feigl, B. J.; Pimentel, L. G.; Lisboa, I. P.; Gmach, M. R.; Varanda, L. L.; Morais, M. C.; Satiro, L. S.; Popin, G. V.; et al. Crop Residue Harvest for Bioenergy Production and Its Implications on Soil Functioning and Plant Growth: A Review. *Sci. Agric.* **2018**, *75* (3), 255–272. <https://doi.org/10.1590/1678-992x-2016-0459>.
- (6) Berendes, D. M.; Yang, P. J.; Lai, A.; Hu, D.; Brown, J. Estimation of Global Recoverable Human and Animal Faecal Biomass. *Nat. Sustain.* **2018**, *1* (11), 679–685. <https://doi.org/10.1038/s41893-018-0167-0>.
- (7) Lu, J.; Watson, J.; Liu, Z.; Wu, Y. Elemental Migration and Transformation during Hydrothermal Liquefaction of Biomass. *J. Hazard. Mater.* **2022**, *423* (PA), 126961. <https://doi.org/10.1016/j.jhazmat.2021.126961>.
- (8) dos Passos, J. S.; Matayeva, A.; Biller, P. Chapter 8 of This Thesis. Manuscript 2 – Enhanced Biocrude and Carbon Recovery from Cow Manure and Wheat Straw Combined Hydrothermal Liquefaction via Mixed Feedstock Optimization: From Batch to Continuous Processing, Aarhus University, 2022.
- (9) Jarvis, J. M.; Billing, J. M.; Corilo, Y. E.; Schmidt, A. J.; Hallen, R. T.; Schaub, T. M. FT-ICR MS Analysis of Blended Pine-Microalgae Feedstock HTL Biocrudes. *Fuel* **2018**, *216* (August 2017), 341–348. <https://doi.org/10.1016/j.fuel.2017.12.016>.
- (10) Sudasinghe, N.; Cort, J. R.; Hallen, R.; Olarte, M.; Schmidt, A.; Schaub, T. Hydrothermal Liquefaction Oil and Hydrotreated Product from Pine Feedstock Characterized by Heteronuclear Two-Dimensional NMR Spectroscopy and FT-ICR Mass Spectrometry. *Fuel* **2014**, *137*, 60–69. <https://doi.org/10.1016/j.fuel.2014.07.069>.
- (11) Elliott, D. C. Historical Developments in Hydroprocessing Bio-Oils. *Energy and Fuels* **2007**, *21* (3), 1792–1815. <https://doi.org/10.1021/ef070044u>.
- (12) Prado, G. H. C.; Rao, Y.; De Klerk, A. Nitrogen Removal from Oil: A Review. *Energy and Fuels* **2017**, *31* (1), 14–36. <https://doi.org/10.1021/acs.energyfuels.6b02779>.
- (13) Biller, P.; Sharma, B. K.; Kunwar, B.; Ross, A. B. Hydroprocessing of Bio-Crude from Continuous Hydrothermal Liquefaction of Microalgae. *Fuel* **2015**, *159*, 197–205. <https://doi.org/10.1016/j.fuel.2015.06.077>.
- (14) Elliott, D. C.; Hart, T. R.; Schmidt, A. J.; Neuenschwander, G. G.; Rotness, L. J.; Olarte, M. V.; Zacher, A. H.; Albrecht, K. O.; Hallen, R. T.; Holladay, J. E. Process Development for Hydrothermal Liquefaction of Algae Feedstocks in a Continuous-Flow Reactor. *Algal Res.* **2013**, *2* (4), 445–454. <https://doi.org/10.1016/j.algal.2013.08.005>.
- (15) Jarvis, J. M.; Sudasinghe, N. M.; Albrecht, K. O.; Schmidt, A. J.; Hallen, R. T.; Anderson, D. B.; Billing, J. M.; Schaub, T. M. Impact of Iron Porphyrin Complexes When Hydroprocessing Algal HTL Biocrude. *Fuel* **2016**, *182*, 411–418. <https://doi.org/10.1016/j.fuel.2016.05.107>.
- (16) Zhao, B.; Wang, Z.; Liu, Z.; Yang, X. Two-Stage Upgrading of Hydrothermal Algae Biocrude to Kerosene-Range Biofuel. *Green Chem.* **2016**, *18* (19), 5254–5265. <https://doi.org/10.1039/c6gc01413e>.
- (17) Albrecht, K. O.; Zhu, Y.; Schmidt, A. J.; Billing, J. M.; Hart, T. R.; Jones, S. B.; Maupin, G.; Hallen, R.; Ahrens, T.; Anderson, D. Impact of Heterotrophically Stressed Algae for Biofuel Production via Hydrothermal Liquefaction and Catalytic Hydrotreating in Continuous-Flow Reactors. *Algal Res.* **2016**, *14*, 17–27. <https://doi.org/10.1016/j.algal.2015.12.008>.
- (18) Castello, D.; Haider, M. S.; Rosendahl, L. A. Catalytic Upgrading of Hydrothermal Liquefaction Biocrudes: Different Challenges for Different Feedstocks. *Renew. Energy* **2019**, *141*, 420–430. <https://doi.org/10.1016/j.renene.2019.04.003>.
- (19) Yu, J.; Biller, P.; Mamahkel, A.; Klemmer, M.; Becker, J.; Glasius, M.; Iversen, B. B. Catalytic Hydrotreatment of Bio-Crude Produced from the Hydrothermal Liquefaction of Aspen Wood: A Catalyst Screening and Parameter Optimization Study. *Sustain. Energy Fuels* **2017**, *1* (4), 832–841. <https://doi.org/10.1039/c7se00090a>.
- (20) Marrone, P. A.; Elliott, D. C.; Billing, J. M.; Hallen, R. T.; Hart, T. R.; Kadota, P.; Moeller, J. C.; Randel, M. A.; Schmidt, A. J. Bench-Scale Evaluation of Hydrothermal Processing Technology for Conversion of Wastewater Solids to Fuels. *Water Environ. Res.* **2018**, *90* (4), 329–342. <https://doi.org/10.2175/106143017x15131012152861>.
- (21) Elliott, D. C.; Hart, T. R.; Neuenschwander, G. G.; Rotness, L. J.; Olarte, M. V.; Zacher, A. H.; Solantausta, Y. Catalytic Hydroprocessing of Fast Pyrolysis Bio-Oil from Pine Sawdust. *Energy and Fuels* **2012**, *26* (6), 3891–3896. <https://doi.org/10.1021/ef3004587>.
- (22) Elliott, D. C.; Wang, H.; French, R.; Deutch, S.; Iisa, K. Hydrocarbon Liquid Production from Biomass via Hot-Vapor-Filtered Fast Pyrolysis and Catalytic Hydroprocessing of the Bio-Oil. *Energy and Fuels* **2014**, *28* (9), 5909–5917. <https://doi.org/10.1021/ef501536j>.
- (23) Verdier, S.; Mante, O. D.; Hansen, A. B.; Poulsen, K. G.; Christensen, J. H.; Ammtziboll, N.; Gabrielsen, J.; Dayton, D. C. Pilot-Scale Hydrotreating of Catalytic Fast Pyrolysis Biocrudes: Process Performance and Product Analysis. *Sustain. Energy Fuels* **2021**, *5* (18), 4668–4679. <https://doi.org/10.1039/d1se00540e>.
- (24) Auersvald, M.; Shumeiko, B.; Vrtiška, D.; Straka, P.; Staš, M.; Šimáček, P.; Blažek, J.; Kubička, D. Hydrotreatment of Straw Bio-Oil from Ablative Fast Pyrolysis to Produce Suitable Refinery Intermediates. *Fuel* **2019**, *238* (June 2018), 98–110. <https://doi.org/10.1016/j.fuel.2018.10.090>.
- (25) Shumeiko, B.; Auersvald, M.; Straka, P.; Šimáček, P.; Vrtiška, D.; Kubička, D. Efficient One-Stage Bio-Oil Upgrading over Sulfided Catalysts. *ACS Sustain. Chem. Eng.* **2020**, *8* (40), 15149–15167. <https://doi.org/10.1021/acssuschemeng.0c03896>.
- (26) Subramaniam, S.; Santosa, D. M.; Brady, C.; Swita, M.; Ramasamy, K. K.; Thorson, M. R. Extended Catalyst Lifetime Testing for HTL Biocrude Hydrotreating to Produce Fuel Blendstocks from Wet Wastes. *ACS Sustain. Chem. Eng.* **2021**, *9* (38), 12825–12832. <https://doi.org/10.1021/acssuschemeng.1c02743>.

- (27) Anastasakis, K.; Biller, P.; Madsen, R. B.; Glasius, M.; Johannsen, I. Continuous Hydrothermal Liquefaction of Biomass in a Novel Pilot Plant with Heat Recovery and Hydraulic Oscillation. *Energies* **2018**, *11* (10), 1–23. <https://doi.org/10.3390/en11102695>.
- (28) Thorson, M. R.; Santosa, D. M.; Hallen, R. T.; Kutnyakov, I.; Olarte, M. V.; Flake, M.; Neuenschwander, G.; Middleton-Smith, L.; Zacher, A. H.; Hart, T. R.; et al. Scaleable Hydrotreating of HTL Biocrude to Produce Fuel Blendstocks. *Energy and Fuels* **2021**, *35* (14), 11346–11352. <https://doi.org/10.1021/acs.energyfuels.1c00956>.
- (29) Channiwala, S. A.; Parikh, P. P. A Unified Correlation for Estimating HHV of Solid, Liquid and Gaseous Fuels. *Fuel* **2002**, *81* (8), 1051–1063. [https://doi.org/10.1016/S0016-2361\(01\)00131-4](https://doi.org/10.1016/S0016-2361(01)00131-4).
- (30) dos Passos, J. S.; Glasius, M.; Biller, P. Hydrothermal Co-Liquefaction of Synthetic Polymers and *Miscanthus Giganteus*: Synergistic and Antagonistic Effects. *ACS Sustain. Chem. Eng.* **2020**, *accschemeng.0c07317*. <https://doi.org/10.1021/accschemeng.0c07317>.
- (31) Castello, D.; Haider, M. S.; Rosendahl, L. A. Catalytic Upgrading of Hydrothermal Liquefaction Biocrudes: Different Challenges for Different Feedstocks. *Renew. Energy* **2019**, *141*, 420–430. <https://doi.org/10.1016/j.renene.2019.04.003>.
- (32) Chang Samuel Hsu, P. R. R. *Springer Handbook of Petroleum Technology*; Hsu, C. S., Robinson, P. R., Eds.; Springer Handbooks; Springer International Publishing: Cham, 2017. <https://doi.org/10.1007/978-3-319-49347-3>.
- (33) Jarvis, J. M.; Albrecht, K. O.; Billing, J. M.; Schmidt, A. J.; Hallen, R. T.; Schaub, T. M. Assessment of Hydrotreatment for Hydrothermal Liquefaction Biocrudes from Sewage Sludge, Microalgae, and Pine Feedstocks. *Energy and Fuels* **2018**, *32* (8), 8483–8493. <https://doi.org/10.1021/acs.energyfuels.8b01445>.
- (34) Jarvis, J. M.; Billing, J. M.; Hallen, R. T.; Schmidt, A. J.; Schaub, T. M. Hydrothermal Liquefaction Biocrude Compositions Compared to Petroleum Crude and Shale Oil. *Energy and Fuels* **2017**, *31* (3), 2896–2906. <https://doi.org/10.1021/acs.energyfuels.6b03022>.
- (35) Madsen, R. B.; Zhang, H.; Biller, P.; Goldstein, A. H.; Glasius, M. Characterizing Semivolatile Organic Compounds of Biocrude from Hydrothermal Liquefaction of Biomass. *Energy and Fuels* **2017**, *31* (4), 4122–4134. <https://doi.org/10.1021/acs.energyfuels.7b00160>.
- (36) Obeid, F.; Chu Van, T.; Johanna Horchler, E.; Guo, Y.; Verma, P.; Miljevic, B.; Brown, R. J.; Ristovski, Z.; Bodisco, T.; Rainey, T. Engine Performance and Emissions from Fuels Containing Nitrogen and Sulphur. *Energy Convers. Manag.* **2022**, *14*, 100179. <https://doi.org/10.1016/j.ecmx.2022.100179>.
- (37) Madsen, R. B.; Anastasakis, K.; Biller, P.; Glasius, M. Rapid Determination of Water, Total Acid Number, and Phenolic Content in Bio-Crude from Hydrothermal Liquefaction of Biomass Using FT-IR. *Energy and Fuels* **2018**, *32* (7), 7660–7669. <https://doi.org/10.1021/acs.energyfuels.8b01208>.
- (38) Watson, J.; Wang, T.; Si, B.; Chen, W. T.; Aierzhati, A.; Zhang, Y. Valorization of Hydrothermal Liquefaction Aqueous Phase: Pathways towards Commercial Viability. *Prog. Energy Combust. Sci.* **2020**, *77*, 100819. <https://doi.org/10.1016/j.peccs.2019.100819>.
- (39) Silva Thomsen, L. B.; Anastasakis, K.; Biller, P. Wet Oxidation of Aqueous Phase from Hydrothermal Liquefaction of Sewage Sludge. *Water Res.* **2022**, *209*, 1–30. <https://doi.org/10.1016/j.watres.2021.117863>.
- (40) Matayeva, A.; Biller, P. Hydrothermal Liquefaction Aqueous Phase Treatment and Hydrogen Production Using Electro-Oxidation. *Energy Convers. Manag.* **2021**, *244* (June), 114462. <https://doi.org/10.1016/j.enconman.2021.114462>.
- (41) Matayeva, A.; Rasmussen, S. R.; Biller, P. Distribution of Nutrients and Phosphorus Recovery in Hydrothermal Liquefaction of Waste Streams. *Biomass and Bioenergy* **2022**, *156* (November 2021), 106323. <https://doi.org/10.1016/j.biombioe.2021.106323>.
- (42) Ovsyannikova, E.; Kruse, A.; Becker, G. C. Valorization of Byproducts from Hydrothermal Liquefaction of Sewage Sludge and Manure: The Development of a Struvite-Producing Unit for Nutrient Recovery. *Energy and Fuels* **2021**, *35* (11), 9408–9423. <https://doi.org/10.1021/acs.energyfuels.1c00561>.

Chapter 10

Thesis conclusions and perspectives

This thesis successfully assessed the potential benefits of combined HTL of synthetic and biological waste materials. Results showed several opportunities to enhance carbon and energy recovery of wastes using HTL, which greatly enlarges the application field for the technology and, by extension, provide better perspectives on economic scenarios of HTL plants. Besides assessing and evaluating these processes from a chemical point of view via batch experiments, pilot processing of the identified promising combinations helped to describe the engineering challenges and benefits involved. During pilot processing, it was possible to highlight the utilities needed for the approach to be implemented and their energetic and practical consequences for HTL.

Among the several types of synthetic polymers tested in Part I, independent of being thermosets or thermoplastics, those containing heteroatoms – either nitrogen or oxygen – in the backbone structure are prone to hydrolysis and depolymerization under HTL subcritical conditions. The hydrolysis yields products mainly in the aqueous phase, with marked exceptions such as epoxy, PC, PUR and PET. For BPA-based polymers (PC and epoxy), oil products contain valuable platform chemicals and their use could be facilitated due to high concentration. For PET, the solid fraction is especially valuable with a very high terephthalic acid recovery. As for PUR, an oil phase containing both amines and glycols can be of great value.

The co-HTL of synthetic polymers and lignocellulosic materials experiments reported in Part II highlighted the importance of chemical mechanisms related to nitrogen. In short, among the synthetic materials tested, a great correlation between nitrogen content and synergistic oil production was found. The reactivity of amino groups was related to these findings, providing good arguments that the presence of reactive organic compounds containing nitrogen can carry carbon to the oil phase and synergistically increase these products. Thus, for synthetic and lignocellulosic materials co-HTL, not only the nitrogen content is important, but the form in which this nitrogen is present. Our findings corroborated by other recent literature studies, identified the most important factors for synergistic effects are the nitrogen content and reactivity.

The specific combination of highly reactive PUR-derived amines with lignocellulosic materials proved to be of great interest. Optimizing the mix ratio and processing temperature proved to be a key element of the concept. This approach resulted in continuous pilot plant processing with 75% energy and 71% carbon recovery in the oil phase. These numbers represent relative increases of energy and carbon recoveries of 53% and 60% for miscanthus and 70% and 74% for PUR single-HTL respectively. Pilot processing also showed that even accounting pumping and heating energy, the total efficiency is about 60%, which can be considered a high conversion efficiency to synthetic oil.

The detailed characterization via FT-ICR high resolution mass spectrometry conducted for these products showed that the lignocellulosic-derived components react with the PUR amines and form highly aromatic and stable compounds, which are the reason for the high synergistic effects observed. Despite that, the resulting heteroatom-containing aromatics are more stable than typical

HTL-derived products, which may reduce fuel applications of these oils. It is nevertheless important to highlight that handling nitrogen in modern combustion engines is already necessary. Thus, the overall effect of having superior HTL efficiencies may be acceptable with minor modifications in downstream uses.

Nevertheless, as PUR is a synthetic polymer typically derived from crude oil, other uses of the HTL products should be considered to decrease further the process CO₂ footprint. For instance, nitrogen-containing heteroatoms are highly valuable in other applications and the biomass-PUR route can be a sustainable option for their production. A mix of these compounds can be a highly promising liquid organic hydrogen carrier^{40,41}, and their application as such can be an opportunity for waste valorization. Thus, despite the fact that traditional oil to fuel approach is hampered, products may still be considered valuable depending on further applications. That is, the investigation of diversified application fields – other than typical biofuels – for oils derived from combined synthetic and biological materials may provide economic feasibility to the process route developed.

Previous literature using model biomolecules to mathematically predict HTL yields identified other interactions as more important than nitrogen-containing molecules with oxygenated groups (e.g. ketones, aldehydes, carboxylic acids) for the increase in biocrude yields. The work presented here on both agricultural waste and synthetic polymers co-HTL optimization showed how nitrogen-containing heteroaromatic compounds are stable when formed in hydrothermal conditions. It is also depicted here how to take advantage of their ability to carry carbon to the oil phase product. Validation of these results in pilot plant processing confirms the great potential that synergistic effects offer to HTL process. Using this approach, energy efficiency is proven to increase by more than 10% in total energy basis (a 25-35 % relative increase for biological waste streams).

The consequences of having stable nitrogen-containing molecules in biocrudes derived from biological waste materials are challenging for the needed downstream upgrading steps for biofuel production. On the other hand, the distillation step after upgrading experiments separated the recalcitrant species into much more specific groups of compounds. These groups contain defined carbon numbers, which may be processed specifically for their respective nitrogen species removal. Either way, if catalytic hydrotreating is applied for these streams, a higher amount of hydrogen and, possibly, more active catalysts, are needed to perform the task.⁴² Literature regarding the development of catalysts specifically targeting biological-derived recalcitrant nitrogen species still requires expansion, with only limited reports targeting this class of compounds.

The results presented in this thesis allowed the generalization of the importance of nitrogen compounds reactivity for synergistic effects both in synthetic-derived and biological-derived waste co-HTL. This was identified as the main cause for high synergistic effects for waste HTL combined processing regardless of waste sources. It was possible to identify two main outcomes of this approach. The first is the increase in biocrude concentration of nitrogen-containing species, which may require further assessment for biofuel production or can be seen as an opportunity to reclaim these molecules. The second consequence is the gain in energy recovery through carbon being carried to the oil phase, which benefits greatly the process overall energy balances and enables more carbon to be converted into biofuels or biochemicals intermediates. Overall, the combined waste processing strategy is very attractive and a promising approach to enhance carbon and energy reclamation as biocrude via hydrothermal liquefaction.

References Part III

- (1) Henrich, E.; Dahmen, N.; Dinjus, E.; Sauer, J. The Role of Biomass in a Future World without Fossil Fuels. *Chemie-Ingenieur-Technik* **2015**, *87* (12), 1667–1685. <https://doi.org/10.1002/cite.201500056>.
- (2) Masson-Delmotte, V.; Zhai, P.; Pirani, A.; Connors, S. L.; Péan, C.; Berger, S.; Caud, N.; Chen, Y.; Goldfarb, L.; Gomis, M. I.; et al. *IPCC, 2021: Climate Change 2021: The Physical Science Basis. Contribution of Working Group I to the Sixth Assessment Report of the Intergovernmental Panel on Climate Change*; Cambridge, 2021.
- (3) IEA. *Key World Energy Statistics 2021*; Paris, 2021.
- (4) IEA. *World Demand by Product Groups, 2018-2019*; Paris.
- (5) Grahn, M.; Hansson, J. Prospects for Domestic Biofuels for Transport in Sweden 2030 Based on Current Production and Future Plans. *Wiley Interdiscip. Rev. Energy Environ.* **2015**, *4* (3), 290–306. <https://doi.org/10.1002/wene.138>.
- (6) de Souza Dias, M. O.; Maciel Filho, R.; Mantelatto, P. E.; Cavalett, O.; Rossell, C. E. V.; Bonomi, A.; Leal, M. R. L. V. Sugarcane Processing for Ethanol and Sugar in Brazil. *Environ. Dev.* **2015**, *15*, 35–51. <https://doi.org/10.1016/j.envdev.2015.03.004>.
- (7) Ricardo, C.; Porto, L.; Vandenberghe, D. S.; Bianchi, A.; Medeiros, P.; Grace, S.; Buckeridge, M.; Pereira, L.; Paula, A.; Ferreira-leitão, V.; et al. Bioethanol from Lignocelluloses: Status and Perspectives in Brazil. *Bioresour. Technol.* **2010**, *101* (13), 4820–4825. <https://doi.org/10.1016/j.biortech.2009.11.067>.
- (8) International Energy Agency. Renewables 2021. **2021**.
- (9) Berendes, D. M.; Yang, P. J.; Lai, A.; Hu, D.; Brown, J. Estimation of Global Recoverable Human and Animal Faecal Biomass. *Nat. Sustain.* **2018**, *1* (11), 679–685. <https://doi.org/10.1038/s41893-018-0167-0>.
- (10) Zeyner, A.; Geißler, C.; Dittrich, A. Effects of Hay Intake and Feeding Sequence on Variables in Faeces and Faecal Water (Dry Matter, PH Value, Organic Acids, Ammonia, Buffering Capacity) of Horses. *J. Anim. Physiol. Anim. Nutr. (Berl.)* **2004**, *88* (1–2), 7–19. <https://doi.org/10.1111/j.1439-0396.2004.00447.x>.
- (11) Choi, H. L.; Sudiarto, S. I. A.; Renggamani, A. Prediction of Livestock Manure and Mixture Higher Heating Value Based on Fundamental Analysis. *Fuel* **2014**, *116*, 772–780. <https://doi.org/10.1016/j.fuel.2013.08.064>.
- (12) Fargione, J.; Hill, J.; Tilman, D.; Polasky, S.; Hawthorne, P. Land Clearing and the Biofuel Carbon Debt. *Science (80-.)*. **2008**, *319* (5867), 1235–1238. <https://doi.org/10.1126/science.1152747>.
- (13) Garcia-Nunez, J. A.; Pelaez-Samaniego, M. R.; Garcia-Perez, M. E.; Fonts, I.; Abrego, J.; Westerhof, R. J. M.; Garcia-Perez, M. Historical Developments of Pyrolysis Reactors: A Review. *Energy and Fuels* **2017**, *31* (6), 5751–5775. <https://doi.org/10.1021/acs.energyfuels.7b00641>.
- (14) Huang, Y.; Li, B.; Liu, D.; Xie, X.; Zhang, H.; Sun, H.; Hu, X.; Zhang, S. Fundamental Advances in Biomass Autothermal/Oxidative Pyrolysis: A Review. *ACS Sustain. Chem. Eng.* **2020**, *8* (32), 11888–11905. <https://doi.org/10.1021/acssuschemeng.0c04196>.
- (15) Eke, J.; Onwudili, J. A.; Bridgwater, A. V. Influence of Moisture Contents on the Fast Pyrolysis of Trommel Fines in a Bubbling Fluidized Bed Reactor. *Waste and Biomass Valorization* **2020**, *11* (7), 3711–3722. <https://doi.org/10.1007/s12649-018-00560-2>.
- (16) Zhang, Y.; Wan, L.; Guan, J.; Xiong, Q.; Zhang, S.; Jin, X. A Review on Biomass Gasification: Effect of Main Parameters on Char Generation and Reaction. *Energy and Fuels* **2020**, *34* (11), 13438–13455. <https://doi.org/10.1021/acs.energyfuels.0c02900>.
- (17) Wittcoff, H. A.; Reuben, B. G.; Plotkin, J. S. *Industrial Organic Chemicals*, 3rd ed.; Wiley: New Jersey, 2013.
- (18) Pereira, E. G.; Da Silva, J. N.; De Oliveira, J. L.; MacHado, C. S. Sustainable Energy: A Review of Gasification Technologies. *Renew. Sustain. Energy Rev.* **2012**, *16* (7), 4753–4762. <https://doi.org/10.1016/j.rser.2012.04.023>.
- (19) Technology, N. I. of S. and. NIST Chemistry WebBook, SRD 69 <https://webbook.nist.gov/cgi/cbook.cgi?ID=C7732185> (accessed Jan 15, 2022).
- (20) Elliott, D. C.; Biller, P.; Ross, A. B.; Schmidt, A. J.; Jones, S. B. Hydrothermal Liquefaction of Biomass: Developments from Batch to Continuous Process. *Bioresour. Technol.* **2015**, *178*, 147–156. <https://doi.org/10.1016/j.biortech.2014.09.132>.
- (21) Biller, P.; Ross, A. B. Potential Yields and Properties of Oil from the Hydrothermal Liquefaction of Microalgae

- with Different Biochemical Content. *Bioresour. Technol.* **2011**, *102* (1), 215–225.
<https://doi.org/10.1016/j.biortech.2010.06.028>.
- (22) Leow, S.; Witter, J. R.; Vardon, D. R.; Sharma, B. K.; Guest, J. S.; Strathmann, T. J. Prediction of Microalgae Hydrothermal Liquefaction Products from Feedstock Biochemical Composition. *Green Chem.* **2015**, *17* (6), 3584–3599. <https://doi.org/10.1039/c5gc00574d>.
- (23) Teri, G.; Luo, L.; Savage, P. E. Hydrothermal Treatment of Protein, Polysaccharide, and Lipids Alone and in Mixtures. *Energy and Fuels* **2014**, *28* (12), 7501–7509. <https://doi.org/10.1021/ef501760d>.
- (24) Yang, J.; He, Q. (Sophia); Corscadden, K.; Niu, H.; Lin, J.; Astatkie, T. Advanced Models for the Prediction of Product Yield in Hydrothermal Liquefaction via a Mixture Design of Biomass Model Components Coupled with Process Variables. *Appl. Energy* **2019**, *233–234* (July 2018), 906–915.
<https://doi.org/10.1016/j.apenergy.2018.10.035>.
- (25) Sheehan, J. D.; Savage, P. E. Bioresource Technology Modeling the Effects of Microalga Biochemical Content on the Kinetics and Biocrude Yields from Hydrothermal Liquefaction. *Bioresour. Technol.* **2017**, *239*, 144–150.
<https://doi.org/10.1016/j.biortech.2017.05.013>.
- (26) Valdez, P. J.; Tocco, V. J.; Savage, P. E. A General Kinetic Model for the Hydrothermal Liquefaction of Microalgae. *Bioresour. Technol.* **2014**, *163*, 123–127. <https://doi.org/10.1016/j.biortech.2014.04.013>.
- (27) Vo, T. K.; Lee, O. K.; Lee, E. Y.; Kim, C. H.; Seo, J. W.; Kim, J.; Kim, S. S. Kinetics Study of the Hydrothermal Liquefaction of the Microalga *Aurantiochytrium* Sp. KRS101. *Chem. Eng. J.* **2016**, *306*, 763–771. <https://doi.org/10.1016/j.cej.2016.07.104>.
- (28) Motavaf, B.; Savage, P. E. Effect of Process Variables on Food Waste Valorization via Hydrothermal Liquefaction. *ACS ES&T Eng.* **2021**. <https://doi.org/10.1021/acsesteng.0c00115>.
- (29) Gopirajan, P. V.; Gopinath, K. P.; Sivaranjani, G. Optimization of Hydrothermal Liquefaction Process through Machine Learning Approach : Process Conditions and Oil Yield. *Biomass Convers. Biorefinery* **2021**.
<https://doi.org/doi.org/10.1007/s13399-020-01233-8>.
- (30) Zhang, W.; Li, J.; Liu, T.; Leng, S.; Yang, L.; Peng, H.; Jiang, S.; Zhou, W.; Leng, L.; Li, H. Machine Learning Prediction and Optimization of Bio-Oil Production from Hydrothermal Liquefaction of Algae. *Bioresour. Technol.* **2021**, *342* (July), 126011. <https://doi.org/10.1016/j.biortech.2021.126011>.
- (31) Li, J.; Zhang, W.; Liu, T.; Yang, L.; Li, H.; Peng, H.; Jiang, S.; Wang, X.; Leng, L. Machine Learning Aided Bio-Oil Production with High Energy Recovery and Low Nitrogen Content from Hydrothermal Liquefaction of Biomass with Experiment Verification. *Chem. Eng. J.* **2021**, *425* (May), 130649.
<https://doi.org/10.1016/j.cej.2021.130649>.
- (32) Déniel, M.; Haarlemmer, G.; Roubaud, A.; Weiss-Hortala, E.; Fages, J. Modelling and Predictive Study of Hydrothermal Liquefaction: Application to Food Processing Residues. *Waste and Biomass Valorization* **2017**, *8* (6), 2087–2107. <https://doi.org/10.1007/s12649-016-9726-7>.
- (33) Aierzhati, A.; Stablein, M. J.; Wu, N. E.; Kuo, C. T.; Si, B.; Kang, X.; Zhang, Y. Experimental and Model Enhancement of Food Waste Hydrothermal Liquefaction with Combined Effects of Biochemical Composition and Reaction Conditions. *Bioresour. Technol.* **2019**, *284* (March), 139–147.
<https://doi.org/10.1016/j.biortech.2019.03.076>.
- (34) Li, J.; Zhang, W.; Liu, T.; Yang, L.; Li, H.; Peng, H.; Jiang, S.; Wang, X.; Leng, L. Machine Learning Aided Bio-Oil Production with High Energy Recovery and Low Nitrogen Content from Hydrothermal Liquefaction of Biomass with Experiment Verification. *Chem. Eng. J.* **2021**, *425* (May), 130649.
<https://doi.org/10.1016/j.cej.2021.130649>.
- (35) Biller, P.; Johannsen, I.; dos Passos, J. S.; Ottosen, L. D. M. Primary Sewage Sludge Filtration Using Biomass Filter Aids and Subsequent Hydrothermal Co-Liquefaction. *Water Res.* **2018**, *130*, 58–68.
<https://doi.org/10.1016/j.watres.2017.11.048>.
- (36) Matayeva, A.; Rasmussen, S. R.; Biller, P. Distribution of Nutrients and Phosphorus Recovery in Hydrothermal Liquefaction of Waste Streams. *Biomass and Bioenergy* **2022**, *156* (November 2021), 106323.
<https://doi.org/10.1016/j.biombioe.2021.106323>.
- (37) Ovsyannikova, E.; Kruse, A.; Becker, G. C. Feedstock-Dependent Phosphate Recovery in a Pilot-Scale Hydrothermal Liquefaction Bio-Crude Production. *Energies* **2020**, *13* (2), 379.
<https://doi.org/10.3390/en13020379>.
- (38) Ovsyannikova, E.; Kruse, A.; Becker, G. C. Valorization of Byproducts from Hydrothermal Liquefaction of

- Sewage Sludge and Manure: The Development of a Struvite-Producing Unit for Nutrient Recovery. *Energy and Fuels* **2021**, *35* (11), 9408–9423. <https://doi.org/10.1021/acs.energyfuels.1c00561>.
- (39) Obeid, F.; Chu Van, T.; Johanna Horchler, E.; Guo, Y.; Verma, P.; Miljevic, B.; Brown, R. J.; Ristovski, Z.; Bodisco, T.; Rainey, T. Engine Performance and Emissions from Fuels Containing Nitrogen and Sulphur. *Energy Convers. Manag. X* **2022**, *14*, 100179. <https://doi.org/10.1016/j.ecmx.2022.100179>.
- (40) He, T.; Pei, Q.; Chen, P. Liquid Organic Hydrogen Carriers. *J. Energy Chem.* **2015**, *24* (5), 587–594. <https://doi.org/10.1016/j.jechem.2015.08.007>.
- (41) Rao, P. C.; Yoon, M. Potential Liquid-Organic Hydrogen Carrier (LOHC) Systems: A Review on Recent Progress. *Energies* **2020**, *13* (22), 6040. <https://doi.org/10.3390/en13226040>.
- (42) Prado, G. H. C.; Rao, Y.; De Klerk, A. Nitrogen Removal from Oil: A Review. *Energy and Fuels* **2017**, *31* (1), 14–36. <https://doi.org/10.1021/acs.energyfuels.6b02779>.

SUPPLEMENTARY INFORMATION – Chapter 2 - Paper 1 - Screening of common synthetic polymers for depolymerization by subcritical hydrothermal liquefaction

Key words: Hydrothermal liquefaction; chemical recycling; depolymerization; circular economy; polymers; plastic

Juliano Souza dos Passos¹, Marianne Glasius², Patrick Biller^{1*}

1. Biological and Chemical Engineering, Aarhus University, Høngøvej 2, DK-8200 Aarhus N, Denmark

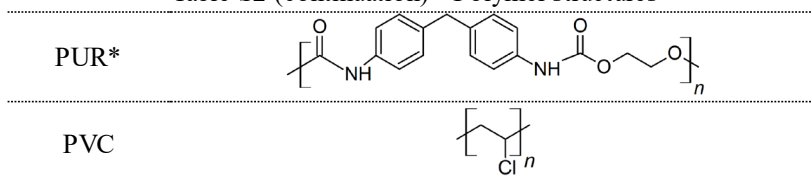
2. Department of Chemistry, Aarhus University, Langelandsgade 140, DK-8000 C, Denmark

*Corresponding author: pbiller@eng.au.dk

Table S1 – Polymer structures

Polymers	Chemical structure
HDPE	
LDPE	
PP	
PS	
ABS	
Monomers	
Epoxy	
Crosslinkers	
PC	
PET	
PA6	
PA66	

Table S2 (continuation) – Polymer structures



R = radicals including H, alkyl and PE (LDPE) – represents branching of LDPE

n = repetition number

a, b and c = different n

* - structure represented with ethylene alcohol unit for illustration purpose. The commercial PUR used has a mixture of

alcohols.

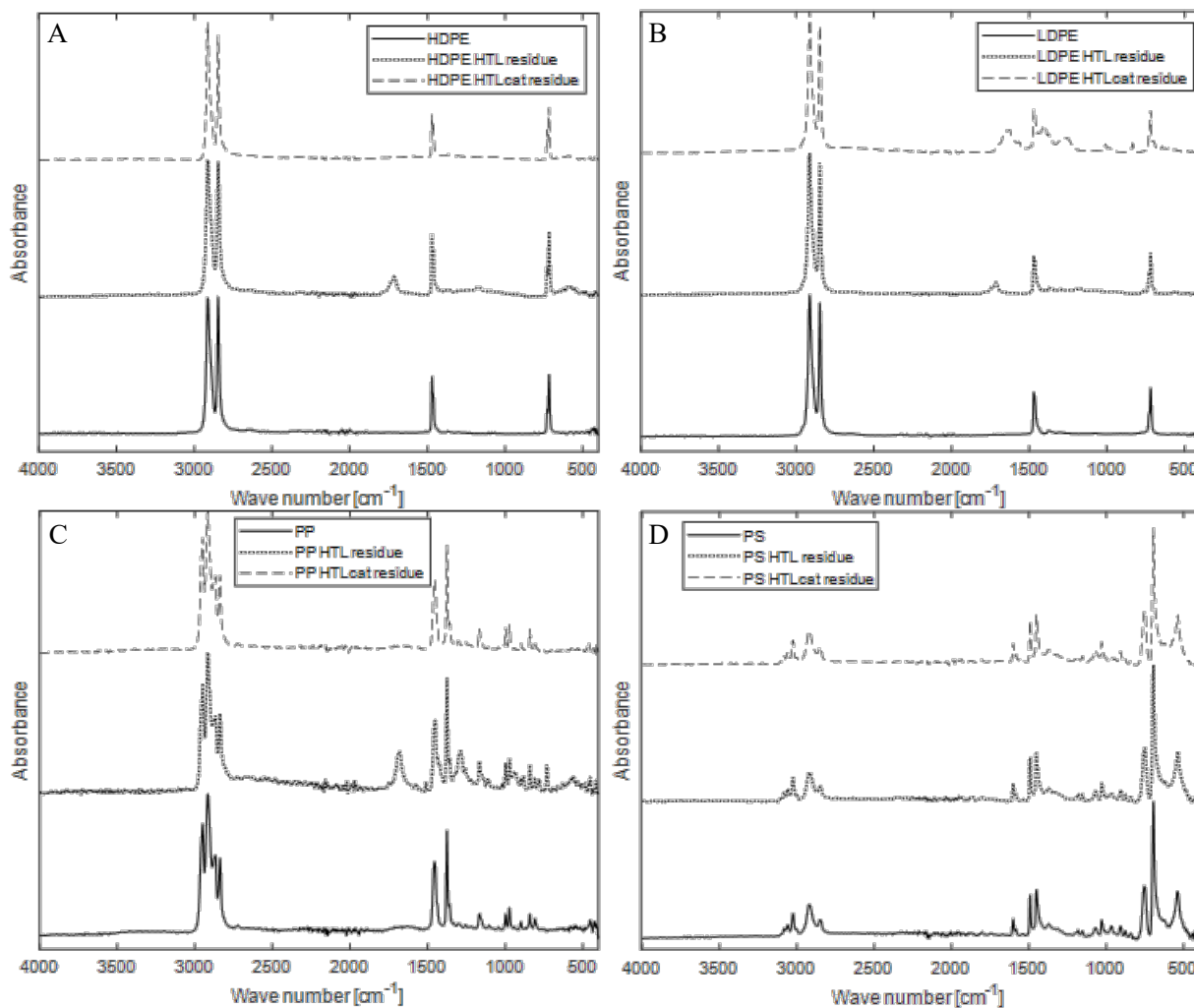


Figure S1 – FTIR HDPE, LDPE, PP and PS – Original polymer and solid residues of HTL procedure without and with catalyst (KOH)

Table S3 – CHNS analysis of raw polymers and its HTL products

HTL	Product	C		H		N		S		Difference
ABS	Raw	86.23%	±0.01%	7.81%	±0.03%	5.13%	±0.00%	0.11%	±0.02%	0.73% ^a
	Oil	N/A	N/A	N/A	N/A	N/A	N/A	N/A	N/A	N/A
	Solid residue	85.82%	±0.06%	7.41%	±0.18%	5.06%	±0.02%	0.03%	±0.02%	1.69% ^a
Epoxi	Raw	68.53%	±0.03%	8.17%	±0.06%	3.19%	±0.00%	0.04%	±0.01%	20.07% ^a
	Oil	72.64%	±1.44%	7.97%	±0.08%	2.57%	±0.11%	0.12%	±0.07%	16.71% ^a
	Solid residue	N/A	N/A	N/A	N/A	N/A	N/A	N/A	N/A	N/A
HDPE	Raw	85.76%	±0.01%	13.87%	±0.15%	0.01%	±0.00%	0.02%	±0.01%	0.34% ^a
	Oil	N/A	N/A	N/A	N/A	N/A	N/A	N/A	N/A	N/A
	Solid residue	85.15%	±0.06%	13.68%	±0.39%	0.00%	±0.00%	0.00%	±0.00%	1.17% ^a
LDPE	Raw	85.78%	±0.05%	14.49%	±0.26%	0.01%	±0.01%	0.00%	±0.00%	-0.27% ^a
	Oil	N/A	N/A	N/A	N/A	N/A	N/A	N/A	N/A	N/A
	Solid residue	84.48%	±0.05%	13.50%	±0.08%	0.17%	±0.01%	0.00%	±0.00%	1.86% ^a
PA6	Raw	62.51%	±0.01%	9.89%	±0.07%	12.11%	±0.01%	0.00%	±0.00%	15.49% ^a
	Oil	59.11%	±0.03%	9.72%	±0.11%	10.98%	±0.31%	0.03%	±0.01%	20.17% ^a
	Solid residue	61.52%	±0.04%	9.96%	±0.09%	11.80%	±0.01%	0.00%	±0.00%	16.73% ^a
PA66	Raw	62.68%	±0.02%	9.82%	±0.03%	12.21%	±0.01%	0.00%	±0.00%	15.30% ^a
	Oil	58.92%	±0.55%	9.26%	±0.09%	10.52%	±0.13%	0.04%	±0.01%	21.27% ^a
	Solid residue	61.92%	±0.02%	9.81%	±0.00%	11.79%	±0.01%	0.00%	±0.00%	16.48% ^a
PET	Raw	62.44%	±0.04%	4.20%	±0.02%	0.00%	±0.00%	0.01%	±0.00%	33.35% ^a
	Oil	57.47%	±0.04%	4.48%	±0.12%	0.67%	±0.24%	0.03%	±0.00%	37.35% ^a
	Solid residue	57.97%	±0.03%	3.58%	±0.00%	0.01%	±0.00%	0.14%	±0.02%	38.30% ^a
PC	Raw	75.73%	±0.01%	5.46%	±0.05%	0.02%	±0.01%	0.01%	±0.00%	18.78% ^a
	Oil	77.51%	±0.47%	6.89%	±0.05%	0.03%	±0.01%	0.02%	±0.01%	15.56% ^a
	Solid residue	N/A	N/A	N/A	N/A	N/A	N/A	N/A	N/A	N/A
PP	Raw	85.77%	±0.00%	13.88%	±0.31%	0.00%	±0.00%	0.00%	±0.00%	0.35% ^a
	Oil	N/A	N/A	N/A	N/A	N/A	N/A	N/A	N/A	N/A
	Solid residue	85.59%	±0.04%	13.24%	±0.17%	0.01%	±0.01%	0.04%	±0.01%	1.13% ^a
PS	Raw	88.64%	±0.02%	7.88%	±0.17%	0.01%	±0.01%	0.00%	±0.00%	3.48% ^a
	Oil	N/A	N/A	N/A	N/A	N/A	N/A	N/A	N/A	N/A
	Solid residue	88.30%	±0.22%	7.69%	±0.16%	0.01%	±0.01%	0.08%	±0.08%	3.93% ^a
PVC	Raw	38.61%	±0.01%	4.70%	±0.06%	0.01%	±0.01%	0.06%	±0.00%	56.63% ^b
	Oil	2.29%	±0.93%	3.97%	±0.29%	0.21%	±0.00%	0.10%	±0.04%	93.45% ^b
	Solid residue	85.67%	±5.31%	6.13%	±1.40%	0.09%	±0.02%	0.04%	±0.04%	8.07% ^b
PUR	Raw	62.33%	±0.04%	8.34%	±0.21%	5.97%	±0.01%	0.00%	±0.00%	23.37% ^a
	Oil	61.82%	±0.14%	9.47%	±0.21%	2.64%	±0.01%	0.02%	±0.01%	26.06% ^a
	Solid residue	76.12%	±0.23%	7.63%	±0.03%	5.92%	±0.05%	0.08%	±0.01%	10.26% ^a

^a – Difference is considered to be oxygen content^b – Difference is considered to be oxygen and chlorine content

N/A – Not available

Table S4 – CHNS analysis of raw polymers and catHTL products

HTL	Product	C		H		N		S		Difference
ABS _{cat}	Raw	86.23%	±0.01%	7.81%	±0.03%	5.13%	±0.00%	0.11%	±0.02%	0.73% ^a
	Oil	54.17%	±0.89%	6.11%	±0.01%	0.29%	±0.07%	0.07%	±0.01%	39.36% ^a
	Solid residue	82.82%	±0.00%	10.02%	±0.24%	0.31%	±0.03%	0.06%	±0.00%	6.81% ^a
Epoxi _{cat}	Raw	68.53%	±0.03%	8.17%	±0.06%	3.19%	±0.00%	0.04%	±0.01%	20.07% ^a
	Oil	65.98%	±0.84%	8.05%	±0.04%	3.71%	±0.03%	0.01%	±0.01%	22.26% ^a
	Solid residue	N/A	N/A	N/A	N/A	N/A	N/A	N/A	N/A	N/A
HDPE _{cat}	Raw	85.76%	±0.01%	13.87%	±0.15%	0.01%	±0.00%	0.02%	±0.01%	0.34% ^a
	Oil	N/A	N/A	N/A	N/A	N/A	N/A	N/A	N/A	N/A
	Solid residue	84.91%	±0.13%	14.30%	±0.24%	0.00%	±0.00%	0.01%	±0.01%	0.78% ^a
LDPE _{cat}	Raw	85.78%	±0.05%	14.49%	±0.26%	0.01%	±0.01%	0.00%	±0.00%	-0.27% ^a
	Oil	N/A	N/A	N/A	N/A	N/A	N/A	N/A	N/A	N/A
	Solid residue	85.44%	±0.01%	14.71%	±0.03%	0.00%	±0.00%	0.00%	±0.00%	-0.16% ^a
PA66 _{cat}	Raw	62.68%	±0.02%	9.82%	±0.03%	12.21%	±0.01%	0.00%	±0.00%	15.30% ^a
	Oil	52.74%	±1.72%	8.48%	±0.25%	9.65%	±0.34%	0.00%	±0.00%	29.13% ^a
	Solid residue	N/A	N/A	N/A	N/A	N/A	N/A	N/A	N/A	N/A
PA6 _{cat}	Raw	62.51%	±0.01%	9.89%	±0.07%	12.11%	±0.01%	0.00%	±0.00%	15.49% ^a
	Oil	47.14%	±0.06%	7.62%	±0.01%	8.35%	±0.10%	0.00%	±0.00%	36.89% ^a
	Solid residue	N/A	N/A	N/A	N/A	N/A	N/A	N/A	N/A	N/A
PC _{cat}	Raw	75.73%	±0.01%	5.46%	±0.05%	0.02%	±0.01%	0.01%	±0.00%	18.78% ^a
	Oil	67.38%	±1.21%	5.17%	±0.61%	0.41%	±0.24%	0.33%	±0.27%	26.71% ^a
	Solid residue	N/A	N/A	N/A	N/A	N/A	N/A	N/A	N/A	N/A
PET _{cat}	Raw	62.44%	±0.04%	4.20%	±0.02%	0.00%	±0.00%	0.01%	±0.00%	33.35% ^a
	Oil	55.94%	±0.39%	3.76%	±0.12%	0.22%	±0.19%	0.03%	±0.01%	40.05% ^a
	Solid residue	55.31%	±0.91%	3.81%	±0.21%	0.10%	±0.06%	0.01%	±0.00%	40.78% ^a
PP _{cat}	Raw	85.77%	±0.00%	13.88%	±0.31%	0.00%	±0.00%	0.00%	±0.00%	0.35% ^a
	Oil	N/A	N/A	N/A	N/A	N/A	N/A	N/A	N/A	N/A
	Solid residue	84.94%	±0.03%	14.45%	±0.19%	0.00%	±0.00%	0.00%	±0.00%	0.62% ^a
PScat	Raw	88.64%	±0.02%	7.88%	±0.17%	0.01%	±0.01%	0.00%	±0.00%	3.48% ^a
	Oil	N/A	N/A	N/A	N/A	N/A	N/A	N/A	N/A	N/A
	Solid residue	87.88%	±0.00%	8.38%	±0.15%	0.00%	±0.00%	0.01%	±0.00%	3.74% ^a
PVC _{cat}	Raw	38.61%	±0.01%	4.70%	±0.06%	0.01%	±0.01%	0.06%	±0.00%	56.63% ^b
	Oil	1.41%	±0.56%	1.58%	±0.20%	0.10%	±0.01%	0.09%	±0.02%	96.83% ^b
	Solid residue	78.55%	±0.24%	7.10%	±0.02%	0.07%	±0.01%	0.02%	±0.00%	14.27% ^b
PUR _{cat}	Raw	62.33%	±0.04%	8.34%	±0.21%	5.97%	±0.01%	0.00%	±0.00%	23.37% ^a
	Oil	61.76%	±0.04%	9.66%	±0.02%	2.02%	±0.01%	0.11%	±0.05%	26.46% ^a
	Solid residue	N/A	N/A	N/A	N/A	N/A	N/A	N/A	N/A	N/A

^a – Difference is considered to be oxygen content^b – Difference is considered to be oxygen and chlorine content

N/A – Not available

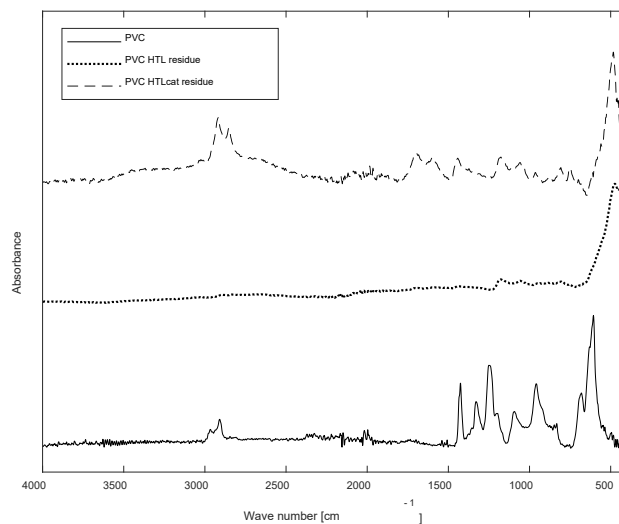


Figure S2 – FTIR PVC – Original polymer and solid residues of HTL procedure without and with catalyst (KOH)

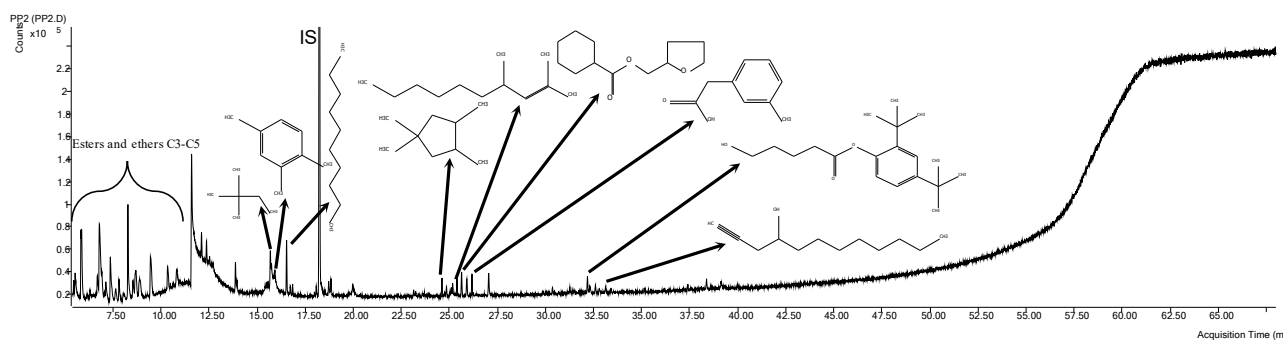


Figure S3 – PP oil GC/MS chromatogram

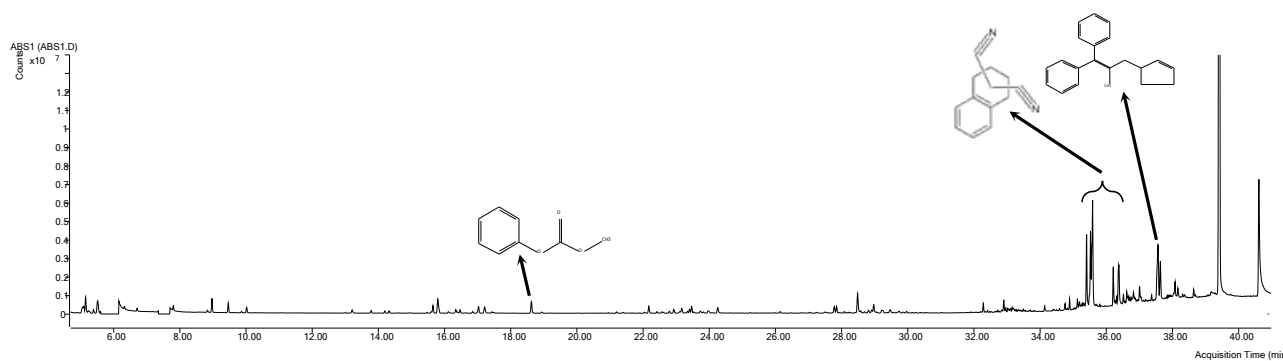


Figure S4 – ABS AP GC/MS chromatogram

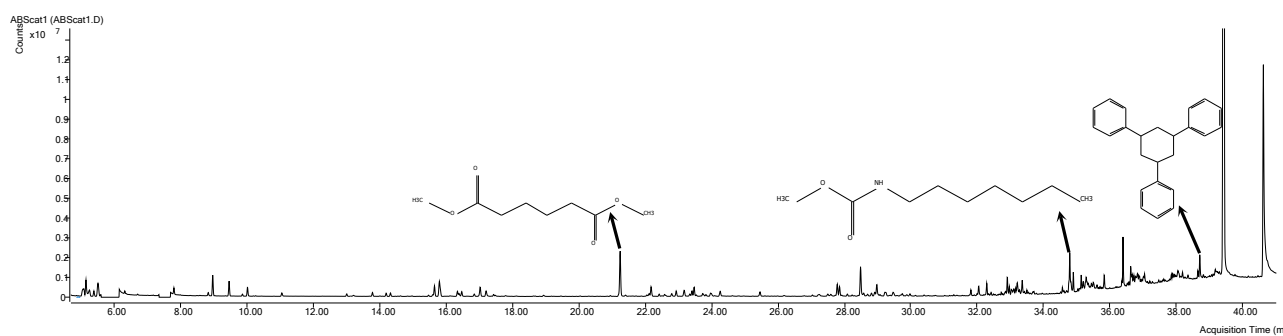


Figure S5 – ABScat AP GC/MS chromatogram

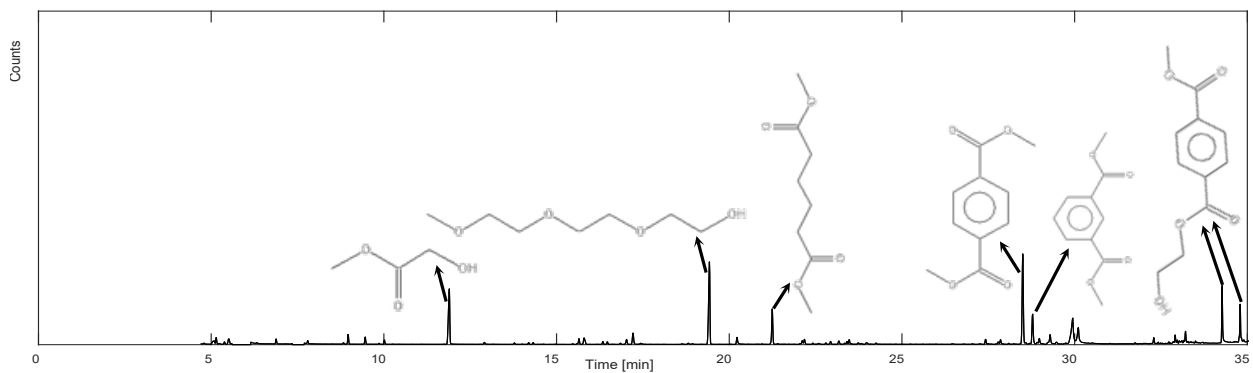


Figure S6 – PET AP GC/MS chromatogram

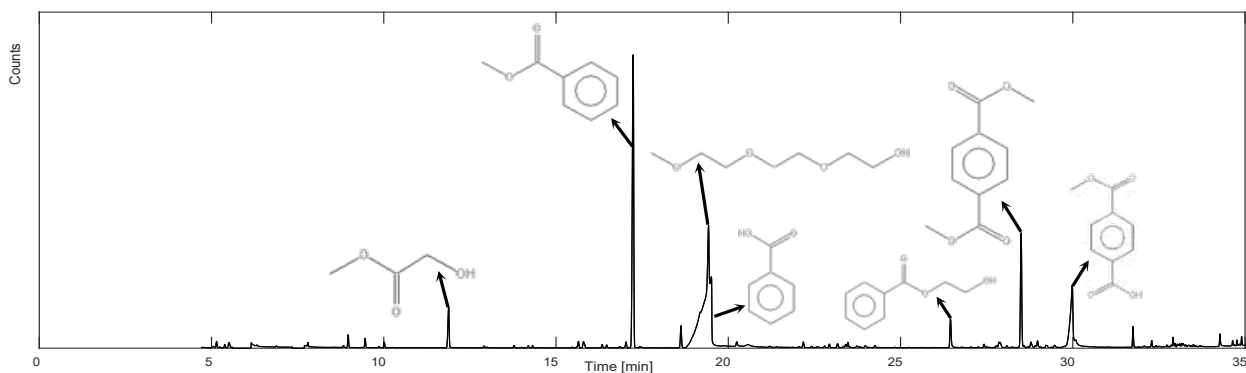


Figure S7 – PETcat AP GC/MS chromatogram

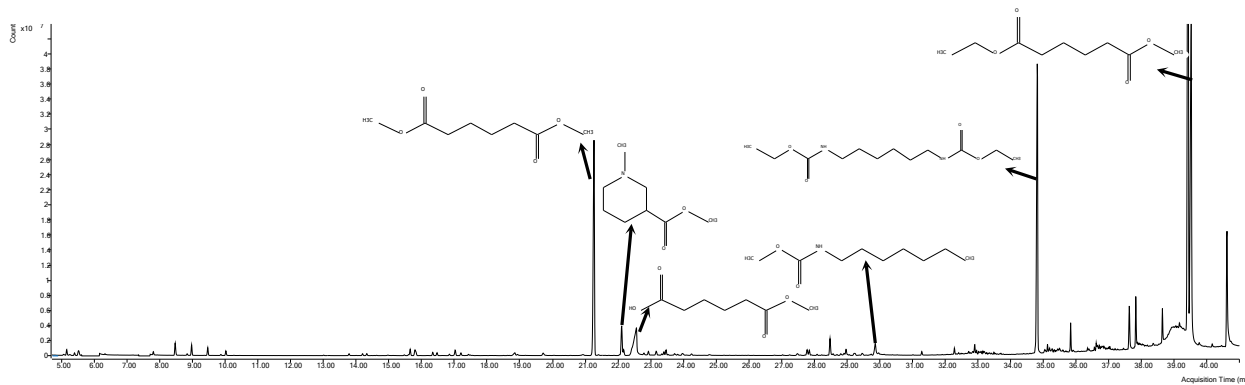


Figure S8 – PA6 AP GC/MS chromatogram

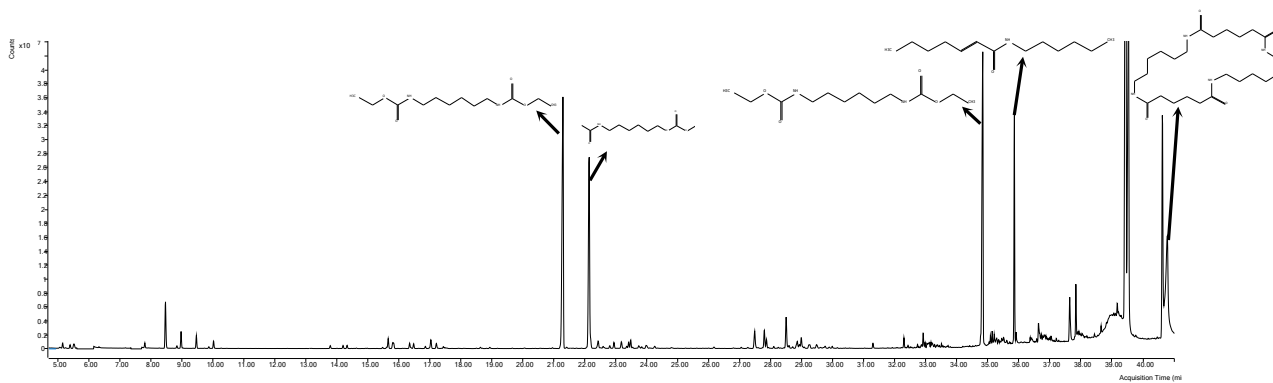


Figure S9 – PA66 AP GC/MS chromatogram

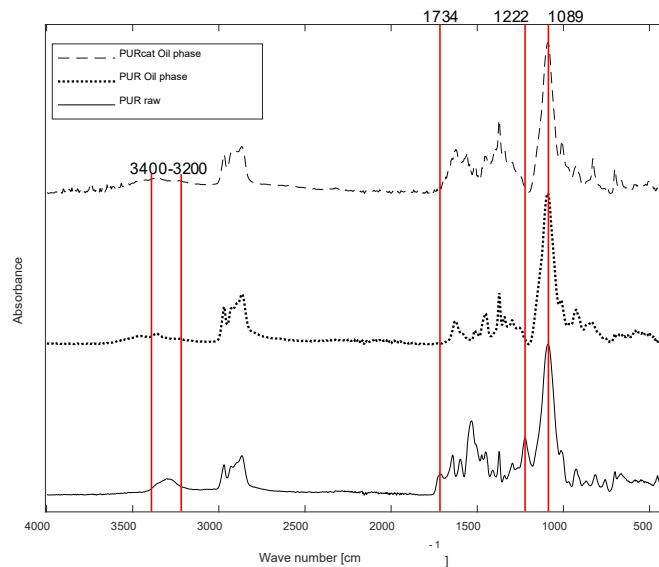


Figure S10 – FTIR of PUR oil phase in comparison to raw material. Highlighted in red: N–H (3400-3200 cm⁻¹); N–C=O (1734 cm⁻¹); C–N (1222 cm⁻¹); C–O–C (1089 cm⁻¹)

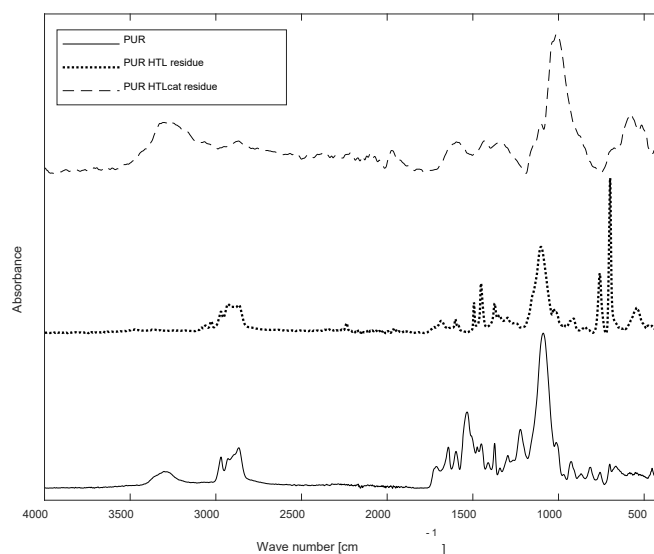


Figure S11 – FTIR of PUR solid residues in comparison to raw material.

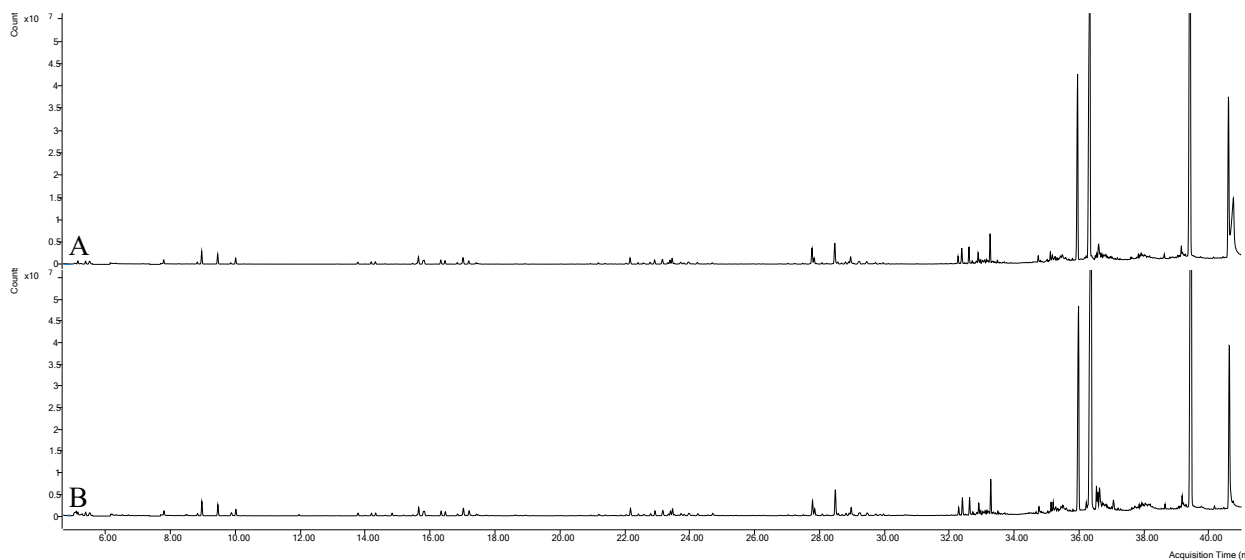


Figure S12 – PUR AP GCMS spectra (A = without catalyst; B = with catalyst).

SUPPLEMENTARY INFORMATION - Chapter 5 - Paper 2 - Hydrothermal co-liquefaction of synthetic polymers and *Miscanthus Giganteus*; synergistic and antagonistic effects

Juliano Souza dos Passos^{1,3}, Marianne Glasius^{2,3}, Patrick Biller^{1,3*}

1 - Biological and Chemical Engineering, Aarhus University, Høngøvej 2, DK-8200 Aarhus N, Denmark

2 - Department of Chemistry, Aarhus University, Langelandsgade 140, DK-8000 Aarhus C, Denmark

3 - Aarhus University Centre for Circular Bioeconomy, Blichers Allé 20, DK-8830, Tjele, Denmark

*Corresponding author: pbiller@eng.au.dk

Key words: Hydrothermal liquefaction; chemical recycling; depolymerization; circular economy; polymers

Number of pages: 11;

Number of figures: 7;

Number of tables: 2.

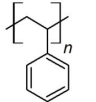
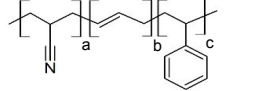
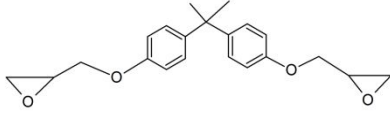
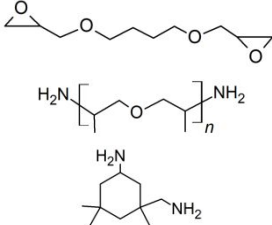
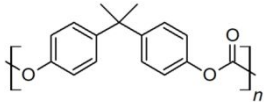
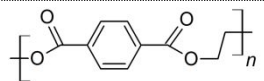
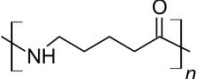
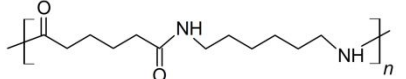
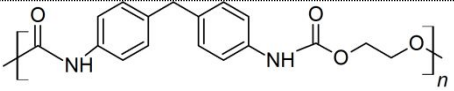
Supporting Information Figures

Figure S1 – Relative concentration changes of selected methoxy- compounds in HDPE, LDPE and PP co-HTL oil measured by GC-MS	2
Figure S2 – Relative concentration change of HDPE, LDPE and PP co-HTL oil measured by GC-MS for selected phenolic compounds. [Pure polymers not available due to lack of conversion to oil]	3
Figure S3 – Relative concentration change of ABS and PS co-HTL oil measured by GC-MS for selected phenolic compounds	3
Figure S4 – Relative concentration change of ABS and PS co-HTL oil measured by GC-MS for selected substituted benzene compounds	4
Figure S5 – Relative concentration change in PET co-HTL oil for selected aromatic (A) and ethylic (B) compounds. (A → → Toluene; → Styrene; → Phenol; → 2-methoxy-Phenol; → methyl ester → 2-methoxy-Benzoic acid; → 4-ethyl-Phenol; → p-Cumenol) (B → → acetic acid methyl ester; → 1,1-dimethoxy-ethane; → 2,2-dimethoxy-propane; → 1,1-dimethoxy-propane; → 1,2-ethanediol; → Cyclopentanone; → 2-Cyclopenten-1-one)	5
Figure S6 – Relative concentration change in PA6 (A) and PA66 (B) co-HTL oil for selected phenolic compounds. (→ Cyclopentanone; → 2-methyl-2-Cyclopenten-1-one; → 2-methoxy-Phenol; → 4-ethyl-Phenol; → 4-ethyl-2-methoxy-Phenol)	5
Figure S7 – Relative concentration change in PA6 (A) and PA66 (B) co-HTL oil for selected compounds. (→ 1,1-Dimethoxycyclopentane; → 1,8-Diazacyclotetradecane-2,7-dione; → 2,2-dimethoxy-Propane; → 3-methylundecane)	6

Supporting Information Tables

Table S1 – Polymer structures and elemental analysis (SD < 0.1% for all values reported).....	1
Table S2 – -Relative composition of oil phase from co-HTL determined by GC/MS analysis	7

Table S1 – Polymer structures and elemental analysis (SD < 0.1% for all values reported).

Polymers	Chemical structure	C (%)	H (%)	N (%)	S (%)	Difference**
HDPE		85.76	13.87	0.01	0.02	0.34
LDPE		85.78	14.49	0.01	0.00	0.00
PP		85.77	13.88	0.00	0.00	0.35
PS		88.64	7.88	0.01	0.00	3.48
ABS		86.23	7.81	5.13	0.11	0.73
Epoxy	Monomers 	68.53	8.17	3.19	0.04	20.07
	Crosslinkers 					
PC		75.73	5.46	0.02	0.01	18.78
PET		62.44	4.20	0.00	0.01	33.35
PA6		62.51	9.89	12.11	0.00	15.49
PA66		62.68	9.82	12.21	0.00	15.30
PUR*		62.33	8.34	5.97	0.00	23.37
PVC		38.61	4.70	0.01	0.06	56.63

R = radicals including H, alkyl and PE (LDPE) – represents branching of LDPE
n = repetition number
a, b and c = different n

* - structure represented with ethylene alcohol unit for illustration purpose. The commercial PUR used has a mixture of alcohols.
** - Difference to be considered oxygen for all polymers except PVC, where chlorine composes most of the value shown.

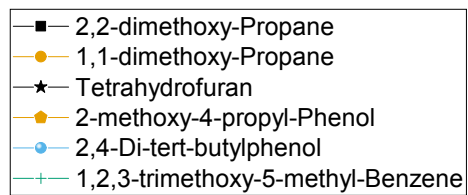
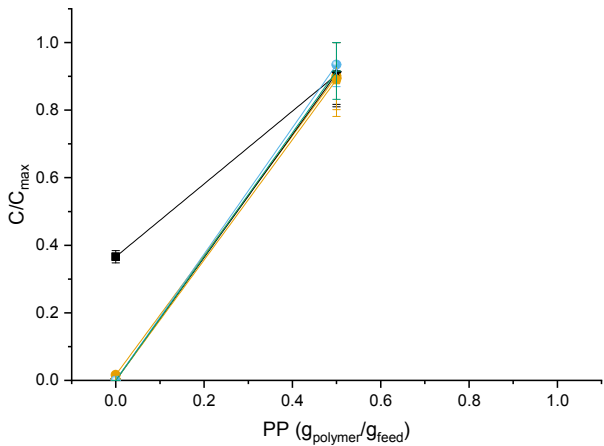
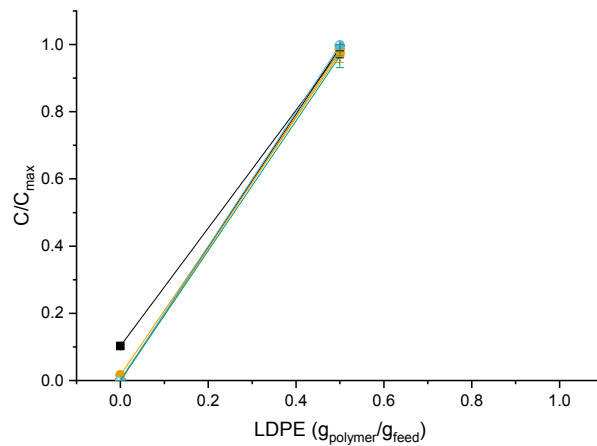
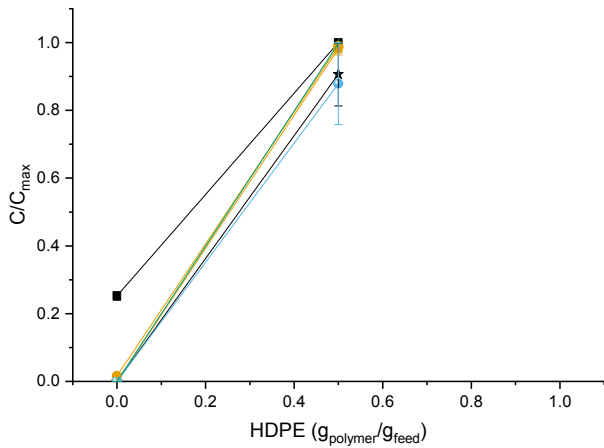


Figure S1 – Relative concentration changes of selected methoxy- compounds in HDPE, LDPE and PP co-HTL oil measured by GC-MS.

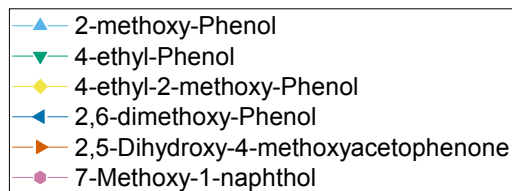
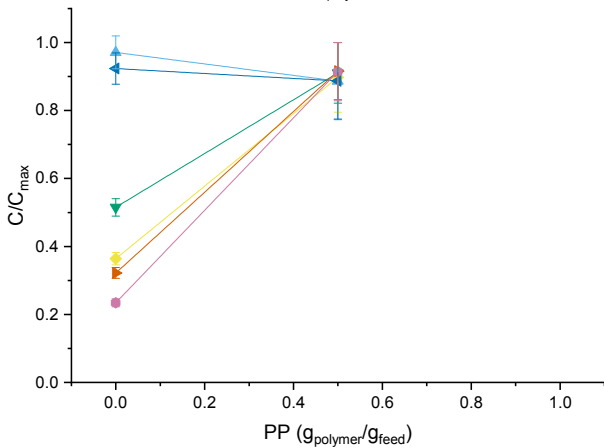
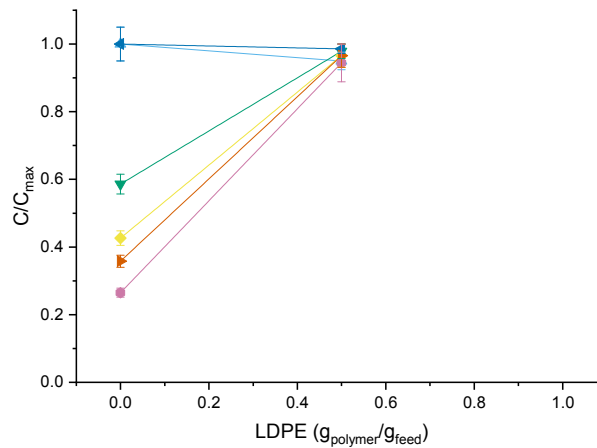
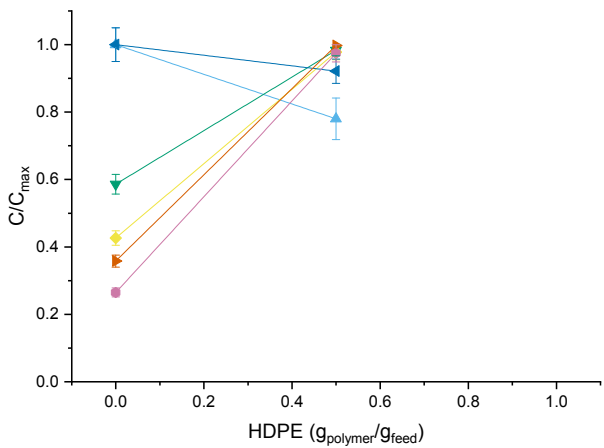


Figure S2 – Relative concentration change of HDPE, LDPE and PP co-HTL oil measured by GC-MS for selected phenolic compounds. [Pure polymers not available due to lack of conversion to oil]

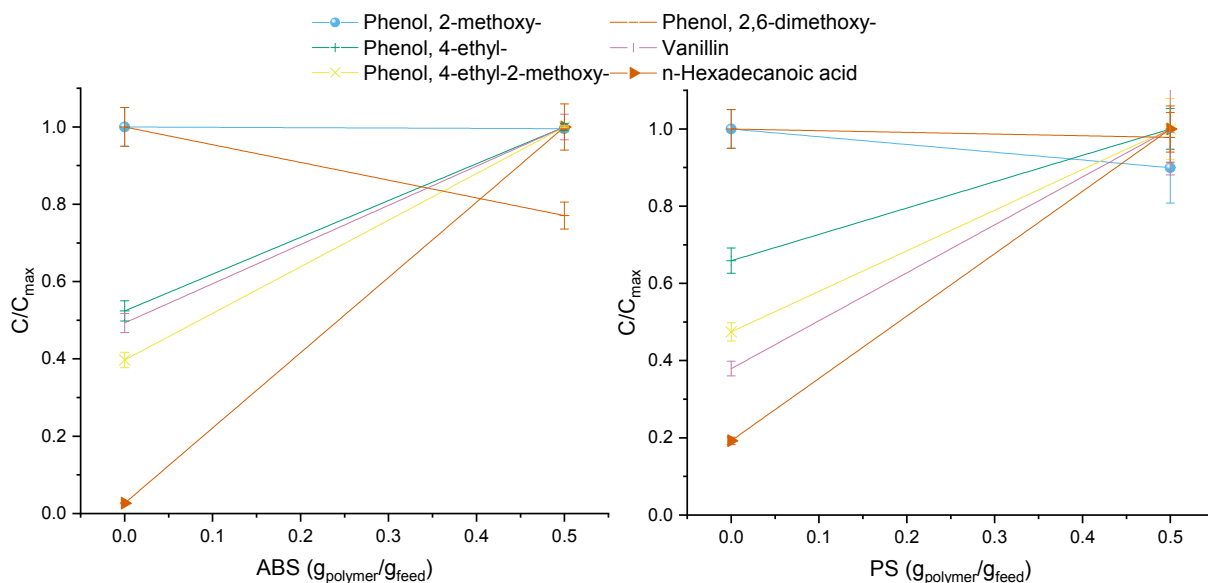


Figure S3 – Relative concentration change of ABS and PS co-HTL oil measured by GC-MS for selected phenolic compounds

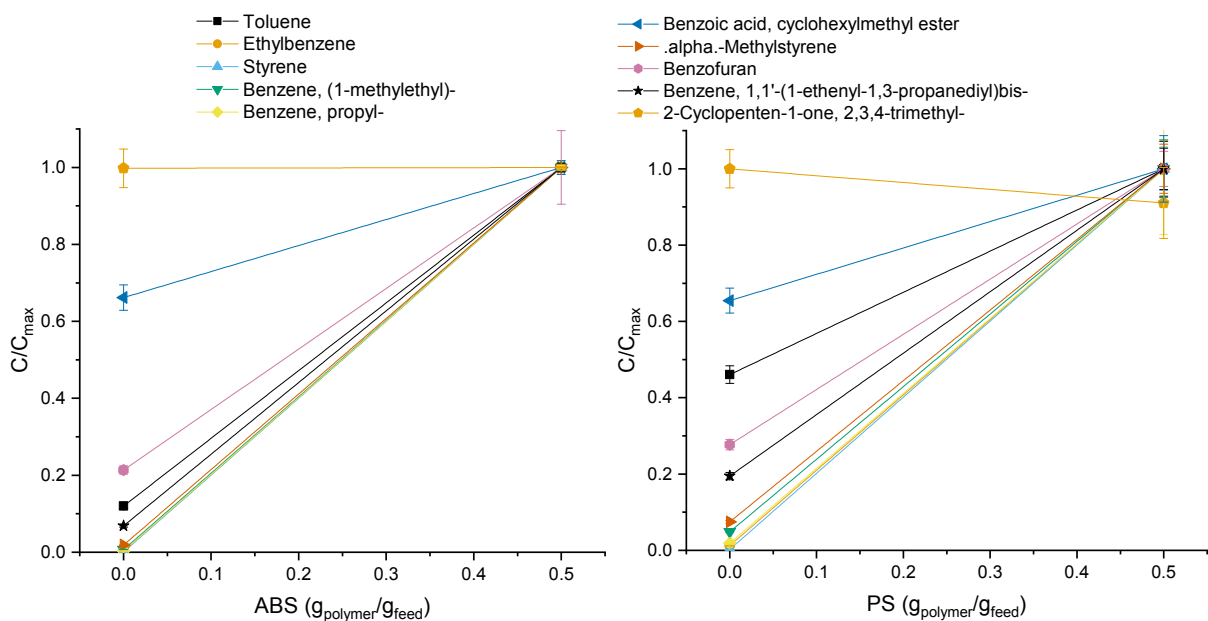


Figure S4 – Relative concentration change of ABS and PS co-HTL oil measured by GC-MS for selected substituted benzene compounds

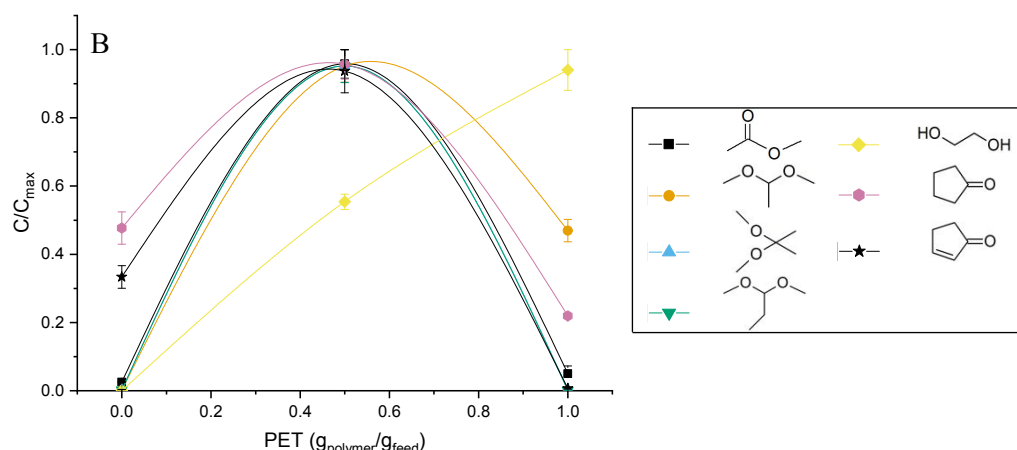
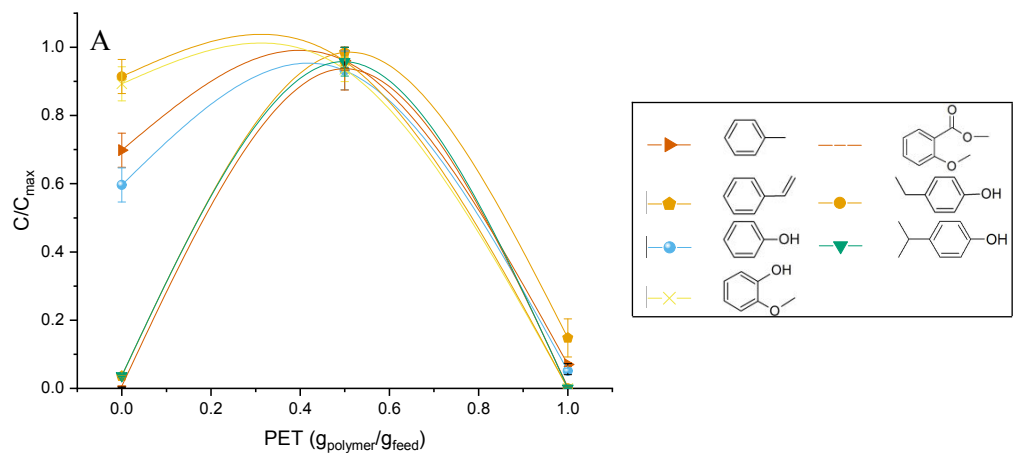


Figure S5 – Relative concentration change in PET co-HTL oil for selected aromatic (A) and ethylic (B) compounds. (A → Toluene; Styrene; Phenol; 2-methoxy-Phenol; methyl ester-2-methoxy-Benzoic acid; 4-ethyl-Phenol; p-Cumenol) (B → acetic acid methyl ester; 1,1-dimethoxy-ethane; 2,2-dimethoxy-propane; 1,1-dimethoxy-propane; 1,2-ethanediol; Cyclopentanone; 2-Cyclopenten-1-one)

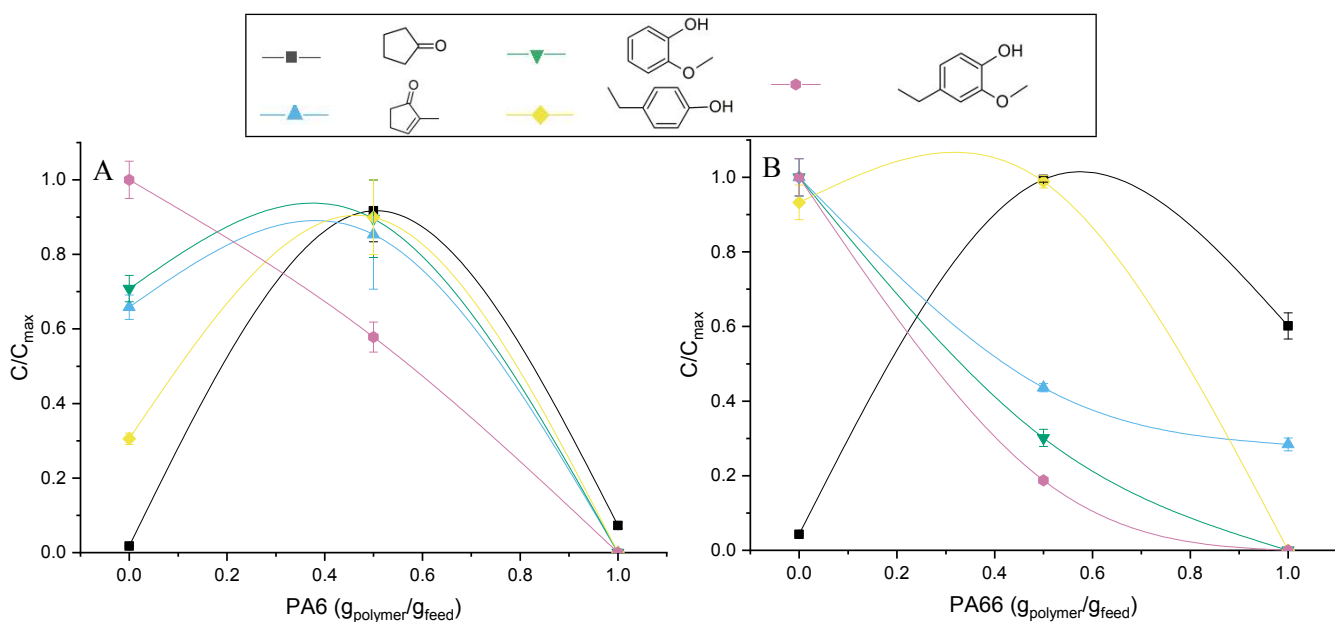


Figure S6 – Relative concentration change in PA6 (A) and PA66 (B) co-HTL oil for selected phenolic compounds. (—■— Cyclopentanone; —▲— 2-methyl-2-Cyclopenten-1-one; —▼— 2-methoxy-Phenol; —◆— 4-ethyl-Phenol; —●— 4-ethyl-2-methoxy-Phenol)

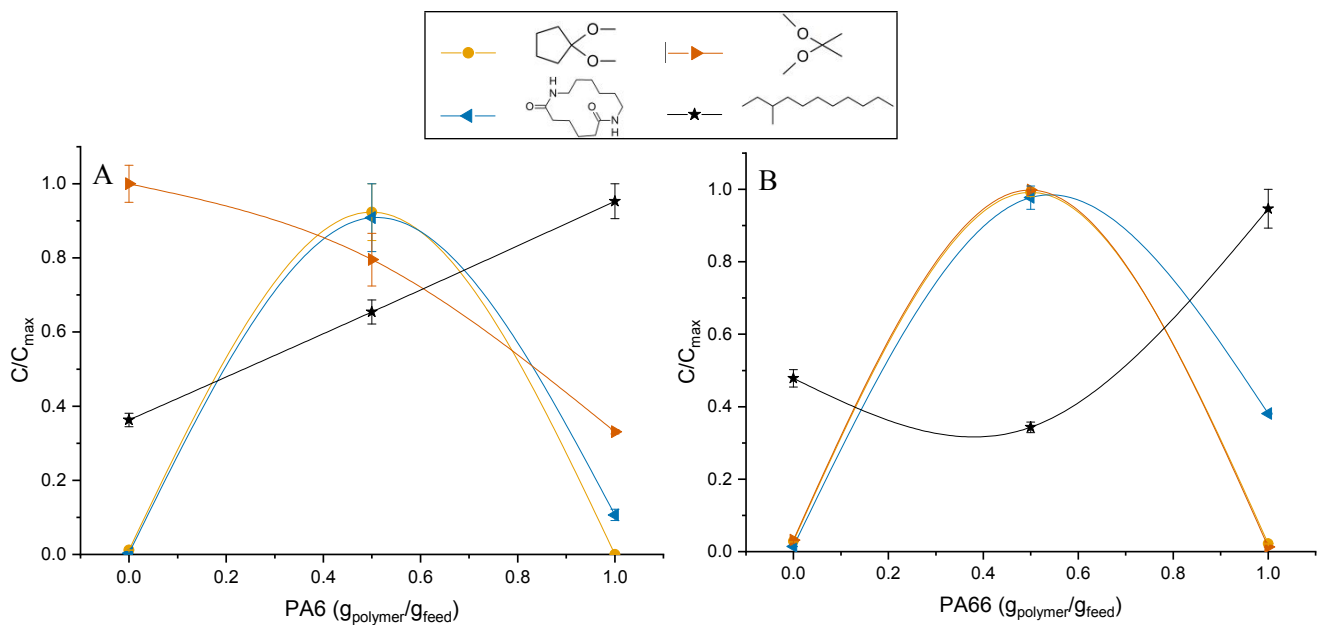


Figure S7 – Relative concentration change in PA6 (A) and PA66 (B) co-HTL oil for selected compounds. (● 1,1-Dimethoxycyclopentane; ▲ 1,8-Diazacyclotetradecane-2,7-dione; ▴ 2,2-dimethoxy-Propane; ★ 3-methylundecane)

Table S2 – -Relative composition of oil phase from co-HTL determined by GC/MS analysis

ABS		PS		Epoxy		PC		PET		HDPE		LDPE	
Compound	%Area	Compound	%Area	Compound	%Area	Compound	%Area	Compound	%Area	Compound	%Area	Compound	%Area
Phenol, 4-ethyl-	7.71%	3-(2-cyclopentenyl)-2-methyl-1,1-diphenyl-1-Propene and similar isomers	13.22%	Phenol	25.49%	p-Isopropenylphenol	35.58%	Ethane, 1,1-dimethoxy-	21.10%	Phenol, 4-ethyl-	12.99%	Phenol, 4-ethyl-	12.77%
Styrene	6.36%	Phenol, 4-ethyl-	6.05%	Phenol, 3-(1-methylethyl)-	29.72%	Phenol, 3-(1-methylethyl)-	26.34%	Acetic acid	6.28%	Phenol, 4-ethyl-2-methoxy-	9.74%	Phenol, 4-ethyl-2-methoxy-	10.18%
Phenol, 4-ethyl-2-methoxy-	5.52%	Phenol, 4-ethyl-2-methoxy-	4.58%	p-Isopropenylphenol	13.41%	Phenol	15.66%	Acetic acid, methyl ester	3.64%	Phenol	5.55%	Ethane, 1,1-dimethoxy-	5.89%
2-Phenyl-2-(prop-2-en-1-yl)pent-4-enenitrile	5.29%	Cyclohexane, 1,3,5-triphenyl-	4.05%	Phenol, 4,4'-(1-methylethylidene)bis-	1.94%	Anisaldehyde dimethyl acetal	5.02%	Phenol, 4-ethyl-	5.19%	Ethane, 1,1-dimethoxy-	4.25%	Acetic acid	5.29%
Benzenebutanenitrile	4.22%	Tetrahydrofuran	2.56%	Acetic acid, methyl ester	1.57%	Phenol, 4,4'-(1-methylethylidene)bis-	4.29%	Methanol, oxo-, benzoate	3.84%	Phenol, 3-(1-methylethyl)-	7.61%	Acetic acid, methyl ester	4.62%
Ethylbenzene	4.27%	Acetic acid	2.35%	Phenol, 4-ethyl-2-methoxy-	1.43%	Phenol, p-tert-butyl-	4.55%	2-Furanethanol, .beta.-methoxy-(S)-	3.81%	Phenol, 2-methoxy-	3.47%	Phenol, 2-methoxy-	4.06%
2-[1-(4-Cyano-1,2,3,4-tetrahydronaphthyl)]propanenitrile	3.03%	Ethane, 1,1-dimethoxy-	2.00%	Anisaldehyde dimethyl acetal	1.41%	Hexestrol	1.66%	Phenol, 4-ethyl-2-methoxy-	3.78%	Acetic acid, methyl ester	3.39%	Phenol, 2,6-dimethoxy-	3.99%
1-Naphthalenecarbonitrile	2.37%	Phenol, 2-methoxy-	1.96%	Phenol, 4-ethyl-	2.05%	Phenol, 4-ethyl-	0.69%	Phenol	2.76%	Phenol, 2,6-dimethoxy-	3.44%	Phenol	3.72%
Benzene, 1,1'-(1,2-dimethyl-1,2-ethanediyl)bis-	1.86%	Phenol, 2,6-dimethoxy-	1.93%	4,4'-Diacetyldiphenylmethane	1.09%	Phenol, 4-ethyl-2-methoxy-	0.39%	Phenol, 2-methoxy-	2.75%	Phenol, p-tert-butyl-	2.82%	2-Furanethanol, .beta.-methoxy-(S)-	2.93%
Phenol, 2-methoxy-	2.15%	Acetic acid, methyl ester	1.70%	Phenol, 2-methoxy-	0.79%	Phenol, 2,6-dimethoxy-	0.39%	p-Cumenol	2.39%	p-Isopropenylphenol	2.74%	p-Cumenol	2.21%
1,3-Butadiene, 1,4-diphenyl-, (E,E)-	2.01%	Styrene	3.53%	Benzofuran, 2-methyl-	0.73%	Phenol, 2-methoxy-	0.30%	1,2-Ethanediol	2.05%	2-Furanethanol, .beta.-methoxy-(S)-	2.06%	2,5-Dihydroxy-4-methoxyacetophenone	2.22%
Ethane, 1,1-dimethoxy-	1.98%	Phenol	1.30%	Benzene, 1,3-bis(1-methylethenyl)-	0.56%	2-Furanethanol, .beta.-methoxy-(S)-	0.28%	Phenol, 2,6-dimethoxy-	2.01%	7-Methoxy-1-naphthol	1.72%	7-Methoxy-1-naphthol	1.93%

Table S2 – Co-HTL oil phase relative composition via GC/MS analysis (continuation)

ABS		PS		Epoxy		PC		PET		HDPE		LDPE	
Compound	%Area	Compound	%Area	Compound	%Area	Compound	%Area	Compound	%Area	Compound	%Area	Compound	%Area
Acetic acid	1.91%	3-Thiophenecarboxylic acid, methyl ester	1.14%	Acetic acid	0.54%	2-Allyl-4-methylphenol	0.28%	2-Propanone, 1-hydroxy-	3.57%	2,5-Dihydroxy-4-methoxyacetophenone	1.67%	Ethanone, 1-(4-hydroxy-3,5-dimethoxyphenyl)-	1.53%
.alpha.-Methylstyrene	1.90%	Ethylbenzene	0.91%	3-Methyl-4-isopropylphenol	0.37%	Benzofuran, 2-methyl-	0.23%	Benzeneacetic acid, alpha.-methoxy-, methyl ester, (.+/-)-	1.69%	Benzaldehyde, 2,4-dihydroxy-6-methyl-	1.55%	4H-1-Benzopyran-4-one, 3-(3,4-dimethoxyphenyl)-6,7-dimethoxy-	1.35%
3-[1-(4-Cyano-1,2,3,4-tetrahydronaphthyl)]propanenitrile	1.72%	7-Methoxy-1-naphthol	0.86%	Phenol, 2,6-dimethoxy-	0.49%	1H-Indene, 2,3-dihydro-1,1,3-trimethyl-	0.18%	Propane, 1,1-dimethoxy-	1.50%	Homosyringaldehyde	1.28%	2-Cyclopenten-1-one, 2-hydroxy-3-methyl-	1.16%
4-Isopropyl-N-[2-(2-methyl-1H-indol-3-yl)-ethyl]-benzenesulfonamide	1.71%	Benzaldehyde, 2,4-dihydroxy-6-methyl-	0.77%	Benzofuran	0.47%	Naphthalene, 1,2,3,4-tetrahydro-1,6,8-trimethyl-	0.17%	Acetoin	1.17%	Phenol, 2-methoxy-4-propyl-	1.27%	Phenol, 2-methoxy-4-propyl-	1.22%
Benzene, 1,1'-(1,2-dimethyl-1,2-ethanediyl)bis-, (R*,S*)-	1.58%	Benzaldehyde dimethyl acetal	0.71%	Phenol, 2-(2-methyl-2-propenyl)-	0.47%	Benzofuran, 3-methyl-2-(1-methylethenyl)-	0.17%	7-Methoxy-1-naphthol	1.04%	Ethanone, 1-(4-hydroxy-3,5-dimethoxyphenyl)-	1.25%	Homosyringaldehyde	1.23%
Acetic acid, methyl ester	1.57%	Ethanone, 1-(4-hydroxy-3,5-dimethoxyphenyl)-	0.70%	p-Hydroxybiphenyl	0.43%	Phenol, 4-(1-methyl-1-phenylethyl)-	0.17%	2,5-Hexanedione	0.80%	Naphthalene, 1,7-dimethoxy-	0.70%	2-Cyclopenten-1-one	1.12%
8-Methyl-5H-pyrido[4,3-b]indole	1.52%	Naphthalene, 1,2,3,4-tetrahydro-1-phenyl-	0.67%	Ethanone, 1-(2,3-dihydro-1H-inden-5-yl)-	0.40%	Benzaldehyde, 4-methyl-	0.13%	Ethanone, 1-(4-hydroxy-3,5-dimethoxyphenyl)-	0.95%	2-Cyclopenten-1-one, 2-methyl-	0.63%	Methyl 3,5-dihydroxybenzoate, 2TMS derivative	1.09%
Cyclohexane, 1,3,5-triphenyl-	1.47%	Phenol, 2-methoxy-4-propyl-	0.57%	3-Cyclohexene-1-carboxaldehyde, 1,3,4-trimethyl-	0.36%	Acetic acid, methyl ester	0.13%	(S)-(+)-1,2-Propanediol	0.98%	Pentanoic acid, 5-hydroxy-, 2,4-di-tert-butylphenyl esters	0.53%	Acetoin	1.04%
Others	39.83%	Others	48.43%	Others	16.26%	Others	3.40%	Others	28.68%	Others	31.36%	Others	30.48%

Table S2 – Co-HTL oil phase relative composition via GC/MS analysis (continuation)

PP		PA6		PA66		PUR		PVC		Miscanthus	
Compound	%Area	Compound	%Area	Compound	%Area	Compound	%Area	Compound	%Area	Compound	%Area
Tetrahydrofuran	21.46%	Phenol, 4-ethyl-	21.27%	Phenol, 4-ethyl-	25.76%	Phenol, 2-methoxy-	12.17%	Acetic acid, methyl ester	23.28%	Phenol, 4-ethyl-	14.89%
Phenol, 4-ethyl-	12.12%	Phenol, 4-ethyl-2-methoxy-	9.08%	Cyclopentanone	11.61%	Phenol	9.45%	Pentanoic acid, 4-oxo-, methyl ester	10.29%	Phenol, 4-ethyl-2-methoxy-	8.07%
Phenol, 4-ethyl-2-methoxy-	9.11%	Phenol	7.81%	Phenol, 4-ethyl-2-methoxy-	9.47%	Phenol, 4-ethyl-	8.21%	Benzene	7.03%	Phenol, 2-methoxy-	7.97%
Acetic acid	3.95%	Hexanedioic acid	7.54%	Phenol	6.69%	Phenol, 4-ethyl-2-methoxy-	6.56%	Methylal	6.14%	Phenol, 2,6-dimethoxy-	7.10%
Phenol, 2-methoxy-	3.40%	Cyclopentanone	5.36%	Acetic acid, methyl ester	4.00%	8-Methyl-5H-pyrido[4,3-b]indole	6.14%	Naphthalene	5.49%	Acetic acid	7.02%
Ethane, 1,1-dimethoxy-	3.45%	Phenol, 2-methoxy-	4.56%	Hydrazine, 1,2-dimethyl-	3.44%	Phenol, 2,6-dimethoxy-	4.44%	Ethane, 1,1-dimethoxy-	3.93%	Phenol	5.08%
Phenol, 2,6-dimethoxy-	3.15%	1,8-Diazacyclotetradecane-2,7-dione	3.28%	1,8-Diazacyclotetradecane-2,7-dione	3.63%	Tetrahydrofuran	3.61%	Methyl propionate	2.06%	2-Cyclopenten-1-one, 2-methyl-	1.65%
Acetic acid, methyl ester	3.18%	Acetic acid	3.36%	1,1-Dimethoxycyclopentane	3.55%	Acetic acid, methyl ester	3.27%	Tetrahydrofuran	2.03%	Phenol, 2-methoxy-4-propyl-	1.59%
Phenol	2.15%	Acetic acid, methyl ester	3.23%	Phenol, 2-methoxy-	3.69%	Acetic acid	2.34%	Butanedioic acid, dimethyl ester	1.69%	Benzene, 1,2,3-trimethoxy-5-methyl-	1.57%
Benzene, 1,2,3-trimethoxy-5-methyl-	1.91%	1,1-Dimethoxycyclopentane	2.48%	Phenol, 2-methoxy-4-propyl-	2.01%	5,7-Dimethylpyrimido[3,4-a]-indole	2.03%	Phenanthrene	1.44%	(E)-3,3'-Dimethoxy-4,4'-dihydroxystilbene	1.56%
7-Methoxy-1-naphthol	1.60%	Phenol, 2,6-dimethoxy-	2.42%	Ethyl pipercolinate	1.25%	1H-Benzimidazole, 1-(2-phenylethenyl)-, (E)-	1.92%	2-Cyclopenten-1-one, 2,3-dimethyl-	1.37%	Pyridine	1.52%
2,4-Di-tert-butylphenol	1.56%	Monobenzene	2.02%	2,3-Dimethoxyphenol	1.41%	Diazene, dimethyl-	1.69%	Hexanoic acid, 4-oxo-, methyl ester	1.21%	2-Propanone, 1-(4-hydroxy-3-methoxyphenyl)-	1.50%

Table S2 – Co-HTL oil phase relative composition via GC/MS analysis (continuation)

PP		PA6		PA66		PUR		PVC		Miscanthus	
Compound	%Area	Compound	%Area	Compound	%Area	Compound	%Area	Compound	%Area	Compound	%Area
Phenol, 2-methoxy-4-propyl-	1.21%	Phenol, 2-methoxy-4-propyl-	1.90%	2,5-Dihydroxy-4-methoxyacetophenone	1.25%	Tert-octyldiphenylamine	1.53%	Propane, 1,1-dimethoxy-	1.17%	Homosyringaldehyde	1.36%
Ethanone, 1-(4-hydroxy-3,5-dimethoxyphenyl)-	1.19%	2-Methoxy-5-methylphenol	1.13%	2-Cyclopenten-1-one, 2-methyl-	1.04%	9H-Xanthen-9-one, 1-hydroxy-3,5,6-trimethoxy-	1.48%	Toluene	1.11%	Ethanone, 1-(4-hydroxy-3,5-dimethoxyphenyl)-	1.40%
Homosyringaldehyde	1.24%	Homosyringaldehyde	1.16%	Homosyringaldehyde	1.00%	Styrene	1.28%	Indane	1.03%	Propanoic acid, 2-methyl-, anhydride	1.35%
4H-1-Benzopyran-4-one, 3-(3,4-dimethoxyphenyl)-6,7-dimethoxy-	1.08%	Pentanoic acid, 5-hydroxy-, 2,4-di-t-butylphenyl esters	0.88%	Pentanoic acid, 5-hydroxy-, 2,4-di-t-butylphenyl esters	0.97%	1-Phenazinol, acetate (ester)	0.91%	2-Cyclopenten-1-one	1.03%	o-cresol	1.16%
2-Cyclopenten-1-one, 2-methyl-	0.97%	2,5-Dihydroxy-4-methoxyacetophenone	0.84%	Methyl propionate	0.94%	Phenol, 2-methoxy-4-propyl-	0.99%	Hexadecanoic acid, methyl ester	0.91%	Ethanone, 1-(3-hydroxy-4-methoxyphenyl)-	1.08%
1,3-Dioxolane, 2-phenyl-2-(phenylmethyl)-	0.90%	Methyl propionate	0.81%	2-Methoxy-5-methylphenol	0.92%	2-Methoxy-5-methylphenol	1.02%	Benzofuran, 2-methyl-	0.85%	Vanillin	1.04%
2-Cyclopenten-1-one	0.85%	3-Hydroxy-4-methoxybenzoic acid	0.61%	1H-Azepine, 1-acetylhexahydro-	0.75%	Phenazine, 1-methyl-	0.91%	Acenaphthene	0.71%	2-Cyclopenten-1-one	0.97%
2-Cyclopenten-1-one, 2-hydroxy-3-methyl-	0.80%	Ethane, 1,1-dimethoxy-	0.55%	Ethane, 1,1-dimethoxy-	0.63%	Homosyringaldehyde	0.85%	Methyl 3,3-dimethoxypropionate	0.76%	p-cresol	0.97%
Others	24.72%	Others	19.70%	Others	15.97%	Others	28.32%	Others	26.46%	Others	31.59%

SUPPLEMENTARY INFORMATION - Chapter 6 - Paper 3 - Combined hydrothermal liquefaction of polyurethane and lignocellulosic biomass for improved carbon recovery

Juliano Souza dos Passos ^{a,b}, Stefano Chiaberge ^c, Patrick Biller* ^{a,b}

^a Department of Biological and Chemical Engineering, Aarhus University, Høngøvej 2, DK-8200 Aarhus N, Denmark

^b Aarhus University Centre for Circular Bioeconomy, DK-8830 Tjele, Denmark

^c Eni s.p.a. Renewable Energy & Environmental R&D, via Fauser 4, 28100, Novara, Italy.

* Corresponding author – e-mail: pbiller@bce.au.dk

Key words: Hydrothermal liquefaction; chemical recycling; circular economy; polymers; polyurethane

Table S1 – Batch experimental plan

N	Temperature	Reaction time min	Miscanthus	PUR	Misc : PUR ratio
	°C		% in feed ash free	% in feed ash free	$\text{g}_{\text{miscanthus}} \cdot \text{g}_{\text{PUR}}^{-1}$
2	350	20	0%	100%	-
2	350	20	100%	0%	-
2	350	20	75%	25%	3.00
2	350	20	50%	50%	1.00
2	350	20	25%	75%	0.33
2	325	20	0%	100%	-
2	325	20	100%	0%	-
2	325	20	75%	25%	3.00
6	325	20	50%	50%	1.00
2	325	20	25%	75%	0.33
2	300	20	0%	100%	-
2	300	20	100%	0%	-
2	300	20	75%	25%	3.00
2	300	20	50%	50%	1.00
2	300	20	25%	75%	0.33

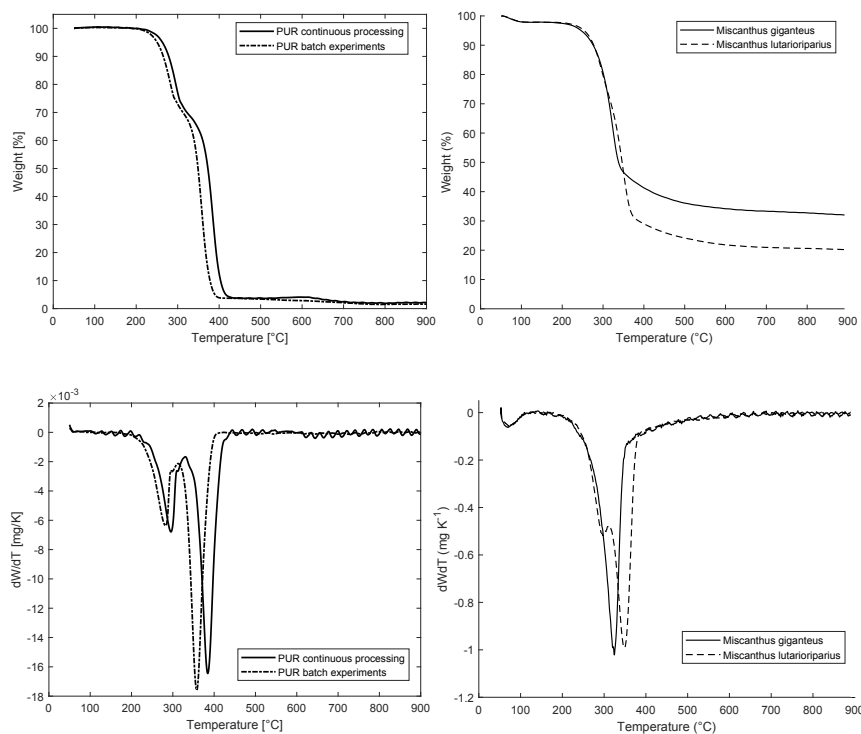


Figure S1 – TGA for miscanthus and PUR batch and continuous

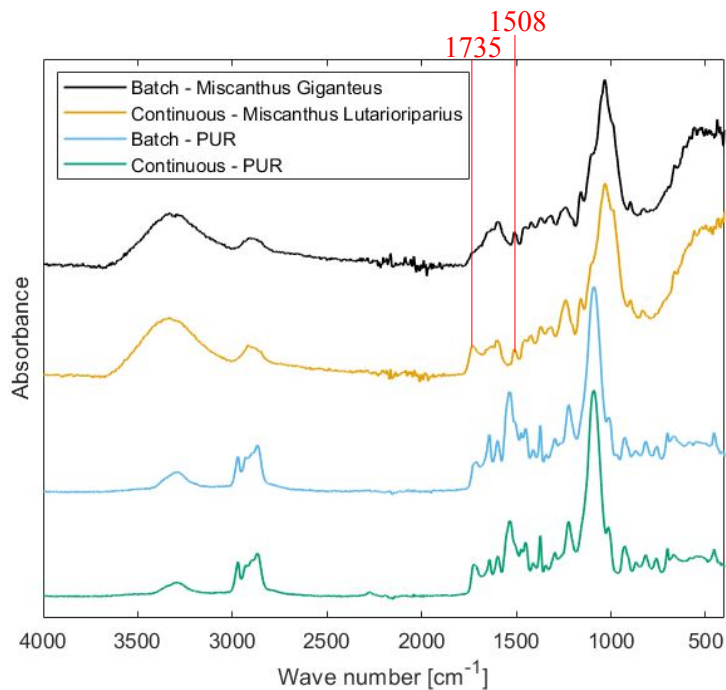


Figure S2 – FTIR for miscanthus and PUR batch and continuous

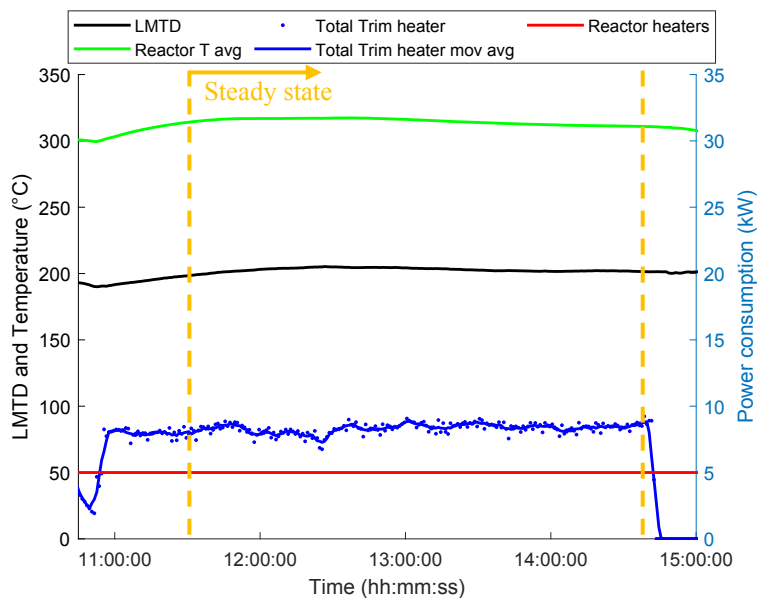


Figure S3 – Continuous campaign temperature and power consumption over time with highlighted steady state operation

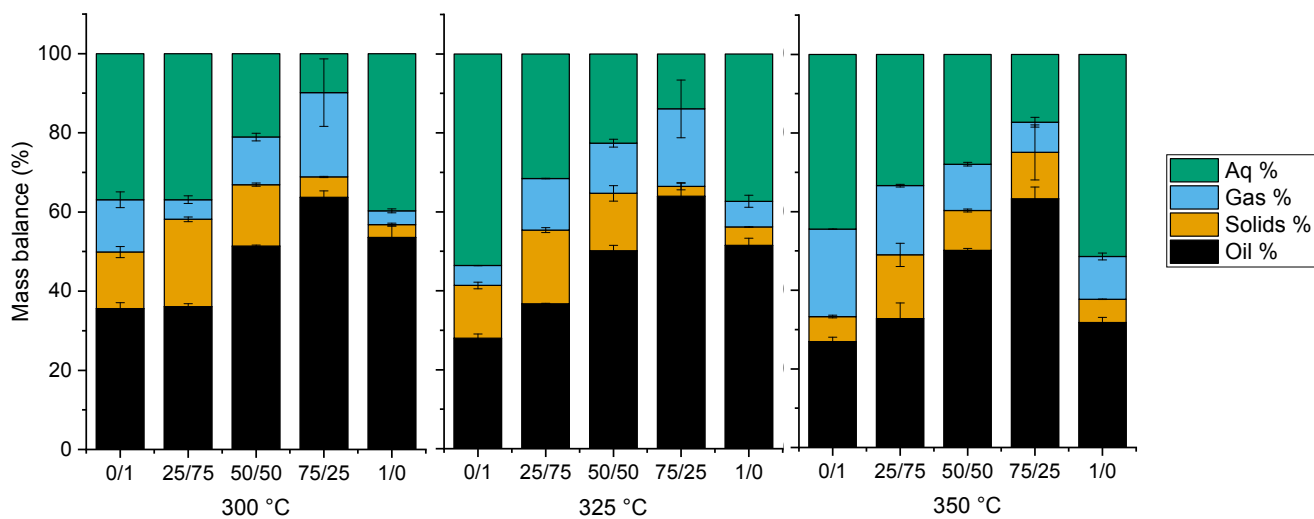


Figure S4 – PUR/Miscanthus batch HTL mass balance results

Table S2 – Feedstock composition

Type	Process	Sample	C [%]	SD	H [%]	SD	N [%]	SD	S [%]	SD	O* [%]	HHV (MJ/kg)
R	C	PUR	61.66	0.00	9.00	0.12	5.70	0.03	0.00	0.00	23.64	29.60
R	B	Batch - PUR	62.33	0.04	8.34	0.21	5.97	0.01	0.00	0.00	23.37	29.08
R	C	Miscanthus Lutarioriparius	45.90	0.00	6.52	0.12	0.14	0.03	0.05	0.05	47.39	18.81
R	B	Miscanthus Giganteus	44.83	0.15	5.82	0.13	0.68	0.02	0.05	0.00	48.63	17.47
O	B	PUR (325 °C)	56.48	2.35	8.95	0.24	2.07	0.08	0.03	0.02	56.48	26.87
O	B	Miscanthus Giganteus (325 °C)	65.81	1.53	6.01	0.05	1.08	0.04	0.09	0.01	65.81	27.25
O	B	75:25 PUR:M (325 °C)	63.82	0.43	8.90	0.23	4.00	0.10	0.03	0.02	63.82	30.31
O	C	PUR:M co-HTL	63.09	0.11	9.74	0.33	3.95	0.14	0.01	0.00	23.21	31.13

* Oxygen by difference

R – raw material

O – oil product

C – Continuous processing

B – Batch experiments

Table S3 – ANOVA analysis for oil yield prediction model

	Sum of Squares	Degrees of Freedom	Mean of Squares	F-Value	p-Value
T	0.0239	1	0.0239	22.10	<0.0001
M	0.2740	1	0.2740	252.96	<0.0001
T ²	0.0016	1	0.0016	1.48	0.2354
T M	0.0044	1	0.0044	4.08	0.0542
M ²	0.1243	1	0.1243	114.75	<0.0001
T ² M	0.0059	1	0.0059	5.42	0.0283
T M ²	0.0231	1	0.0231	21.32	0.0001
M ³	0.1262	1	0.1262	116.49	<0.0001
Error	0.0271	25	0.0011	-	-

Table S4 – ANOVA analysis for carbon yield prediction model

	Sum of Squares	Degrees of Freedom	Mean of Squares	F-Value	p-Value
T	0.0131	1	0.0131	13.67	0.0010
M	0.0727	1	0.0727	75.67	<0.0001
T M	0.0034	1	0.0034	3.53	0.0714
M ²	0.0157	1	0.0157	16.30	0.0004
T ²	0.2022	1	0.2022	210.49	<0.0001
T M ²	0.0135	1	0.0135	14.01	0.0009
M ³	0.1518	1	0.1518	158.08	<0.0001
Error	0.0250	26	0.0010	-	-

Table S5 – ANOVA analysis for energy yield prediction model

	Sum of Squares	Degrees of Freedom	Mean of Squares	F-Value	p-Value
T	0.0159	1	0.0159	12.63	0.0014
M	0.0543	1	0.05427	43.16	<0.0001
T M	0.0155	1	0.0155	12.31	0.0016
M ²	0.2523	1	0.2523	200.67	<0.0001
T M ²	0.0184	1	0.0184	14.65	0.0007
M ³	0.1629	1	0.1629	129.54	<0.0001
Error	0.0340	27	0.0013	-	-

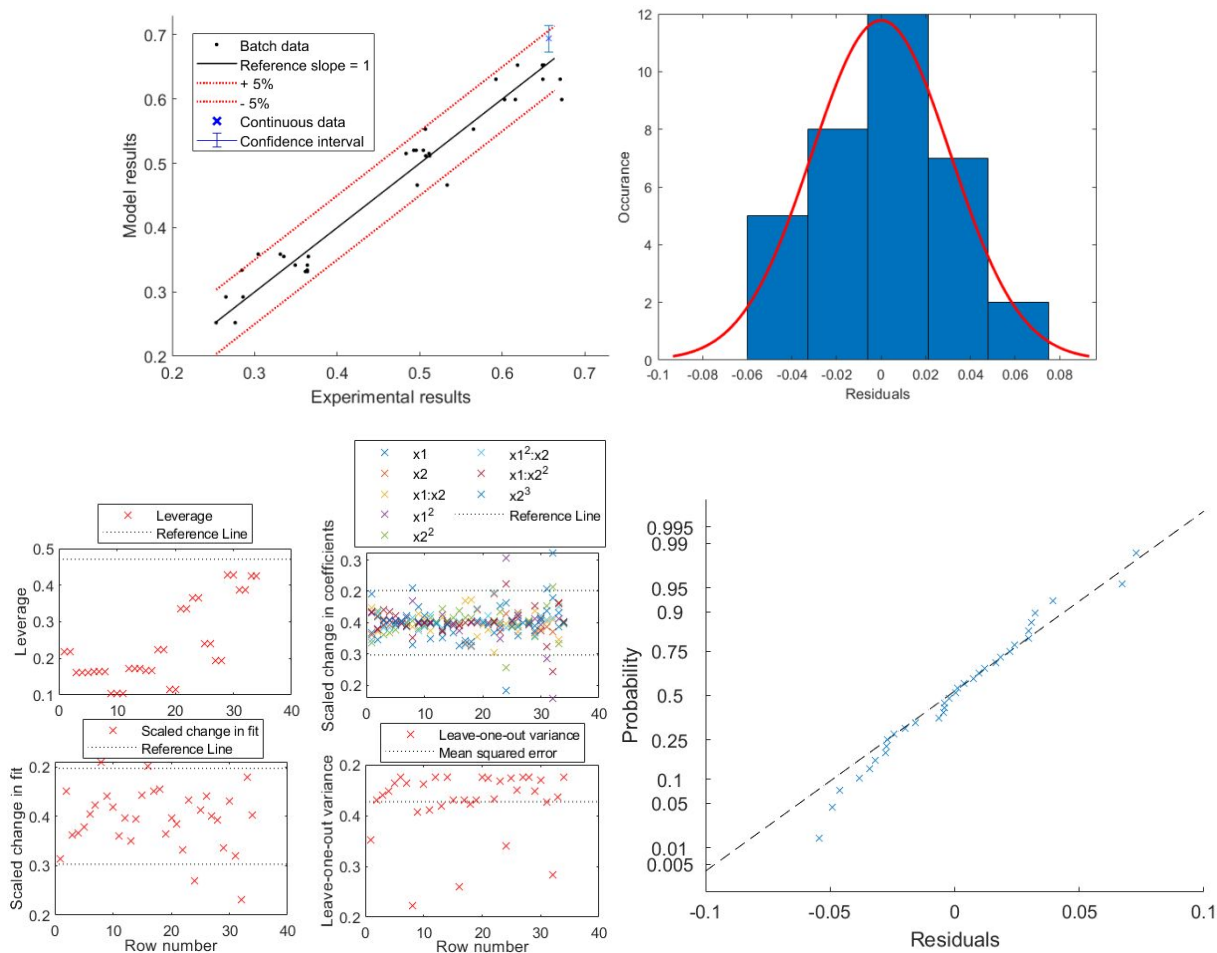


Figure S5 – Model prediction and experimental comparison, residual histogram, leverage, scaled change in coefficients, scaled change in fit, leave-one-out variance and residuals normal probability plots for oil yield prediction model

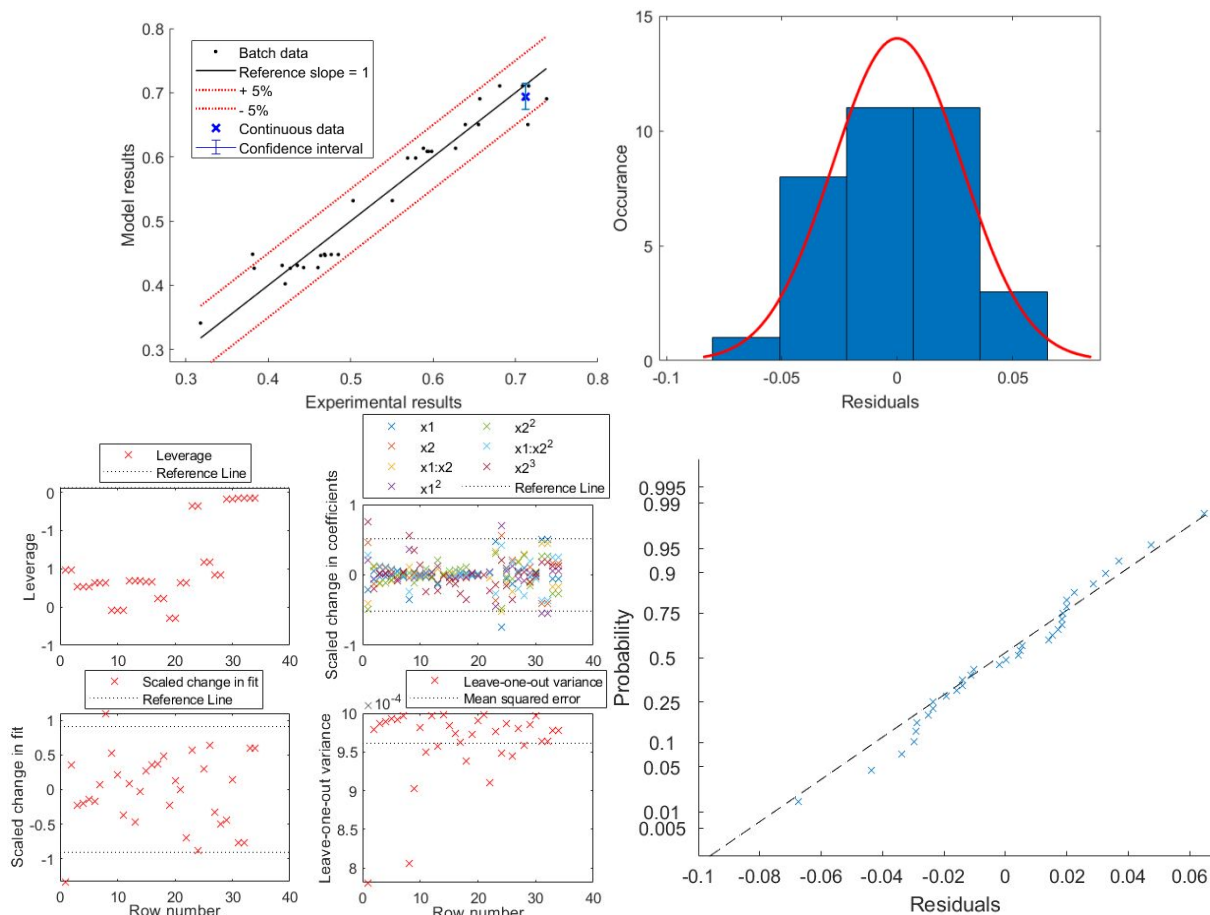


Figure S6 – Model prediction and experimental comparison, residual histogram, leverage, scaled change in coefficients, scaled change in fit, leave-one-out variance and residuals normal probability plots for carbon yield prediction model

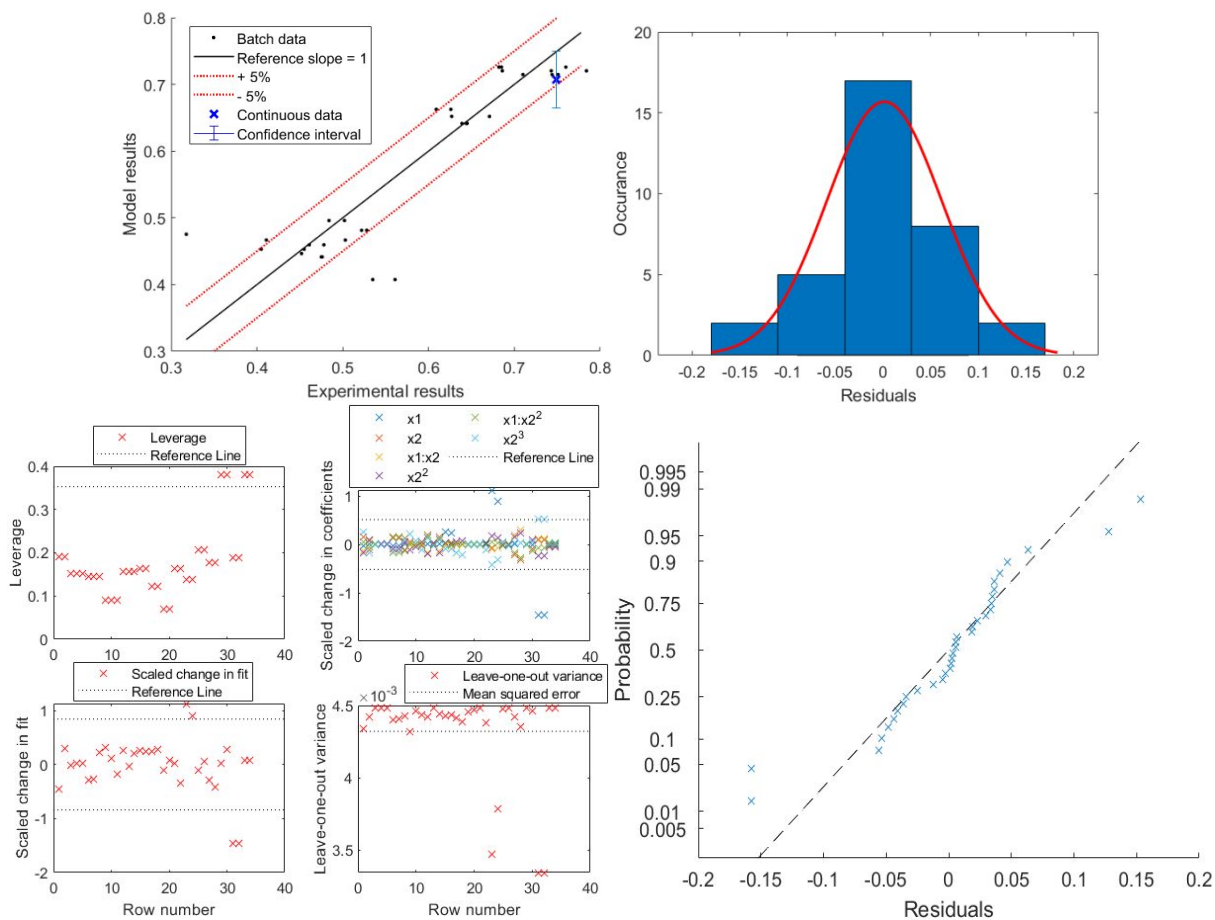


Figure S7 – Model prediction and experimental comparison, residual histogram, leverage, scaled change in coefficients, scaled change in fit, leave-one-out variance and residuals normal probability plots for energy yield prediction model

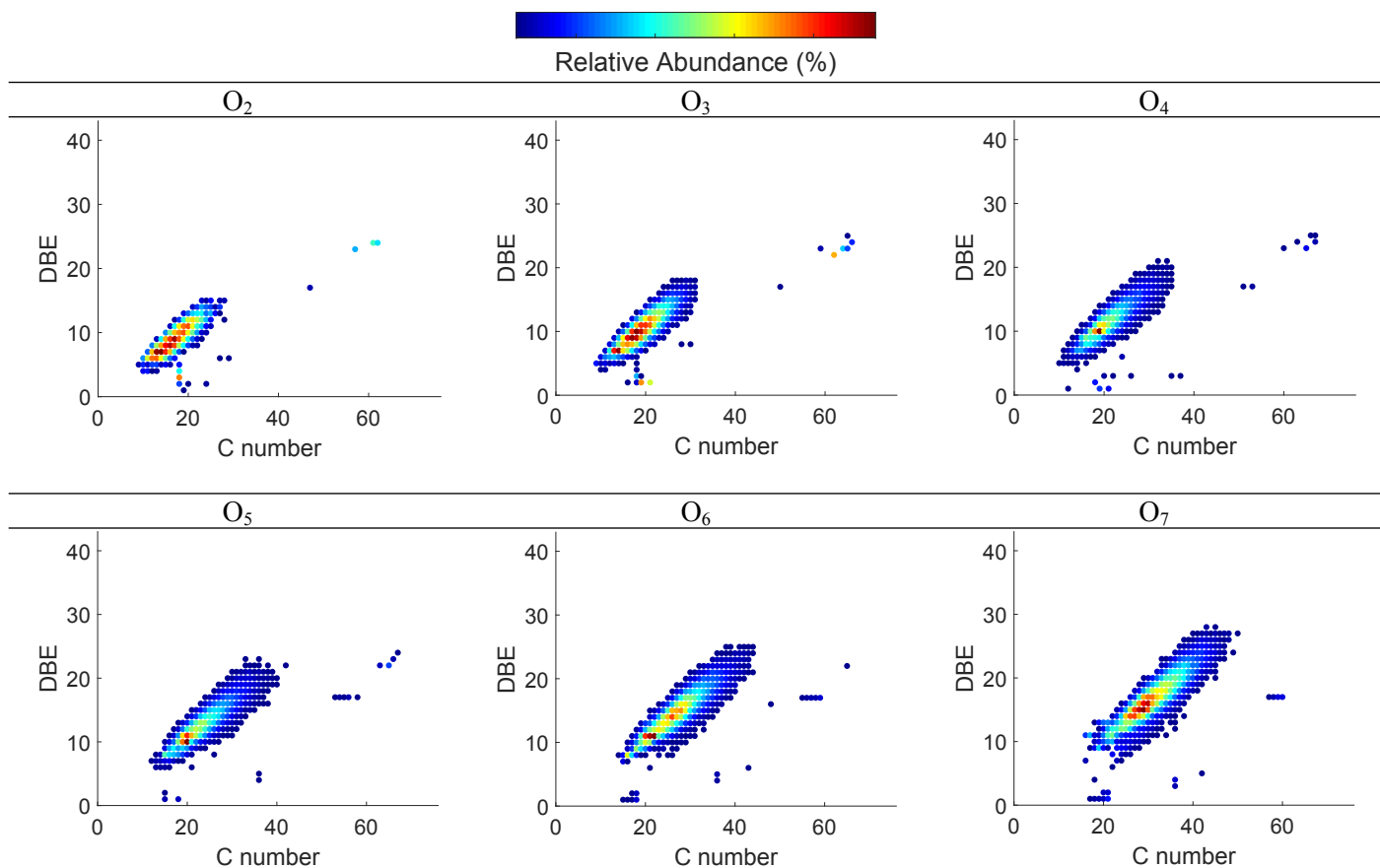


Figure S8 – DBE versus carbon number for miscanthus biocrude according to family

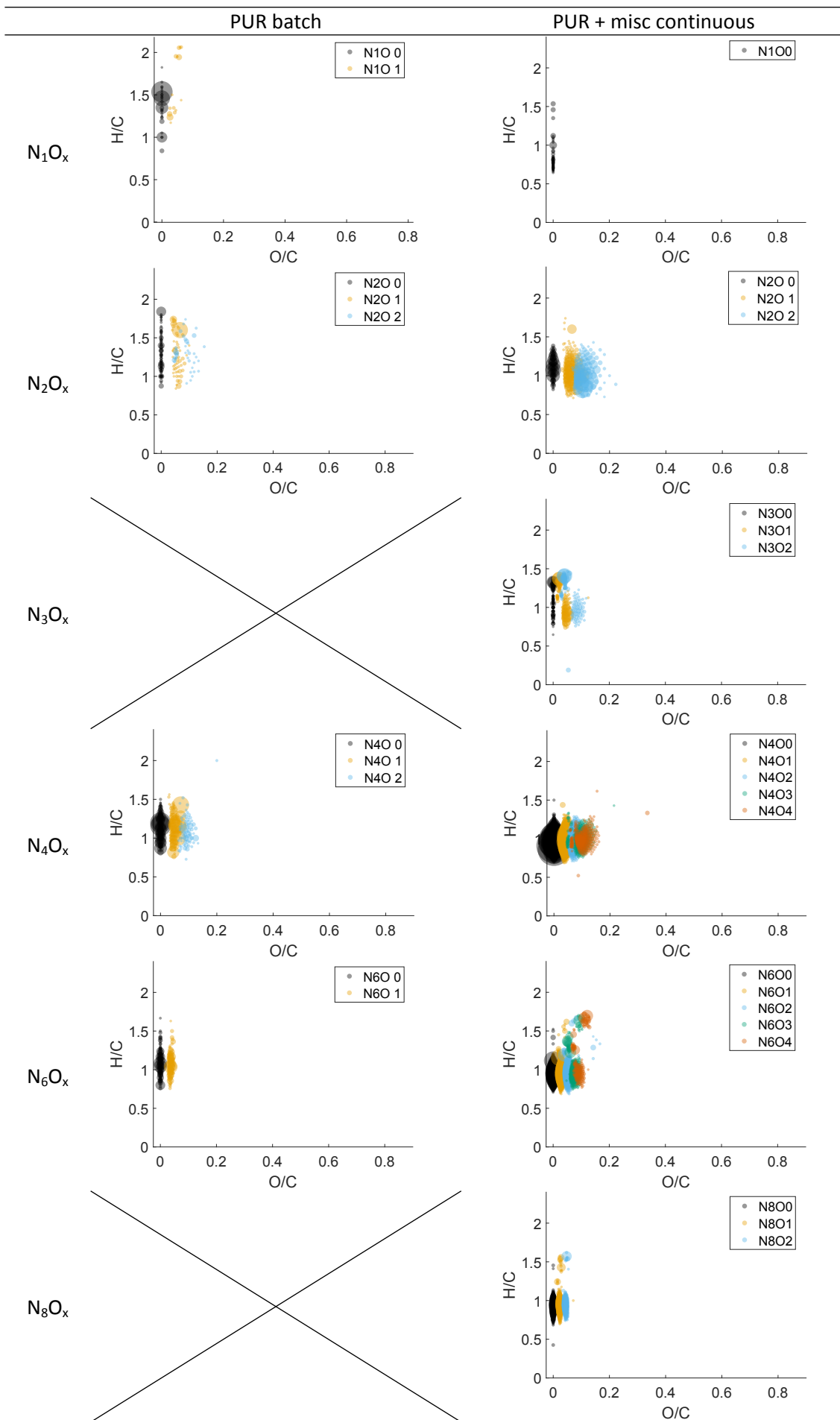


Figure S9 – Van-Krevelen diagram for all different nitrogen containing compounds identified

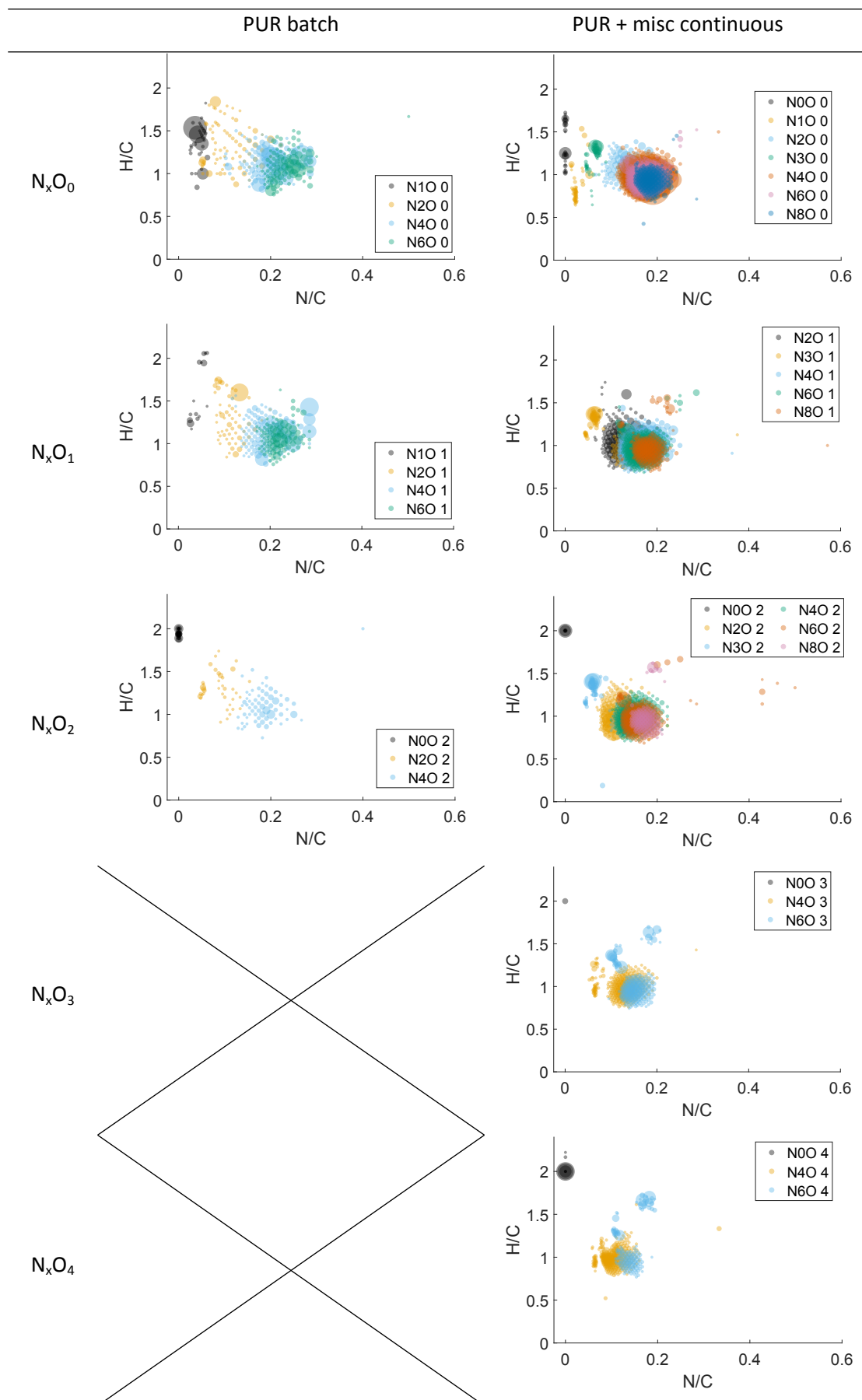


Figure S10 – Modified Van-Krevelen diagram for all different nitrogen containing compounds identified

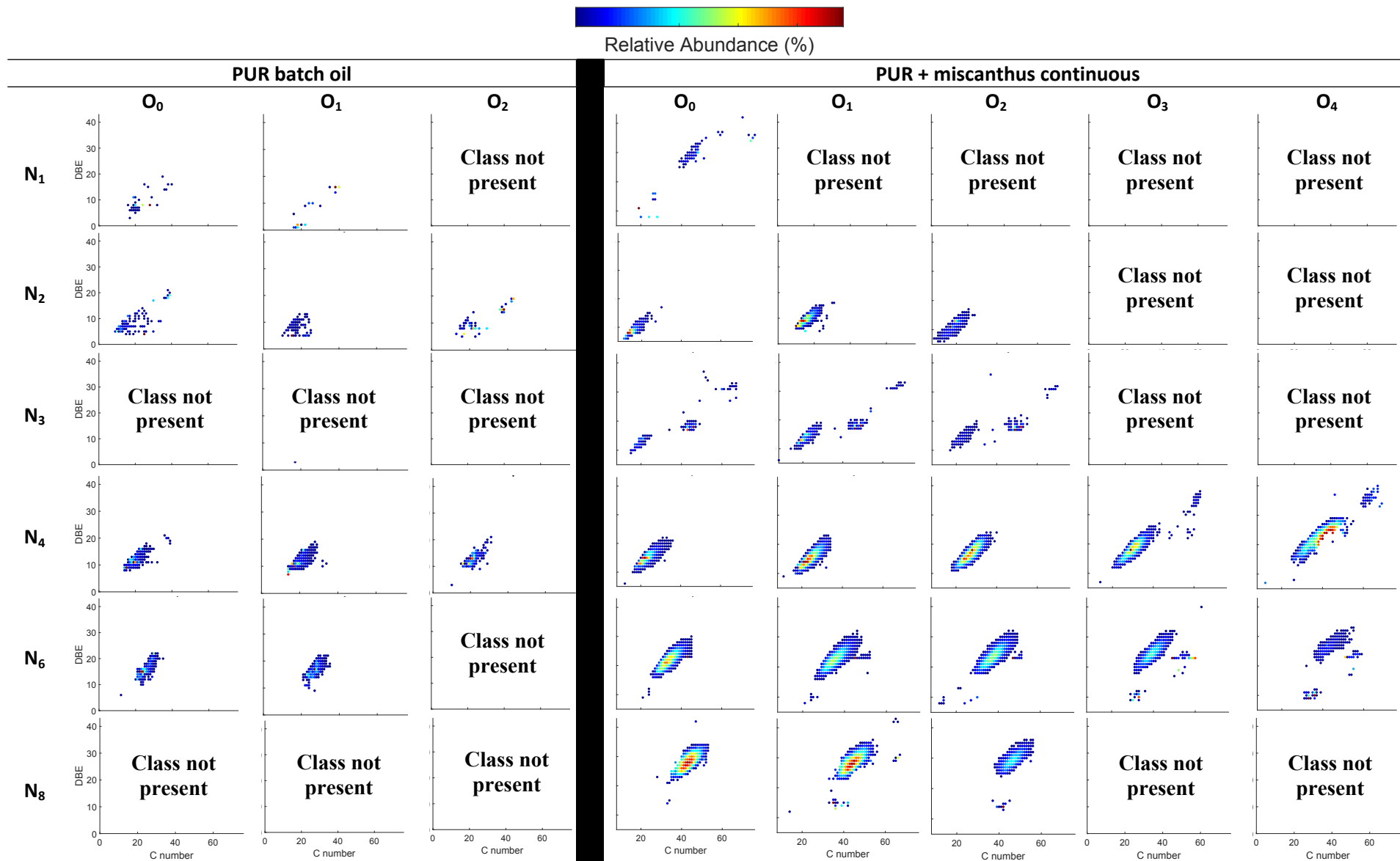


Figure S11 – DBE over carbon number according to nitrogen and oxygen number

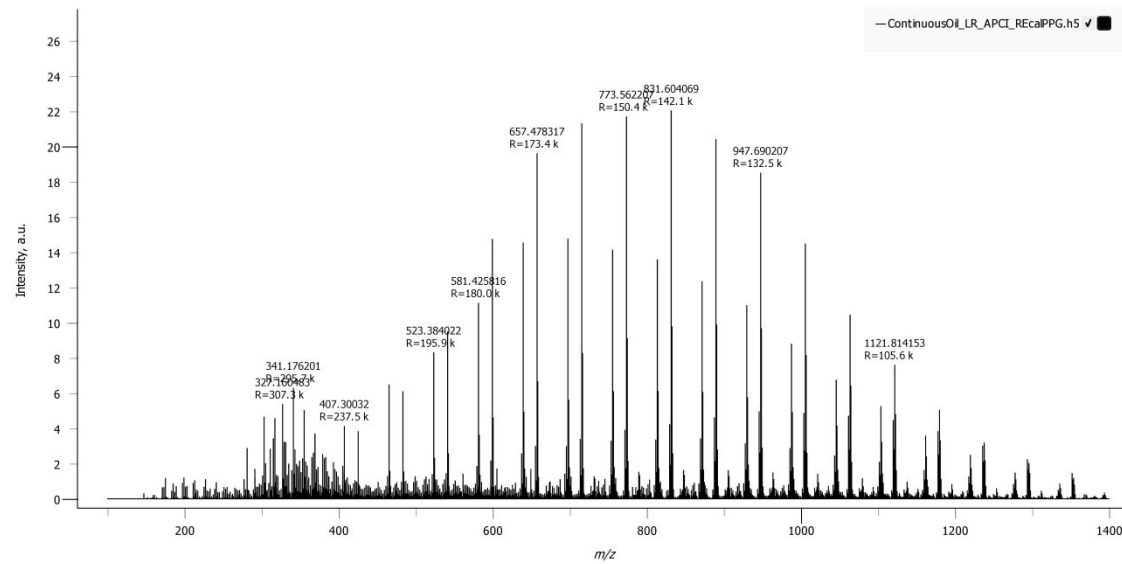


Figure S12 – APCI(+)-FTICR mass spectrum of oil from HTL experiments in continuous campaign – polyurethane and miscanthus co-HTL

SUPPLEMENTARY INFORMATION – Chapter 8 – Manuscript 2 – Enhanced biocrude and carbon recovery from cow manure and wheat straw combined hydrothermal liquefaction via mixed feedstock optimization: from batch to continuous processing

Juliano Souza dos Passos ^{a,b}, Aisha Matayeva^a, Patrick Biller* ^{a,b}

^a Department of Biological and Chemical Engineering, Aarhus University, Hångøvej 2, DK-8200 Aarhus N, Denmark

^b Aarhus University Centre for Circular Bioeconomy, DK-8830 Tjele, Denmark

* Corresponding author – pbiller@bce.au.dk

Key words: Hydrothermal liquefaction; waste valorization; manure; wheat straw; biofuel

Table S1 – Elemental analysis and moisture of manure and wheat straw

Biomass	C, %	H, %	N, %	S, %	O, %*	Ash, %	Moisture, %	HHV, MJ/kg
Manure	41.76	5.71	2.16	0.51	28	16.14	5.85	17.3
Wheat straw	42.96	5.98	0.55	0.091	46.16	2.7	5.7	14.8

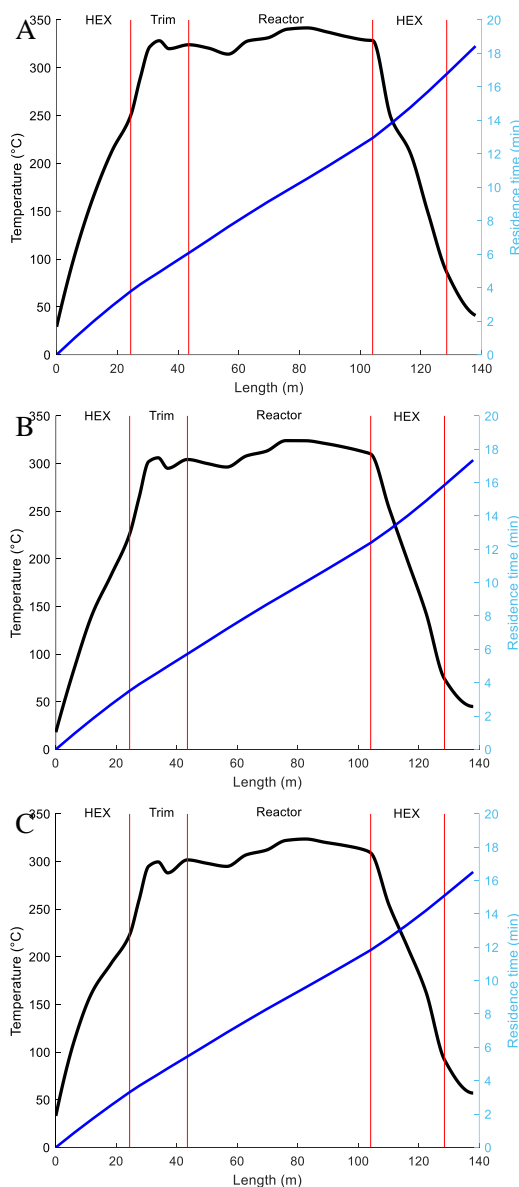


Figure S1 – Continuous production campaign in HTL pilot plant. Temperature profiles and residence times for Wheat Straw (A), Cow Manure (B) and co-HTL of both (C)

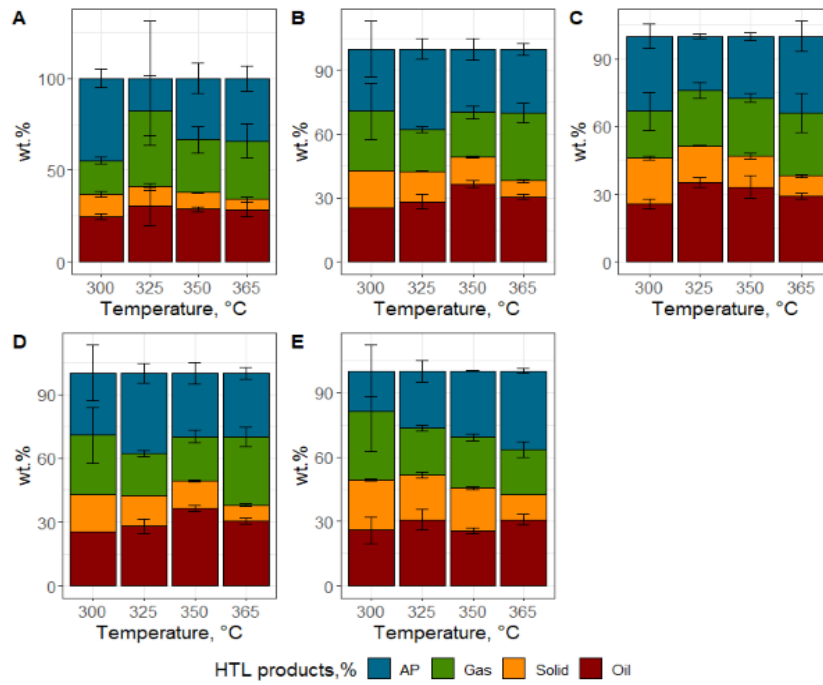


Figure S2 – HTL product yields: A) Manure, 0 %, B) Manure, 25%, C) Manure 50%, D) Manure 75, E) Manure 100%. (AP – Aqueous Phase)

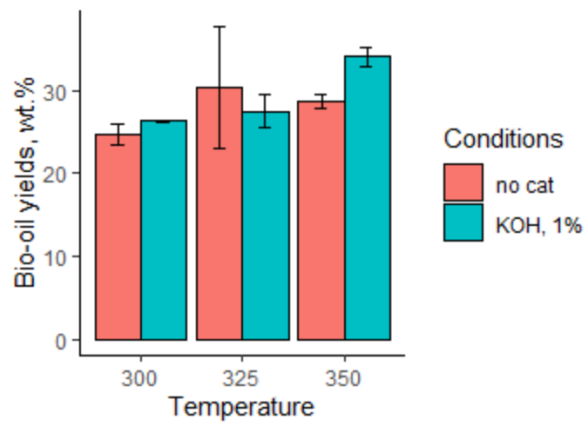


Figure S3 - The bio-oil yields from wheat straw using no cat and 1% KOH

Table S2 - Experimental design and raw results

Temperature ^a , z	Manure ^b , x ₁	Wheat straw ^b , x ₂	Oil yield, y ₁	ER, y ₂	CR, y ₃
-1	0	1	22.11231	37.76353	35.17224
-1	0	1	24.49436	41.83161	38.96117
-0.23	0	1	35.53431	64.44167	58.66822
-0.23	0	1	21.60711	39.18461	35.67399
0.538	0	1	26.13858	51.21013	44.17382
0.538	0	1	27.897	54.65519	47.14552
1	0	1	29.6125	53.61148	48.76532
1	0	1	24.2375	43.8804	39.91387
1	0.246914	0.753086	29.65432	53.76033	48.75686
0.538	0.248842	0.751158	33.38263	61.35275	54.31788
-0.23	0.249312	0.750688	24.31184	44.2062	40.05918
-1	0.248572	0.751428	24.02994	41.7607	38.62493
0.538	0.252948	0.747052	35.45031	65.14156	57.68894
-0.23	0.253482	0.746518	28.91897	52.57409	47.65606
-1	0.257863	0.742137	24.0379	41.75814	38.64783
1	0.259259	0.740741	28.02469	50.77948	46.09348
-1	0.490542	0.509458	22.69861	38.12832	35.01792
1	0.493827	0.506173	26.5679	48.24777	43.7735
1	0.5	0.5	28.23171	51.25604	46.52294
-0.23	0.501465	0.498535	31.83594	53.83087	49.1183
0.538	0.502059	0.497941	34.62582	61.95313	56.29323
-0.23	0.502336	0.497664	34.83448	58.8989	53.74595
0.538	0.507949	0.492051	28.04384	50.16419	45.60014
-1	0.508339	0.491661	25.83638	43.36674	39.87875
-1	0.74525	0.25475	29.57326	46.81496	43.81776
-0.23	0.746542	0.253458	47.72499		
1	0.746988	0.253012	24.0241	45.46637	41.3781
-0.23	0.74813	0.25187	34.90876	63.63523	57.81157
-0.23	0.747559	0.252441	28.4	51.76537	47.03927
-0.23	0.747845	0.252155	26.4	48.11992	43.72664
0.538	0.749178	0.250822	30.77996	54.72018	48.0626
0.538	0.749676	0.250324	35.34285	62.83073	55.18829
1	0.75	0.25	23.6125	44.68184	40.67268
-1	0.750643	0.249357	29.40653	46.54063	43.57742
-1	1	0	20.52328	35.47786	32.95701
-1	1	0	28.71549	49.63944	46.11235
-0.23	1	0	32.37736	54.93608	50.87871
-0.23	1	0	25.98146	44.08387	40.828
0.538	1	0	23.54273	43.29897	39.85716
0.538	1	0	25.29315	46.51827	42.82056
1	1	0	30.7875	58.65369	53.97797
1	1	0	27.39506	52.19071	48.0302

^a Temperature was coded: -1 (300°C), -0.23 (325°C), 0.538 (350°C), +1(365°C)

^b the mass ratio of manure and wheat straw was normalized due to the constriction of the mixture model $x_1+x_2=1$

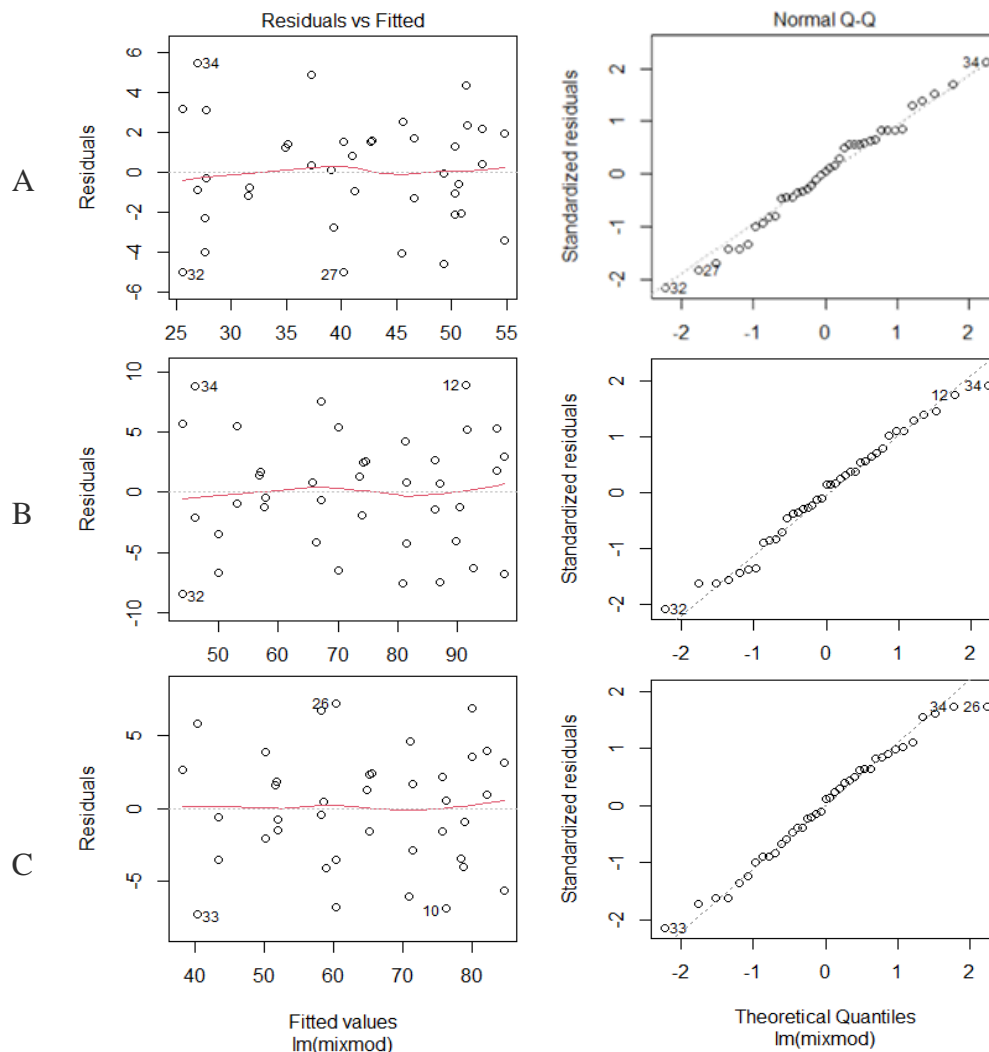


Figure S4 - The diagnostic plots of three models for the prediction of a) bio-oil yield, %, b) ER, %, c) CR, %

Table S3 – ANOVA for oil yield, ER and CR

Terms	Bio-oil yield		ER		CR	
	Coef.	p	Coef.	p	Coef.	p
x_1	27.16	5.17e-14	42.30	5.46e-11	38.94	1.15e-11
x_2	24.12	1.79e-4	46.73	1.13e-08	40.69	8.52e-09
$x_1x_2(x_1-x_2)$	9.69	0.56	24.50	0.3760	16.08	0.51
x_1x_2	32.15	0.001	58.31	0.001	4.92	0.00
x_1z	1.06	0.47	5.61	0.03	4.42	0.03
x_2z	2.23	0.14	5.76	0.03	-36.5	0.06
$x_1x_2(x_1-x_2)z$	-26.72	0.04	-36.50	0.11	6.25	0.06
x_1z^2	-0.57	0.83	6.59	0.77	0.51	0.17
x_2z^2	1.30	0.67	-1.80	0.72	6.24	0.90
$x_1x_2(x_1-x_2)z^2$	-11.93	0.61	-42.17	0.28	0.51	0.35
x_1x_2z	-2.96	0.65	-7.15	0.62	-31.38	0.48
$x_1x_2z^2$	-30.10	0.01	-61.06	0.007	-57.67	0.003
<i>Regression</i>		0.005		0.001		0.001
<i>Residuals</i>	3.187		5.48		4.71	
<i>F-statistic</i>	3.316		4.21		4.08	

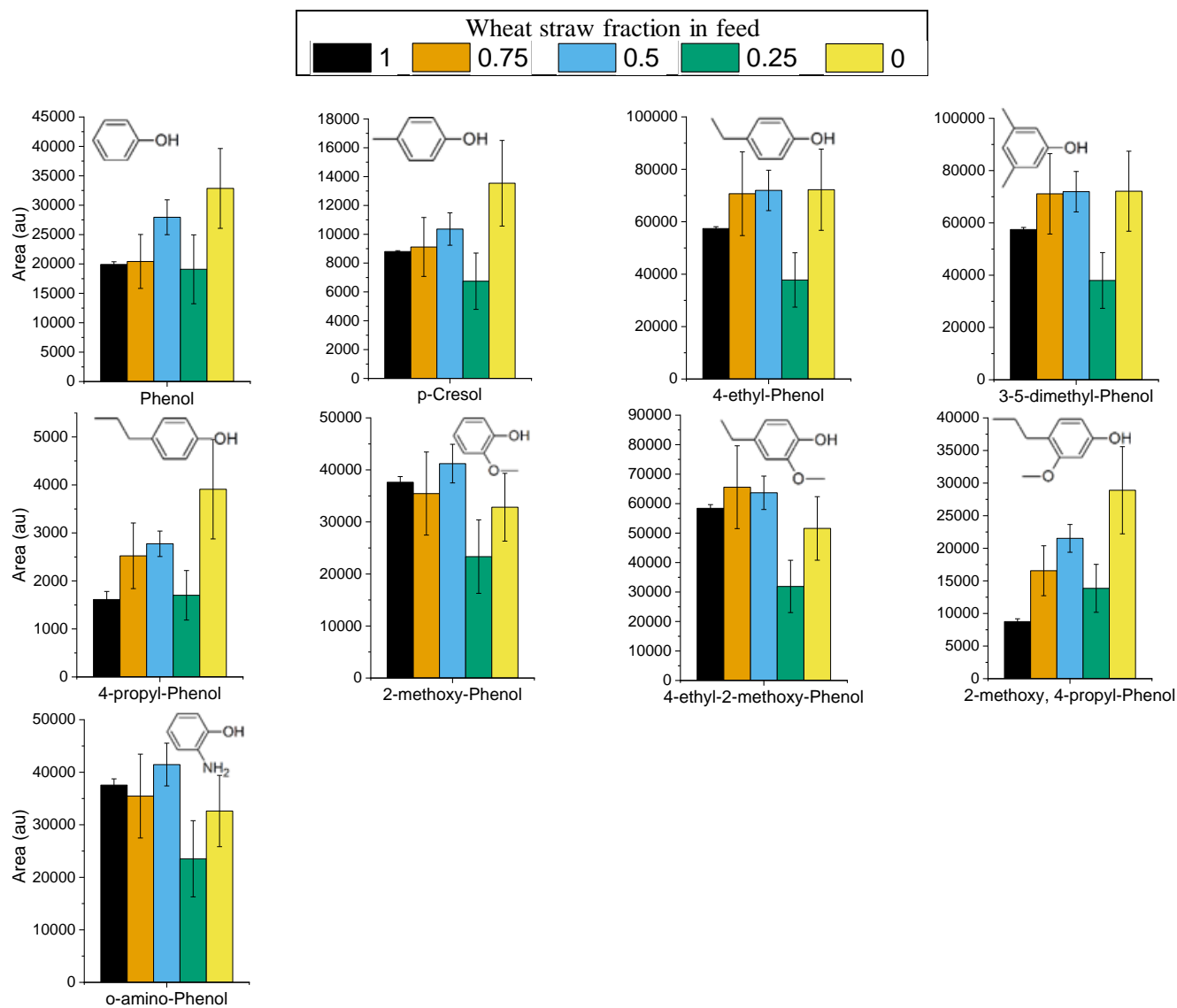


Figure S5 - Phenolic compounds WS fraction comparison @ 325 °C

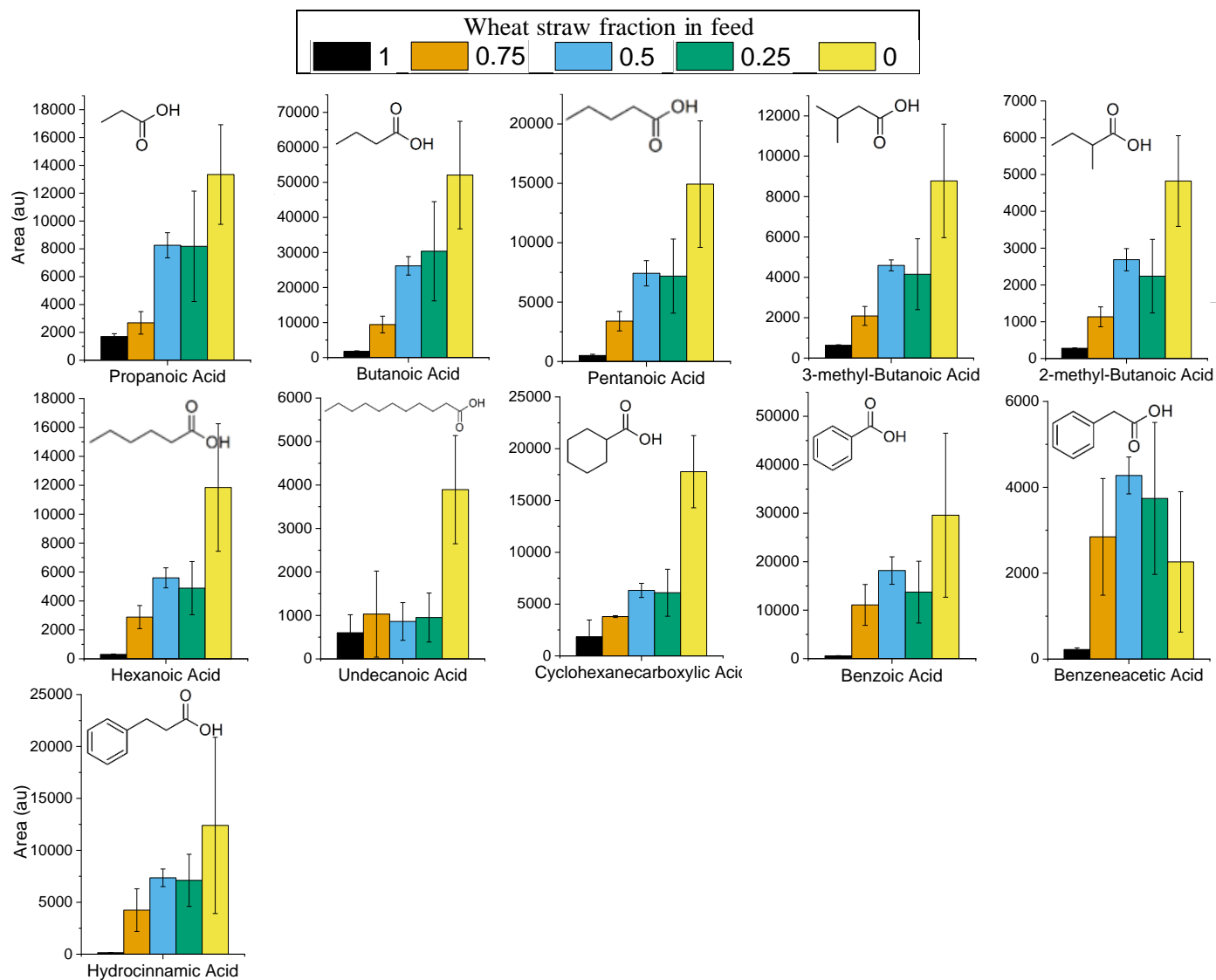


Figure S6 - Carboxylic acids WS fraction comparison @ 325 °C

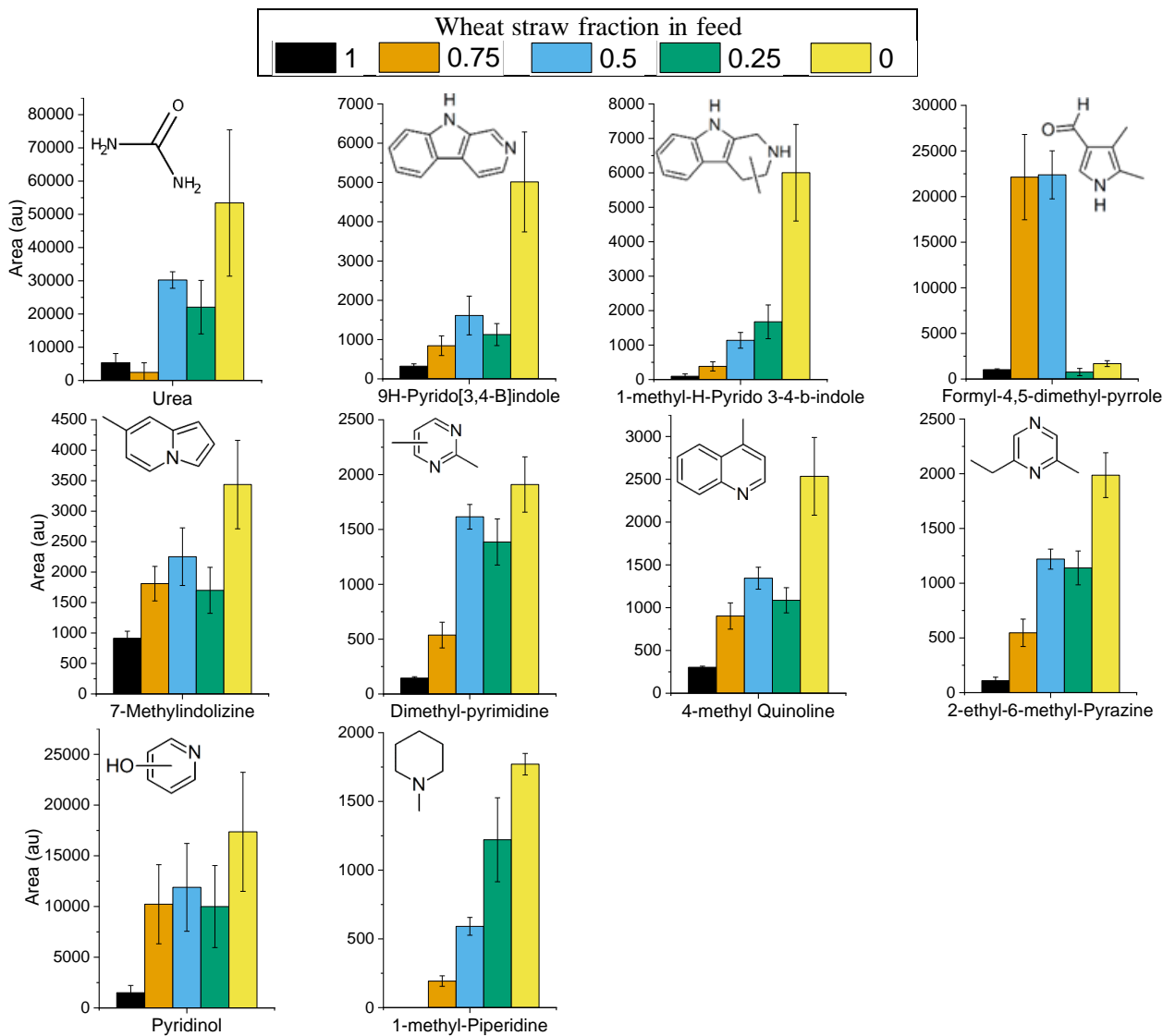
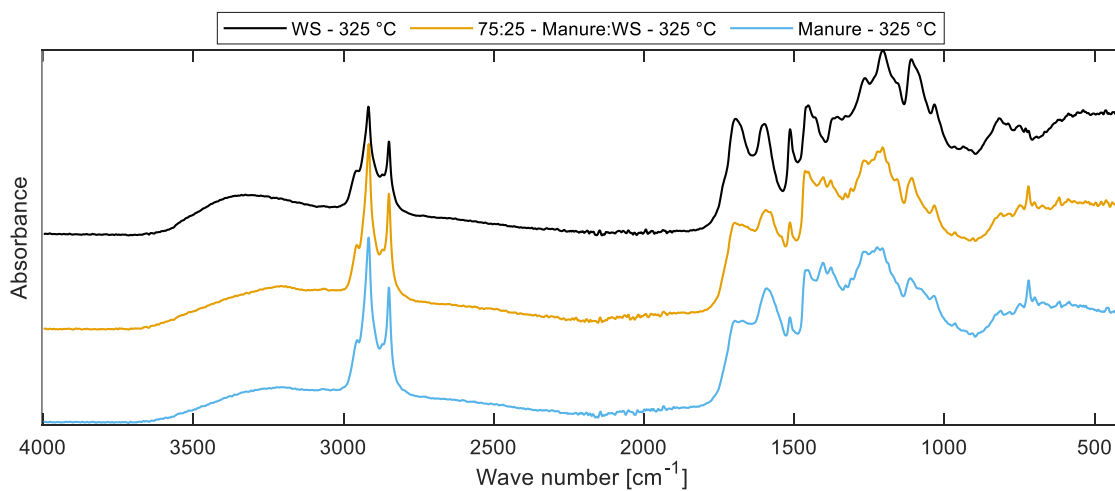
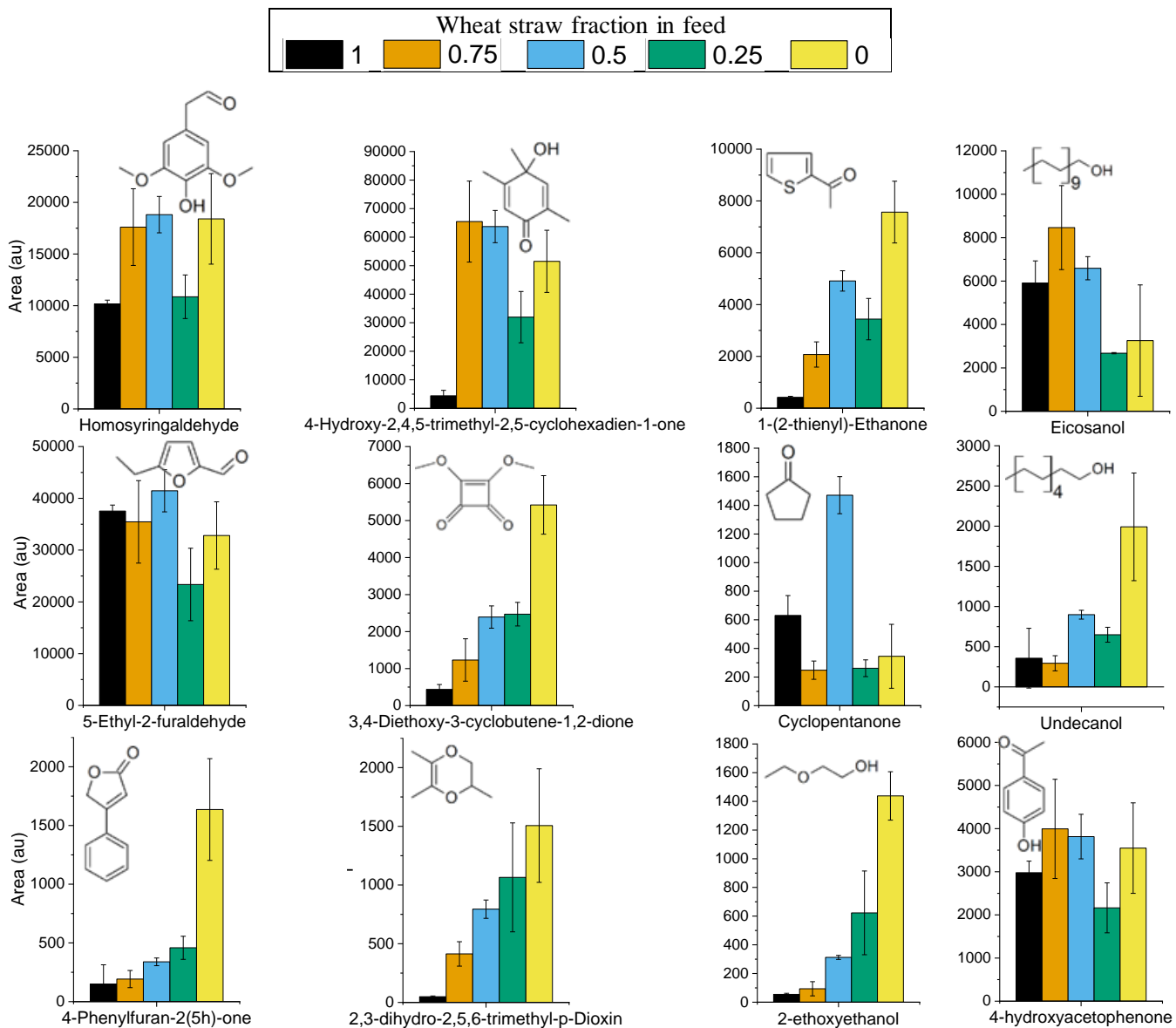


Figure S7 - N-compounds WS fraction comparison @ 325 °C



SUPPLEMENTARY INFORMATION – Chapter 9 – Manuscript 3 – Upgrading of hydrothermal liquefaction biocrudes from mono- and co-liquefaction of cow manure and wheat straw via hydrotreating and distillation

Juliano Souza dos Passos ^{a,b}, Petr Straka ^c, Miloš Auersvald ^c, Patrick Biller* ^{a,b}

^a Department of Biological and Chemical Engineering, Aarhus University, Hångøvej 2, DK-8200 Aarhus N, Denmark

^b Aarhus University Centre for Circular Bioeconomy, DK-8830 Tjele, Denmark

* Corresponding author – pbiller@bce.au.dk

Key words: Hydrothermal liquefaction; waste valorization; manure; wheat straw; biofuel

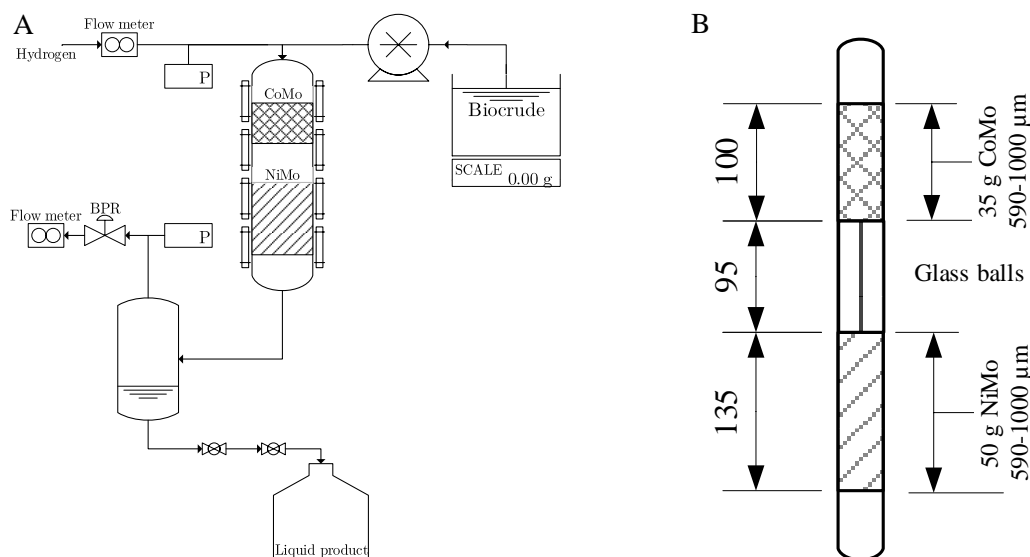


Figure S1 – Hydrotreatment setup simplified process diagram (A) and reactor packing detail (out of scale) in mm (B)

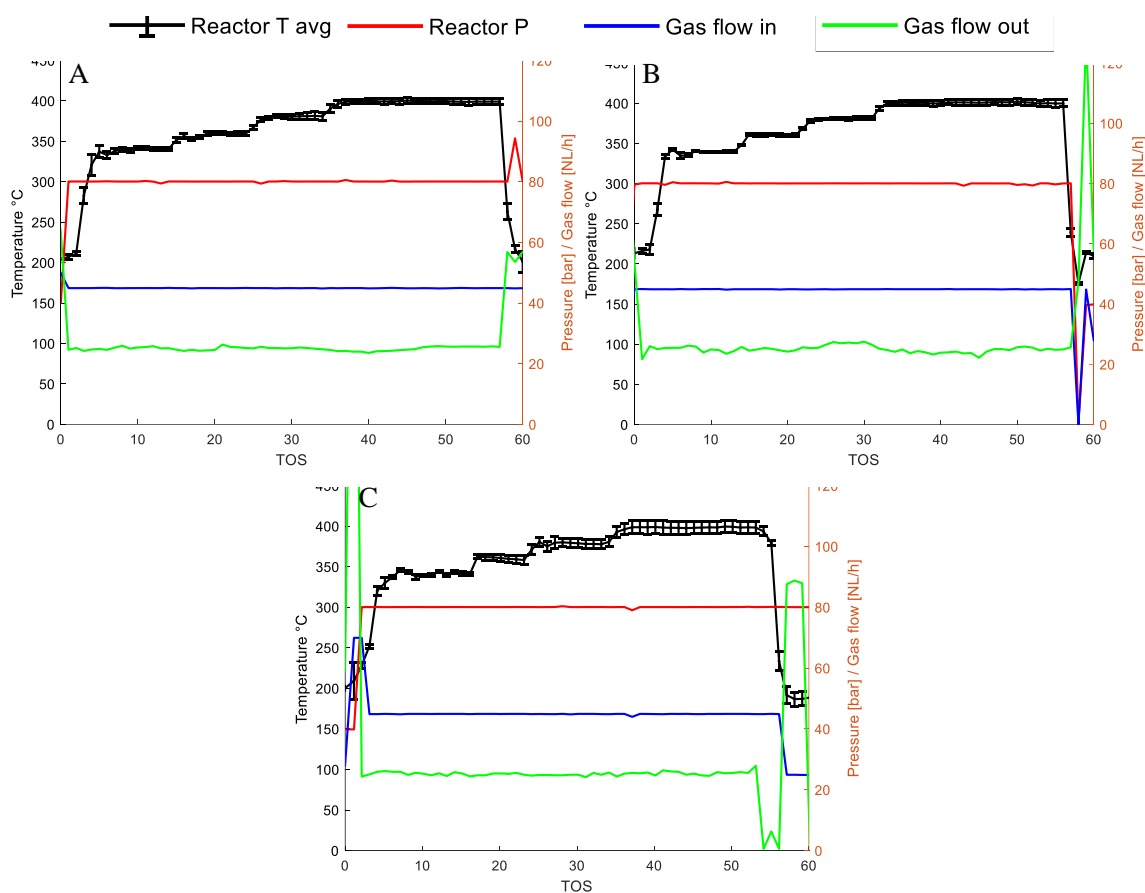


Figure S2 – Reactor average temperature (four first thermocouples in the NiMo catalyst section), pressure, gas flow in and out during hydrotreatment. A – Wheat straw; B – Cow Manure; C – Combined biocrude

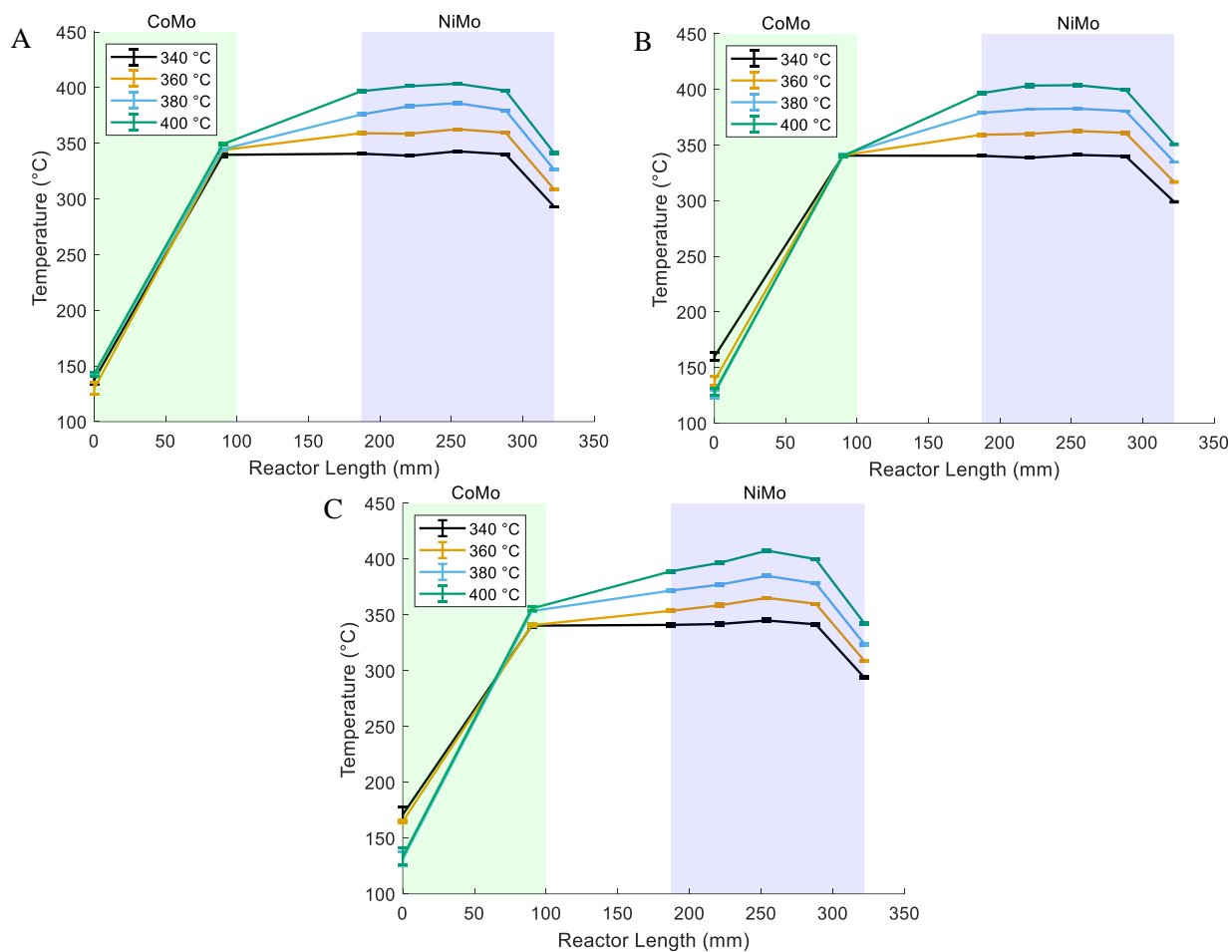


Figure S3 – Reactor temperature profile for all temperatures tested. A – Wheat straw; B – Cow Manure; C – Combined biocrude

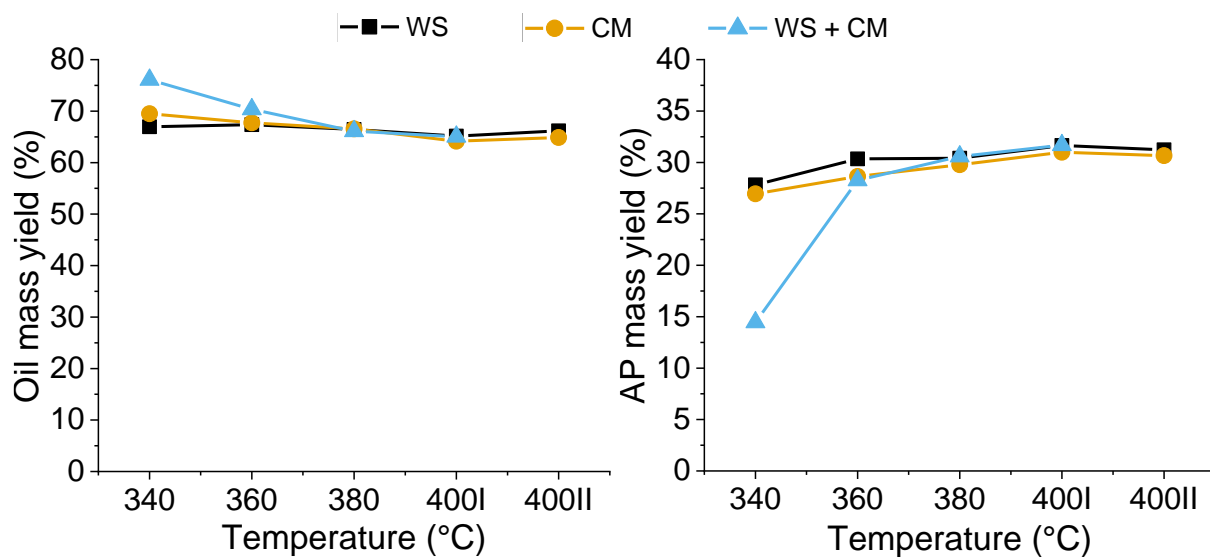


Figure S4 – Oil (A) and aqueous phase (AP) (B) mass yields

Table S1 – Elemental composition of biocrudes and hydrotreated products, deoxygenation and hydrogen consumption

Feed		C	H	N	S	O*	DO**	DN**	H ₂ cons.
		%	%	%	%	%	%	%	gH ₂ /kg _{oil} DB
Straw	Biocrude	63.2 ± 0.3	8.0 ± 0.0	0.7 ± 0.0	0.1 ± 0.0	27.9	-	-	-
	340 °C	85.3 ± 0.0	11.1 ± 0.0	1.1 ± 0.1	0.1 ± 0.0	2.4	91	-54	18.1
	360 °C	86.1 ± 0.0	11.3 ± 0.0	1.1 ± 0.1	0.0 ± 0.0	1.4	95	-50	27.8
	380 °C	87.1 ± 0.1	11.8 ± 0.0	0.5 ± 0.1	0.0 ± 0.0	0.5	98	27	25.2
	400 °CI	87.5 ± 0.0	11.9 ± 0.0	0.6 ± 0.0	0.0 ± 0.0	0.0	100	19	35.7
	400 °CII	87.4 ± 0.0	11.8 ± 0.0	0.5 ± 0.0	0.0 ± 0.0	0.3	99	29	30.8
Manure	Biocrude	66.1 ± 0.3	8.2 ± 0.1	3.4 ± 0.0	0.7 ± 0.0	21.6	-	-	-
	340 °C	83.1 ± 0.1	11.3 ± 0.0	3.4 ± 0.1	0.1 ± 0.0	2.1	90	0	13.5
	360 °C	84.9 ± 0.0	11.8 ± 0.0	2.5 ± 0.1	0.0 ± 0.0	0.8	97	26	23.4
	380 °C	85.8 ± 0.0	12.3 ± 0.0	2.3 ± 0.2	0.0 ± 0.0	0.0	100	34	30.7
	400 °CI	86.4 ± 0.0	12.6 ± 0.0	1.7 ± 0.2	0.0 ± 0.0	0.0	100	51	30.3
	400 °CII	86.2 ± 0.0	12.4 ± 0.0	1.8 ± 0.2	0.0 ± 0.0	0.0	100	48	29.1
Combi ned	Biocrude	65.3 ± 1.9	8.5 ± 0.0	2.7 ± 0.2	0.4 ± 0.0	23.2	-	-	-
	340 °C	82.9 ± 0.1	11.0 ± 0.0	3.2 ± 0.1	0.0 ± 0.0	2.9	88	-18	10.8
	360 °C	84.7 ± 0.0	11.4 ± 0.0	3.2 ± 0.1	0.0 ± 0.0	0.7	97	-17	14.1
	380 °C	85.4 ± 0.0	11.5 ± 0.0	3.2 ± 0.2	0.0 ± 0.0	0.0	100	-17	14.1
	400 °CI	85.8 ± 0.1	11.5 ± 0.0	3.1 ± 0.0	0.0 ± 0.0	0.0	100	-17	17.7
	400 °CII	85.6 ± 0.0	11.3 ± 0.0	3.2 ± 0.1	0.0 ± 0.0	0.0	100	-20	16.5

* - Oxygen by difference

** - DO = Deoxygenation; DN = Denitrogenation

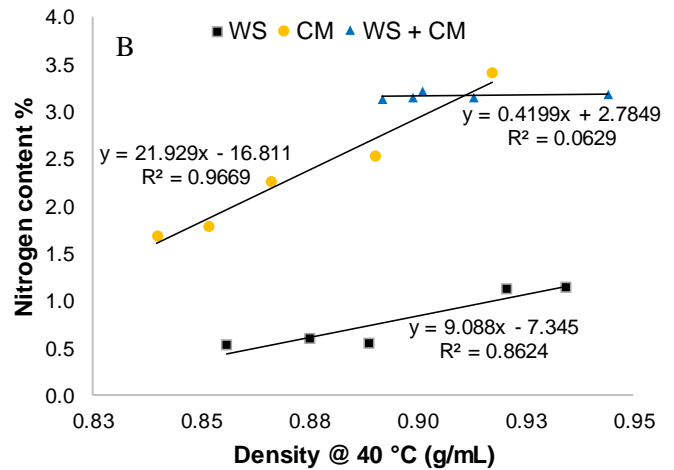
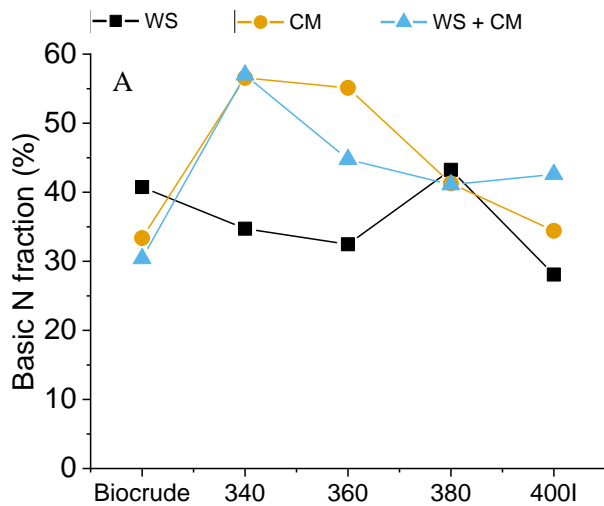


Figure S5 – Basic nitrogen fraction in total nitrogen oil content (A) and nitrogen content to density correlation

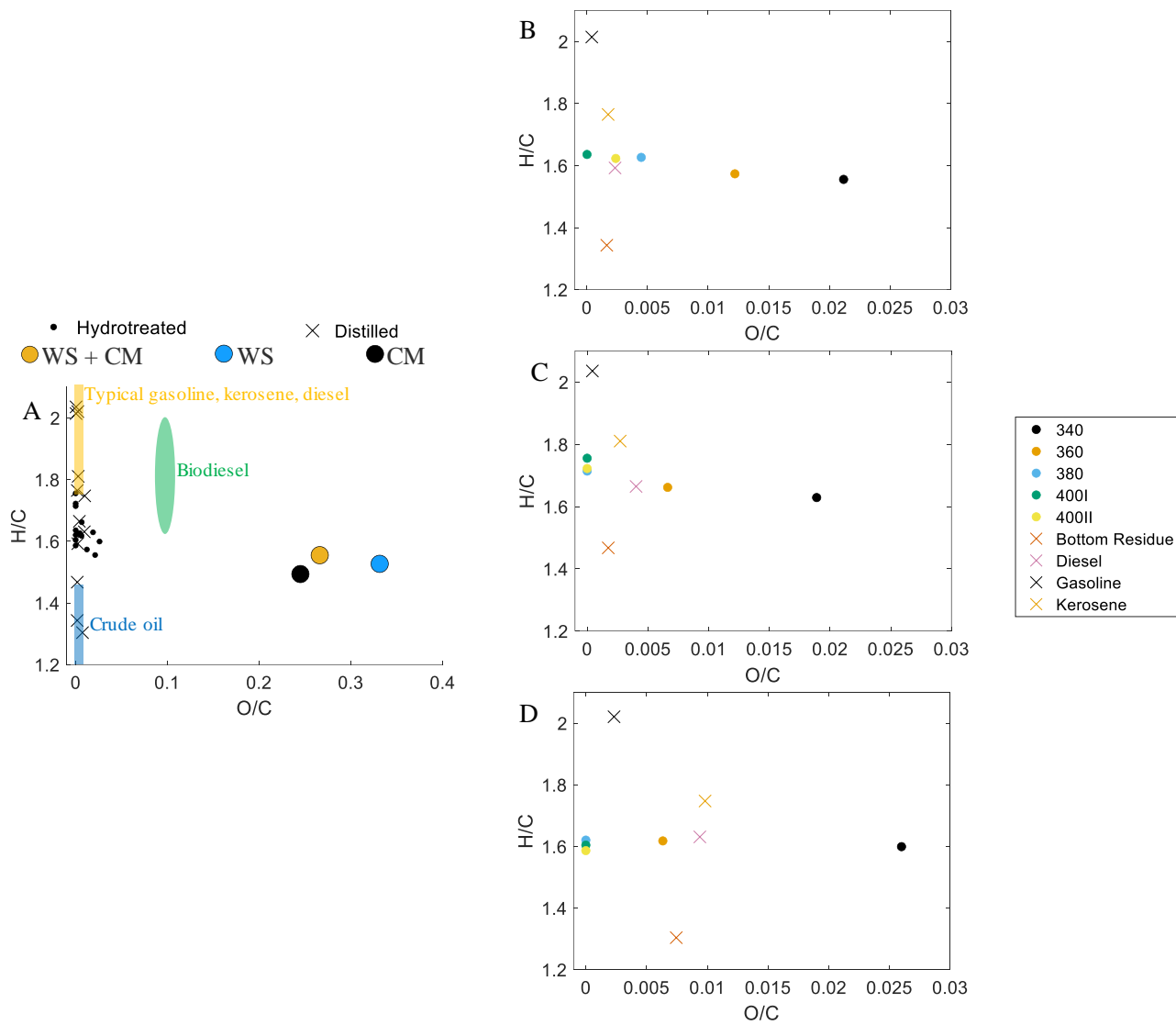


Figure S6 – Van Krevelen diagram of hydrotreated and distilled products. A – All samples and biocrudes; B – Wheat straw products; C – Cow manure products; D – Combined biocrude products

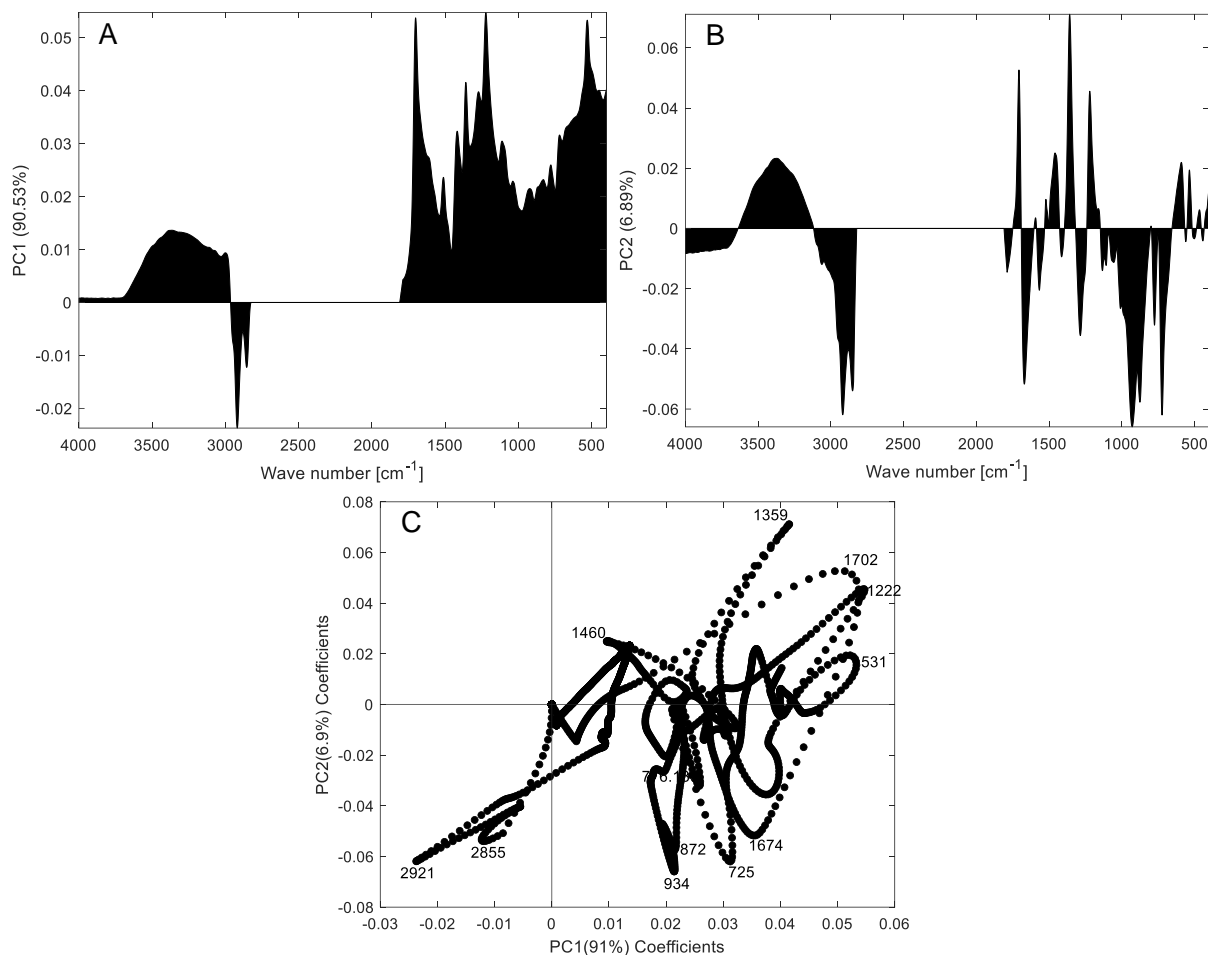


Figure S7 – Principal components 1 and 2 loadings for FTIR PCA

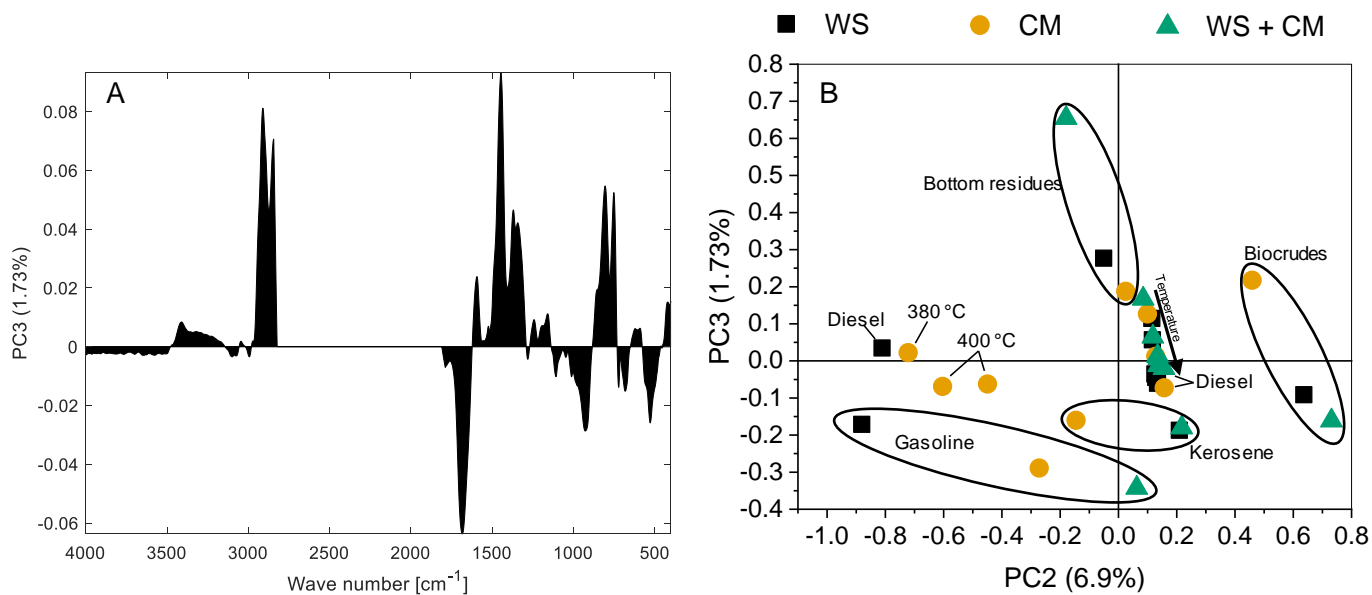


Figure S8 – PC3 loading plot and PC2 versus PC3 scores for FTIR PCA